SEMIANNUAL REPORT NO. 5

DEVELOPMENT OF COMPRESSOR END SEALS STATOR INTERSTAGE SEALS, AND STATOR PIVOT SEALS IN ADVANCED AIR-BREATHING PROPULSION SYSTEMS

Prepared for

NATIONAL AERONAUTICS AND SPACE ADMINISTRATION

20 January 1968

CONTRACT NAS3-7605

Technical Management
NASA Lewis Research Center
Cleveland, Ohio
Air-Breathing Engine Division
D. P. Townsend
Project Manager
L. P. Ludwig
Research Advisor

Written by: R. M. Hawkins, A. H. McKibbin

R. M. Hawkins
Project Manager

A. H. McKibbin
Assistant Project Engineer-
Analytical

Dr. Charles C. W. Ng
Assistant Project Engineer-
Analytical

Approved by:
R. P. Shevchenko
Senior Project Engineer

Pratt & Whitney Aircraft
DIVISION OF UNITED AIRCRAFT CORPORATION

EAST HARTFORD, CONNECTICUT

PREFACE

This report describes the progress of work conducted between 1 July 1967 and 31 December 1967 by the Pratt & Whitney Aircraft Division of United Aircraft Corporation, East Hartford, Connecticut on Contract NAS3-7605, Development of Compressor End Seals, Stator Interstage Seals, and Stator Pivot Seals in Advanced Air-Breathing Propulsion Systems, for the Lewis Research Center of the National Aeronautics and Space Administration.

The authors wish to acknowledge the assistance of Messrs. H. L. Northup, P. E. Nicolich, H. Shaffer, P. R. Lawell, R. E. Turley, and P. A. Rubenstein in the preparation of material for this report.

Roger M. Hawkins is Project Manager for Pratt & Whitney Aircraft for this program.

The following National Aeronautics and Space Administration personnel have been assigned to this project:

Contract Officer	-	J. H. DeFord
Project Manager	-	D. P. Townsend
Research Advisor	-	L. P. Ludwig
Contract Administrator	-	E. Schiopota

SUMMARY

This report describes the work accomplished during the fifth six-month period of an analytical, design, and experimental program directed at developing compressor end seals, stator interstage seals, and stator pivot seals for advanced air-breathing propulsion systems.

Feasibility analyses of the OC diaphragm thin-strip seal, the semirigid one-piece seal, and the flexure-mounted shoe seal have been completed. Each of these three concepts has been analyzed in both an end seal configuration and an interstage seal configuration, thus completing the Task I work. Results of the analyses indicated that the best configurations were the OC diaphragm end seal and the semirigid interstage seal. Both of these seals have been chosen for further evaluation under Task II.

Most of the work under Tasks II and IV has been concerned with procurement and fabrication of the seals, instrumentation, and test equipment. In addition, a gas-film analysis and a thermal analysis of the one-side floated-shoe end and interstage seals were performed under Task II. Testing has started on the single-bellows vane pivot seal, (Task IV) but no results are available as yet.

No work has been performed under Task III in the last six months.

Milestone Charts are presented at the end of this report.

SEMIANNUAL REPORT NO. 5

DEVELOPMENT OF COMPRESSOR END SEALS, STATOR INTERSTAGE SEALS, AND STATOR PIVOT SEALS IN ADVANCED AIR-BREATHING ENGINES

by

R. M. Hawkins, A. H. McKibbin, and C. C. W. Ng

ABSTRACT

Tracking analyses and thermal analyses of the OC diaphragm thin-strip seal, the semirigid interstage seal, and the flexure-mounted shoe seal are discussed. The tracking analysis includes the effects of seal tilt angle, engine speed (take-off, cruise, and idle conditions), and natural frequencies of the seal. Primary emphasis is placed on the OC diaphragm end seal and the semirigid interstage seal, since these designs were chosen for further evaluation. In addition the preparations for testing the end and interstage seals and the vane pivot seals are discussed.

TABLE OF CONTENTS

		Page
PREFACE		ii
SUMMARY		iii
ABSTRACT		iv
LIST OF ILLUSTRATIONS		vii
LIST OF TABLES		xi
NOMENCLATURE		xiii
INTRODUCTION		1
I.	TASK I	3
	A. Introduction	3
	B. Seal Tracking Analysis	7
	C. OC Diaphragm Thin-Strip Seal	49
	D. Semirigid Interstage Seal Design	74
II.	TASK II	93
	A. Introduction	93
	B. One-Side Floated-Shoe Seal	94
	C. OC Diaphragm End Seal and Semirigid Interstage Seal	98
	D. Test Rig and Test Stand	102
III.	TASK III	103
IV.	TASK IV	105
	A. Introduction	105
	B. Description of Seals and Test Rig	106
MILESTONE CHARTS		119
APPENDICES		123
	A. Flexible Seal Tracking Analysis Computer Program	123
	B. Thermal Analysis	141
	C. OC Diaphragm End Seal Task I Thermal Calculations	149
	D. Temperature Analysis of the Semirigid Interstage Seal	179

TABLE OF CONTENTS (Contd)

	Page
E. Stiffness and Displacement Calculations for Composite Thin Rings	197
F. Thermal Rotation Calculations for the Semirigid Interstage Seal	211
REFERENCES	215
DISTRIBUTION LIST	216

LIST OF ILLUSTRATIONS

Figure	Title	Page
1	OC Diaphragm End Seal	4
2	Semirigid Interstage Seal	5
3	Geometry of the Flexure-Mounted Shoe Seal	8
4	Free-Body Diagram of the Shoe	8
5	Beam Analogy for the Tab Spring	11
6	Tab Load Diagram	12
7	Dimensions of the Flexure-Mounted Shoe Seal	12
8	Axial Oscillation of the Hoop	14
9	Angular Oscillation of the Shoe	15
10	Axial Oscillation of the Shoe	16
11	OC Diaphragm Thin-Strip Seal Concept	19
12	Semirigid One-Piece Seal Concept	19
13	Rotor Contour, Seal-Ring Instantaneous Deflection, and Seal-Ring Initial Distortion	20
14	Free-Body Diagram of a Seal-Ring Segment	21
15	Bending of a Seal Segment Because of Angular Displacement α	23
16	Seal-Ring Segment	25
17	Lumped-Parameter Model of the Carrier-Ring System	36
18	Schematic for Mathematical Model of Angular Vibration	39
19	Typical Single-Pad Seal	44

LIST OF ILLUSTRATIONS (Contd)

Figure	Title	Page
20	Gas-Film Forces on a Double Pad	46
21	OC Diaphragm End Seal Restoring Moment and Minimum Film Thickness	51
22	OC Diaphragm End Seal Film Thickness	52
23	OC Diaphragm End Seal Leakage	53
24	Critical Tolerances in the OC Diaphragm End Seal	55
25	Modes of Seal and Runner Distortion Used in Tracking Analysis	60
26	Helical Coil Spring Rate	68
27	Simplified Diagram of the OC Diaphragm Seal	69
28	Force and Moment Diagram for the OC Diaphragm Seal Carrier	71
29	Cross Section of the Semirigid One-Piece Seal	76
30	Cross Section of the Semirigid One-Piece Seal with Insulating Cut Out	77
31	Minimum Film Thickness and Center of Pressure for the Semirigid Interstage Seal at Cruise	80
32	Leakage and Stiffness of the Semirigid Interstage Seal at Cruise	80
33	Minimum Film Thickness and Center of Pressure for the Semirigid Interstage Seal at Idle	81
34	Leakage and Stiffness of the Semirigid Interstage Seal at Idle	82
35	Minimum Film Thickness and Center of Pressure For the Semirigid Interstage Seal at Take-Off	83
36	Leakage and Stiffness of the Semirigid Interstage Seal at Take-Off	84
37	Diagram of Nodal Points and Subvolumes for Thermal Analysis of the Semirigid Interstage Seal	86

LIST OF ILLUSTRATIONS (Contd)

Figure	Title	Page
38	Temperature Distribution (in °F) in the Semirigid Interstage Seal	87
39	One-Side Floated-Shoe End Seal Gas Film Calculation	94
40	One-Side Floated-Shoe Interstage Seal Gas Film Calculation	96
41	Thermal Map of the One-Side Floated-Shoe Interstage Seal at Cruise Conditions	97
42	Semirigid Interstage Seal	98
43	Semirigid Interstage Seal Thermal Deflection	99
44	Pressure-Induced Deflections in the Semirigid Interstage Seal. Runner in Retracted and Extended Position	101
45	Single-Bellows Vane Pivot Seal	107
46	Instrumentation on Single-Bellows Vane Pivot Seal (XP-80138)	108
47	Seal (Left) for Single-Bellows Vane Pivot Seal, and Bellows (Right) (VP-79777)	109
48	Seal Housing with Bellows Seal Installed (XP-80136)	110
49	Push Rod and 25X View of Strain Gauge (XP-78644, XP-80223)	111
50	Vane Actuation Link (XP-80487)	112
51	Strain Gauge for Vane Actuation Link (XP-80488)	113
52	Test Rig and Instrumentation (XP-80959)	114
53	Instrumentation and Control Panel (XP-80960)	115
54	Close-Up of Thermocouple Leads (XP-8093)	116
55	Thermal Network for Internal and Surface Nodal Points	142
56	Thermal Network for Nodal Points in the Gap between Seal and Seal Plate	143

LIST OF ILLUSTRATIONS (Contd)

Figure	Title	Page
57	Temperature Distribution (in Degrees Fahrenheit) in the OC Diaphragm End Seal at Cruise Conditions	150
58	Nodal Network for the OC Diaphragm End Seal	152
59	Model and Heat Flow Path for Heat Transfer in the Region of Metal Nodes 13, 14, and 15	176
60	Flow Chart of the Entire Fluid Heat Transfer Path for the OC Diaphragm End Seal	177
61	Rotation of the Cross Section of a Ring Around a Prescribed Center of Rotation	197
62	Free-Body Diagram of One Half of a Ring	199
63	Free-Body Diagram of One Half of a Ring with a Uniform Radial Force (Q_o) Applied Outward through the Centroid	200
64	Mismatch Conditions for a Two-Section Ring	202
65	Rotation of a Thin Ring with a Linear Axial Temperature Gradient	209
66	Thermal Rotation Model of the Semirigid Interstage Seal	212

LIST OF TABLES

Table	Title	Page
I	Adjusted Residual Moments in the OC Diaphragm End Seal	54
II	Combined Residual Moments for the OC Diaphragm End Seal	57
III	Mean and Minimum Film Thickness Resulting From Residual Moments in the OC Diaphragm End Seal	58
IV	Tilted- and Parallel-Film Maximum Seal Leakage in the OC Diaphragm End Seal	58
V	Results of Tracking Analysis of the OC Diaphragm End Seal	61
VI	Influence Coefficients for the OC Diaphragm End Seal	62
VII	Natural Frequencies of the OC Diaphragm End Seal in Rad/Sec	64
VIII	Carrier and Seal Ring Rigid-Body Response Ratios	64
IX	Final Minimum Film Thickness of the OC Diaphragm End Seal During Operation	65
X	Balance Results for the OC Diaphragm End Seal	72
XI	Film Thickness and Residual Moment Tabulation for the Semirigid Interstage Seal	79
XII	Input Distortions Used in the Tracking Analysis of the Semirigid End and Interstage Seals	88
XIII	Influence Coefficients for the Tracking Analysis of the Semirigid Interstage Seal	90
XIV	Semirigid Interstage Seal Tracking Results	91
XV	Design Point Gas Film Characteristics	95
XVI	Heat Generation	151
XVII	Weighted Axial Clearance	153

LIST OF TABLES (Contd)

Table	Title	Page
XVIII	Input Data for Admittance Calculation	156
XIX	Output Data from Admittance Calculation	166
XX	Input Data for Admittance Calculation on the Semirigid Interstage Seal	183
XXI	Output Data from Admittance Calculation on the Semirigid Interstage Seal	190

NOMENCLATURE

A	ring cross sectional area (in^2)
B_{ss}	flex shoe tab transverse stiffness (lb/in)
$B_{s\alpha}$	flex shoe tab cross coupling stiffness (lb/rad)
$B_{\alpha s}$	flex shoe tab cross coupling stiffness (in-lb/in)
$B_{\alpha\alpha}$	flex shoe tab angular stiffness (in-lb/rad)
C_{A1}, C_{A2}	influence coefficients associated with α_n
C_{B1}, C_{B2}	influence coefficients associated with β_n
C_{u1}, C_{u2}	influence coefficients associated with u_n
C_{v1}, C_{v2}	influence coefficients associated with v_n
C_1, C_2, C_3	magnitude of $\gamma_1, \gamma_2, \gamma_3$
E	modulus of elasticity (lb/in^2)
F_1, F_2, F_3	forces on semi-rigid seal (lb/in)
F_3	"O" diaphragm pressure load (lb/in)
F_S	helical coil spring force (lb/in)
F_{S1}, F_{S2}	C and O diaphragm spring reactions (lb/in)
F_o	carrier axial pressure load (lb/in)
F_y	carrier radial pressure load (lb/in)
G	modulus of rigidity (lb/in^2), shear modulus of elasticity (lb/in^2)
I	area moment of inertia (in^4)
I_1, I_2, I_{tt}	mass moment of inertia (in-lb-sec^2)
I_p	area moment of inertia (in^4)

K_{ss}	axial gas film stiffness (lb/in/in)
$\overline{K}_{ss}$	carrier spring stiffness (lb/in/in)
K'_{ss}	axial gas film stiffness per unit area ($lb/in/in^2$)
$K_{\alpha\alpha}$	angular gas film stiffness (in-lb/in. rad)
$K_{s\alpha}$	cross coupling film stiffness (lb/in-rad)
$K_{\alpha s}$	cross coupling film stiffness (in–lb/in/in)
K^*_r	bending stiffness of seal ring $= \frac{EI}{R^2}$ (in-lb/in-rad)
K^*_{ss}	OC diaphragm stiffness, (lb/in/in)
$K^*_{s\alpha}$	OC diaphragm cross coupling stiffness (lb/in-rad)
$K^*_{\alpha s}$	OC diaphragm cross coupling stiffness (lb/in/in)
$K^*_{\alpha\alpha}$	OC diaphragm angular stiffness (in-lb/in-rad)
K_1, K_2, K_3	spring constants (lb/in) (See Figure 17)
M	moment (in-lb/in)
ΔM	gas film restoring moment (in-lb/in)
M_b	bending moment (in-lb/in)
M_c	residual moment due to "C" diaphragm tolerance,
M_o	residual moment due to "O" diaphragm tolerance
M_{oc}	combined residual moment due to tolerances $= M_o + M_c$ (in-lb/in)
M_R	carrier residual moment (in-lb/in)
M_{res}	residual moment (in-lb/in)
M_t	flexible ring twisting moment (in-lb/in)

P_1, P_2	dimensionless quantity defined by Equation 40
Q_1, Q_2	unit flow rate (lb/sec-in)
Q_T	total flow rate (lb-sec)
Q_{PR}	piston ring flow rate (lb/sec)
R	gas constant ($in^2/^o$ R-sec^2)
R	seal ring radius (inches)
S_s	combined radial stiffness of seal ring (lb/in/in)
S_{oc}	radial stiffness of OC spring diaphragm (lb/in/in)
T	temperature (°R or °F)
U	velocity (in/sec)
V	shearing force (lb/in)
W_1, W_2	seal or bearing reactions (lb/in)
$\overline{W}_1, \overline{W}_2$	dimensionless seal or bearing loads
a	orifice radius, (inches)
a	seal radius (inches)
a_g	groove width (inches)
a_r	ridge width (inches)
b	pad width (inches)
$b_1 \ldots\ldots b_4$	width dimensions, (inches)
c	pad length (inches)
e	strain (in/in)
g	gravitational constant (in/sec^2)
h_m	mean film thickness (inches)

h_1	step bearing land clearance (inches)
h_2	step bearing recess clearance (inches)
Δh	Rayleigh pad recess depth (inches)
h_{min}	minimum gas film thickness (inches)
$h_{T\,min}$	combined mode minimum film thickness (in)
$h_{R\,min}$	minimum film thickness resulting from residual moments (in)
$h_{R\,m}$	mean film thickness resulting from residual moments (in)
h_F	final, combined minimum film thickness (in)
k	thermal conductivity $\left(\frac{BTU}{(hr\text{-}^{O}F\text{-}ft}\right)$
k_2	back up spring stiffness for flexure-mounted shoe seal (lb/in)
ℓ	beam length (inches)
ℓ	net change in axial film thickness (inches)
m	mass in flow (lb-sec/in^2)
m_1, m_2	mass (lb-sec^2/in)
n	number of orifice holes
n	operational mode (1, 2, 3 .....etc.)
p_1, p_2	ambient and supplied pressure respectively (psia)
Δp	pressure difference (psi)
q_a	restoring force (lb/in)
q	restoring moment (in-lb/in)
r	radial coordinate
t	thickness (inches)

t	time (sec)
u_1	transverse seal ring displacement (inches)
u_2	transverse carrier displacement (inches)
u_n	dynamic seal ring transverse response to runner deformations δ_n and ϵ_n
v_n	static seal ring transverse response to seal-ring deformation (ζ_n and η_n) (dimensionless)
w	flow rate (lb/hr)
$\overline{x}_c$	dimensionless center of pressure
x^*	centroid, x coordinates (in)
x_c	center of pressure = $b\overline{x}_c$ (inches)
x_c, x_{To}, x_{Bo}	radial displacements of spring diaphragms (inches)
x_1, x_2, x_3	rigid body displacements (inches)
$\overline{x}_1, \overline{x}_2, \overline{x}_3$	radial displacements of ring centroid, (inches)
x_{12}, x_{23}	radial thermal mismatch (inches)
$\overline{y}_c$	dimensionless center of pressure
y	transverse displacement (inches)
y	beam deflection (inches)
y_1, y_2, y_3	force moment arms (in)
y^*	centroid y coordinate (in)
z	axial coordinate (inches)
z	axial displacement of OC springs
z_o	initial axial position of OC springs
$\overline{z}$	net axial displacement of OC springs = $z - z_o$ (inches)

α	seal tilt angle (radians)
α	coefficient of thermal expansion (in/in/°F)
α_n	dynamic seal ring angular response to runner deformations ϵ_n and δ_n
β	spiral groove angle (degrees)
β_n	static seal ring angular response to seal ring deformation ζ_n and η_n
$\gamma_1, \gamma_2, \gamma_3$	rigid body angular displacement
$\Gamma_1, \Gamma_2, \ldots \Gamma_{10}, \Gamma_{11}$	special parameters defined in Equation 27
δ	initial transverse deformation of rotor surface (inches)
δ	thermal radial mismatch (inches)
δ_n	n-th component of dimensionless, initial transverse rotor deformation
ϵ	initial angular rotor deformation (radians)
ϵ_n	n-th component of initial angular rotor deformation (radians)
ζ	initial angular deformation of seal ring (radian)
ζ_n	nth component of initial angular deformation of seal ring
η	initial transverse distortion of seal ring (inches)
η_n	nth component of dimensionless initial seal ring transverse deformation
θ	coordinate
θ	seal tilt angle due to restraining effect of OC springs
ν	frequency, (rad/sec.)
ν_{n1}, ν_{n2}	natural frequencies of flexible seal ring (rad/sec)
Λ_y	bearing compressibility number, $6\mu Vb/ph^2$
μ	viscosity (lb-sec/in^2)
ξ	$\frac{EI}{GI_p}$

ρ	mass density ($lb\text{-}sec^2/in^4$)
τ	shear stress (lb/in^2)
ϕ	net angle between rotor and seal ring, (radians)
ψ	wedge angle of shoe section (degrees)
ω	angular speed (rad/sec)

INTRODUCTION

High performance, modern multistage axial-flow compressors built with state-of-the-art features incorporate several air leak paths which are detrimental to compressor performance. Elimination or significant reduction of these leaks would result in a compressor of higher efficiency and possibly smaller size. Some typical areas of leak paths with estimates of percent air loss and potential effect on compressor performance are:

	Air Loss	Effect on Compressor Efficiency
End Seal	0.6%	1.0%
Interstage Stator Seals (ten stages)	0.9%	1.0%
Vane Pivot Seals (variable stator)	0.2% per stage	0.2% per stage

Increases in compressor efficiency are traditionally sought by means of compressor geometry redesign. A few extra points in efficiency often mean the difference between a successful or an unsuccessful engine design. These increases as a result of geometry change are always very expensive and not always successful. On the other hand, the losses to efficiency as a result of air leaks are strikingly large, and real gains are within reach at a relatively low cost. The gains in efficiency, however, must be balanced against any detrimental effect that improved sealing may have on the engine, such as lower reliability or increased weight.

This program will provide for a research, analytical, and test program having as its goal the development of compressor end seals, stator interstage seals, and vane pivot seals which exhibit lower air leakage rates than those currently in use. This will be accomplished using components of such size, materials, and designs as to be considered applicable to compressors for engines capable of supersonic aircraft propulsion.

I. TASK I

CONCEPT FEASIBILITY ANALYSIS PROGRAMS FOR COMPRESSOR END SEALS AND STATOR INTERSTAGE SEALS

A. INTRODUCTION

In the initial feasibility analyses, a one-side floated-shoe seal and a two-side floated shoe seal were developed. These designs, however, were sufficiently similar in their basic design concepts that they would leave the program without a radically different conceptual backup if they failed to meet design requirements on test. Therefore, Contract Amendment Number 2 was authorized, providing for the feasibility analysis of an OC diaphragm thin-strip seal. In addition to performing a feasibility analysis of that seal, the contractor has considered two backup seal concepts: the flexure-mounted shoe seal and the semirigid one-piece seal.

The feasibility analysis conducted on all three seals (OC diaphragm, flexure-mounted shoe, and semirigid) has been completed. Both the OC diaphragm and the semirigid seal concepts appear to yield satisfactory predicted performance characteristics. The contractor has therefore requested and received approval to finalize the designs of the OC diaphragm thin-strip seal for the end seal application (shown in Figure 1) and the semirigid one-piece seal for the interstage location (shown in Figure 2). The flexure mounted shoe seal was removed from further consideration at the completion of the Task I feasibility analysis.

Under the terms of the contract, four seals are to be provided by the contractor: two compressor end seals and two stator interstage seals. NASA approval has already been granted for detailing and hardware procurement of the one-side floated-shoe end seal and the one-side floated-shoe interstage seal under Task II. At the present time, the one-side floated-shoe end seal is being fabricated. The one-side floated-shoe interstage seal has been detailed, but procurement had been held in abeyance until the conclusion of the feasibility analysis conducted on the OC diaphragm and the semirigid seal concepts. Since the one-side floated-shoe interstage seal design appears to be competitive with the OC diaphragm and semirigid seal concepts from the standpoint of predicted performance characteristics, the contractor has started procurement of this segmented seal.

1. DESCRIPTION OF THE TWO SEAL CONCEPTS OF CONTRACT AMENDMENT NUMBER 2 SELECTED FOR FINAL DESIGN

The OC diaphragm end seal (Figure 1) employs a thin, flexible, one-piece, annular strip as the primary seal element, providing a high degree of conformability to runner distortion. The thin strip is supported by three C-shaped semitoroidal diaphragms mounted on a floating secondary seal carrier. The secondary carrier provides for axial travel relative to the main engine structure, and a piston ring seal is used between the carrier and the engine structure. One of the C diaphragms forms a seal between the high-pressure and the low-pressure areas. The other two C diaphragms face each other and form a chamber to which the high pressure air flows before reaching the primary seal face. This design, therefore, permits direct balancing of the moments on the thin strip. Further, the thin-strip

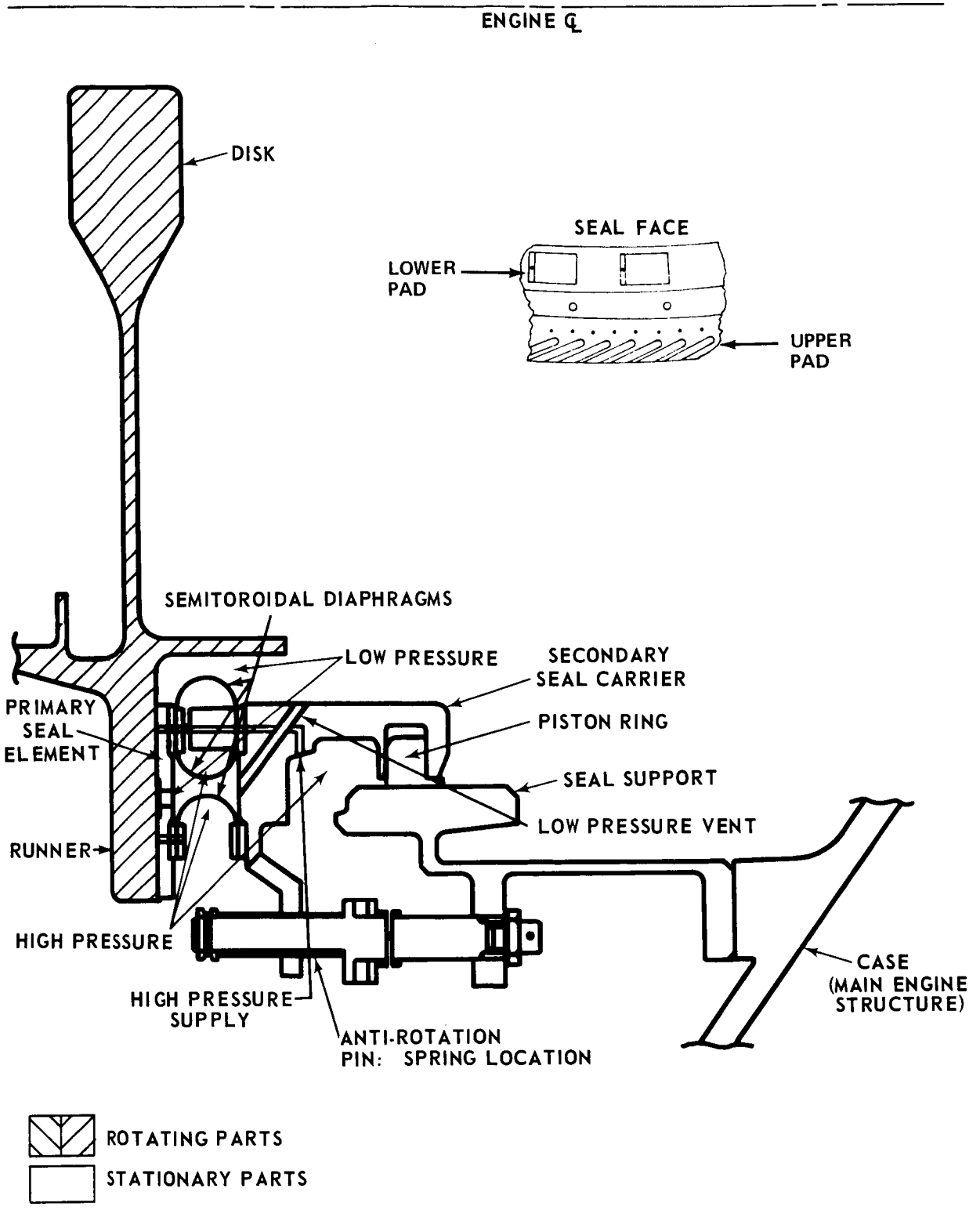

Figure 1 OC Diaphragm End Seal

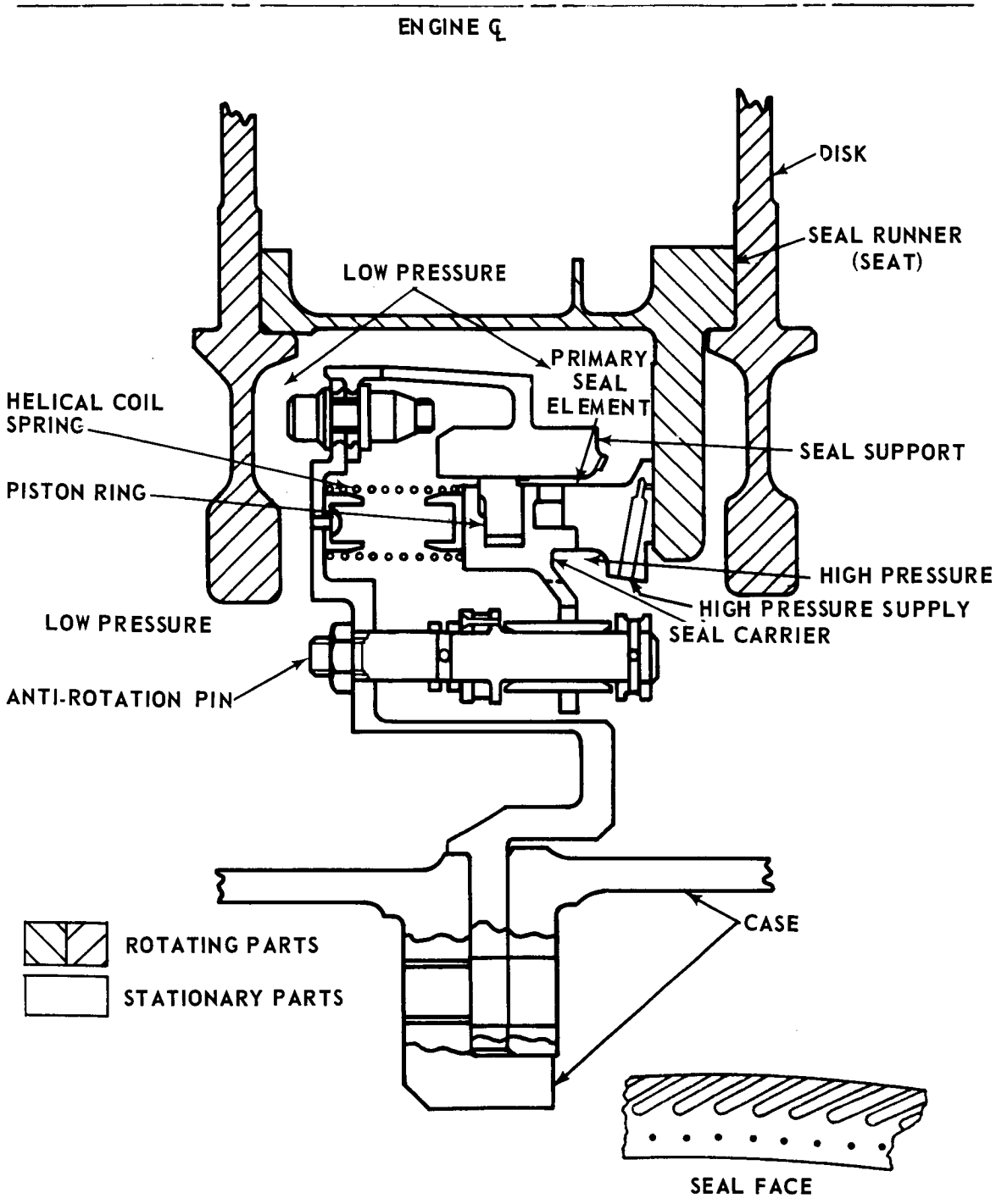

Figure 2 Semirigid Interstage Seal

primary sealing element provides flexibility, and, therefore, tracking capability. The moment balance is achieved with methods which are nearly independent of angular displacements of the strip, making low residual moment imbalance easy to achieve. See page 49 for a detailed description of the seal.

The semirigid interstage seal (Figure 2) recognizes the possibility that a semirigid one-piece primary seal element might be provided with a combination of high gas-film stiffness and low structural stiffness so that adequate gas film thickness is maintained during all operating conditions. The feasibility of this design rests primarily on the ability of the seal to perform satisfactorily with a conically tilted seal face, the tilt resulting primarily from axial thermal gradients. The design also requires that runner conical distortion be relatively low and in the same direction as the seal distortion. The seals's cross-sectional stiffness must be high enough to render the seal insensitive to residual moment imbalance resulting from design drawing tolerances or change in operating conditions, yet low enough to allow the seal to conform to runner waviness. See page 74 for a detailed description of the seal.

2. COMPARISON OF THE RELATIVE MERITS AND POSSIBLE SHORTCOMINGS OF THE TWO SEAL CONCEPTS OF CONTRACT AMENDMENT NUMBER 2

- The leakage rates of the OC diaphragm seal are approximately twice as high as those of the semirigid seal.
- Approximate weights of the main seal assemblies are 18 pounds for the OC diaphragm seal and 10 pounds for the semirigid seal.
- Dynamic seal performance characteristics are satisfactory for both end seal designs, and interstage seal designs at cruise and take off conditions. In the interstage location at idle operating conditions, both seals yield low minimum film thicknesses.
- Heat generation and thus frictional power losses are nearly 50 percent lower with the semirigid seal design than those obtained with the OC diaphragm seal.
- The semirigid seal design is simpler, and thus can be manufactured more economically than the OC diaphragm.
- Based upon the above comparison, the semirigid seal has many inherent advantages over the OC diaphragm seal. The OC diaphragm seal may, however, find application in cases where high seal ring flexibility is required to conform to runner distortions and where thermal gradients across the semirigid seal render this design impractical.

B. SEAL TRACKING ANALYSIS

This portion of the report is concerned with the formulation of the tracking analysis for each of the three seal configurations considered under Contract Amendment No. 2. Once formulated and programmed, this analysis should serve as a valuable tool in establishing the seal's response under dynamic conditions. The analysis consists of two parts: one covering the flexure-mounted shoe seal design, and a second part covering the OC diaphragm thin strip seal design and the semirigid design. The second part has been programmed for the IBM-360 computer. The program has been checked out, and solutions to a typical sample problem obtained. The program listing is presented in Appendix A.

1. TRACKING ANALYSIS OF THE FLEXURE-MOUNTED SHOE SEAL

In designing a flexure-mounted shoe seal (Figure 3), it is necessary to know how closely the shoe will track with various modes of rotor oscillation. In this section, the motion of each shoe is analyzed by assuming that each individual shoe and the hoop are represented by a system of two rigid masses connected by a beam spring and that the system's internal shear and moment can be characterized by four spring stiffnesses.

This system of two masses and two springs is depicted in Figure 4. The mass of the shoe is denoted by m_1, and the equivalent mass (m_2) or the hoop assignable to each shoe is considered to be the total hoop mass divided by the number of shoes. Each shoe is attached to the frame by a back-up spring having a spring rate k_2 and is connected to the hoop by means of a beam spring. The gas film is represented by a spring system having two direct- and two cross-coupling stiffnesses.

The imposed motion of the rotor face is denoted by δ and ϵ, where δ is the axial motion and ϵ the twist motion. δ is defined as positive downward, and ϵ is positive in the direction as shown in Figure 4. The shoe is assumed to have a plane motion which is constrained to oscillate in the y and α directions, i.e. the axial and angular directions. The axial oscillation is denoted by u_1, defined as positive downward, and the angular motion is denoted by α, defined as positive counterclockwise. The hoop is assumed to have an axial oscillation only, and is represented by u_2 (defined as positive downward). A free-body diagram of the shoe is also shown in Figure 4. The gas film's forces are represented by an upward force acting through the centroid of the shoe section having a magnitude $K_{ss}(u_1 - \delta) + K_s (a - \epsilon)$ wise moment having a magnitude $K_{\alpha s}(u_1 - \delta) + K_{\alpha\alpha}(\alpha - \epsilon)$. The forces exerted by the beam spring are likewise represented by an upward force, $B_{ss}(u_1 - u_2) + B_{s\alpha}\,\alpha$, acting at a distance b_2 from the centroid, and by a clockwise moment having a magnitude of $B_{\alpha s}(u_1 - u_2) + B_{\alpha\alpha}\,\alpha$. The inertia forces of the flex-shoe are an upward force, $m_1 \ddot{u}_1$, acting through centroid and a clockwise moment, $I_p \ddot{\alpha}$. The equations of motion of the flex-shoe and the hoop become

$$k_2 u_1 + B_{ss}(u_1 - u_2) + B_{s\alpha}\alpha + K_{ss}(u_1 - \delta) + K_{s\alpha}(\alpha - \epsilon) + m_1 \ddot{u}_1 = 0$$

$$K_{\alpha s}(u_1 - \delta) + K_{\alpha\alpha}(\alpha - \epsilon) + B_{\alpha s}(u_1 - u_2) + B_{\alpha\alpha}\,\alpha + I_p \ddot{\alpha} + k_2 u_1 b_1 + \left[B_{ss}(u_1 - u_2) + B_{s\alpha}\alpha\right] b_2 = 0$$

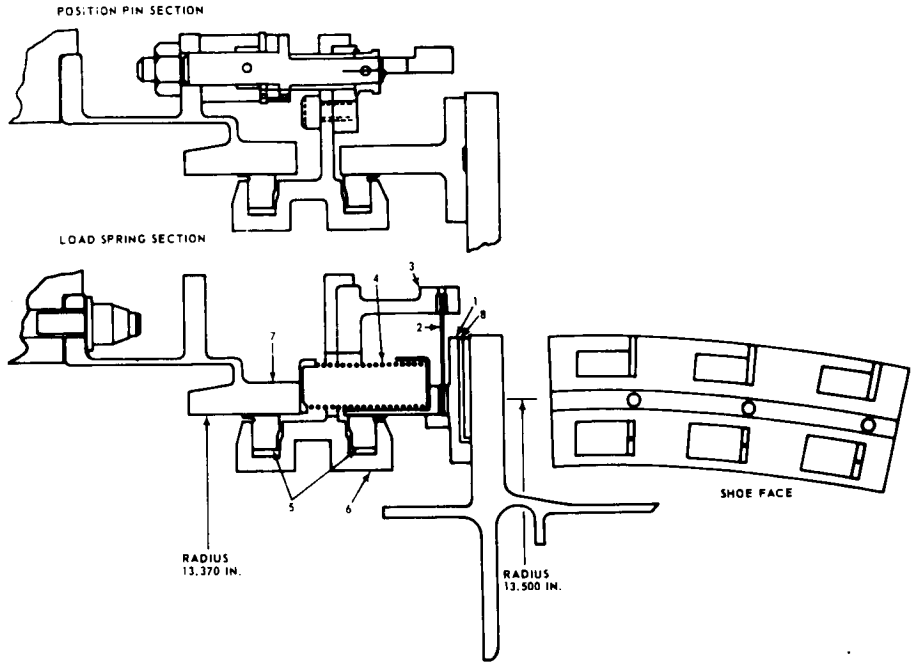

Figure 3 Flexure-Mounted Shoe End Seal.
1. Shoe 2. Flexure Tab 3. Carrier 4. Coil Spring 5. Piston Rings
6. Carrier 7. Test-Rig Adapter 8. Air Passage

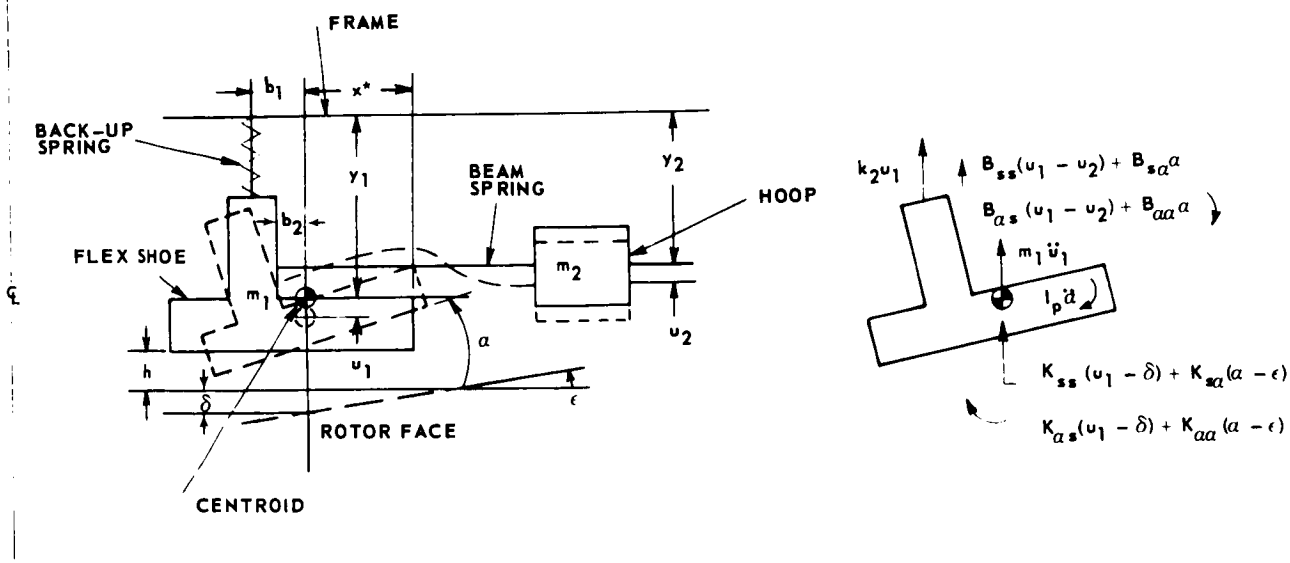

Figure 4 Geometry and Free-Body Diagram of the Flexure-Mounted Shoe Seal

$$m_2 \ddot{u}_2 - B_{ss}(u_1 - u_2) - B_{s\alpha} a = 0$$

Let

$$\begin{aligned} u_1 &= u_{1a} e^{i\omega t} \\ u_2 &= u_{2a} e^{i\omega t} \\ a &= a_a e^{i\omega t} \end{aligned} \tag{1}$$

and the motion of the rotor face be given by

$$\begin{aligned} \epsilon &= \epsilon_a e^{i\omega t} \\ \delta &= \delta_a e^{i\omega t} \end{aligned} \tag{2}$$

the equations of motion after substitution of Equations 1 and 2 can be put into the matrix notation as

$$A \begin{vmatrix} \bar{u}_{1a} \\ \bar{u}_{2a} \\ a_a \end{vmatrix} = C \bar{\delta}_a + D \epsilon_a \tag{3}$$

where

$$\bar{u}_{1a} = \frac{u_{1a}}{b}$$

$$\bar{u}_{2a} = \frac{u_{2a}}{b}$$

$$\bar{\delta}_a = \delta_a / b$$

and,

$$A = \begin{vmatrix} \left(\frac{k_2 + B_{ss} + K_{ss}}{m_1} - \omega^2\right) b & \left(-\frac{B_{ss}}{m_1}\right) b & \frac{B_{s\alpha} + K_{s\alpha}}{m_1} \\ -\frac{B_{ss}}{m_2} b & \left(\frac{B_{ss}}{m_2} - \omega^2\right) b & -\frac{B_{s\alpha}}{m_2} \\ \frac{\left(K_{\alpha s} + B_{\alpha s} + k_2 b_1 + B_{ss} b_2\right)}{I_p} b & -\frac{\left(B_{\alpha s} + B_{ss} b_2\right)}{I_p} b & \frac{B_{\alpha\alpha} + K_{\alpha\alpha} + B_{s\alpha} b_2}{I_p} - \omega^2 \end{vmatrix}$$

$$C = \begin{vmatrix} \frac{bK_{ss}}{m_1} \\ 0 \\ \frac{bK_{\alpha s}}{I_p} \end{vmatrix}$$

$$D = \begin{vmatrix} \frac{K_{s\alpha}}{m_1} \\ 0 \\ \frac{K_{\alpha\alpha}}{I_p} \end{vmatrix}$$

The value of ω for which the determinant of the matrix "A" becomes zero represents a natural frequency of this system. By calculating the determinant of "A" for a range of ω, and plotting these values against ω, the natural frequencies of the system can be determined.

Equation 3 can be inverted to obtain

$$\begin{aligned} \bar{u}_1 &= \left| (u_{1\delta})\ \bar{\delta}_a \right| + \left| (u_{1\epsilon})\ \epsilon \right| \\ \bar{u}_2 &= \left| (u_{2\delta})\ \bar{\delta}_a \right| + \left| (u_{2\epsilon})\ \epsilon \right| \\ a &= \left| (a_\delta)\ \bar{\delta}_a \right| + \left| (a_\epsilon)\ \epsilon \right| \end{aligned} \qquad (4)$$

A computer program was written to calculate the above six coefficients and determinant A for various values of ω. These coefficients can be used to determine the response according to Equation 4.

The gas film's stiffnesses can be calculated from the basic gas-film performance data by using a computer subroutine "KCAL", as described in Appendix A. The stiffnesses of the tab spring can be derived from the formulas for the deflections of a beam fixed at two ends. Consider a beam whose two ends are displaced axially from each other, as shown in Figure 5a. Because of symmetry, the bending moment at the center vanishes and the beam can be regarded as being composed of two identical cantilever sections, as shown in Figure 5b.

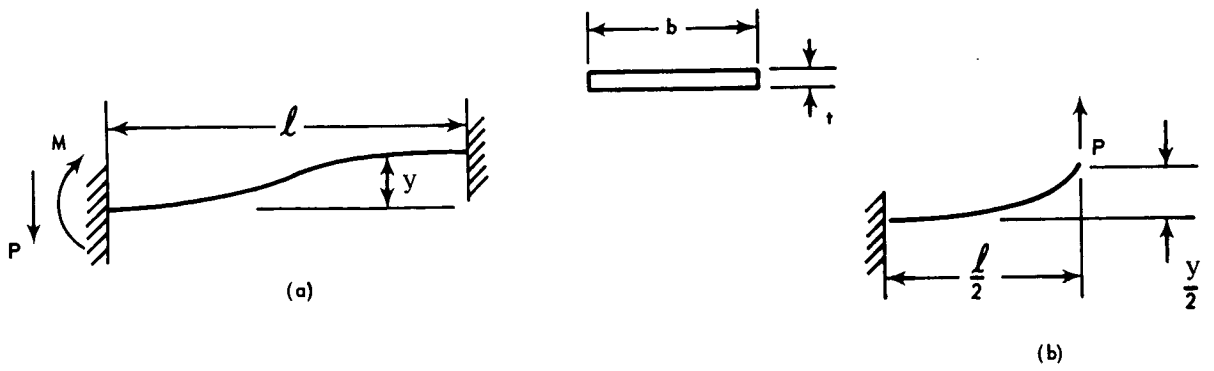

Figure 5 Beam Analogy for the Tab Spring

It follows that

$$\frac{y}{2} = \frac{P}{3EI}\left(\frac{\ell}{2}\right)^3$$
$$M = -\frac{P\ell}{2} \qquad (5)$$

According to the definition,

$$B_{ss} = \frac{P}{y}$$
$$B_{\alpha s} = \frac{M}{y} \qquad (6)$$

Hence

$$B_{ss} = \frac{12EI}{\ell^3}$$
$$B_{\alpha s} = -\frac{6EI}{\ell^2}$$

To determine $B_{s\alpha}$ and $B_{\alpha\alpha}$, one may consider the tab as a beam with one end fixed and the other end constrained to move in a horizontal plane containing the two ends as shown in Figure 6.

Referring to Reference 1,

$$\alpha = \frac{M\ell}{4EI}$$
$$P = \frac{3M}{2\ell}$$

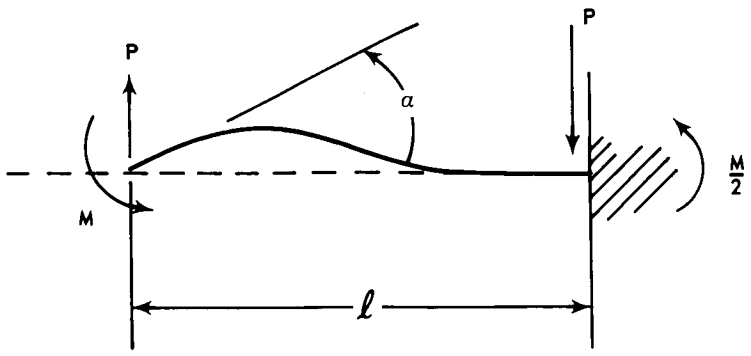

Figure 6 Tab Load Diagram

Following the convention used in Figure 3,

$$B_{s\alpha} = -\frac{P}{\alpha} = \frac{6EI}{\ell^2}$$

$$B_{\alpha\alpha} = \frac{4EI}{\ell}$$

where $I = \frac{bt^3}{12}$

For a numerical example, consider a flexure-mounted shoe seal with dimensions as shown in Figure 7.

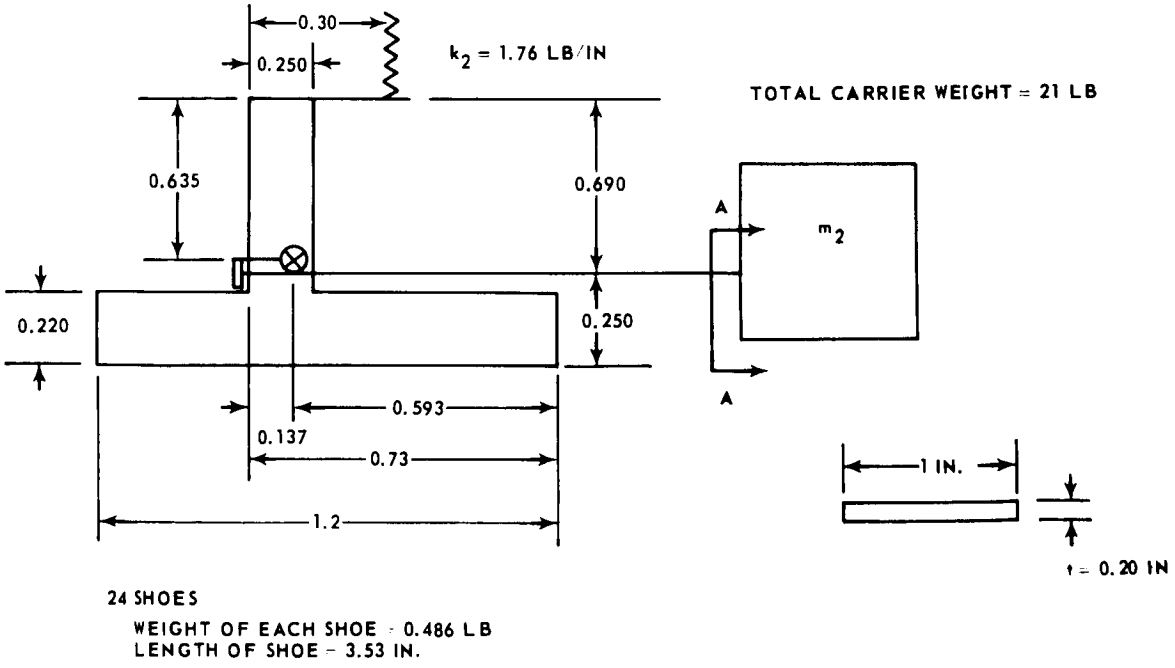

Figure 7 Dimensions of the Flexure-Mounted Shoe Seal

The masses of shoe and carrier are 0.00126 lb-sec^2/in. and 0.00226 lb-sec^2/in., respectively. The polar moment of inertia of the shoe about its centroid is 0.000185 in-lb-sec^2. The gas film stiffnesses are given as:

$$K_{ss} = 17{,}600 \text{ lb/in}^2$$

$$K_{s\alpha} = 3{,}500 \text{ lb/rad-in}$$

$$K_{\alpha s} = 2{,}048 \text{ in-lb/in}^2$$

$$K_{\alpha\alpha} = 1711 \text{ in-lb/rad-in}$$

The backup spring stiffness is given by

$$k_2 = 1.76 \text{ lb/in}$$

and

$$b_1 = 0.137 - 0.30 = -0.163 \text{ in}$$
$$b_2 = 0.137 \text{ in}$$

For the beam spring stiffnesses,

$$B_{ss} = \frac{12EI}{\ell^3} = \frac{12 \times 30 \times 10^6 \times 1 \times (.02)^3}{12 \times 1.2^3} = 138.5 \text{ lb/in}$$

$$B_{s\alpha} = -\frac{6EI}{\ell^2} = -83.0 \text{ lb/rad}$$

$$B_{\alpha s} = -\frac{6EI}{\ell^2} = -83.0 \text{ in-lb/in}$$

$$B_{\alpha\alpha} = \frac{4EI}{\ell} = +66.7 \text{ in-lb/rad}$$

The input data based on the above calculations can be listed as follows:

Analytical Symbol	Computer Symbol	Numerical Value	Units
m_1	SM1	0.00126	lb-sec^2/in
m_2	SM2	0.00226	lb-sec^2/in
I_p	FIP	0.000185	in-lb-sec^2
b	B	1.2	in
b_1	B1	-0.163	in
b_2	B2	0.137	in
ℓ	FL	3.53	in

K_{ss}	CKSS	17,600	lb/in^2
$K_{s\alpha}$	CKSA	3500	lb/rad-in
$K_{\alpha s}$	CKAS	2048	$in\text{-}lb/in^2$
$K_{\alpha\alpha}$	CKAA	1711	in-lb/rad-in
k_2	CK2	1.76	lb/in
δ	DELTA	1.0	in
ϵ	EPSLON	1.0	radian
B_{ss}	BSS	138.5	lb/in
$B_{s\alpha}$	BSA	-83.0	lb/rad
$B_{\alpha s}$	BAS	-83.0	in-lb/in
$B_{\alpha\alpha}$	BAA	66.7	in-lb/rad
N	W(NW)	2000-18000	rpm

The results from the computer are expressed in terms of $u_{1\delta}$, $u_{2\delta}$; $u_{1\epsilon}$; etc. These are given below and also plotted in Figures 8 to 10.

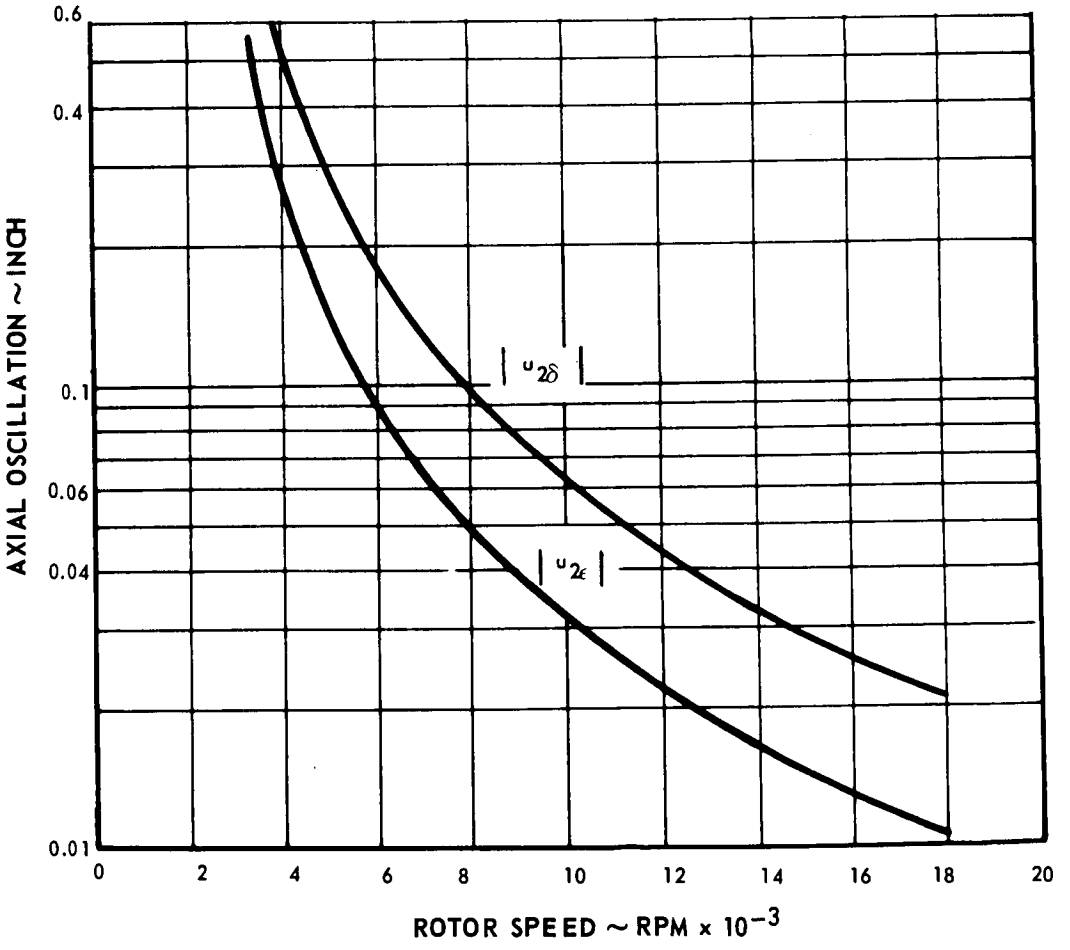

Figure 8 Axial Oscillation of the Hoop

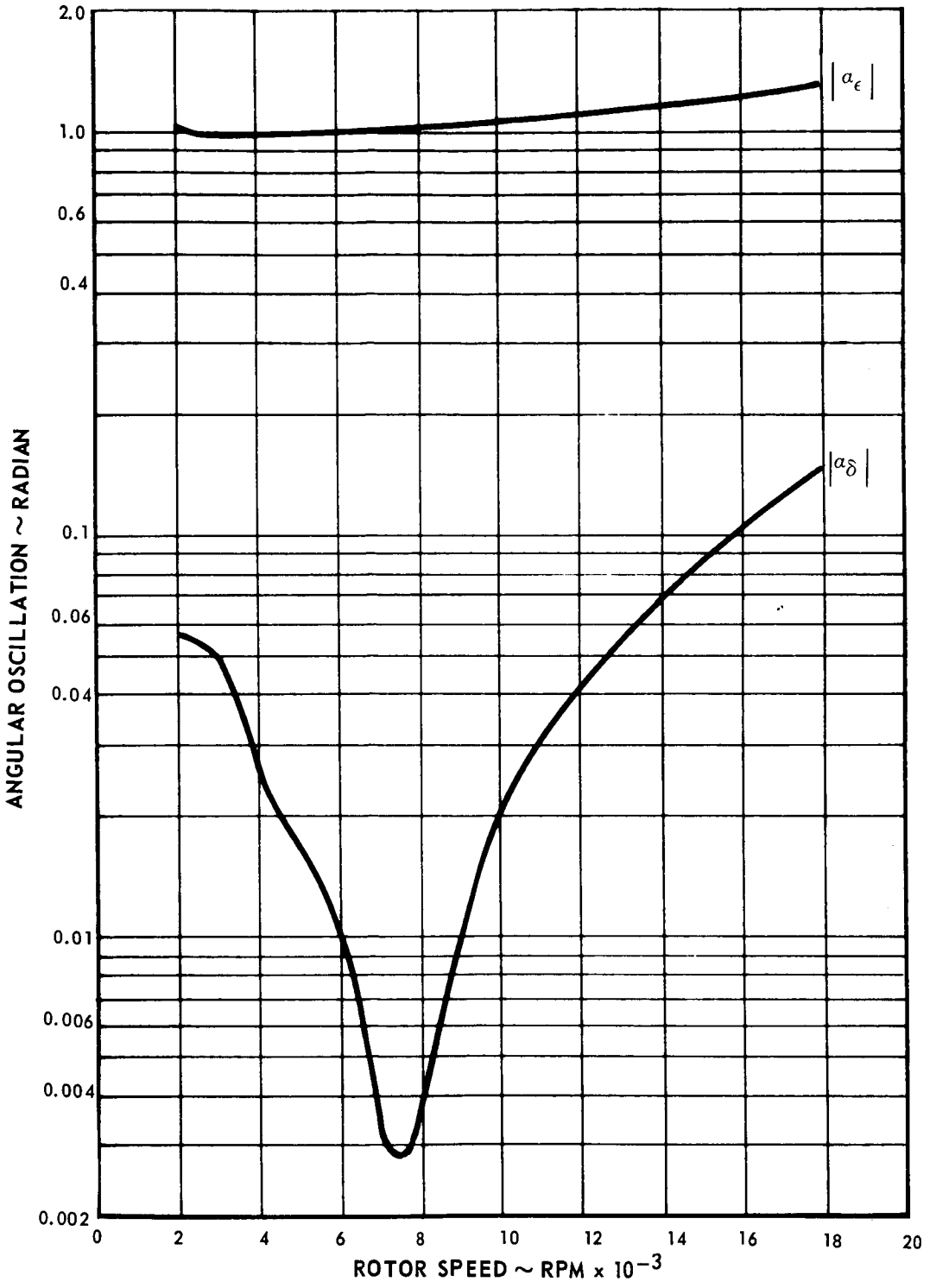

Figure 9 Angular Oscillation of the Shoe

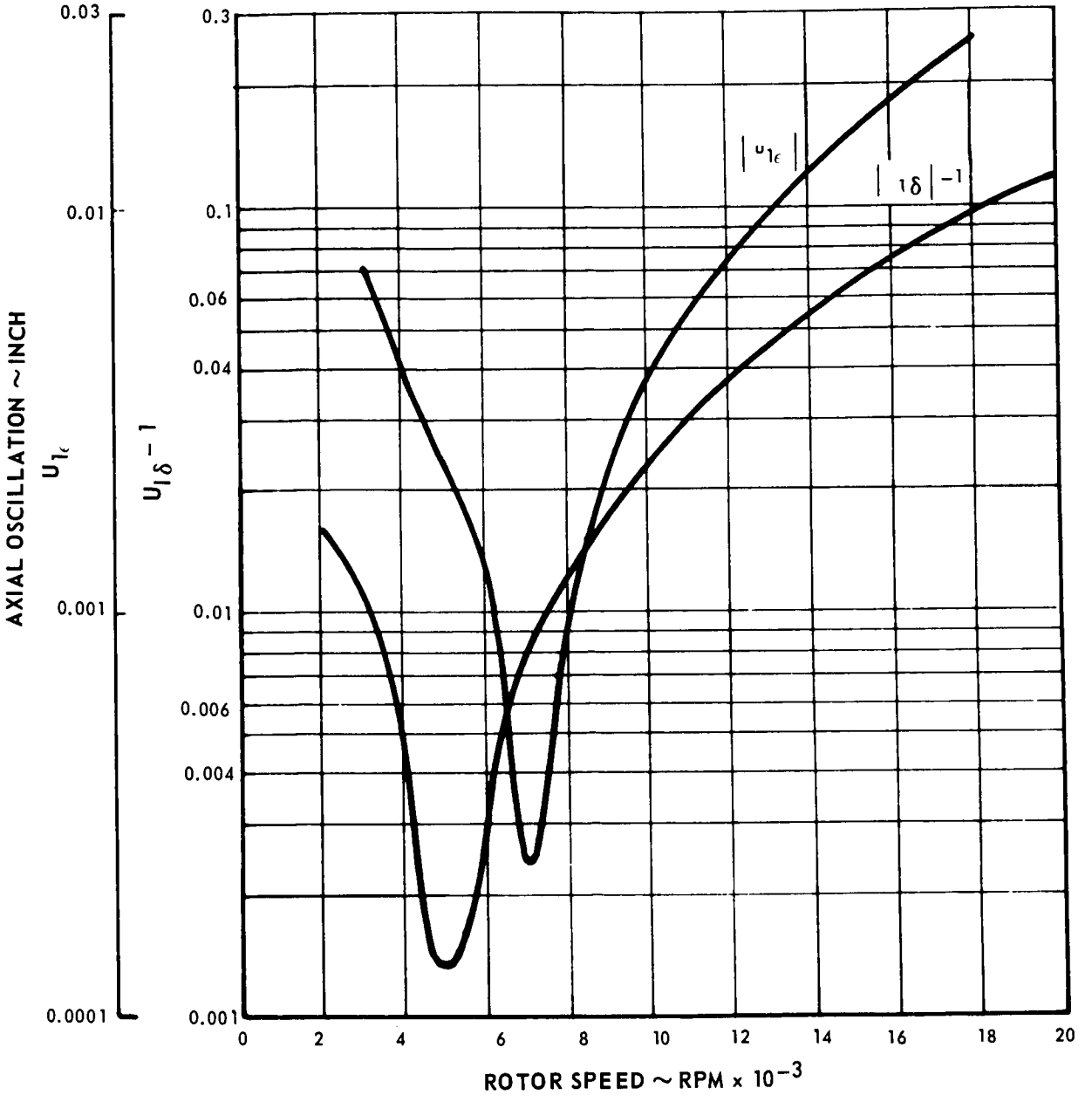

Figure 10 Axial Oscillation of the Shoe

If the seal shoe tracks the rotor surface exactly, and if the hoop is to be isolated from the shoe oscillations, then the following ideal conditions must prevail:

$$u_1 = \delta$$

$$a = \epsilon$$

$$u_2 = 0$$

To determine how closely the shoe tracks the rotor, it is most convenient to calculate $(u_1 - \delta)$, $(a - \epsilon)$, and u_2. Perfect tracking demands that all three quantities be zero.

Now using Equations 4, one obtains:

$$u_1 - \delta = \left|(u_{1\delta} - 1)\ \delta\right| + \left|u_{1\epsilon}\ \ \epsilon\, b\right|$$

$$u_2 = \left|u_{2\delta}\ \ \delta\right| + \left|u_{2\epsilon}\ \ \epsilon\, b\right|$$

$$a - \epsilon = \left|a_\delta\ \ \left(\frac{\delta}{b}\right)\right| + \left|(a_\epsilon - 1)\,\epsilon\right|$$

If for the wobbling mode, the rotor oscillation is given to be

$$\delta = 1.5 \times 10^{-3} \text{ inch}$$

$$\epsilon = 0.5 \times 10^{-3} \text{ radian}$$

Then Figures 8 and 9 give the following coefficients at cruise:

N	$u_{1\delta}$	$u_{2\delta}$	a_δ	$u_{1\epsilon}$	$u_{2\epsilon}$	a_ϵ
7100	1.0083	-0.125	0.003	0.000245	0.0635	1.007

Using Equations 6, one obtains at cruise

$$u_1 - \delta = 1.245 \times 10^{-5} \text{ inch}$$

$$u_2 = 2.25 \times 10^{-4} \text{ inch}$$

$$a - \epsilon = 7.25 \times 10^{-6} \text{ radian}$$

For the saddle mode, the rotor oscillation is given to be

$$\delta = 0.5 \times 10^{-3} \text{ inches}$$

$$\epsilon = 0.3 \times 10^{-3} \text{ rad.}$$

Figures 8 to 10 give the following coefficients at the cruise conditions:

2N	$u_{1\delta}$	$u_{2\delta}$	a_{δ}	$u_{1\epsilon}$	$u_{2\epsilon}$	a_{ϵ}
14,200	1.0568	-0.03	-0.0742	-0.0127	0.0157	1.08

Using Equations 6, one obtains at cruise

$$u_1 - \delta = 3.29 \times 10^{-5} \text{ inch}$$

$$u_2 = 2.05 \times 10^{-5} \text{ inch}$$

$$a - \epsilon = 5.48 \times 10^{-5} \text{ radian}$$

Superimposing the saddle and wobbling motion, the minium gas-film thickness at cruise becomes

$$h_{min} = h_o - (u_1 - \delta)_{wobble} - (u_1 - \delta)_{saddle} - \left[(a-\epsilon)_{wobble} + (a-\epsilon)_{saddle}\right] \times \frac{b}{2}$$

$$h_{min} = 0.001 - 1.245 \times 10^{-5} \times 3.29 \times 10^{-5} - (7.25 \times 10^{-6} + 5.48 \times 10^{-5}) \times 0.6 = 0.0009185 \text{ inch}$$

The corresponding motion of the hoop at cruise becomes

$$(u_2)_{cruise} = 2.25 \times 10^{-4} + 2.05 \times 10^{-5} = 0.000245 \text{ inch}$$

These figures indicate that at cruise, tracking will be satisfactory if the flexure-mounted shoe seal is used in the end-seal position.

2. FLEXIBLE SEAL RING VIBRATION

The vibration of a flexible seal ring supported by a gas film will be analyzed in this section. Two design concepts are under consideration, a thin-strip seal ring with OC diaphragm, and a semirigid one-piece seal ring; they are respectively shown in Figures 11 and 12.

a. OC DIAPHRAGM SEAL

It is seen from Figure 11 that the seal ring is separated from the rotor by a gas film, and is connected to the carrier by the OC diaphragm. Having a much higher rigidity than the seal ring, the carrier can vibrate only in a rigid-body fashion. On the other hand, the seal ring can vibrate both as an elastic ring and as a rigid body.

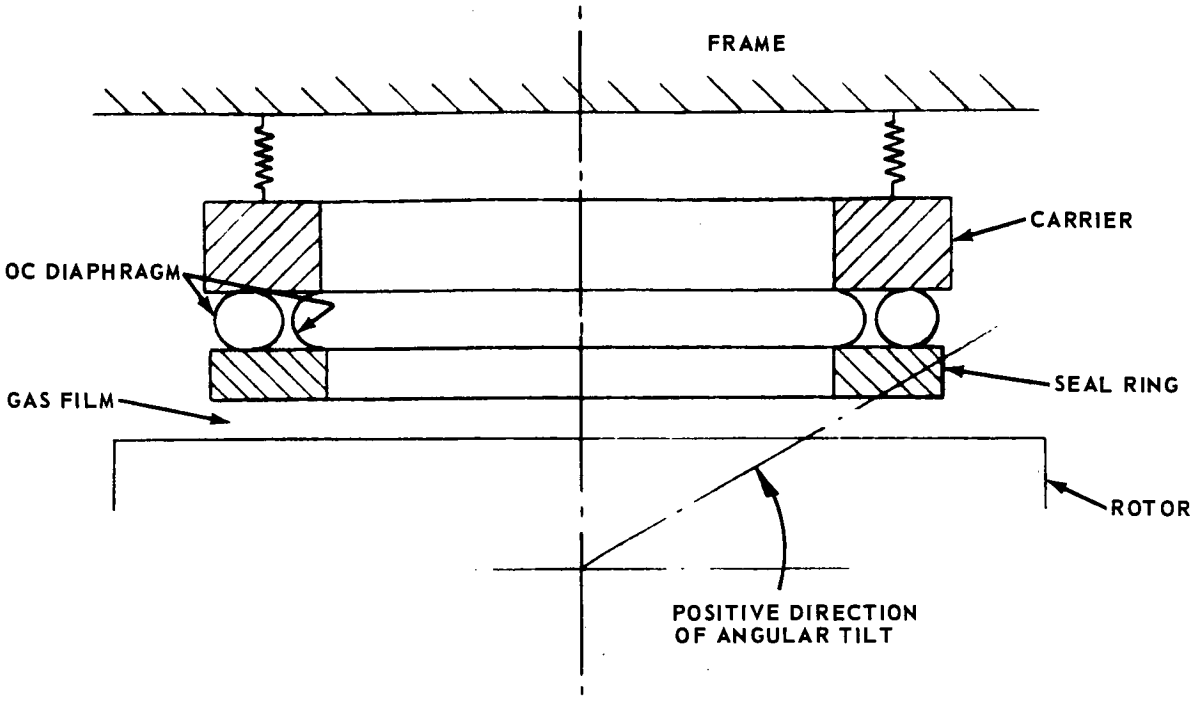

Figure 11 OC Diaphragm Thin-Strip Seal Concept

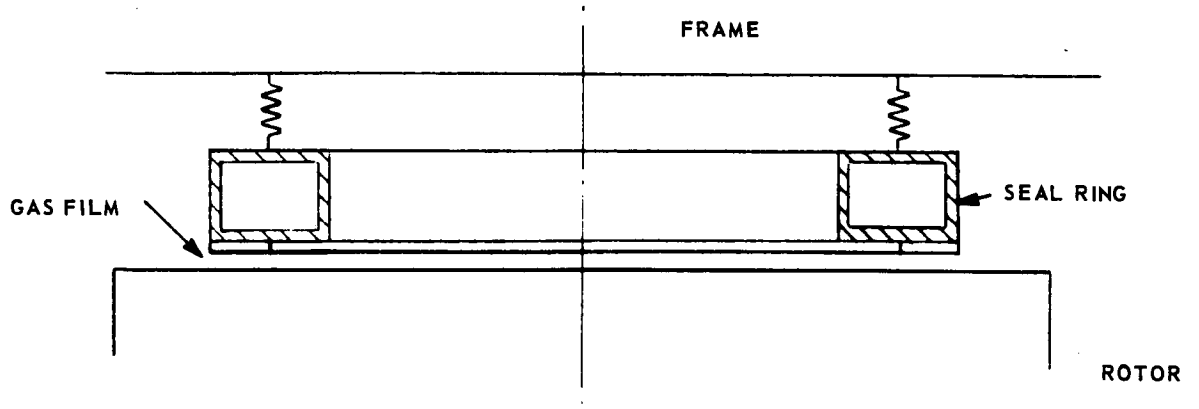

Figure 12 Semirigid One-Piece Seal Concept

Consider the situation that the rotor surface facing the seal ring may be distorted so that it is not perfectly flat. This can be classified into two categories: transverse (axial) distortion ($\delta = \Sigma_n \delta_n \cos n\theta$) and angular distortion ($\epsilon = \Sigma_n \epsilon_n \cos n\theta$). Since the rotor is rotating at an angular speed of ω_1, the deviation of the rotor surface from its perfectly flat position at any particular instant of time can be represented by

$$\delta = b \sum_n \delta_n \cos n(\theta + \omega t) \tag{7}$$

$$\epsilon = \sum_n \epsilon_n \cos n(\theta + \omega t) \tag{8}$$

Similarly, assume that the seal ring has initial transverse and angular deformation.

$$\eta = b \sum_n \eta_n \cos n\theta \tag{9}$$

$$\zeta = \sum_n \zeta_n \cos n\theta \tag{10}$$

respectively. The sign convention for all angular deformations is given in Figure 11.

(1) Elastic Ring Vibrations

Let y be the instantaneous local deflection of the seal ring. Now, for the purpose of illustration, let us set, for the time being, $\epsilon = \zeta = 0$. Then the film thickness is given by

$$h = h_m - y + \delta$$

where h_m is the nominal mean film thickness.

Note that y is the deflection from the perfectly flat position. Both y and δ are defined as positive in the downward direction, as shown in Figure 13.

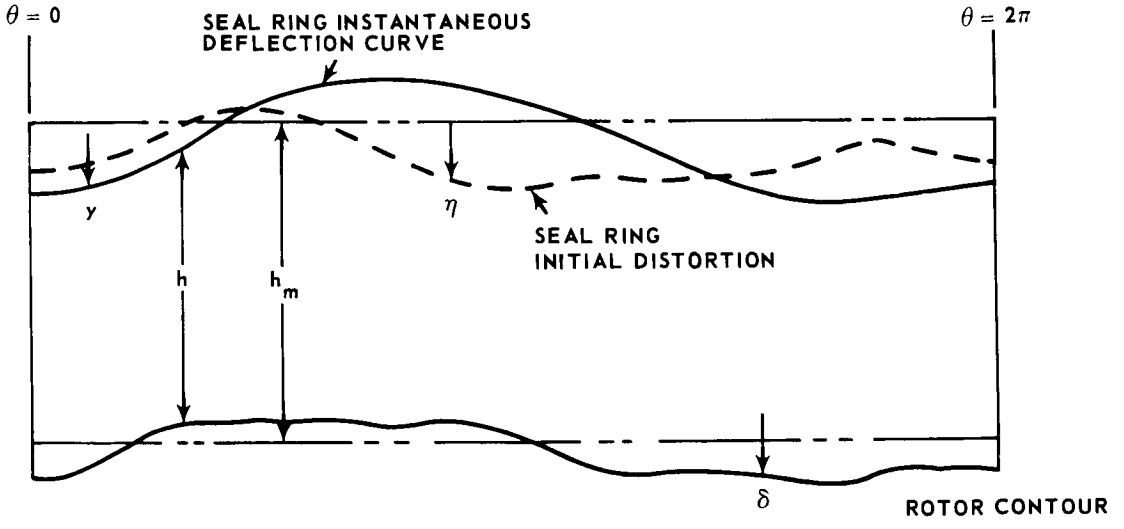

Figure 13 Rotor Contour, Seal-Ring Instantaneous Deflection, and Seal-Ring Initial Distortion

The free-body diagram of a differential element of the seal ring is shown in Figure 14. The forces and moments acting on this element are shear forces (V), the gas-film restoring force (q), the bending moment (M_b), the twisting moment (M_t), and the gas film's restoring moment ($q\alpha$). A double arrowhead denotes vector representation (right-hand system) of angular quantities. The equations of motion can be written as follows:

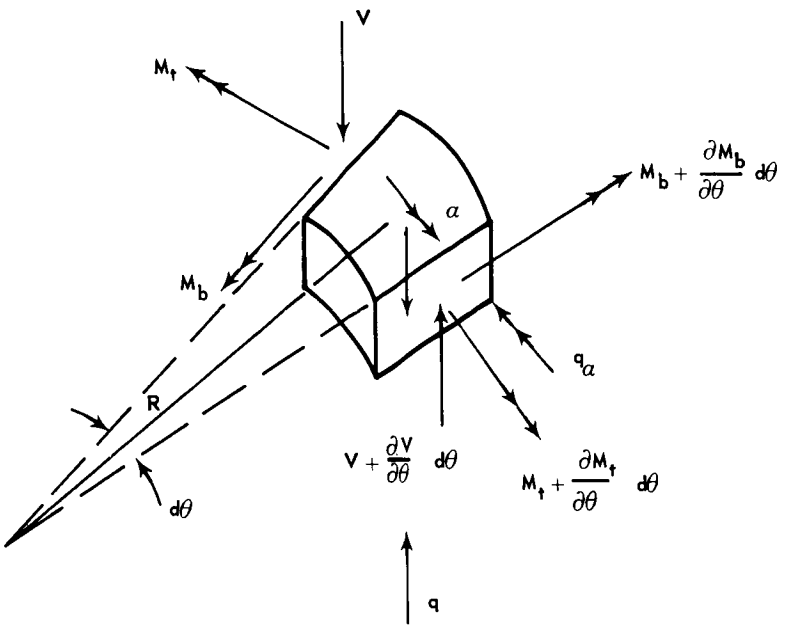

Figure 14 Free-Body Diagram of a Seal-Ring Segment

Transverse motion (linear translation):

$$-\frac{\partial V}{\partial \theta} d\theta - qRd\theta = (\rho ARd\theta)\,\ddot{y} \tag{11}$$

Radial equilibrium of all moments:

$$\frac{\partial M_b}{\partial \theta} d\theta - M_t d\theta - VRd\theta = I_{rr} \frac{\partial \ddot{y}}{\partial \theta} \frac{1}{R} \tag{12}$$

Tangential equilibrium of all moments:

$$M_b d\theta + \frac{\partial M_t}{\partial \theta} d\theta - q_\alpha Rd\theta = I_{tt}\,\ddot{\alpha} \tag{13}$$

where

ρ = density of the seal ring

A = cross-sectional area (ab) of the seal ring

M = mass of the differential element = $\rho ARd\theta$

$$I_{rr} = \frac{M(R^2 d\theta^2 + a^2)}{12} = \frac{Ma^2}{12} \qquad (14)$$

$$I_{tt} = \frac{M(a^2 + b^2)}{12}$$

q = restoring force per unit circumferential length

q_α = restoring moment for unit circumferential length

Before we express q and q_α in terms of displacement, let us define a set of spring constants for the gas film. K_{ss}, $K_{s\alpha}$, $K_{\alpha s}$ and $K_{\alpha\alpha}$, and a set of spring constants for the OC diaphragm, K_{ss}^*, $K_{s\alpha}^*$, $K_{\alpha s}^*$ and $K_{\alpha\alpha}^*$. Here, K_{ss} is the y-direction restoring force per unit circumferential length due to unit displacement in the y- direction, $K_{s\alpha}$ is the y-direction restoring force per unit circumferential length due to a unit angular displacement in the α-direction, and so on. The units are as follows:

K_{ss} and K_{ss}^* (lb/in/in)

$K_{s\alpha}$ and $K_{s\alpha}^*$ (lb/rad/in)

$K_{\alpha s}$ and $K_{\alpha s}^*$ (in.lb/in/in)

$K_{\alpha\alpha}$ and $K_{\alpha\alpha}^*$ (in.lb/rad/in)

When the seal ring is displaced from its perfectly flat position by an amount y, the resulting restoring forces from the gas film and the OC diaphragm are respectively $K_{ss}y$ and K_{ss}^*y. In the meantime, let us assume that the rotor deviates from its perfectly flat position by an amount δ (in the same direction as y). This will decrease the gas film restoring force $K_{ss}y$ by $K_{ss}\delta$. A similar argument can be applied to the angular displacement. Thus, we can write

$$\begin{aligned} q &= K_{ss}(y-\delta) + K_{ss}^* y + K_{s\alpha}(\alpha-\epsilon) + K_{\alpha\alpha}^* \alpha \\ q_\alpha &= K_{\alpha s}(y-\delta) + K_{\alpha s}^* y + K_{\alpha\alpha}(\alpha-\epsilon) + K_{\alpha\alpha}^* \alpha \end{aligned} \qquad (15)$$

At this stage of the analysis, it appears proper to obtain relationships between M_b, M_t, and the displacements y and α. Again, take a differential element of the seal ring with length $Rd\theta$. Because of angular (twisting) displacement α, the upper portion is compressed, while the lower portion is stretched (see Figure 15). At an arbitrary location z, the stretched length of the element is $(R + z\alpha)d\theta$. Hence, deformation = $z\alpha d\theta$

$$e_\alpha = \text{strain due to } \alpha = \frac{z\alpha d\theta}{Rd\theta} = \frac{z\alpha}{R}$$

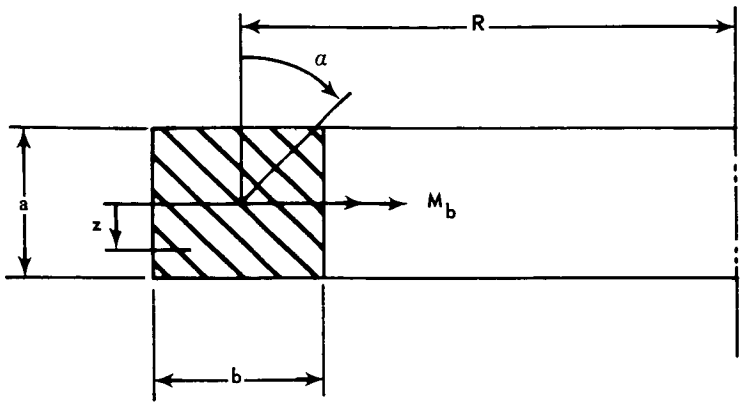

Figure 15 Bending of a Seal Segment Because of Angular Displacement α

We also know that strain due to transverse bending is

$$e_b = -\frac{z}{\bar{\rho}} = \text{strain due to transverse bending}$$

where $\bar{\rho}$ = radius of curvature $= \left(\frac{d^2y}{R^2 d\theta^2}\right)^{-1}$

Thus,

$$e = \text{total strain} = e_\alpha + e_b$$

$$= z\left(\frac{\alpha}{R} - \frac{1}{R^2}\frac{d^2y}{d\theta^2}\right)$$

The bending moment is readily obtained

$$M_b = -\int_{-a/2}^{a/2} Eezbdz = E\left(\frac{1}{R^2}\frac{d^2y}{d\theta^2} - \frac{\alpha}{R}\right)\int_{-a/2}^{a/2} z^2 bdz \qquad (16)$$

$$= EI\left(\frac{1}{R^2}\frac{d^2y}{d\theta^2} - \frac{\alpha}{R}\right)$$

where E = Young's Modulus

$$I = \text{area of moment of inertia} = \int_{-a/2}^{a/2} z^2 bdz$$

As for the twisting moment, we have the well-known formula:

$$M_t = GI_p \frac{\partial a}{R\partial\theta}$$

for a bar under torsion.

In the case of a circular ring, there is an additional term in the twisting moment. Consider a segment under torsion. The segment has linear displacement y and angular displacement a. It is convenient to use cylindrical coordinates r, θ, and z as shown in Figure 16. The shear stresses contributing towards the twisting moment are

$$\tau_{\theta r} = 2Ge_{\theta r} \qquad \tau_{\theta z} = 2Ge_{\theta z} \tag{17}$$

Also, the strain displacement relationships are (Reference 2, page 183).

$$e_{\theta r} = \frac{1}{2}\left(\frac{\partial u_r}{r\partial\theta} + \frac{\partial u_\theta}{\partial r} - \frac{u_\theta}{r}\right)$$

$$e_{\theta z} = \frac{1}{2}\left(\frac{\partial u_z}{r\partial\theta} + \frac{\partial u_\theta}{\partial z}\right) \tag{18}$$

where u_r, u_θ and u_z are the displacements in the respective direction. From Figure 16, it is clear that:

$$u_r = az$$

$$u_\theta = -\frac{\partial y}{R\partial\theta} z$$

$$u_z = y - a\bar{r}$$

Thus, from Equation 18,

$$e_{\theta r} = \frac{1}{2}\left(\frac{\partial a}{r\partial\theta} + \frac{1}{r}\frac{\partial y}{R\partial\theta}\right)z$$

$$e_{\theta z} = \frac{1}{2}\left(\frac{\partial y}{r\partial\theta} - \bar{r}\frac{\partial a}{r\partial\theta} - \frac{\partial y}{R\partial\theta}\right)$$

Substituting into Equations 17, we have

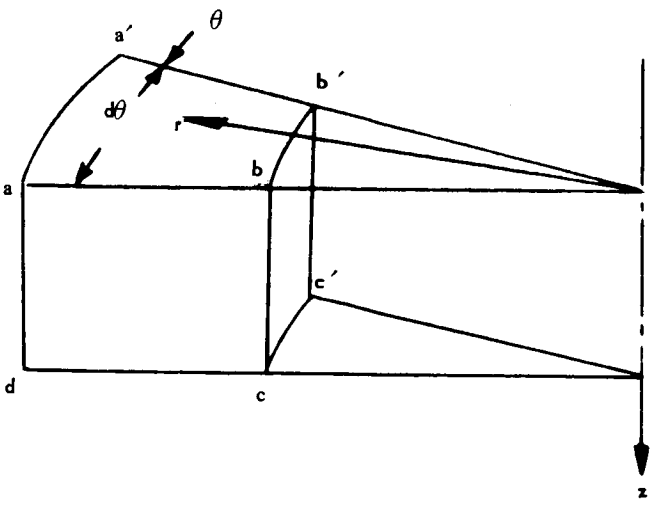

a. CYLINDRICAL COORDINATES

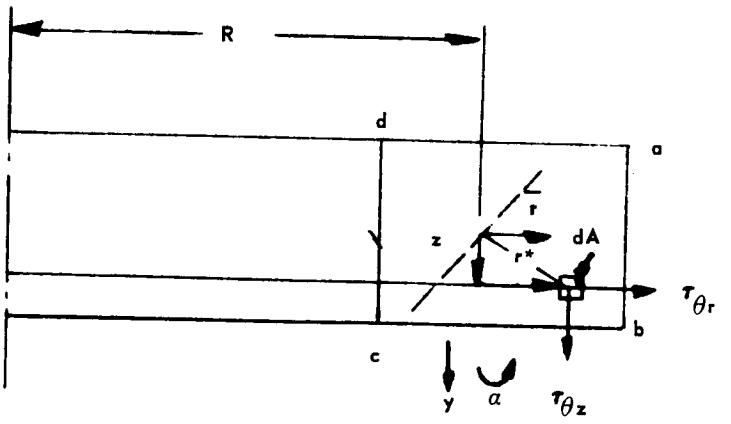

b. SHEAR STRESSES ON A DIFFERENTIAL ELEMENT dA

Figure 16 Seal-Ring Segment

$$\tau_{\theta r} = G\left(\frac{\partial a}{r\partial\theta} + \frac{1}{r}\frac{\partial y}{R\partial\theta}\right)z$$

$$\tau_{\theta z} = G\left(\frac{\partial y}{r\partial\theta} - \bar{r}\frac{\partial a}{r\partial\theta} - \frac{\partial y}{R\partial\theta}\right)$$

The twisting moment can be obtained by integrating the moments resulting from the shear stresses.

$$M_t = -\int_A \tau_{\theta z}\,\bar{r}\,dA + \int_A \tau_{\theta r}\,z\,dA$$

$$= -G\int_A\left[\frac{\partial y}{r\partial\theta} - \bar{r}\left(\frac{\partial a}{r\partial\theta}\right) - \frac{\partial y}{R\partial\theta}\right]\bar{r}\,dA + G\int_A\left(\frac{\partial a}{r\partial\theta} + \frac{1}{r}\frac{\partial y}{r\partial\theta}\right)z^2\,dA$$

Observe that from geometry,

$$r = R + \bar{r}$$

For the seal ring application, R is much greater than $\bar{r}$. Therefore, we can make the approximation that

$$\frac{1}{r} = \frac{1}{R+\bar{r}} = \frac{1}{R(1+\frac{\bar{r}}{R})} \cong \frac{1}{R}\left(1-\frac{\bar{r}}{R}\right)$$

Thus, the twisting moment is readily obtained,

$$M_t = -G\int_A\left[\frac{1}{R}\left(1-\frac{\bar{r}}{R}\right)\frac{\partial y}{\partial\theta} - \bar{r}\,\frac{1}{R}\left(1-\frac{\bar{r}}{R}\right)\frac{\partial a}{\partial\theta} - \frac{\partial y}{R\partial\theta}\right]\bar{r}\,dA$$

$$+G\int_A\left[\frac{1}{R}\left(1-\frac{\bar{r}}{R}\right)\frac{\partial a}{\partial\theta} + \frac{1}{R}\left(1-\frac{\bar{r}}{R}\right)\frac{\partial y}{R\partial\theta}\right]z^2\,dA$$

Using the condition that

$$\int_A \bar{r}\,dA = \int_A \bar{r}^3\,dA = 0$$

we obtain

$$M_t = G\frac{\partial y}{R^2\partial\theta}\int_A \bar{r}^2 dA + G\frac{\partial a}{R\partial\theta}\int_A \bar{r}^2 dA$$

$$+ G\frac{\partial a}{R\partial\theta}\int_A z^2 dA + G\frac{\partial y}{R^2\partial\theta}\int_A z^2 dA$$

$$= G\left(\frac{\partial y}{R^2\partial\theta} + \frac{\partial a}{R\partial\theta}\right)\int_A (\bar{r}^2 + z^2)dA \qquad (19)$$

$$= GI_p\left(\frac{\partial y}{R^2\partial\theta} + \frac{\partial a}{R\partial\theta}\right)$$

where

I_p = the polar moment of inertia

$$= \int_A (\bar{r}^2 + z^2)dA$$

The same expression for M_t is given in (Reference 3, page 451). It is important to note that when a rectangular cross section (thin-strip seal ring) or a hollow cross section (semirigid one-piece ring) is under consideration, I_p should be replaced by its equivalent polar moment of inertia calculated from the membrane analogy for a bar under torsion (see Reference 4). Thus, for a thin strip seal ring (Reference 4, page 15)

$$I_p = \frac{1}{3}ba^3$$

To summarize, the bending moment and the twisting moment are given by Equations 16 and 19 respectively. If the initial transverse and angular deformations of the ring, η and ζ, are taken into account, then the bending and twisting moments are

$$M_b = EI\left[\frac{1}{R^2}\frac{d^2(y-\eta)}{d\theta^2} - \frac{a-\zeta}{R}\right] \qquad (20)$$

$$M_t = GI_p\left[\frac{\partial(y-\eta)}{R^2\partial\theta} + \frac{\partial(a-\zeta)}{R\partial\theta}\right] \qquad (21)$$

We now proceed to simplify the equations of motion (11, 12, and 13), and express them in terms of y and a and their derivatives. Differentiating Equation 12 with respect to θ,

$$\frac{\partial^2 M_b}{\partial \theta^2} - \frac{\partial M_t}{\partial \theta} - R\frac{\partial V}{\partial \theta} = \frac{\rho A a^2 \partial^2 \ddot{y}}{12 \partial \theta^2} \tag{22}$$

Multiplying both sides of Equation 11 by $\frac{R}{d\theta}$,

$$-R\frac{\partial V}{\partial \theta} - qR^2 = \rho A R^2 \ddot{y} \tag{23}$$

Subtracting Equation 23 from Equation 22,

$$\frac{\partial^2 M_b}{\partial \theta^2} - \frac{\partial M_t}{\partial \theta} + qR^2 = \frac{\rho A a^2}{12}\frac{\partial^2 \ddot{y}}{\partial \theta^2} - \rho A R^2 \ddot{y} \tag{24}$$

Since

$$\frac{\partial^2 \ddot{y}}{\partial \theta^2} \sim \ddot{y}$$

Therefore

$$\frac{\frac{\rho A a^2}{12}\frac{\partial^2 \ddot{y}}{\partial \theta^2}}{\rho A R^2 \ddot{y}} \sim \frac{a^2}{R^2} \ll 1$$

where $\sim$ denotes "of the order of".

For seal ring applications, a is much smaller than R, so that $\frac{a}{R} \ll 1$. Thus, Equation 24 reduces to

$$\frac{\partial^2 M_b}{\partial \theta^2} - \frac{\partial M_t}{\partial \theta} + qR^2 + \rho A R^2 \ddot{y} = 0$$

Substituting Equations 14, 20, and 21 into the above equation, we have

$$EI\left[\frac{\partial^4 (y-\eta)}{R^2 \partial \theta^4} - \frac{\partial^2 (\alpha-\zeta)}{R \partial \theta^2}\right] - GI_p\left[\frac{\partial^2 (y-\eta)}{R^2 \partial \theta^2} + \frac{\partial^2 (\alpha-\zeta)}{R \partial \theta^2}\right]$$
$$+ R^2\left[(K_{ss}^* + K_{ss})\, y + (K_{s\alpha} + K_{s\alpha}^*)\,\alpha\right] + \rho A R^2 \ddot{y} \tag{25}$$
$$= R^2 (K_{ss}\,\delta + K_{s\alpha}\,\epsilon)$$

and substituting Equations 15, 20, and 21 into Equation 7, we have

Equations 25 and 26 become

$$\frac{\partial^2 a}{\partial\theta^2} - \Gamma_1 a - \Gamma_9 \frac{\partial^4 u}{\partial\theta^4} + \Gamma_{10} \frac{\partial^2 u}{\partial\theta^2} - \Gamma_2 u - \frac{1}{f_1^{\,2}} \frac{\partial^2 u}{\partial t^2}$$

$$= -\Gamma_3 \epsilon - \Gamma_4 \frac{\delta}{b} + \frac{\partial^2 \zeta}{\partial\theta^2} - \Gamma_9 \frac{\partial^4 \eta}{\partial\theta^4} + \Gamma_{10} \frac{\partial^2 \eta}{\partial\theta^2} \tag{29}$$

$$\frac{\partial^2 a}{\partial\theta^2} - \Gamma_5 a - \frac{1}{f_2^{\,2}} \frac{\partial^2 a}{\partial t^2} + \Gamma_{11} \frac{\partial^2 u}{\partial\theta^2} - \Gamma_6 u$$

$$= -\Gamma_7 \epsilon - \Gamma_8 \frac{\delta}{b} + \frac{\partial^2 \zeta}{\partial\theta^2} - \xi\zeta + \Gamma_{11} \frac{\partial^2 \eta}{\partial\theta^2} \tag{30}$$

Differential operators D_1 through D_4 are defined as follows:

$$D_1 = \frac{\partial^2}{\partial\theta^2} - \Gamma_1$$

$$D_2 = -\Gamma_9 \frac{\partial^4}{\partial\theta^4} + \Gamma_{10} \frac{\partial^2}{\partial\theta^2} - \Gamma_2 - \frac{1}{f_1^{\,2}} \frac{\partial^2}{\partial t^2}$$

$$D_3 = \frac{\partial^2}{\partial\theta^2} - \Gamma_5 - \frac{1}{f_2^{\,2}} \frac{\partial^2}{\partial t^2}$$

$$D_4 = \Gamma_{11} \frac{\partial^2}{\partial\theta^2} - \Gamma_6$$

Then we can write Equations 29 and 30 in the form,

$$D_1 a + D_2 u = -\Gamma_3 \epsilon - \Gamma_4 \frac{\delta}{b} + \frac{\partial^2 \zeta}{\partial\theta^2} - \Gamma_9 \frac{\partial^4 \eta}{\partial\theta^4} + \Gamma_{10} \frac{\partial^2 \eta}{\partial\theta^2} \tag{31}$$

and

$$D_3 a + D_4 u = -\Gamma_7 \epsilon - \Gamma_8 \frac{\delta}{b} + \frac{\partial^2 \zeta}{\partial\theta^2} - \xi\zeta + \Gamma_{11} \frac{\partial^2 \eta}{\partial\theta^2} \tag{32}$$

Apply D_4 on Equation 31 and D_2 on Equation 32 and subtract:

$$\frac{EI}{R}\left[\frac{\partial^2(y-\eta)}{R\partial\theta^2} - (\alpha-\zeta)\right] + \frac{GI_p}{R}\left[\frac{\partial^2(y-\eta)}{R\partial\theta^2} + \frac{\partial^2(\alpha-\zeta)}{\partial\theta^2}\right]$$
$$- R\left[(K_{\alpha\alpha} + K_{\alpha\alpha}^*)\,\alpha + (K_{\alpha s} + K_{\alpha s}^*)\,y - K_{\alpha\alpha}\epsilon - K_{\alpha s}\,\delta\right] \qquad (26)$$
$$= \frac{1}{12}\,\rho AR\,(a^2 + b^2)\,\ddot{\alpha}$$

Defining the following dimensionless quantities:

$$u = \frac{y}{b}$$

$$\xi = \frac{EI}{GI_p}$$

$$\Gamma_1 = \frac{(K_{s\alpha} + K_{s\alpha}^*)R^3}{EI + GI_p} \qquad \Gamma_7 = \frac{K_{\alpha\alpha}R^2}{GI_p}$$

$$\Gamma_2 = \frac{(K_{ss} + K_{ss}^*)\,bR^3}{EI + GI_p} \qquad \Gamma_8 = \frac{K_{\alpha s}\,bR^2}{GI_p}$$

$$\Gamma_3 = \frac{K_{s\alpha}R^3}{EI + GI_p} \qquad \Gamma_9 = \frac{b}{R}\,\frac{\xi}{1+\xi}$$

$$\Gamma_4 = \frac{K_{ss}\,bR^3}{EI + GI_p} \qquad \Gamma_{10} = \frac{b}{R}\,\frac{1}{1+\xi}$$

$$\Gamma_5 = \xi + \frac{(K_{\alpha\alpha} + K_{\alpha\alpha}^*)\,R^2}{GI_p} \qquad \Gamma_{11} = \frac{b}{R}\,(1+\xi) \qquad (27)$$

$$\Gamma_6 = \frac{(K_{\alpha s} + K_{\alpha s}^*)\,b\,R^2}{GI_p}$$

and two typical frequencies

$$f_1 = \left[\frac{EI + GI_p}{\rho AbR^3}\right]^{1/2}$$

$$f_2 = \left[\frac{12\,GI_p}{\rho AR^2\,(a^2 + b^2)}\right]^{1/2} \qquad (28)$$

$$
\begin{aligned}
&(D_1 D_4 - D_2 D_3)\, a \\
&= D_4 \left[-\Gamma_3 \epsilon - \Gamma_4 \frac{\delta}{b} + \frac{\partial^2 \zeta}{\partial \theta^2} + \left(-\Gamma_9 \frac{\partial^4}{\partial \theta^4} + \Gamma_{10} \frac{\partial^2}{\partial \theta^2} \right) \eta \right] \\
&\quad - D_2 \left[-\Gamma_7 \epsilon - \Gamma_8 \frac{\delta}{b} + \left(\frac{\partial^2}{\partial \theta^2} - \xi \right) \zeta + \Gamma_{11} \frac{\partial^2 \eta}{\partial \theta^2} \right]
\end{aligned} \tag{33}
$$

Similarly, apply D_3 on Equation 31 and D_1 on Equation 32 and subtract,

$$
\begin{aligned}
&(D_1 D_4 - D_2 D_3)\, u \\
&= D_1 \left[-\Gamma_7 \epsilon - \Gamma_8 \frac{\delta}{b} + \left(\frac{\partial^2}{\partial \theta^2} - \xi \right) \zeta + \Gamma_{11} \frac{\partial^2 \eta}{\partial \theta^2} \right] \\
&\quad - D_3 \left[-\Gamma_3 \epsilon - \Gamma_4 \frac{\delta}{b} + \frac{\partial^2 \zeta}{\partial \theta^2} + \left(-\Gamma_9 \frac{\partial^4}{\partial \theta^4} + \Gamma_{10} \frac{\partial^2}{\partial \theta^2} \right) \eta \right]
\end{aligned} \tag{34}
$$

Thus, we have obtained Equation 33 for a and Equation 34 for u. The right-hand sides of Equations 31 and 32 are the respective forcing functions for a-motion and u-motion. Note that in the left-hand sides of Equations 33 and 34 the differential operators are identical. This is because they are the results of solving coupled linear systems.

(2) Natural frequencies of flexible seal ring vibrations

To find the natural frequencies, we solve the homogeneous system

$$(D_1 D_4 - D_2 D_3)\, a = 0 \tag{35}$$

or

$$(D_1 D_4 - D_2 D_3)\, u = 0$$

Either equation will, of course, yield the same natural frequencies.

Expanding the differential operator in Equation 35 we obtain

$$
\begin{aligned}
&\left\{ -\frac{1}{f_1^2 f_2^2} \frac{\partial^4}{\partial t^4} + \left[\frac{1}{f_1^2} \left(\frac{\partial^2}{\partial \theta^2} - \Gamma_5 \right) + \frac{1}{f_2^2} \left(-\Gamma_9 \frac{\partial^4}{\partial \theta^4} + \Gamma_{10} \frac{\partial^2}{\partial \theta^2} - \Gamma_2 \right) \right] \frac{\partial^2}{\partial t^2} \right. \\
&\quad + \left[\Gamma_9 \frac{\partial^6}{\partial \theta^6} + (\Gamma_{11} - \Gamma_{10} - \Gamma_5 \Gamma_9) \frac{\partial^4}{\partial \theta^4} + (\Gamma_2 - \Gamma_6 + \Gamma_5 \Gamma_{10} - \Gamma_1 \Gamma_{11}) \frac{\partial^2}{\partial \theta^2} \right. \\
&\quad \left. \left. - (\Gamma_1 \Gamma_6 - \Gamma_2 \Gamma_5) \right] \right\} a = 0
\end{aligned} \tag{36}
$$

Because of the cross-differentiation terms in Equation 36, e.g. $\frac{1}{f_1^2}\frac{\partial^4}{\partial\theta^2\partial t^2}$, the method of separation of variables cannot be applied in general. However, since we are dealing with a ring geometry, the displacements must be continuous and periodic in θ. This strongly suggests that the θ dependence is of the form of $e^{in\theta}$. Thus, assume that

$$a = e^{in\theta}\, T(t), \quad n = 1, 2, 3 \ldots \tag{37}$$

Substituting Equation 37 into Equation 36 yields

$$\frac{d^4T}{dt^4} + \left[f_2^2 (n^2 + \Gamma_5) + f_1^2 (\Gamma_9 n^4 + \Gamma_{10} n^2 + \Gamma_2) \right] \frac{d^2T}{dt^2}$$

$$- f_1^2 f_2^2 \left[- \Gamma_9 n^6 + (\Gamma_{11} - \Gamma_{10} - \Gamma_5\Gamma_9) n^4 - (\Gamma_2 - \Gamma_6 + \Gamma_5\Gamma_{10} - \Gamma_1\Gamma_{11}) n^2 . \right. \tag{38}$$

$$\left. + (\Gamma_1\Gamma_6 - \Gamma_2\Gamma_5) \right] T = 0$$

For natural frequency calculations assume

$$T = C e^{i\nu t}$$

where C is an arbitrary constant, and ν, a frequency.

Then Equation 38 becomes

$$\nu^4 - P_1 \nu^2 + f_1^2 f_2^2 P_2 = 0 \tag{39}$$

where

$$\left.\begin{aligned} P_1 &= f_2^2 (n^2 + \Gamma_5) + f_1^2 (\Gamma_9 n^4 + \Gamma_{10} n^2 + \Gamma_2) \\ P_2 &= \Gamma_9 n^6 - (\Gamma_{11} - \Gamma_{10} - \Gamma_5\Gamma_9) n^4 \\ &\quad + (\Gamma_2 - \Gamma_6 + \Gamma_5\Gamma_{10} - \Gamma_1\Gamma_{11}) n^2 - (\Gamma_1\Gamma_6 - \Gamma_2\Gamma_5) \end{aligned}\right\} \tag{40}$$

Equation 39 is the characteristic equation. The number n = 1, 2, 3, ... represents different modes of vibration. For a given n, Equation 39 has two positive roots. Let them be denoted by ν_{n1} and ν_{n2}. They are given by

$$\nu_{n1} = \left[\frac{1}{2} P_1 + \frac{1}{2} (P_1^2 - 4 f_1^2 f_2^2 P_2)^{1/2} \right]^{1/2} \tag{41}$$

$$\nu_{n2} = \left[\frac{1}{2} P_1 - \frac{1}{2} (P_1^2 - 4 f_1^2 f_2^2 P_2)^{1/2} \right]^{1/2} \tag{42}$$

where ν_{n1} and ν_{n2} are the two natural frequencies at mode n.

(3) Dynamic Response

As indicated before, the right-hand sides of Equations 33 and 34 are the forcing functions. They consist of influences from the angular and transverse displacements of the rotor surface, ϵ and δ, and the angular and the transverse displacement of the seal ring, ζ and η. Let us re-write Equations 7 through 10.

$$\delta = b \sum_{n} \delta_n \cos n(\theta + \omega t) \tag{7a}$$

$$\epsilon = \sum_{n} \epsilon_n \cos n(\theta + \omega t) \tag{8a}$$

$$\eta = b \sum_{n} \eta_n \cos n\theta \tag{9a}$$

$$\zeta = \sum_{n} \zeta_n \cos n\theta \tag{10a}$$

Thus, it is clear that δ and ϵ give rise to dynamic forces, and η and ζ, to static (time-independent) forces.

Based on the above, we can assume that the dynamic response, a, and u, can be expressed in the form,

$$a = \sum_{n} \left[a_n \cos n(\theta + \omega t) + \beta_n \cos n\theta \right] \tag{43}$$

$$u = \sum_{n} \left[u_n \cos n(\theta + \omega t) + v_n \cos n\theta \right] \tag{44}$$

Here, a_n and u_n are the response to δ and ϵ. Let the seal ring have initial deformation, η and ζ. Then, through the action of the gas film, the seal ring will reach a static equilibrium position which is indicated by β_n and v_n.

Substituting Equations 7a, 8a, 9a, 10a, 39, and 40 into Equation 33, we obtain

$$\left\{ -\frac{1}{f_1^2 f_2^2} n^4 \omega^4 + \left[\frac{-1}{f_1^2} (n^2 + \Gamma_5) - \frac{1}{f_2^2} (\Gamma_9 n^4 + \Gamma_{10} n^2 + \Gamma_2) \right] (-n^2 \omega^2) \right.$$

$$- \Gamma_9 n^6 + (\Gamma_{11} - \Gamma_{10} - \Gamma_5 \Gamma_9) n^4 - (\Gamma_2 - \Gamma_6 + \Gamma_5 \Gamma_{10} - \Gamma_1 \Gamma_{11}) n^2 + \Gamma_1 \Gamma_6$$

$$\left. - \Gamma_2 \Gamma_5 \right\} a_n \cos n(\theta + \omega t) + \left\{ - \Gamma_9 n^6 + (\Gamma_{11} - \Gamma_{10} - \Gamma_5 \Gamma_9) n^4 - (\Gamma_2 - \Gamma_6 \right.$$

$$\left. + \Gamma_5 \Gamma_{10} - \Gamma_1 \Gamma_{11}) n^2 + \Gamma_1 \Gamma_6 - \Gamma_2 \Gamma_5 \right\} \beta_n \cos n\theta - \left\{ (\Gamma_3 Q_1 + \Gamma_7 Q_2) \epsilon_n \right.$$

$$\left. + (\Gamma_4 Q_1 + \Gamma_8 Q_2) \delta_n \right\} \cos n(\theta + \omega t) - \left\{ [n^2 Q_1 + (n^2 + \xi) Q_{20}] \zeta_n + [(\Gamma_9 n^4 \right.$$

$$\left. + \Gamma_{10} n^2) Q_1 + n^2 \Gamma_{11} Q_{20}] \eta_n \right\} \cos n\theta = 0$$

where

$$Q_1 = \Gamma_{11} n^2 + \Gamma_6$$

$$Q_2 = -\Gamma_9 n^4 - \Gamma_{10} n^2 - \Gamma_2 + \frac{n^2 \omega^2}{f_1^{\,2}}$$

$$Q_{20} = \Gamma_9 n^4 - \Gamma_{10} n^2 - \Gamma_2$$

Since $\cos n\theta$ and $\cos n(\theta + \omega t)$ are two independent functions, their coefficients must be equal to zero separately.

$$\Delta_n a_n = (\Gamma_3 Q_1 + \Gamma_7 Q_2)\,\epsilon_n + (\Gamma_4 Q_1 + \Gamma_8 Q_2)\,\delta_n \tag{45}$$

$$-P_2 \beta_n = [n^2 Q_1 + (n^2 + \zeta)\,Q_{20}]\,\zeta_n + [(\Gamma_9 n^4 + \Gamma_{10} n^2)\,Q_1 + n^2 \Gamma_{11} Q_{20}]\,\eta_n \tag{46}$$

where

$$\Delta_n = -\frac{n^4 \omega^4}{f_1^{\,2} f_2^{\,2}} + \frac{n^2 \omega^2}{f_1^{\,2} f_2^{\,2}}\,P_1 - P_2 \tag{47}$$

P_1 and P_2 are defined in Equation 40.

Similarly, from Equation 34 we obtain

$$\Delta_n u_n = (\Gamma_7 Q_3 + \Gamma_3 Q_4)\,\epsilon_n + (\Gamma_8 Q_3 + \Gamma_4 Q_4)\,\delta_n \tag{48}$$

$$-P_2 v_n = [(n^2 + \zeta)\,Q_3 + n^2 Q_{40}]\,\zeta_n + [n^2\,\Gamma_{11} Q_3 + (\Gamma_9 n^4 + \Gamma_{10} n^2)\,Q_{40}]\,\eta_n \tag{49}$$

where

$$Q_3 = n^2 + \Gamma_1$$

$$Q_4 = -n^2 - \Gamma_5 + \frac{n^2 \omega^2}{f_2^{\,2}}$$

$$Q_{40} = -n^2 - \Gamma_5$$

We can rewrite Equations 45, 46, 48, and 49 in the form of influence coefficients,

$$a_n = C_{A1} \epsilon_n + C_{A2} \delta_n$$

$$\beta_n = C_{B1} \zeta_n + C_{B2} \eta_n \tag{50}$$

$$u_n = C_{u1}\epsilon_n + C_{u2}\delta_n$$

$$v_n = C_{v1}\zeta_n + C_{v2}\eta_n$$

C_{A1}, C_{A2}, etc. are the influence coefficients. They are defined as follows:

$$\left.\begin{aligned}
C_{A1} &= \frac{\Gamma_3 Q_1 + \Gamma_7 Q_2}{\Delta_n} \\
C_{A2} &= \frac{\Gamma_4 Q_1 + \Gamma_8 Q_2}{\Delta_n} \\
C_{B1} &= \frac{n^2 Q_1 + (n^2 + \xi) Q_{20}}{-P_2} \\
C_{B2} &= \frac{(\Gamma_9 n^4 + \Gamma_{10} n^2) Q_1 + n^2 \Gamma_{11} Q_{20}}{-P_2} \\
C_{u1} &= \frac{\Gamma_7 Q_3 + \Gamma_3 Q_4}{\Delta_n} \\
C_{u2} &= \frac{\Gamma_8 Q_3 + \Gamma_4 Q_4}{\Delta_n} \\
C_{v1} &= \frac{(n^2 + \xi) Q_3 + n^2 Q_{40}}{-P_2} \\
C_{v2} &= \frac{n^2 \Gamma_{11} Q_3 + (\Gamma_9 n^4 + \Gamma_{10} n^2) Q_{40}}{-P_2}
\end{aligned}\right\} \quad (51)$$

It is to be noted that different modes of vibratory response can be calculated separately. For example, for n = 1, we can calculate a_1, β_1 etc, for n = 2 we can calculate a_2 β_2, etc. Then the total response will be $a = a_1 + a_2 \ldots, \beta = \beta_1 + \beta_2 \ldots$ etc.

These computations have been included in the computer program discussed in Appendix A.

(4) Rigid-Body Vibrations

In the last section, the vibration of a flexible seal ring was considered. There, the carrier was unable to vibrate as an elastic body, and was assumed to be fixed in space.

Now let us consider the rigid-body vibration of the carrier and the seal ring. It can be visualized that the carrier-ring system can have two linear degrees of freedom x_1 and x_2, and two angular degrees of freedom γ_1 and γ_2. Because of axial symmetry, the other two angular degrees of freedom with axes of rotation perpendicular to those of γ_1 and γ_2 need not be considered, as they would yield identical results.

(5) Rectilinear Vibrations

The lumped-parameter model of the carrier-ring system is shown in Figure 17.

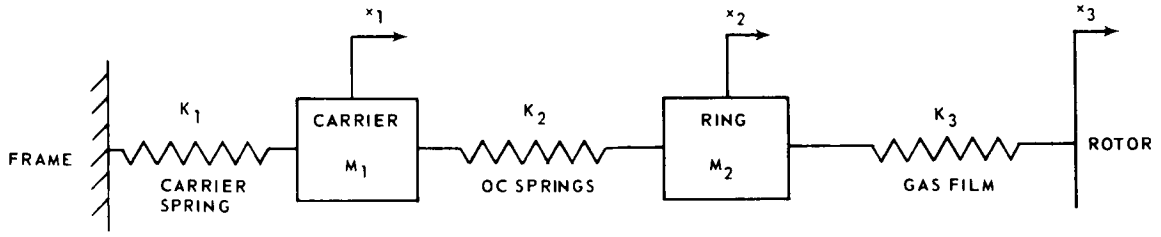

Figure 17 Lumped-Parameter Model of the Carrier-Ring System

The displacements of the carrier and the ring are represented by x_1 and x_2, while the motion of the rotor is prescribed by x_3. This system was considered in Reference 5, and an explicit solution was obtained in page V-5, Reference 1. Results are summarized as follows:

The natural frequency is given by the roots of the characteristic equation,

$$\nu^4 - A_1\nu^2 + A_2 = 0 \tag{52}$$

where

$$A_1 = \frac{K_1 + K_2}{m_1} + \frac{K_2 + K_3}{m_2}$$

$$A_2 = \frac{K_1K_2 + K_2K_3 + K_3K_1}{m_1m_2} \tag{53}$$

Thus

$$\nu_1 = \left[\frac{A_1 + \sqrt{A_1^2 - 4A_2}}{2}\right]^{1/2}$$

$$\nu_2 = \left[\frac{A_1 - \sqrt{A_1^2 - 4A_2}}{2}\right]^{1/2} \tag{54}$$

The motions of the carrier and the ring, x_1 and x_2, expressed relative to the rotor imposed motion, x_3, are obtained as:

$$\frac{x_1}{x_3} = \frac{K_2 K_3}{\left[-m_1\omega^2 + K_1 + K_2\right]\left[-m_2\omega^2 + K_2 + K_3 - \dfrac{K_2^2}{-m_1\omega^2 + K_1 + K_2}\right]} \tag{55}$$

$$\frac{x_2}{x_3} = \frac{K_3}{-m_2\omega^2 + K_2 + K_3 - \dfrac{K_2^2}{-m_1\omega^2 + K_1 + K_2}} \tag{56}$$

where ω is the frequency of the imposed motion x_3.

Equations 55 and 56 represent the response of the undamped vibration. They would become very large as ω approaches ν_1 or ν_2.

Although the natural frequencies ν_1 and ν_2 can be easily calculated from Equation 54, let us obtain a simplified expression from which we will be able to predict how to increase (or decrease) the natural frequency by varying certain parameters.

In seal ring application, it is known that the gas film is much stiffer than the OC diaphragm, which is much stiffer than the carrier spring. Thus,

$$K_3 \gg K_2 \gg K_1 \tag{57}$$

Also, we have

$$m_1 \gtrapprox m_2 \tag{58}$$

Therefore, from Equation 53

$$A_1 \cong \frac{K_3}{m_2}$$

$$A_2 \cong \frac{K_2 K_3}{m_1 m_2} \tag{59}$$

Observe that

$$\sqrt{A_1^2 - 4A_2} \cong \left[\left(\frac{K_3}{m_2}\right)^2 - 4\frac{K_2 K_3}{m_1 m_2}\right]^{1/2}$$

$$= \frac{K_3}{m_2}\left[1-4\left(\frac{K_2}{K_3}\right)\left(\frac{m_2}{m_1}\right)\right]^{1/2} \qquad (60)$$

$$= \frac{K_3}{m_2}\left[1-2\left(\frac{K_2}{K_3}\right)\left(\frac{m_2}{m_1}\right)\right]$$

We have used the binomial expansion and the condition that

$$\frac{K_2}{K_3}\,\frac{m_2}{m_1} \ll 1$$

Using Equations 59 and 60, the natural frequencies given by Equation 54 are reduced to

$$\nu_1 = \left[\frac{K_3}{m_2}\right]^{1/2}$$

$$\nu_2 = \left[\frac{K_2}{m_1}\right]^{1/2} \qquad (61)$$

Thus, we see that under the conditions of Equations 57 and 58, the system is decoupled into two subsystems, namely, the seal ring supported by the gas film, and the carrier supported by the OC diaphragm. In the numerical example, it will be shown that since the gas film is very stiff, ν_1 is much higher than the rotating speed of the rotor. The lower mode ν_2, however, is quite close to the idling speed (based on an estimated $m_1 = 30$ pounds and $K_2 = 17100$ lb/in). Efforts should be made according to Equation 61 to vary either m_1 or K_2 (or both) so that ν_2 is sufficiently different from the speed range of the rotor. For actual calculation of the natural frequencies, the exact expressions of Equation 54 should be used.

(6) Angular Vibration

The two angular degrees of freedom are described by γ_1 and γ_2 as shown in Figure 18. The axes of γ_1 and γ_2 are perpendicular to the paper. Suppose that the rotor has a face runout with half amplitude C_3. Then

$$\gamma_3 = C_3 \cos \omega t$$

where ω = rotational speed of rotor

The equations of motion are

$$I_1\ddot{\gamma}_1 + K_{\gamma 1}\gamma_1 + K_{\gamma 2}(\gamma_1 - \gamma_2) = 0 \qquad (62)$$

$$I_2\ddot{\gamma}_2 + K_{\gamma 2}(\gamma_2 - \gamma_1) + K_{\gamma 3}\gamma_2 = K_{\gamma 3}\gamma_3 \qquad (63)$$

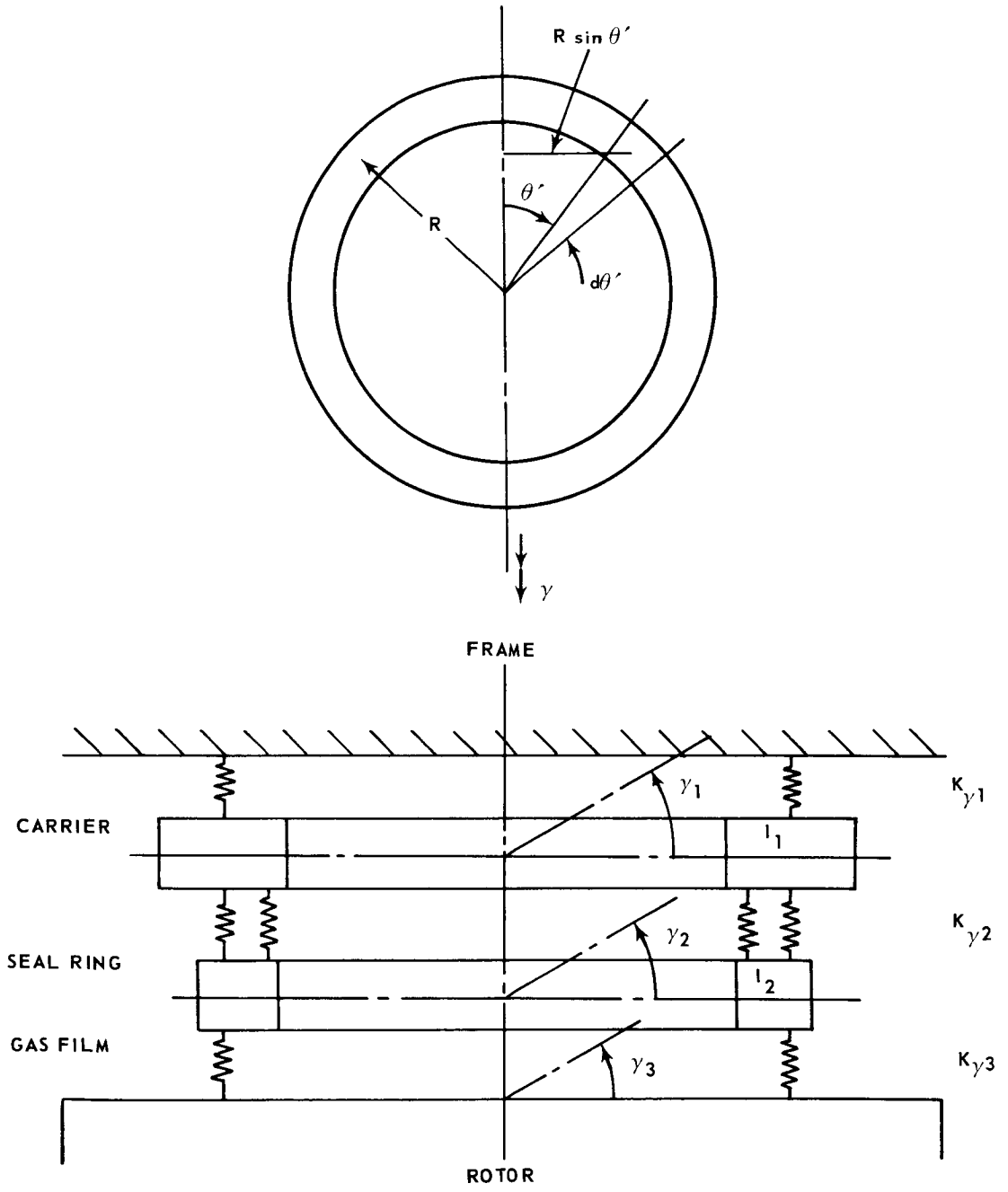

Figure 18 Schematic for Mathematical Model of Angular Vibration

$$\left.\begin{aligned} &\text{where } I_1 = \frac{1}{2} m_1 R^2 = \text{moment of inertia of the carrier} \\ &\text{and } I_2 = \frac{1}{2} m_2 R^2 = \text{moment of inertia of the seal ring} \end{aligned}\right\} \quad (64)$$

To obtain the spring constant $K_{\gamma 3}$, consider the restoring moment of the gas film due to a rigid body rotation γ.

$$\text{Moment from } K_{ss} = \int_0^{2\pi} (\gamma R \sin\theta')(K_{ss} R d\theta') R \sin\theta'$$

$$= R^3 K_{ss} \gamma \int_0^{2\pi} \sin^2 \theta' d\theta'$$

$$= \pi R^3 K_{ss} \gamma$$

$$\text{Moment from } K_{\alpha\alpha} = \int_0^{2\pi} (\gamma \sin\theta')(K_{\alpha\alpha} R\, d\theta') \sin\theta'$$

$$= R K_{\alpha\alpha} \gamma \int_0^{2\pi} \sin^2\theta' d\theta'$$

$$= \pi R K_{\alpha\alpha} \gamma$$

There is no contribution from $K_{s\alpha}$ and $K_{\alpha s}$. Thus,

$$\text{Restoring Moment} = (\pi R^3 K_{ss} + \pi R K_{\alpha\alpha})\gamma$$

The spring constant is by definition:

$$K_{\gamma 3} = \frac{\text{Restoring Moment}}{\gamma} = \pi R^3 K_{ss} + \pi R K_{\alpha\alpha}$$

Similarly,

$$K_{\gamma 2} = \pi R^3 K_{ss}^* + \pi R K_{\alpha\alpha}^*$$

But, because $R^2 K_{ss} \gg K_{\alpha\alpha}$

and $R^2 K_{ss}^* \gg K_{\alpha\alpha}^*$

we obtain

$$K_{\gamma 3} = \pi R^3 K_{ss}$$

$$K_{\gamma 2} = \pi R^3 K_{ss}^* \qquad (65)$$

Equations 62 and 63 can be solved by assuming that

$$\gamma_1 = C_1 \cos \omega t$$
$$\gamma_2 = C_2 \cos \omega t$$

Using the same procedure in solving the rectilinear vibration, it is found that the natural frequency will satisfy

$$\nu^4 - B_1 \nu^2 + B_2 = 0 \tag{66}$$

where $B_1 = \dfrac{K_{\gamma 1} + K_{\gamma 2}}{I_1} + \dfrac{K_{\gamma 2} + K_{\gamma 3}}{I_2}$

$$B_2 = \frac{K_{\gamma 1}K_{\gamma 2} + K_{\gamma 2}K_{\gamma 3} + K_{\gamma 3}K_{\gamma 1}}{I_1 I_2}$$

and the dynamic responses of the carrier and seal ring with respect to unit rotor input can be respectively expressed by

$$\frac{C_1}{C_3} = \frac{K_{\gamma 2}K_{\gamma 3}}{\left(-I_1\omega^2 + K_{\gamma 1} + K_{\gamma 2}\right)\left(-I_2\omega^2 + K_{\gamma 2} + K_{\gamma 3} - \dfrac{K_{\gamma 2}^{\,2}}{I_1\omega^2 + K_{\gamma 1} + K_{\gamma 2}}\right)} \tag{67}$$

$$\frac{C_2}{C_3} = \frac{K_{\gamma 3}}{-I_2\omega^2 + K_{\gamma 2} + K_{\gamma 3} - \dfrac{K_{\gamma 2}^{\,2}}{-I_1\omega^2 + K_{\gamma 1} + K_{\gamma 2}}} \tag{68}$$

From Equation 64 and 65 we can write

$$B_1 = \frac{\pi R^3 (\bar{K}_{ss} + K_{ss}^*)}{\frac{1}{2} m_1 R^2} + \frac{\pi R^3 (K_{ss}^* + K_{ss})}{\frac{1}{2} m_2 R^2}$$

$$= \frac{2\pi R (\bar{K}_{ss} + K_{ss}^*)}{m_1} + \frac{2\pi R (K_{ss}^* + K_{ss})}{m_2}$$

It is easily identified that

$$2\pi R\, \bar{K}_{ss} = K_1$$

$$2\pi R\, K_{ss}^* = K_2$$

$$2\pi R\, K_{ss} = K_3$$

Hence,

$$B_1 = \frac{K_1 + K_2}{m_1} + \frac{K_2 + K_3}{m_2} = A_1$$

Similarly,

$$B_2 = \frac{K_1 K_2 + K_2 K_3 + K_3 K_1}{m_1 m_2} = A_2$$

Thus, Equations 52 and 66 are identical. The natural frequencies of the angular vibration are the same as those of the rectilinear vibration. Utilizing the identities

$$\frac{K_{\gamma 2}}{-I_1 \omega^2 + K_{\gamma 1} + K_{\gamma 2}} = \frac{\pi R^3 K_{ss}^*}{-\frac{1}{2} m_1 R^2 \omega^2 + \pi R^3 \bar{K}_{ss} + \pi R^3 K_{ss}^*}$$

$$= \frac{2\pi R K_{ss}^*}{-m_1 \omega^2 + 2\pi R \bar{K}_{ss} + 2\pi R K_{ss}^*}$$

$$= \frac{K_2}{-m_1 \omega^2 + K_1 + K_2}, \text{ etc.}$$

We can easily see that the dynamic response C_1/C_3 and C_2/C_3 as given by Equations 67 and 68 reduce to Equations 55 and 56 respectively.

Thus, the rigid-body vibrations of the carrier-ring system can be predicted by considering either the rectilinear vibration or the angular vibration, because they are completely analogous to each other. The flexible seal tracking analysis computer program discussed in Appendix A includes calculations of the natural frequencies and the dynamic response.

b. SEMIRIGID SEAL RING

The analysis and computer program for vibration of the thin-strip seal ring in the OC diaphragm seal are quite general. They can be easily applied to the semirigid seal ring's vibration if the following quantities are properly identified: K_{ss}^*, $K_{s\alpha}^*$, $K_{\alpha s}^*$, $K_{\alpha\alpha}^*$, I, I_p, A and I_{tt}.

The seal ring is again supported by a gas film on one side, but on the other side there is no OC diaphragm. A mechanical spring is used instead to hold the ring down. Let the spring constant of this spring be K_1, then

$$K_{ss}^* = \frac{K_1}{2\pi R}$$

$$K_{s\alpha}^* = K_{\alpha s}^* = K_{\alpha\alpha}^* = 0$$

Consider the case that the cross section of the ring is a rectangular hollow section with uniform thickness. Then, the moment of inertia and the equivalent polar moment of inertia are

$$I = \frac{1}{12}(b_1 a_1^{\,3} - b_2 a^3{}_2)$$

$$I_p = \frac{4\bar{A}^2 t}{\ell}$$

where

a_1, b_1 = outer dimension of rectangular ring

a_2, b_2 = inner dimension of rectangular ring

t = thickness (uniform)

ℓ = linear length = $2a_1 + 2b_1 - 4t$

$\bar{A}$ = area = $(a_1 - t)(b_1 - t)$

See Reference 4, page 27.

Let

$A_1 = a_1 b_1$

$A_2 = a_2 b_2$

$M_1 = \rho A_1 R d\theta$ = mass of an element with area A_1 and thickness $Rd\theta$

$M_2 = \rho A_2 R d\theta$ = mass of an element with area A_2 and thickness $Rd\theta$

Then, from Equation 14,

$$I_{tt} = \frac{M_1(a_1^{\,2} + b_1^{\,2})}{12} - \frac{M_2(a_2^{\,2} + b_2^{\,2})}{12}$$

and A = net area = $a_1 b_1 - a_2 b_2$

c. GAS FILM CROSS-COUPLING STIFFNESS EVALUATION

(1) Derivation of Angular and Cross-Coupling Stiffness for Single Pad Configuration

In studying the tracking capability of the seal ring with respect to the rotor face distortions, it is convenient to approximate the behavior of the air film by two direct stiffnesses, K_{ss}, $K_{\alpha\alpha}$ and two cross-coupling stiffnesses, $K_{s\alpha}$, $K_{\alpha s}$. Referring to a typical single pad seal as shown in Figure 19, these stiffnesses may be mathematically defined as follows:

$$K_{ss} = -\frac{\partial W}{\partial h}$$

$$= K'_{ss}\ b\ (\text{lb/in})/\text{in}$$

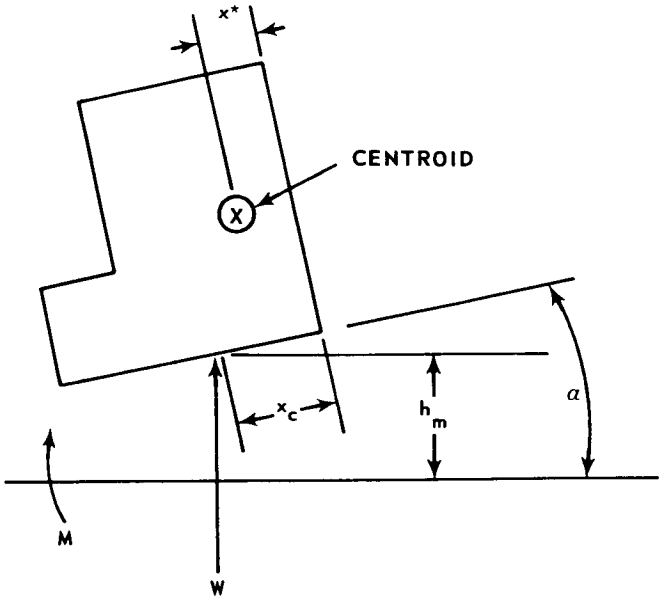

Figure 19 Typical Single-Pad Seal

where W is the upward restoring force per unit circumferential length, h_m the mean film thickness, K_{ss} the axial stiffness per unit sealing area, and b the seal width. K_{ss} can be found in the tabulated performance data.

$$K_{\alpha\alpha} = \frac{M}{\alpha}$$

$$= \frac{\partial[W(x_c - x^*)]}{\partial \alpha}$$

$$= (x_c - x^*)\frac{\partial W}{\partial \alpha} + W\frac{\partial x_c}{\partial \alpha} \text{ in-lb/in/rad}$$

M is the counterclockwise restoring moment about the centroid of the cross section per unit circumferential length, α the clockwise tilting angle, x_c the coordinate of the center of pressure, and x^* the centroid coordinate.

Similarly

$$K_{s\alpha} = \frac{\partial W}{\partial \alpha} \text{ lb/in/rad}$$

$$K_{\alpha s} = -\frac{\partial M}{\partial h} = -\left[\frac{\partial W}{\partial h}(x_c - x^*) + W\frac{\partial x_c}{\partial h}\right]$$

$$= K'_{ss}\, b\,(x_c - x^*) - W\frac{\partial x_c}{\partial h} \text{ (in-lb/in)/in}$$

$$W = K_{ss}(-\Delta h) + K_{s\alpha}\Delta\alpha$$

$$M = K_{\alpha s}(-\Delta h) + K_{\alpha\alpha}\Delta\alpha$$

In calculating the derivatives, one may make the following approximations.

$$\frac{\partial W}{\partial \alpha} = \frac{W|_{\alpha=\Delta\alpha} - W|_{\alpha=-\Delta\alpha}}{2\Delta\alpha}$$

$$\frac{\partial x_c}{\partial \alpha} = \frac{x_c|_{\alpha=\Delta\alpha} - x_c|_{\alpha=-\Delta\alpha}}{2\Delta\alpha}$$

$$\frac{\partial x_c}{\partial h} = \frac{x_c|_{h=h_o+\Delta h} - x_c|_{h=h_o-\Delta h}}{2\Delta h}$$

The equations derived above are for direct use in the tracking analyses of the single-pad semi-rigid seal configuration.

(2) Derivation of Angular and Cross-Coupling Stiffness for Double Pad Configurations

For the double pad, the expression of the film stiffnesses is more complex than for the single pad.

Referring to Figure 20,

$$K_{ss} = -\frac{\partial W}{\partial h}$$

$$= \left(-\frac{\partial W_1}{\partial h}\right) + \left(-\frac{\partial W_2}{\partial h}\right)$$

$$= (K'_{ss})_1 \, b_1 + (K'_{ss})_2 \, b_2 \quad \text{(lb/in)/in}$$

and

$$K_{\alpha\alpha} = \frac{\partial W}{\partial \alpha} (x_c - x^*) + W \frac{\partial x_c}{\partial \alpha}$$

where $x_c = \dfrac{W_2 (b - x_2) + W_1 x_1}{W_1 + W_2}$ and $\dfrac{\partial W}{\partial \alpha} = \dfrac{\partial W_1}{\partial \alpha} + \dfrac{\partial W_2}{\partial \alpha}$

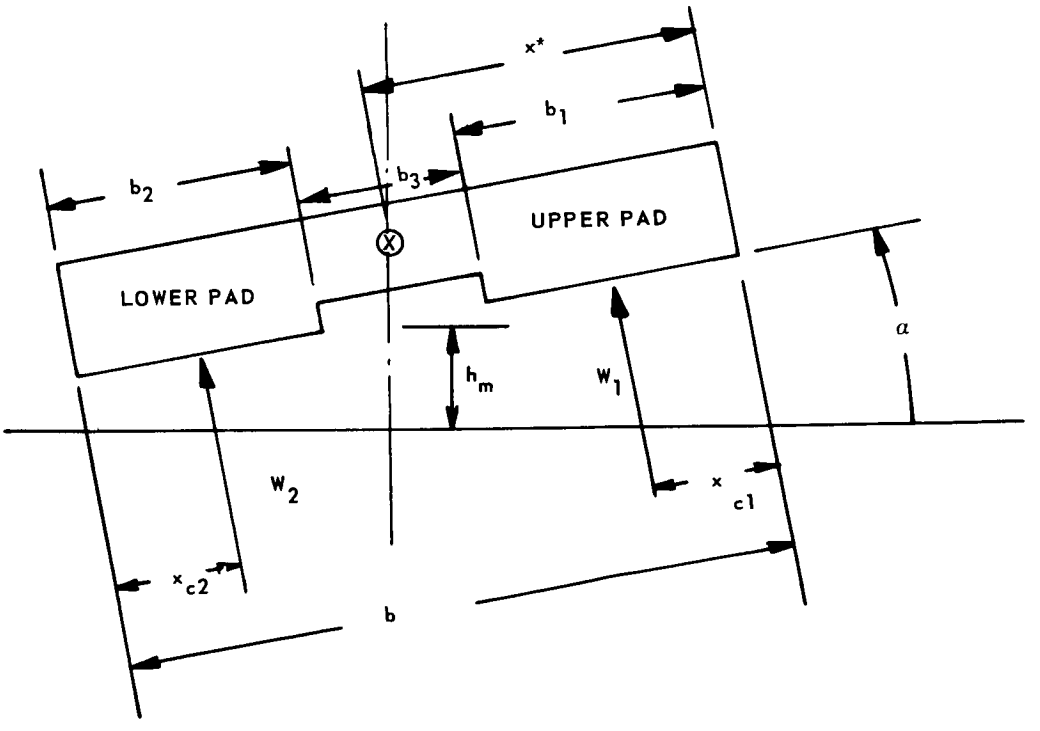

Figure 20 Gas-Film Forces on a Double Pad

Similarly, the cross-coupling coefficients are defined by

$$K_{s\alpha} = \frac{\partial W}{\partial \alpha}$$

$$K_{\alpha s} = \frac{-\partial M}{\partial h} = -\left[\frac{\partial W}{\partial h}(x_c - x^*) + W\frac{\partial x_c}{\partial h}\right]$$

$$= \left[(K'_{ss})_1 b_1 + (K'_{ss})_2 b_2\right](x_c - x^*) - W\frac{\partial x_c}{\partial h}$$

where

$$\frac{\partial W}{\partial \alpha} = \left(\frac{W_1^+ - W_1^-}{2\Delta\alpha}\right) + \left(\frac{W_2^+ - W_2^-}{2\Delta\alpha}\right)$$

$$\frac{\partial x_c}{\partial \alpha} = \frac{1}{2\Delta\alpha}\left[\frac{W_2^+(b - x_2^+) + W_1^+ x_1^+}{W_1^+ + W_2^-}\right] - \left[\frac{W_2^-(b - x_2^-) + W_1^- x_1^-}{W_1^- + W_2^-}\right]$$

$$\frac{\partial x_c}{\partial h} = \frac{1}{2\Delta h}\left[\frac{W_2(b_2 - x_2) + W_1 x_1}{W_1 + W_2}\right]_{h = h_o + \Delta h}$$

$$- \frac{1}{2\Delta h}\left[\frac{W_2(b_2 - x_2) + W_1 x_1}{W_1 + W_2}\right]_{h = h_o + \Delta h}$$

and

$$W_2^+ = W_2 \;\Big|\; \alpha = \Delta\alpha,\quad h_2 = h - \frac{\Delta\alpha}{2}(b_3 + b_2)$$

$$W_2^- = W_2 \;\Big|\; \alpha = \Delta\alpha,\quad h_2 = h + \frac{\Delta\alpha}{2}(b_3 + b_2)$$

$$W_1^+ = W_1 \;\Big|\; \alpha = \Delta\alpha,\quad h_1 = h + \frac{\Delta\alpha}{2}(b_3 + b_1)$$

$$W_1^- = W_1 \;\Big|\; \alpha = \Delta\alpha,\quad h_1 = h - \frac{\Delta\alpha}{2}(b_3 + b_1)$$

$$x_2^+ = x_2 \quad \left| \begin{array}{l} a = \Delta a \\ h_2 = h - \dfrac{\Delta a}{2}\ (b_3 + b_2) \end{array} \right.$$

$$x_2^- = x_2 \quad \left| \begin{array}{l} a = \Delta a \\ h_2 = h + \dfrac{\Delta a}{2}\ (b_3 + b_2) \end{array} \right.$$

$$x_1^+ = x_1 \quad \left| \begin{array}{l} a = \Delta a \\ h_1 = h + \dfrac{\Delta a}{2}\ (b_3 + b_1) \end{array} \right.$$

$$x_1^- = x_1 \quad \left| \begin{array}{l} a = \Delta a \\ h_1 = h - \dfrac{\Delta a}{2}\ (b_3 + b_1) \end{array} \right.$$

Since the calculation of these stiffnesses for the double pad from the basic performance data is quite involved, hand computation is not feasible and a computer subroutine has been prepared. This subroutine is used in conjunction with the tracking computer program and requires the basic primary seal data described in Appendix A.

region at the concave side of the upper diaphragm spring. The air passes through the seal gap to the vent recess and proceeds through the gap between the springs to holes drilled in the carrier. The holes vent directly to the low-pressure area.

The lower seal pad is fed through radial holes in the carrier and the O-diaphragm air pocket formed by the lower diaphragm spring. Air enters the individual pads through 154 feed holes 1/16 of an inch in diameter, and is distributed over the Rayleigh recess by means of a 1/16 wide and 0.030 inch deep groove located at the leading edge of the recess.

Secondary sealing between the carrier and the stationary support structure is accomplished through the use of a piston ring. The design details of the piston ring are the same as those of the one-sided floated-shoe seal discussed in Reference 6, page 23. The piston ring's outer surface includes a step bearing configuration which helps to establish an air film between piston ring and seal support.

2. SEAL CONSTRUCTION

The OC diaphragm end seal consists of a seal ring supported on O- and C-diaphragm springs. The springs are welded on one side to the seal ring and on the other to the carrier.

The carrier in turn is preloaded by virtue of 24 helical coil preload springs which rest on riveted spring guides on the carrier and seal support. The carrier is centered and held in place by four antirotation pins similar to the ones employed in the one-sided floated-shoe design (Reference 6, page 7). The seal support separates the high-pressure from the low-pressure chamber and provides the secondary sealing surface for the piston ring to ride on.

The O-and C-diaphragm springs are of toroidal and semitoroidal cross section. These springs are to be fabricated or formed from 0.006-inch stock and welded into separate subassemblies with the use of spring supports for the O- and C-spring sections, respectively. The subassemblies are then electron-beam welded onto the seal ring and carrier. To avoid prestressing and distortion of the spring diaphragms, and to contain the diaphragm subassemblies prior to final welding onto the seal ring and carrier, the spring assemblies are rabbeted onto the seal ring with light clearance fits.

The seal face is hard coated with aluminum oxide (Linde LC-1C) or Chrome Carbide (Linde LW-5), whichever is more suitable for the etching and/or machining of the spiral groove and Rayleigh recess profiles. The major seal parts are made of Inconel X750.

3. OC DIAPHRAGM STATIC SEAL PERFORMANCE AT CRUISE, IDLE, AND TAKE-OFF

a. STATIC PERFORMANCE CURVES

The static seal performance curves for the double-pad OC diaphragm end seal are shown in Figures 21 through 23. The arbitrarily arrived at limits based upon the cruise static performance curves appear to apply also to the take-off and idle conditions: in order not to fall below 70 percent of the design film thickness, the tilt angle should be restricted to 0.0007 radians for positive and 0.0004 radians for negative tilt.

C. OC DIAPHRAGM THIN-STRIP SEAL

The final configuration of the OC diaphragm end seal is shown in Figure 1. Both the end and interstage configurations of the OC diaphragm seal are similar in design and materials. Because the OC diaphragm interstage seal will not be investigated under Task II, the discussion below is directed primarily toward the end seal configuration. With minor exceptions, however, it also applies to the interstage seal.

1. PRINCIPLE OF OPERATION

The OC diaphragm end seal shown in Figure 1 is a flexibly supported, flexible ring seal operating on the principle of the controlled seal gap. The gap control is achieved through the incorporation of gas bearing profiles in the seal face which are designed to yield gaps or air films between the stationary seal rings and runner.

The end and interstage seals have been designed for operation at steady-state cruise, idle, and take-off conditions as simulated on a Pratt & Whitney Aircraft test rig. Air-film thickness is a function of speed, air temperature, and air pressure. Thus, at standstill, the seal is in direct contact with the runner and the film thickness is zero. The film thickness develops as the engine reaches the design operating conditions. In order to secure safe starts and stops, the seal ring and runner faces are hardcoated. The hard coats are selected on the basis of their compatibility of operation up to 1400 degrees Fahrenheit, mutual material compatibility, and resistance to wear.

As shown in Figure 1, the seal ring surface is divided into two bearing lands, the two lands being separated by a recessed vent groove. The outer land, henceforth referred to as the upper pad, serves the function of a bearing-seal combination. This pad is designed to maintain a small air film to separate the high from the low air-pressure areas, providing at the same time sufficient stiffness for proper seal operation at dynamic conditions. The upper pad consists of a hybrid combination of a spiral groove pattern and inherently compensated orifices. The spiral groove pattern provides hydrodynamic lift-off capability at conditions when the compressor discharge pressure is low, as at idle, start-up, and shutdown. The inherently compensated orifices enhance the rquired stiffness characteristics during operation.

The inner land, (or the lower pad) serves as a bearing. This pad includes Rayleigh shrouded-step recesses, the function of which is to strengthen the film-generating performance characteristics of the seal. It provides, in combination with the upper pad, the high angular stiffness which is a prerequisite to proper operation of a flexible seal ring and early liftoff capabilities.

The high-pressure areas, as shown in Figure 1, are located on the outside of the seal's outer surface and within the O-diaphragm spring. The low-pressure areas are on the seal's inner surface and on the inner surface and right side of the carrier.

During operation, the upper pad is fed with high-pressure air through the air gap at its outer edge and through the line of 360 orifices connecting the air-film gap to the high-pressure

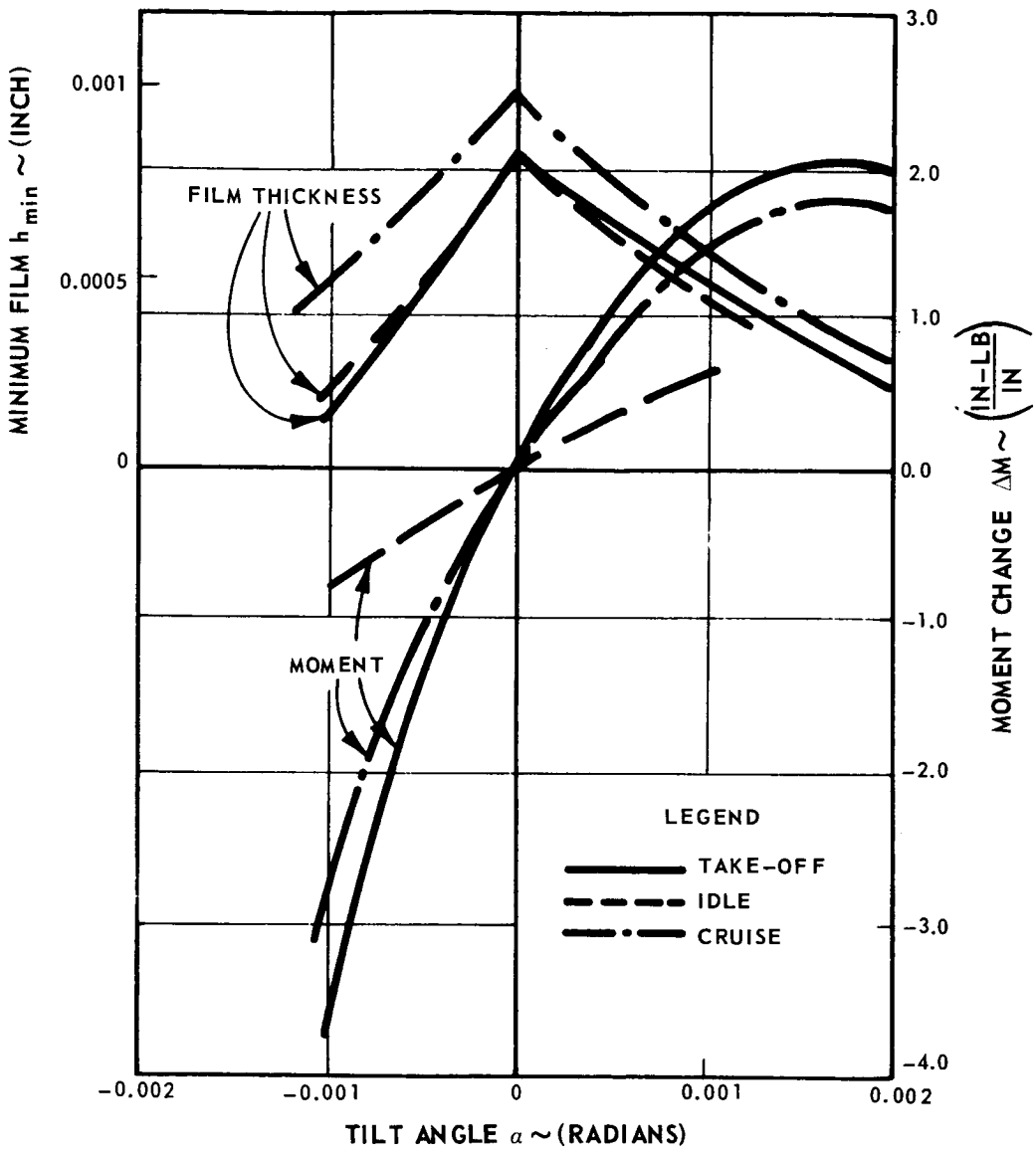

Figure 21 OC Diaphragm End Seal Restoring Moment and Minimum Film Thickness

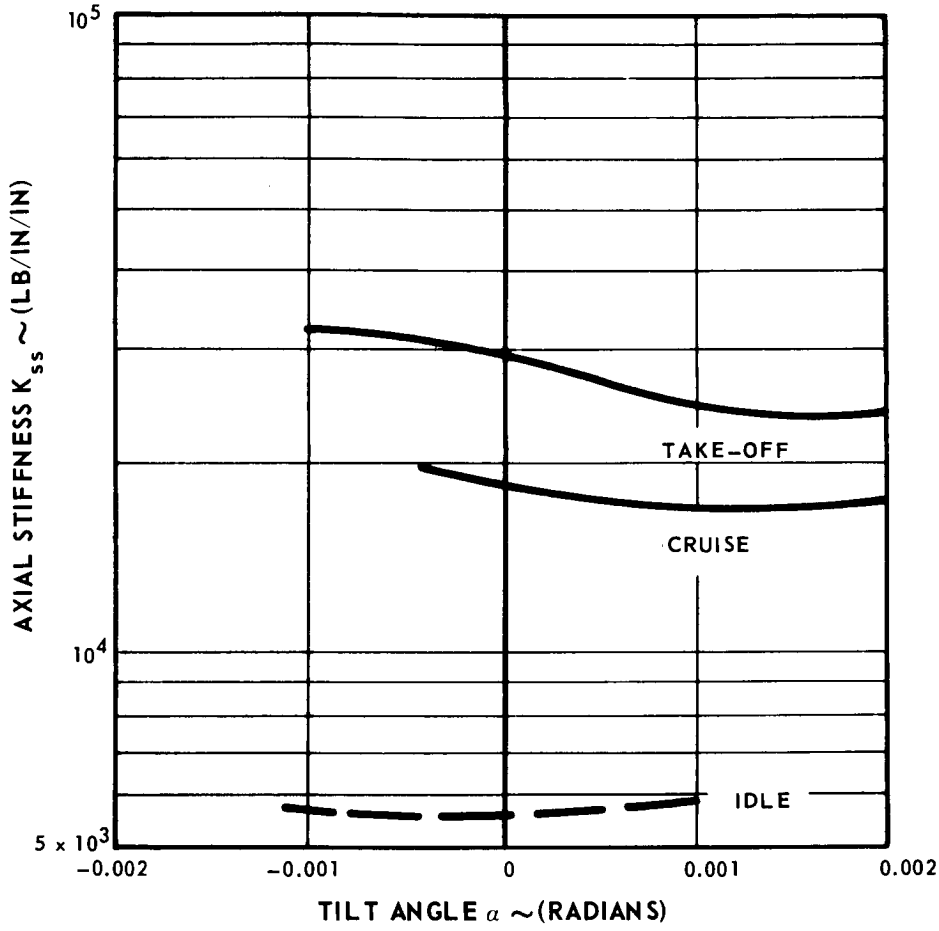

Figure 22 OC Diaphragm End Seal Film Thickness

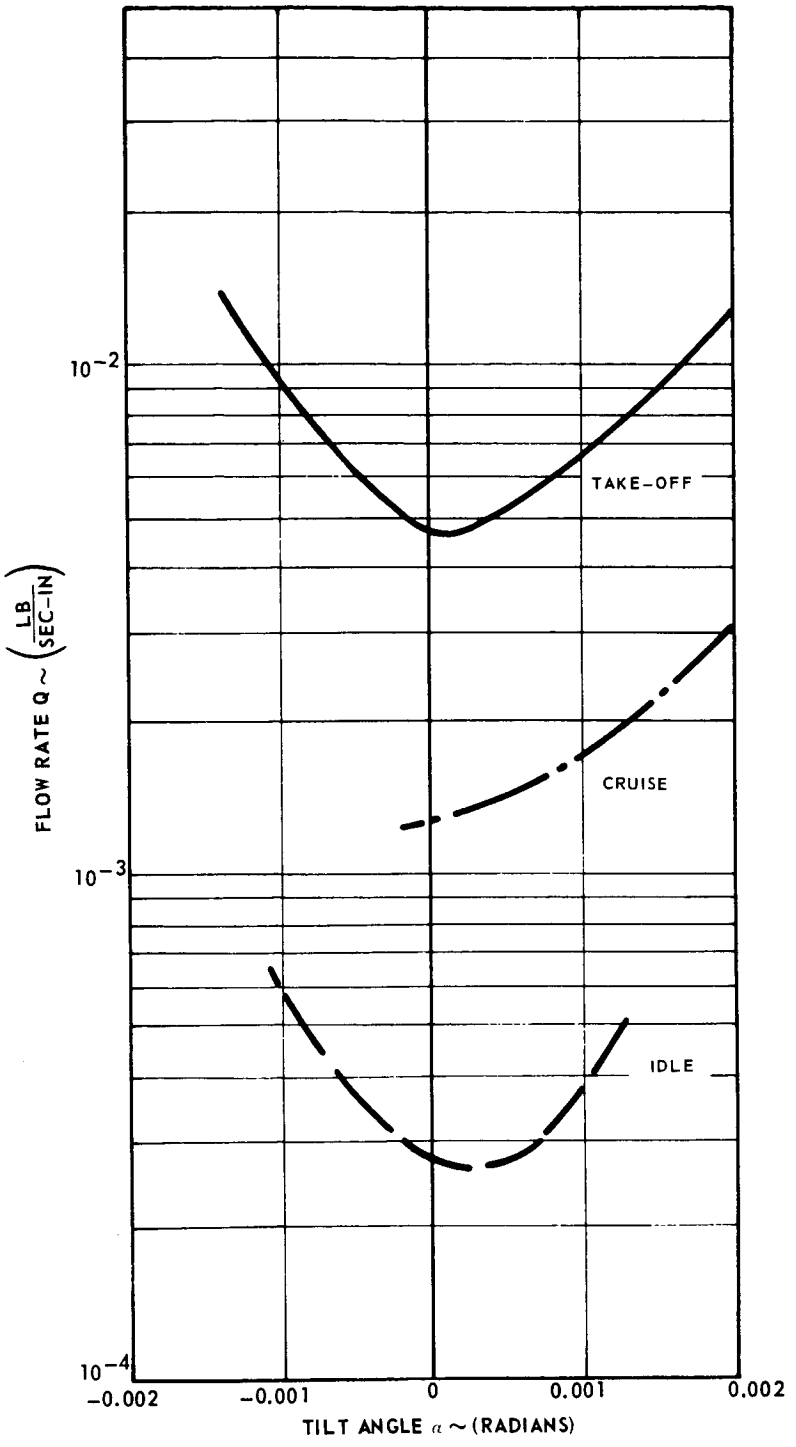

Figure 23 OC Diaphragm End Seal Leakage

Because of the flexibility of the OC diaphragm seal, the chances are very good that the seal ring will follow conical runner distortion, as can be seen from the following comparison of the seal-ring and air-film angular stiffnesses. The bending stiffness of the ring can be calculated, assuming that the ring tilts as a solid body, from

$$K_r^* = \frac{EI}{R^2}$$

where

$$I = \frac{bh^3}{12} = 0.211\,(10^{-3})\ \text{in}^4$$

$$E = 23 \times 10^6\ \text{psi}$$

$$R = 13.5\ \text{in}$$

K_r^* = seal ring bending stiffness = 27.0 in-lb/radian

The restoring moments of the gas film are much higher than those required to overcome the seal ring's internal resistance to bending. The seal ring also can be subjected to tilt in another way, through the application of residual moments. These moments arise as result of changes in operating conditions, dimensional seal variations due to manufacturing tolerances, and thermal deformation. The effects of the residual moments are discussed below.

b. RESIDUAL MOMENTS DUE TO CHANGE IN OPERATING CONDITIONS

The residual moments resulting from change in operating conditions have been previously calculated in Reference 7. Neglecting the seal ring's resistance to tilt, the seal ring will tilt until the imposed residual moment is balanced by a restoring moment created by the tilt angle a. Hence, knowing the residual bending moments, angle a can be directly determined from Figure 22. The tilt angles obtained are high in particular at take-off for the end stage seal. A significant reduction in tilt angle can be achieved through slight increase of the gas-force moment-arm between the lower pad and the centroid from 0.474 inch to 0.494 inch. The resulting residual moments are shown in Table I.

TABLE I

ADJUSTED RESIDUAL MOMENTS IN THE OC DIAPHRAGM END SEAL

	M_{res} lb-in/in	a Milliradians
Cruise	0.40	0.2
Idle	0.236	0.38
Take-Off	−0.70	−0.32

The adjustment in the moment arm produces a residual moment on the seal at cruise and slightly increases the residual moment at idle. The residual moments at take-off, however, are reduced from −1.35 in-lb/in. to −0.70 in-lb/in. As a result of these changes, the tilt angles all fall within the specified range of 0.0007 to −0.0004 milliradian.

c. RESIDUAL MOMENTS DUE TO DRAWING TOLERANCES

The most critical tolerances in terms of their contribution to the residual moment change are the tolerances of the spring diameters (A, B, and C in Figure 24) and their respective concentricities. Based on these tolerances, the residual moment change for all applicable operating conditions can be calculated as shown in the following sample calculation for the end seal at cruise.

(1) Sample Calculation for C-Diaphragm at Cruise

$$\Delta p = 80 \text{ psi}$$

Tolerance on diameter "C" is ± 0.004 inch, therefore, radial distance x_1 in Figure 24 can vary by ± 0.002 inch.

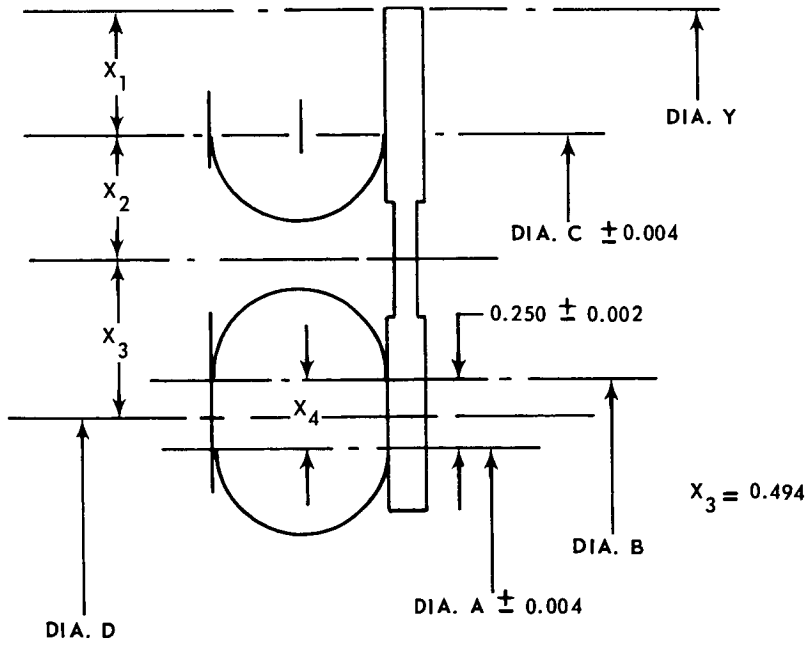

Figure 24 Critical Tolerances in the OC Diaphragm End Seal

Tolerance on eccentricity of diameter "C" with respect to diameter "Y" is ± 0.004 inch. This permits an additional change in distance x_1 by ± 0.002 inch.

Based on the above tolerances, the total increase or decrease in x_1 is 0.004 inch.

The net gas-force change is thus

$$F_{r1} = \Delta p \, \Delta x_1 = \pm 80 \, (0.004) = \pm 0.320 \text{ lb/in.}$$

The moment arm of the $\Delta p \, \Delta x_1$, gas force is 0.175 ± 0.002 inch.

It should be noted that when the gas force decreases (Δx_1 is negative), the moment arm increases by one half the magnitude of the decrease in Δx_1

In the case of cruise and idle conditions we are only interested in the positive residual moments developed, inasmuch as the residual moments at cruise and idle are positive, and the positive moments due to tolerance changes will be directly additive to yield the worst possible case. At take-off where the residual moments due to change in operating conditions are negative, the problem is not so severe. The total moment change at cruise is thus

$$M_c = F_{r1} \, x_2 = +0.320 \, (0.175 + 0.002) = 0.056 \, \frac{\text{in-lb}}{\text{in}}$$

(2) **Sample Calculation for O-Diaphragm At Cruise**

Tolerance on Diameter A in Figure 24 is ±0.004 inch and moment arm x_3 due to this tolerance will vary by ±0.002 inch.

Tolerance on dimension x_4 over which Δp acts is ±0.002. This will affect gas force F_{r2} since $F_{r2} = \Delta p \Delta x_4$. This tolerance also effects x_3 by ±0.001 inch.

To obtain a positive residual moment at cruise,

$$F_{r2} = \Delta p \Delta x_4$$

$$= 80 \, (0.002) = 0.16 \text{ lb/in.}$$

The moment arm x_3, adding 0.002 inches of possible eccentricity effect is

$$x_3 = 0.494 + 0.002 + 0.001 + 0.002$$
$$= 0.499 \text{ inch}$$

The net moment at cruise due to "O" diaphragm tolerance is thus

$$M_o = F_{r2} \, x_3 = 0.16 \, (0.499) = 0.08 \, \frac{\text{in-lb}}{\text{in}}$$

and the total moment on the seal due to the combined tolerance effect $M_{oc} = M_o + M_c = 0.14$.

The residual moment values calculated for all specified conditions are given below.

Cruise	0.14
Idle	0.02
Take-Off	−0.25

d. RESIDUAL MOMENTS DUE TO THERMAL EFFECTS

Due to lack of thermal data at off-design conditions, the over-all effects of residual moments due to thermal gradients cannot be calculated at this time. The major contribution to the residual moments from thermal effects is expected to come from the thermal gradients existing in the seal support O- and C-diaphragm springs and temperature differences between the diaphragm springs and seal ring. (See Appendix C)

e. COMBINED RESIDUAL MOMENTS

The residual moments due to change in operating conditions, as well as the moments due to drawing tolerances can now be added to yield the worst possible residual moment combinations. The combined residual moments are listed in Table II.

TABLE II

COMBINED RESIDUAL MOMENTS FOR THE OC DIAPHRAGM END SEAL

	M_{res} (in-lb/in)	Tilt Angle (milliradians)
Cruise	0.564	0.32
Idle	0.263	0.40
Take-Off	−1.01	−0.40

f. EFFECT OF RESIDUAL BENDING MOMENTS ON FILM THICKNESS

The effect of residual bending moments on film thickness during operation can be found using the data obtained from Table II to find the minimum film thickness from the static performance characteristics shown in Figure 21. The values of minimum film thickness h_{min} and mean film thickness h_m are given in Table III. These values will be later used to adjust the results of the tracking analysis to account for the residual moment effects. Note, that the values given here are conservative, inasmuch as the internal seal ring resistance to tilt is assumed to be zero.

TABLE III

MEAN AND MINIMUM FILM THICKNESSES RESULTING FROM RESIDUAL MOMENTS IN THE OC DIAPHRAGM END SEAL

	h_{Rmin} (in x 10^3)	h_{Rm} (in x 10^3)	a (rad x 10^3)
Cruise	0.84	1.386	0.32
Idle	0.68	0.94	0.40
Take-Off	0.55	0.81	–0.40

g. EFFECT OF SEAL RING TILT ON SEAL LEAKAGE

Seal leakages have been calculated and tabulated in Reference 7 for all operating conditions at parallel film thicknesses. Having established the maximum residual moments expected during operation and the resulting tilt angles (see Table III), the effect of the seal ring angular tilt on leakage can now be determined from Figure 23.

The net results are shown in Table IV where values of parallel film thickness leakage rates are compared to tilted seal ring leakage rates. The results indicate only slight increases in leakage at cruise and idle. The only appreciable increase in leakage due to tilt (about 25 percent) occurs at the take-off condition. Considering the fact that the calculated tilt angles represent conservative estimates of the expected maximum, the increase in leakage shown at this condition represents also a highly conservative estimate.

TABLE IV

TILTED- AND PARALLEL-FILM MAXIMUM SEAL LEAKAGE IN THE OC DIAPHRAGM END SEAL

	Parallel Film (lb/sec)	Tilted Film (lb/sec)	Tilt Angle a (rad)
Cruise	0.113	0.116	0.00032
Idle	0.024	0.022	0.00040
Take-Off	0.390	0.490	0.00040

h. OC DIAPHRAGM SEAL DYNAMIC PERFORMANCE

(1) Tracking Analysis

The tracking analysis employed to investigate the dynamic seal performance characteristics is described in detail in Section IB of this report. In the course of evaluation of seal tracking performance, the seal is subjected to three runner input modes. In the n = 0 mode, no

axial runner input deflection exists but the seal ring (or the runner) is tilted by an angle ξ_n, the seal tilt angle being uniform all around the circumference. This condition is representative of the state in which the seal or runner is initially coned or is subjected to thermal tilt or coning. The gas film characteristics required for the input, such as $K_{\alpha\alpha}$, $K_{s\alpha}$, $K_{\alpha s}$ and K_{ss} have been calculated based on a seal tilt angle of 0.0004 radian.

In the n = 1 mode the runner exhibits an 0.003-inch full indicator runout resulting in a ±0.0015-inch wobble once per revolution.

In the n = 2 mode, the runner is distorted in a saddle shape, exhibiting two high and two low spots symetrically spaced, the maximum deformation being 0.001 inch from planar. At this condition, the runner deformation occurs at a frequency equal to twice the runner frequency of rotation.

The n = 0, n = 1 and n = 2 modes of distortions are graphically shown in Figure 25. The tracking results based upon the seal distortions discussed above are given in Table V. In this table, n, ξ_n, h_m, δ_n, and ϵ_n are inputs into the computer program. The minimum film thickness for each mode of distortion is calculated from the following relationships established in Section IB.

$$\alpha_n = C_{A1}\,\epsilon_n + C_{A2}\,\delta_n$$

$$\beta_n = C_{B1}\,\zeta_n + C_{B2}\,\eta_n$$

$$u_n = C_{u1}\,\epsilon_n + C_{u2}\,\delta_n$$

$$v_n = C_{v1}\,\zeta_n + C_{v2}\,\eta_n$$

where ϵ_n is the seal to rotor angle as shown in Figure 25, $\delta_n = \delta/b$ (δ being the axial rotor displacement shown in Figure 25), and b the radial width of the seal face. The "C's" are influence coefficients calculated through the use of the computer program. These are listed in Table VI for all operating conditions.

The minimum film thickness is calculated using the following relationships

$$h_{min} = h_m - \frac{b}{2}\,|\epsilon_n - \alpha_n - \beta_n| - b\,|-\delta_n + u_n + v_n\,|$$

The results indicate that at most conditions, with the given input distortions, the seal would still operate at reasonably safe minimum film thicknesses even if all distortions were to fall in phase in such a manner that the film thickness loss ($h_m - h_{min}$) resulting from each mode of distortion would be directly additive yielding the combined h_{min} shown in Table V.

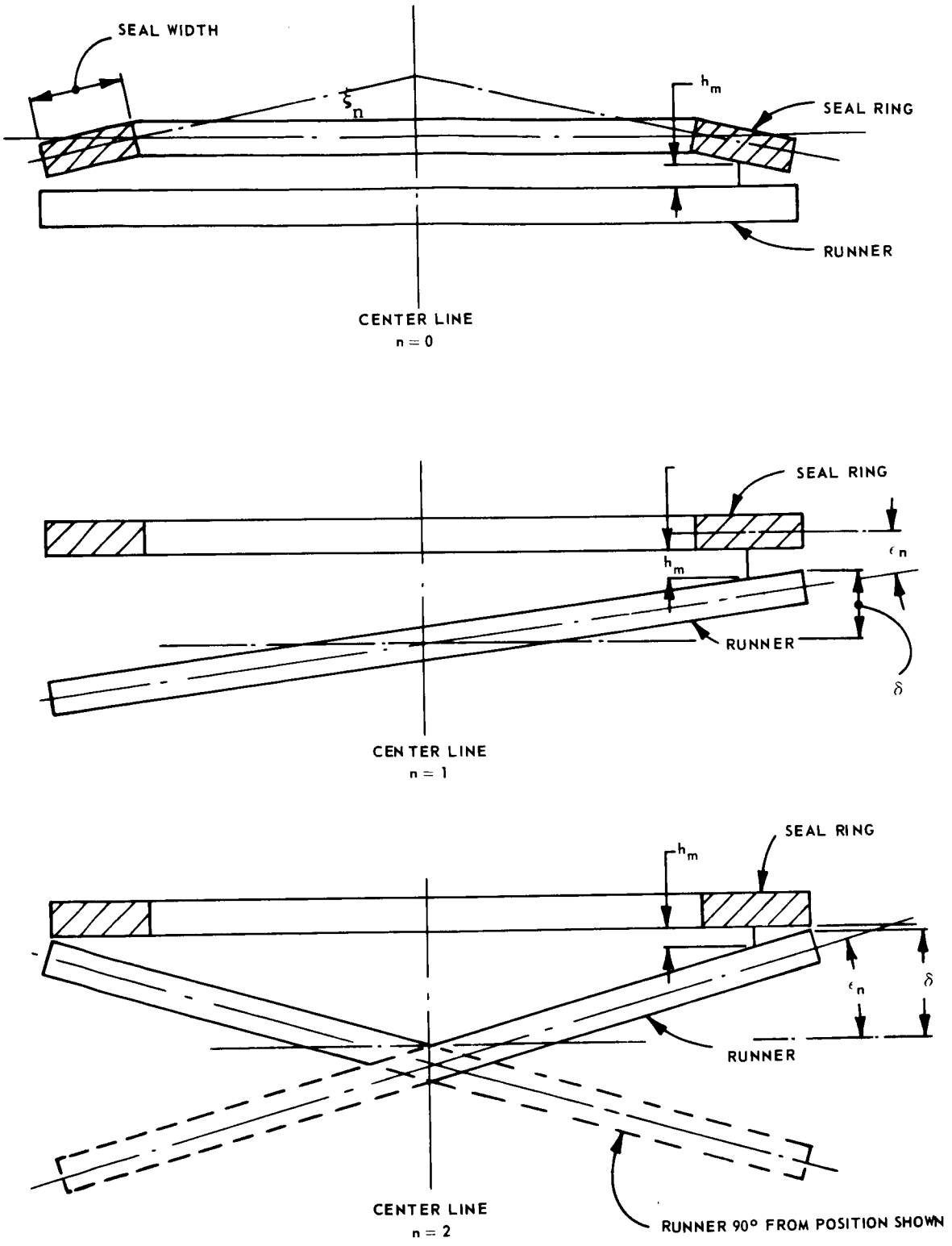

Figure 25 Modes of Seal and Runner Distortion Used in Tracking Analysis

TABLE V

RESULTS OF TRACKING ANALYSIS OF OC DIAPHRAGM END SEAL

Mode Number n	Mode 1 Angular Deflection ξ_n (radian)	Mean Film Thickness h_m (inches)	Centroid Deflection δ (inches)	Angular Deflection ϵ_n	Minimum Film Thickness h_{min} (inches)	Combined Minimum Film Thickness* h_{Tmin} (inches)
			Cruise			
0	0.0004	0.001	0.0	0.0	0.000995	
1		0.001	−0.0015	0.00011	0.000872	0.000840
2		0.001	−0.0005	0.000037	0.000973	
			Idle			
0	0.0004	0.00085	0.0	0.0	0.00085	
1		0.00085	−0.0015	0.00011	0.00068	0.000630
2		0.00085	−0.0005	0.000037	0.00080	
			Takeoff			
0	0.0004	0.00085	0.0	0.0	0.000845	
1		0.00085	−0.0015	0.00011	0.000764	0.000740
2		0.00085	−0.0005	0.000037	0.000831	

$$*h_{Tmin} = h_m - \sum_n (h_m - h_{min})$$

TABLE VI

INFLUENCE COEFFICIENTS FOR THE OC DIAPHRAGM END SEAL

	Mode Number	Cruise	Idle	Takeoff
C_{A1}	0	0.920	0.9411	0.935
	1	0.9043	0.9237	0.9180
	2	0.8580	0.8752	0.8696
C_{A2}	0	0.0983	0.0603	0.0625
	1	0.0839	0.0549	0.0534
	2	0.0431	0.0397	0.0271
C_{B1}	0	0.0141	0.0131	0.0136
	1	0.0320	0.0313	0.0320
	2	0.0818	0.0822	0.0832
C_{B2}	0	0.0000	0.0000	0.0000
	1	0.0031	0.0030	0.0031
	2	0.0114	0.0113	0.0115
C_{u1}	0	0.0111	0.0055	0.0104
	1	0.0133	0.0066	0.0131
	2	0.0196	0.0098	0.0206
C_{u2}	0	0.9576	0.9171	0.9715
	1	0.9625	0.9196	0.9745
	2	0.9769	0.9267	0.9834
C_{v1}	0	−0.0020	−0.0012	−0.0022
	1	−0.0043	−0.0024	0.0050
	2	−0.0109	−0.0057	0.0129
C_{v2}	0	0.0000	0.0000	0.0000
	1	−0.0004	−0.0002	0.0005
	2	−0.0015	−0.0006	0.0017

(2) Natural Frequencies

The OC diaphragm seal system yields four natural frequencies. Two of these, resulting from the seal-ring vibration analysis, are

$$\nu_{n1} = \left[\frac{1}{2} P_1 + \frac{1}{2} (P_1^2 - 4f_1^2 f_2^2 P_2)^{1/2}\right]^{1/2}$$

$$\nu_{n2} = \left[\frac{1}{2} P_1 - \frac{1}{2} (P_1^2 - 4f_1^2 f_2^2 P_2^2)^{1/2}\right]^{1/2}$$

For details, the reader is referred to Section IB. The calculated values of ν_{n1} and ν_{n2} fall far beyond the operating speed range, imposing no problems directly related to the design. The other two natural frequencies, ν_1 and ν_2, result from the behavior of the entire system in terms of rigid body vibrations. As previously discussed, ν_1 and ν_2 can be closely approximated using the following relationships:

$$\nu_1 = \left[\frac{K_3}{m_2}\right]^{1/2}$$

$$\nu_2 = \left[\frac{K_2}{m_1}\right]^{1/2}$$

where

K_3 = gas film stiffness (lb/in)

K_2 = spring diaphragm stiffness (lb/in)

m_2 = seal ring mass (lb-sec^2/in)

m_1 = carrier mass (lb-sec^2/in)

As has been shown in Section IB, ν_1 is far beyond the operating speed range and thus also imposes no particular problem on the design: ν_2, however, depends upon the selected OC spring geometry and carrier mass. Consequently, the ratio of K_2/m_1, due to practical design limitations, had to be carefully selected so that the resulting critical speed (ν_2) fell above the operating speed of 8000 rpm.

The final values of natural frequencies for all operating points under consideration are listed in Table VII with the corresponding operating frequencies (ν_o).

TABLE VII

NATURAL FREQUENCIES OF THE OC DIAPHRAGM END SEAL IN RAD/SEC

	Mode Number	ν_{n1}	ν_{n2}	ν_1	ν_2	ν_o
Cruise	0	46,789	11,337	13,123	1,273	760
	1	47,069	11,370	13,123	1,273	760
	2	47,899	11,466	13,123	1,273	760
Idle	0	46,728	8,220	7,983	1,240	1,273
	1	47,145	8,223	7,983	1,240	1,273
	2	48,372	8,232	7,983	1,240	1,273
Takeoff	0	54,152	13,746	16,319	1,280	1,280
	1	54,465	13,792	16,319	1,280	1,280
	2	55,393	13,925	16,319	1,280	1,280

Examining the values of the lowest natural frequency (ν_2) and comparing these to the approximate operating frequencies (ν_o) at each condition, the conclusion may be drawn that the lowest natural frequencies of the system fall safely above the operating frequencies.

(3) Carrier and Seal Ring Rigid Body Response

In the analysis of rigid body vibrations discussed in Section IB, the dynamic rigid body responses of the carrier and the seal ring with respect to the unit runner input, are expressed by C_1/C_3, C_2/C_3 respectively. From Table VIII, the relative motions of seal diaphragm and carrier can be found. The carrier response C_1/C_3 indicates that the carrier motion at cruise will be highest and approximately equal to 1.5 times the runner input displacement. Due to the damping action of the torque pins, a good percentage of the indicated gain will probably be damped out. The seal diaphragm follows the input motion almost perfectly as indicated by the C_2/C_3 ratios of close to 1.0.

TABLE VIII

CARRIER AND SEAL RING RIGID-BODY RESPONSE RATIOS

	C_1/C_3	C_2/C_3
Cruise	1.57	1.02
Idle	1.12	1.01
Takeoff	1.42	1.01

i. COMBINED STATIC AND DYNAMIC SEAL PERFORMANCE

The results of the tracking analysis discussed above show that the gas film possesses sufficient restoring moment capabilities to counteract initial seal ring deformation within reasonable limits of seal ring tilt angle when the deformations are not produced by residual moments.

When residual moments are present, the seal ring (neglecting its internal resistance to tilt) will tilt to the point where a restoring moment of equal and opposite magnitude is developed by the gas film. The effects of seal ring tilt due to residual moments are not considered in the tracking analysis aside from the fact that the gas film characteristics are calculated at expected tilt angles.

To take into account the residual moment contribution to the minimum film thickness during operation, the difference between parallel film thickness h (listed in Table V) for all running condition's, and minimum film thickness h_{Rmin} (listed in Table III) resulting from the residual bending moment, is subtracted from the minimum film thickness h_{Tmin} (listed in Table V) obtained in the tracking analysis, or

$$h_{Tmin} - (h_m - h_{Rmin}) = h_{Fmin}$$

where h_{Fmin} is the final combined minimum film thickness. This approach is conservative, since it assumes that all deformations act in phase and are thus directly additive. It also assumes no internal resistance of the ring and a worst-tolerance stackup. The values calculated using this procedure are shown in Table IX.

TABLE IX

FINAL MINIMUM FILM THICKNESS OF THE OC DIAPHRAGM END SEAL DURING OPERATION

Conditions	h_m (in x 10^3)	h_{Rmin} (in x 10^3)	h_{Tmin} (in x 10^3)	h_{Fmin} (in x 10^3)
Cruise	1.00	0.84	0.84	0.68
Idle	0.85	0.68	0.63	0.46
Takeoff	0.85	0.55	0.74	0.44

The addition of the residual moment effects obviously lowers the operational film thickness. The final values, with the exception of one condition, indicate less than 50 percent film loss for the worst cases considered. OC diaphragm end seal performance should thus be satisfactory over almost the entire range of conditions.

4. OC DIAPHRAGM SEAL THERMAL ANALYSIS

Thermal maps showing the temperature distribution of the seal's cross section and the immediate surrounding areas have been computed at cruise conditions. The detailed analytical procedure and results are given in Appendix C.

The results for the end seal are slightly different from those reported in Reference 7. The differences are mainly due to the assumption of reduced air temperature at the-low pressure side. According to the latest thermal analysis, this temperature is expected to be 1136 degrees Fahrenheit instead of the originally assumed 1200 degrees Fahrenheit.

In summary, the end seal temperature distribution yields reasonably low temperature gradients. Although the thermal gradients in the seal section will produce a seal face deformation with a slope of –0.0027 in/in, this will be entirely offset by counteracting pressure forces.

5. OC DIAPHRAGM END SEAL ORIFICE PRESSURE DROP CALCULATIONS

The analysis of the OC diaphragm end seal assumes that no pressure drop occurs at the lower pad orifices which admit pressurized air to the Rayleigh shrouded pads and that no pressure drop occurs at the vent holes incorporated in the seal ring and carrier. To ensure that these pressure drops are minimized in the actual design, the number of orifices and orifice diameters must be kept as large as physically possible within the design limits.

a. PRESSURE DROP THROUGH RAYLEIGH PAD FEED HOLES

The maximum possible Rayleigh shrouded step feed orifice diameter is 0.062 inch. Since there are 77 pads in the end seal, there are also 77 feed orifices present. The air flow through the lower pad at cruise is 0.084 lb/sec.

$$G = \frac{m\sqrt{RT}}{p_2\, \pi a^2\, C_d\, n g} \tag{69}$$

where

G = dimensionless flow

p_2 = supply pressure = 100 psia

R = gas constant = $2.47\,(10^5)$ in^2/sec^2 – ^{o}R

T = supply temperature = 1660^{o}F

a = orifice radius = 0.01325 in

C_d = coefficient of discharge = 0.8

n = number of orifices = 77

g = gravitational constant = 386 in/sec^2

m = flow = 0.084 lb/sec

Therefore, for the end seal cruise condition, G = 0.233.

From Figure 12, Reference 8, for G = 0.233, $\left(\frac{p_1}{p_2}\right)^2 = 0.92$

$$\frac{p_2}{p_1} = 0.96$$

The pressure drop across the Rayleigh pad feed holes is thus only 4 percent of the supply pressure and should not appreciably affect seal performance. At take-off, the lower pad flow is increased, but due to an increase in supply pressure and a decrease in temperature, the pressure ratio across the orifice will remain essentially the same as at cruise.

b. PRESSURE DROP THROUGH VENT HOLES

The pressure drop through the vent holes is calculated in a similar manner. The following specific values apply:

p_2 = 20 psia n = 154

a = 0.0625 inch m = 0.017 lb/sec

All other values are the same as those used in the Rayleigh pad feeder hole calculations. Substituting in Equation 69, G = 0.123 and $P_2/P_1 = 0.98$, which is low enough to be considered negligible. Again, at take-off, in spite of the increased flow, no appreciable increase in pressure ratio is expected due to compensating temperature effects. Nevertheless, in the final detailed layouts the vent hole sizes should be increased to the maximum possible to avoid pressure buildups.

6. PRELOAD HELICAL COIL SPRINGS

To save on design and manufacturing expense, the helical coil springs used in the OC diaphragm can be exactly the same as those used in the one-side floated-shoe design.

The spring specifications are as follows:

Wire size (inches)	0.035 ±0.008 dia
Coil outside diameter (inches)	0.445 Reference
Spring rate at 70°F	1.942 lb/in Reference
Solid height (inches)	0.601 to 0.671
Free heights (inches)	1.870 Reference
Total number of coils	18 Reference
First load	0 lb, 7 oz to 0 lb 9 oz at 1.612 inches length
Second load	1 lb 12 ox to 2 lb 0 oz at 0.904 inches length
End Condition	Close ends and grind square to within 2°

The spring rate variations according to the above specifications are plotted in Figure 26. For the end seal, the nominal spring length is 1.130 inches. At this length the load can vary

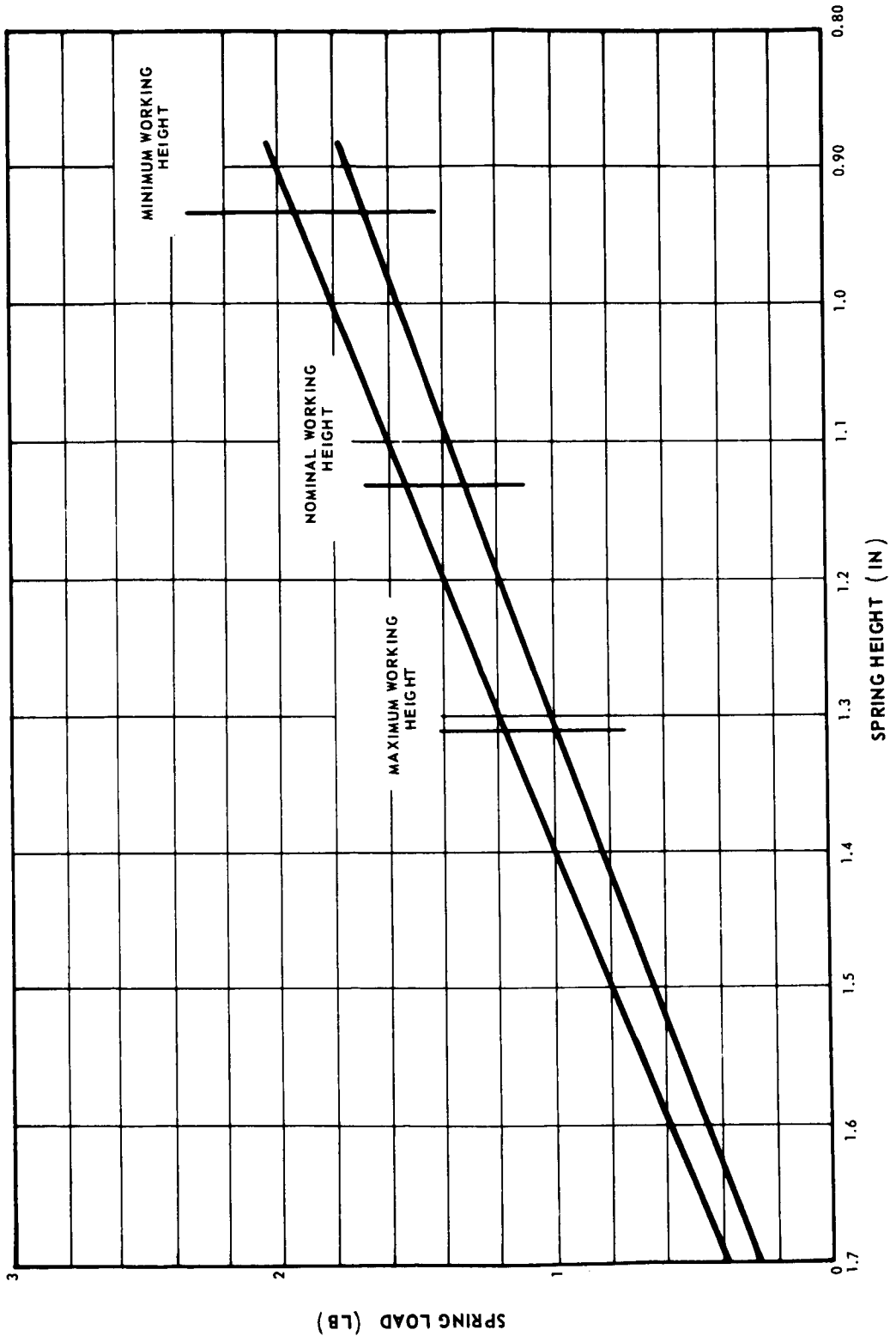

Figure 26 Helical Coil Spring Rate

between 1.54 and 1.32 pounds. For 24 springs, the total spring load variation is thus 37.0 to 31.7 pounds. Using a mean seal diameter of 27.050 inches, the variation in terms of spring load per inch of circumference is 0.437 lb/in to 0.373 lb/in. Similarly, at the minimum working length (nominal length less 0.2 inches) the load variation in pounds per inch of circumference is 0.553 to 0.482 lb/in, and at the maximum working length (nominal length plus 0.2 inches) the load can vary between 0.333 and 0.277 lb/in. The over-all spring load variation (taking into account the change in the spring's working length because of differential thermal expansion of test parts and spring tolerances) is 0.277 to 0.553 lb/in. In the original seal balance calculations, a constant spring load of 0.5 lb/in. was assumed to be acting on the seal at all conditions. Due to the fact that the spring load is not constant, what remains now to be established is the effect of spring load variation on film thickness and residual moments, and the minimum spring load sufficient to overcome friction at the antirotation pins.

a. EFFECTS OF SPRING LOAD VARIATION ON FILM THICKNESS AND RESIDUAL MOMENTS

To be conservative, let us assume that the entire spring load variation can occur at end idle conditions (the worst conditions), where the over-all pressure loading is lowest. The change from 0.5 lb/in assumed load to 0.553 lb/in maximum possible load will have negligible effects. Considering now the minimum possible spring load, the loss in seal face loading is $0.5 - 0.227 = 0.223$ lb/in. The total load at the interstage seal is 20.0 lb/in, (Table V, Ref. 7) thus the load loss of 0.223 lb/in represents a decrease of about 1 percent which is still within the over-all design accuracy and should not appreciably effect the operating seal clearance.

To determine residual moment effects, the simplified OC diaphragm seal model shown in Figure 27 can be used.

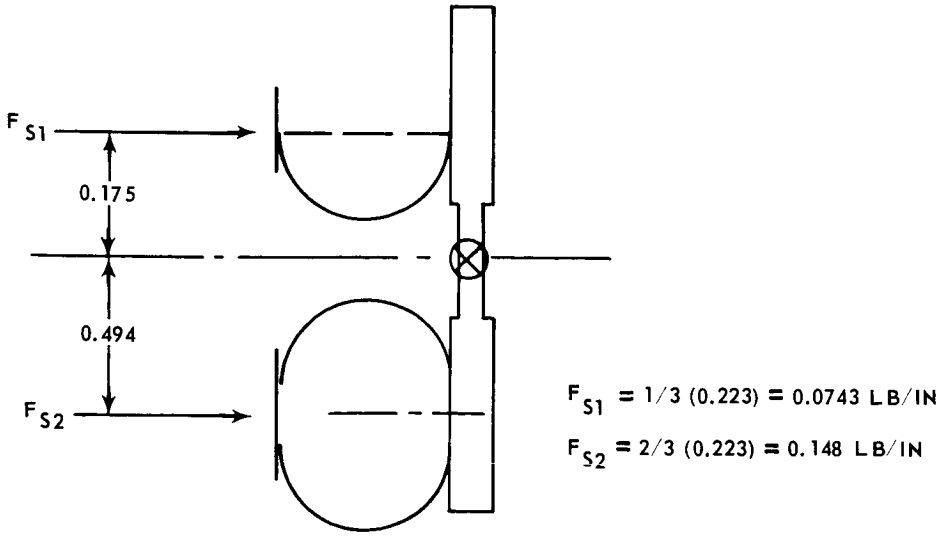

Figure 27 Simplified Diagram of the OC Diaphragm Seal

Summing up the spring moments about the centroid

$$-0.148\,(-0.494) + 0.0743\,(0.175) = 0.060 \text{ in.lb./in.}$$

This moment is extremely low, and in any event will subtract from the original residual moment in all cases (with exception of end seal take-off) thus actually reducing the tilt angle (a). Based upon the above calculations, it can be concluded that the effects of spring length and spring gradient variations on seal performance are negligible.

b. MINIMUM SPRING LOAD REQUIREMENTS TO OVERCOME FRICTION

Let us assume conservatively that only the spring load acts on the seal in the axial direction at cruise. From Reference 7, the power loss generated by the OC diaphragm end seal at cruise is 6.3 horsepower. At $\omega = 757$ rad/sec,

$$\text{Torque} = \frac{(550)\,(6.3)\,(12)}{(757)} = 55 \text{ in/lb}$$

The frictional force to be overcome by the spring is

$$F_f = \text{coefficient of friction} \times \frac{\text{Torque}}{\text{Radius}}$$

Assuming a coefficient of friction of 0.5 and a radius of 14.5 inches,

$$F_f = 0.5\,\frac{55}{14.5} \approx 2.0 \text{ pounds}$$

The minimum available spring force from Figure 26 is 0.98 lb/in, so that for 24 springs the total spring force is approximately 23.5 pounds, which is an order of magnitude higher than the frictional force to be overcome. The helical coil springs as specified can thus be used safely in the seal designs.

7. CARRIER BALANCE

The force and moment diagram for the OC diaphragm carrier cross section is shown in Figure 28. The carrier is designed so that the net resultant moment about the centroid of the cross section is small and bending stiffness high, thus minimizing carrier rotation. Furthermore, to make sure that the OC diaphragm springs remain slightly compressed during operation, the carrier is balanced to yield an additional 0.5 lb/in of pressure loading at cruise. This load acts in the same direction as the spring load. The forces acting on the carrier are:

F_s Helical coil spring load = 0.5 lb/in

F_{s1} C-diaphragm spring reaction

F_{s2} O-diaphragm spring reaction

F_2 C-diaphragm radial pressure load = .2Δp

F_3 O-diaphragm pressure load = 0.25 Δp

F_o Carrier axial pressure load = y_1 Δp

F_y Carrier radial pressure load = 1.255 Δp

Furthermore,

$$F_{s1} = 0.167 + 2.09\,(10^{-3})\,\Delta p$$

$$F_{s2} = 0.333 + 4.18\,(10^{-3})\,\Delta p$$

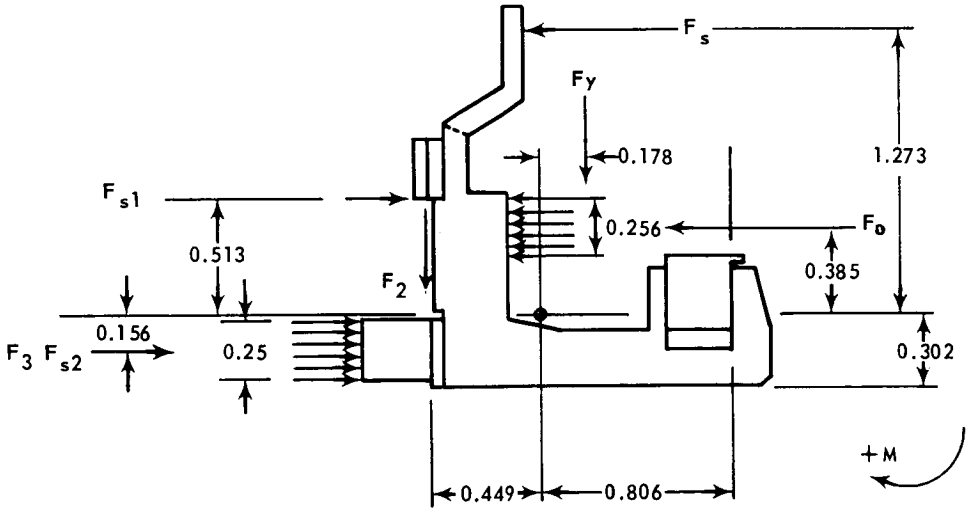

Figure 28 Force and Moment Diagram for the OC Diaphragm Seal Carrier

The left-hand terms of F_{s1} and F_{s2} are the reactions to the helical coil spring load and the right-hand terms are reactions to the carrier imbalance of 0.5 lb/in at cruise.

For balance, $\Sigma F = 0$

$$F_{s1} + F_{s2} + F_3 - F_o - F_s = 0$$

Substituting the given values in the above equation

$$0.167 + 2.09\,(10^{-3})\,\Delta p + 0.333 + 4.18\,(10^{-3})\,\Delta p + 0.25\,\Delta p - y_1\,\Delta p - 0.5 = 0$$

or

$$0.256\,\Delta p - y_1\,\Delta p = 0$$

$$y_1 = 0.256 \text{ inch}$$

For $\Sigma F_y = 0$, the only loads acting on the carrier is F_y and F_2. The internal ring reaction to these loads will, assuming no ring distortion, pass through the centroid of the ring's cross section, and thus is of little interest in the moment balance when moments are taken around the centroid. The centroid coordinates x* and y* for the given cross section are calculated using the moment area method to be x* = .449 inch and y* = .302 inch.

Note that $M_x \neq 0$, but equals M_R, the residual carrier moment. Referring to Figure 28,

$$M_R = .513\,F_{s1} - 1.273\,F_s + .178\,F_y - .385\,F_o - .156\,F_3 - .156\,F_{s2} - .449\,F_2$$

$$= -.0035\,\Delta p - .6027$$

Pressure differentials corresponding to the end seal design conditions can now be easily substituted and carrier residual moments obtained. These moments are given in Table X.

TABLE X

BALANCE RESULTS FOR THE OC DIAPHRAGM END SEAL

$I = .165 \text{ in}^2$

$R = 13.0 \text{ in}$

	ΔP (psi)	Residual Carrier Moment M_R (in-lb/in)	Modulus of Elasticity E (psi)	Angle of Carrier Rotation θ (rad x 10^3)
Cruise	80	− .883	24	.038
Idle	13	− .648	30	.022
Take-Off	150	−1.128	28	.041

The moment of inertia around the centroidal "y" axis is calculated to be 0.1251 in^4, from Reference 1.

$$\theta = \frac{M_R R^2}{EI}$$

Where θ is the angle of carrier rotation, E is the modulus of elasticity, I is the moment of inertia around the centroidal "y" axis, R is the mean carrier ring radius, and M_R is the residual carrier moment. Assuming a carrier radius of 13 inches, the values of θ listed in Table X were obtained for all design conditions. The angular carrier rotation, in all cases, is of small magnitude.

D. SEMIRIGID INTERSTAGE SEAL DESIGN

The final Task I design for the semirigid interstage seal is shown in Figure 2. Because the semirigid end seal will not be evaluated in Task II, the following discussion will be concentrated on the semirigid interstage seal. As was the case with the OC diaphragm seal, there are only minor differences between the end and interstage configurations of the semirigid seal design.

1. PRINCIPLE OF OPERATION

The semirigid seal, although differing in other major respects, operates on the same basic principle as the OC diaphragm seal, inasmuch as in this case too, the principle of clearance controlled leakage is applied.

Primary sealing is accomplished at the seal face, which consists of a single land. This land has a spiral-groove inherently compensated orifice profile, and acts as a bearing and seal combination. The angular stiffness of a single land bearing is very low. As a result, the seal ring must be rigid enough to absorb residual bending moments without appreciable deformation of the seal face. To accomplish this, substantial seal-ring length is required. Moreover, the seal ring must also serve as a housing for the piston ring required for secondary sealing, one of the secondary seals being formed by contact between the side of the piston ring and the seal ring. It should be noted that the combination of seal length and piston ring contact is conducive to the generation of high thermal gradients. Thermal gradients in turn cause the seal surface to deform and through this deformation may seriously affect seal performance. In order to minimize the extent of thermal gradients and seal deformations the following steps have been taken:

- The seal material was selected to provide high thermal conductivity in combination with a low coefficient of thermal expansion.
- The piston ring was insulated through the inclusion of a thermal barrier in the form of a radially annular slot.
- The seal's cross section was designed to minimize thermal distortions through the addition of a relatively constant temperature ring on the seal's outer edge close to the seal face.
- The seal's tracking performance characteristics indicate tolerance to some degree of distortion. Since slight distortion may be beneficial, the seal is designed so that sufficient distortion occurs, the net result of which is an increase in film clearance at high pressure ratios, reduction in heat generation at the seal face, and an increase in leakage flow. The increased air flow also carries more heat away from the seal face, leaving less heat to be dissipated by the seal, and therefore lower thermal gradients.

The seal ring is preloaded with 24 helical coil springs to ensure contact at start and permit development of separating air films at relatively low speeds. The seal face and runner coating materials were also selected with regard to compatibility at high temperature and resistance to wear. They are identical to the ones used in the OC diaphragm seal.

2. SEAL CONSTRUCTION

The semirigid seal is a one-piece design. The seal basically consists of a ring composed of front and rear sections welded together to form a thermal barrier. The rear section of the ring includes 24 tabs for piston-ring retention and for spring-guide mounting. This same section includes also four protruding slotted tabs for engagement of the antirotation pins. The antirotation pins are the same as those used in the OC diaphragm seal. The front portion of the seal includes the primary seal face and 360 orifices feeding in directly from the high pressure cavity.

Calculations of force and moment balancing for the piston ring are not discussed in this volume, since they were previously described in Reference 6, page 23. The piston ring is of the same cross-sectional design as the OC diaphragm piston ring, but in this case the ring rides on the seal's inner edge. This change required a modification of the piston-ring spring design. The piston ring rides on the seal support which connects through the support case to the test housing.

The seal ring is made of Duranickel 301, a material of substantial high-temperature strength combined with good thermal conductivity and relatively low thermal expansion. The seal face is coated with aluminum oxide or chrome carbide, for the same considerations of profile manufacturability mentioned in the OC diaphragm seal description. The seal supports are made of Inconel X750.

3. MODIFICATION OF CROSS-SECTION

The semirigid seal cross section arrived at in Reference 7 and shown in Figure 29 exhibits one basic drawback: the axial thermal gradients at cruise are high enough to cause end seal distortions of 0.003 radians in the end seal application and higher in the interstage seal. (See page 49, Ref. 7) The axial thermal gradients result from heat flow originating at the seal interface and from heat flow due to radial temperature differences between the high- and low-pressure test-rig areas.

The axial heat flow is enhanced by the fact that the seal and piston ring are in intimate metal-to-metal contact, providing an excellent conductive path down to the seal support, which extends through the low-temperature area to the housing walls. Thus, in order to reduce the effectiveness of this built-in heat sink, the piston ring has to be isolated from the seal ring. Since contact between piston ring and seal walls is absolutely necessary to maintain good sealing, it becomes advisable to introduce a thermal barrier in the seal proper, close to the piston ring, leaving the back of the ring against which the piston ring rests unaltered. This can be accomplished through the introduction of a radial cut out.

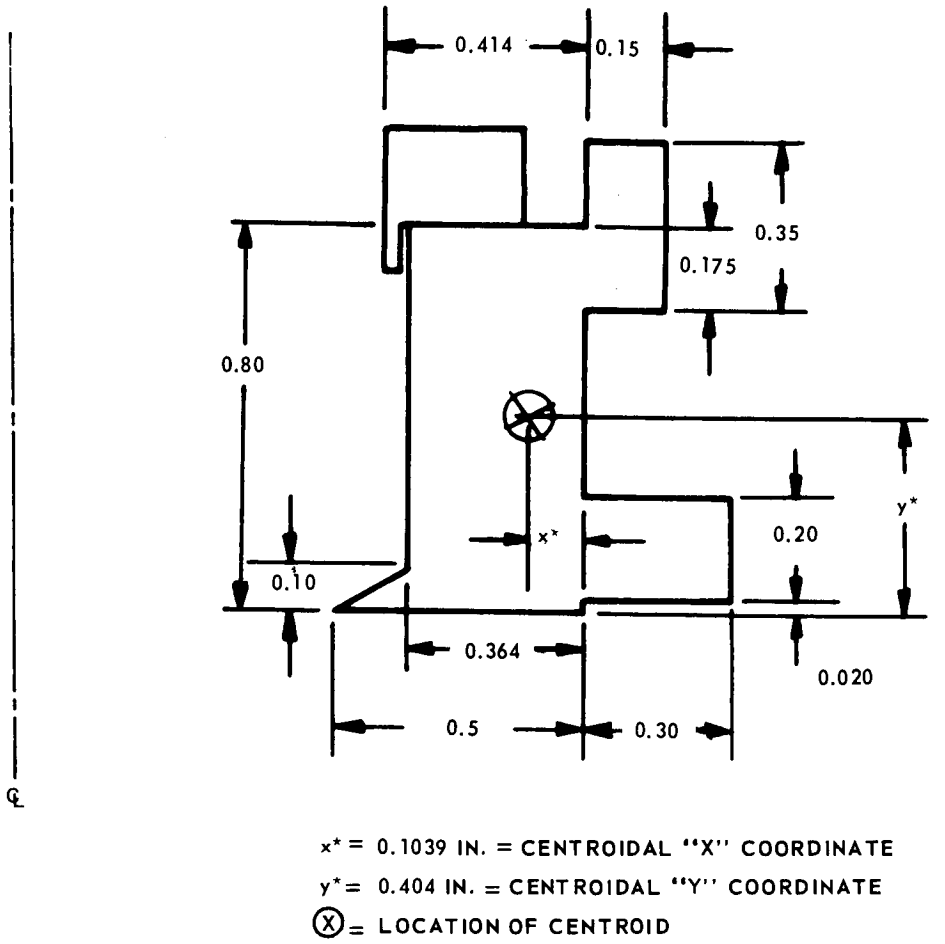

Figure 29 Cross Section of the Semirigid One-Piece Seal

The air in this cut out is relatively stagnant and thus acts as a fairly good insulator. In order to maintain seal rigidity and to prevent the gas loading applied by the piston ring onto the seal wall from deflecting it excessively, the ring is welded at 180 points around the inside circumference.

The introduction of the thermal barrier cut out necessitates rebalancing the cross section through minor dimensional adjustments so that the location of the centroid is not appreciably altered. This is important since the magnitude of the residual bending moments is dependent upon the force moment arm to the centroid. The final adjusted, configuration is shown in Figure 30. It forms the basis for the final seal design.

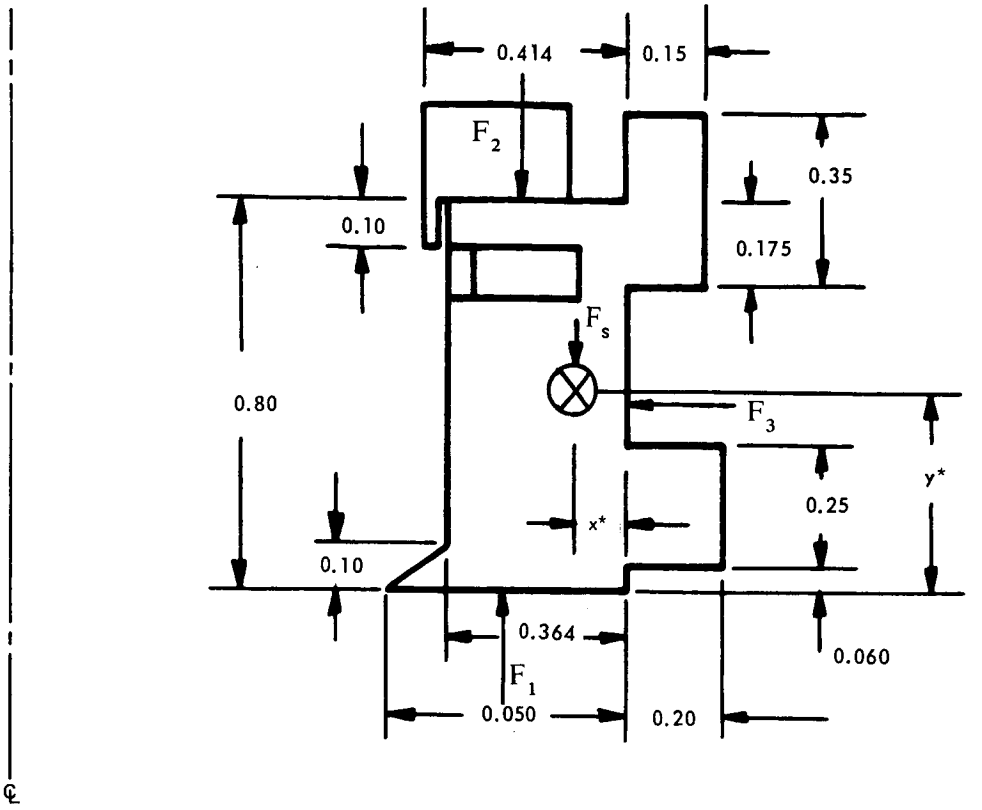

x* = 0.1056 IN. = CENTROIDAL "X" COORDINATE

y* = 0.403 IN. = CENTROIDAL "Y" COORDINATE

⊗ = LOCATION OF CENTROID

Figure 30 Cross Section of the Semirigid One-Piece Seal with Insulating Cut Out

4. SEAL BENDING STIFFNESS

The bending stiffness of the seal can now be calculated from:

$$K_r^* = \frac{M}{\theta} = \frac{EI}{R^2}$$

where $E = 23 \times 10^6$ psi, $I = 0.0255$ in^4, $R = 13.5$ in.

then,

$$K_r^* = 3218 \frac{\text{in-lb}}{\text{rad}}$$

This represents only a slight reduction in stiffness over the 3820 in-lb/rad. of the original "E" configuration discussed in Reference 7.

5. STATIC SEAL PERFORMANCE

a. RESIDUAL MOMENTS

The seal modifications described in the previous section have slightly altered the seal shape, but the air-pressure forces acting on the modified seal remain essentially the same as on the original cross-section. Consequently, neither the seal's air-film forces nor centers of pressure have been changed. The change in seal shape, however, brings about a slight change in centroid location and bending stiffness of the seal ring, resulting in a change in residual moments and tilt angle. These changes are tabulated in Table XI together with the magnitudes of all forces, centers of pressure and minimum film thickness. Examining the new results, the seal ring's tilt at all operating conditions still remains negligible. In all cases the small tilt angles are negative and acting in the direction of tilt opposite to that imposed by thermal gradients. This will slightly alleviate the negative effects of thermal seal rotation.

b. GENERAL PERFORMANCE CHARACTERISTICS

The static seal performance characteristics at cruise conditions for the end and interstage seals are discussed in detail in Reference 7. The basic performance curves at cruise are here supplemented with the performance characteristics at idle and take-off conditions. These curves are presented in Figures 31 through 36.

In general terms the comments made in the discussion of the end seal in Reference 7 also apply to the interstage seal. Due, however, to the lower pressure differentials existing at the interstage seal the latter's characteristics are more sensitive to tilt.

(1) Minimum Film Thickness

At take-off conditions (Figure 35), the pressure differentials are still sufficiently high to produce a slight increase in minimum film thickness at positive tilt angles. At cruise conditions (Figure 31), the minimum film thickness begins to decrease with positive tilt. The rate of decrease, however, is still low in comparison to that at negative tilt. At idle conditions (Figure 33), where the pressure differential is down to 2 psi, the rate of decrease in minimum film thickness at positive tilt angles exceeds the rate at negative tilt. Obviously, tilt angles of 0.002 radians cannot be tolerated at these conditions. Neither, however, are such high tilt angles to be expected to be present merely due to the fact that at idle the over-all ambient temperature and heat generation at the seal interface drastically decrease.

(2) Air-Film Stiffness

The film stiffnesses, K_{ss}, of the interstage seal are generally lower than the stiffness of the end seal at corresponding conditions, mainly due to the reduced hydrostatic effects. As will be shown in the tracking analyses, the stiffnesses are still sufficient to maintain sufficiently large air films during operation.

TABLE XI

FILM THICKNESS AND RESIDUAL MOMENT TABULATION FOR THE SEMIRIGID INTERSTAGE SEAL

Condition	Dimensionless Load $\overline{W}$	Dimensionless Center of Pressure $\overline{x}_c$	F_1* (lb/in^2)	F_2† (lb/in^2)	F_3‡ (lb/in^3)	Mean Film Thickness h_m (x 10^3 inch)	Residual Moments M_{res}‡ (in.lb/in)	Bending Stiffness K^*_r in.lb x 10^{-3} / in. rad	Seal Tilt Angle α (rad x 10^3)
Cruise	0.8695	0.422	10.87	10.37	20.0	1.02	-.15	3.22	-.045
Idle	1.3295	0.437	1.329	0.829	1.6	0.80	-.07	3.22	-.022
Take-Off	0.8495	0.418	21.237	20.737	40.0	0.79	-.21	3.22	-.065

* F_1 is the resultant force of the gas film pressure on the semi-rigid seal

† F_2 is the axial pressure differential force in the semi-rigid seal

‡ F_3 is the radial pressure differential force on the semi-rigid seal

ǂ M_{res} is given by Equation (8) of Reference 7

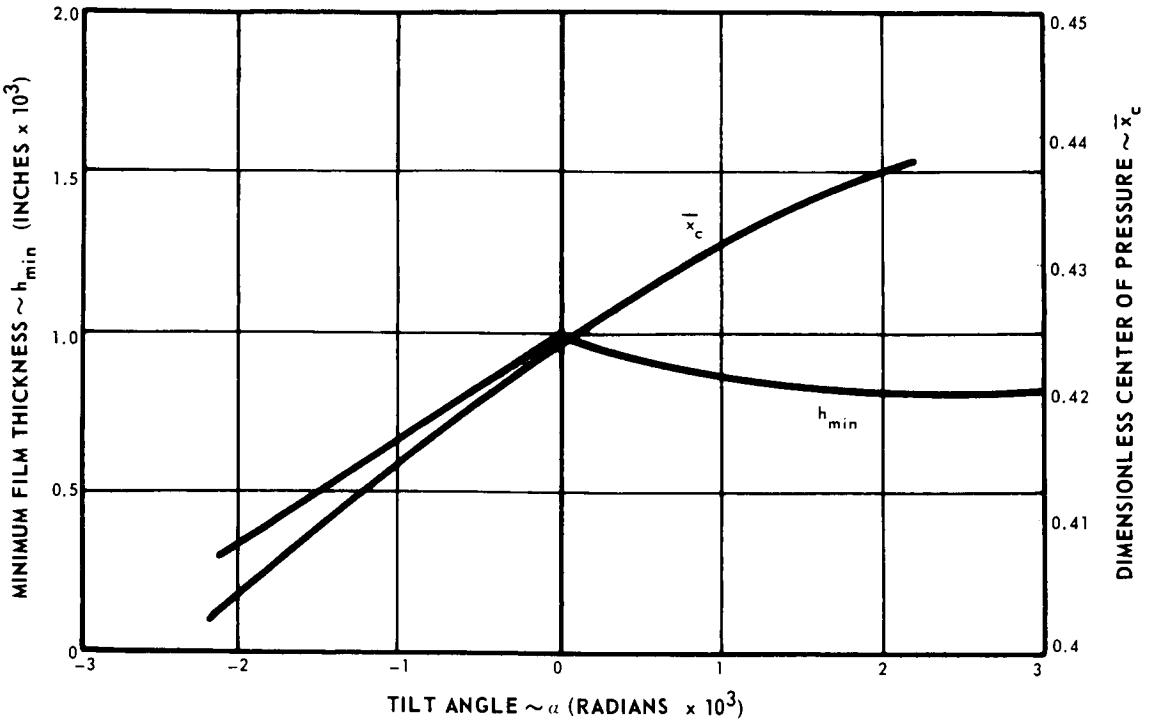

Figure 31 Minimum Film Thickness and Center of Pressure for the Semirigid Interstage Seal at Cruise

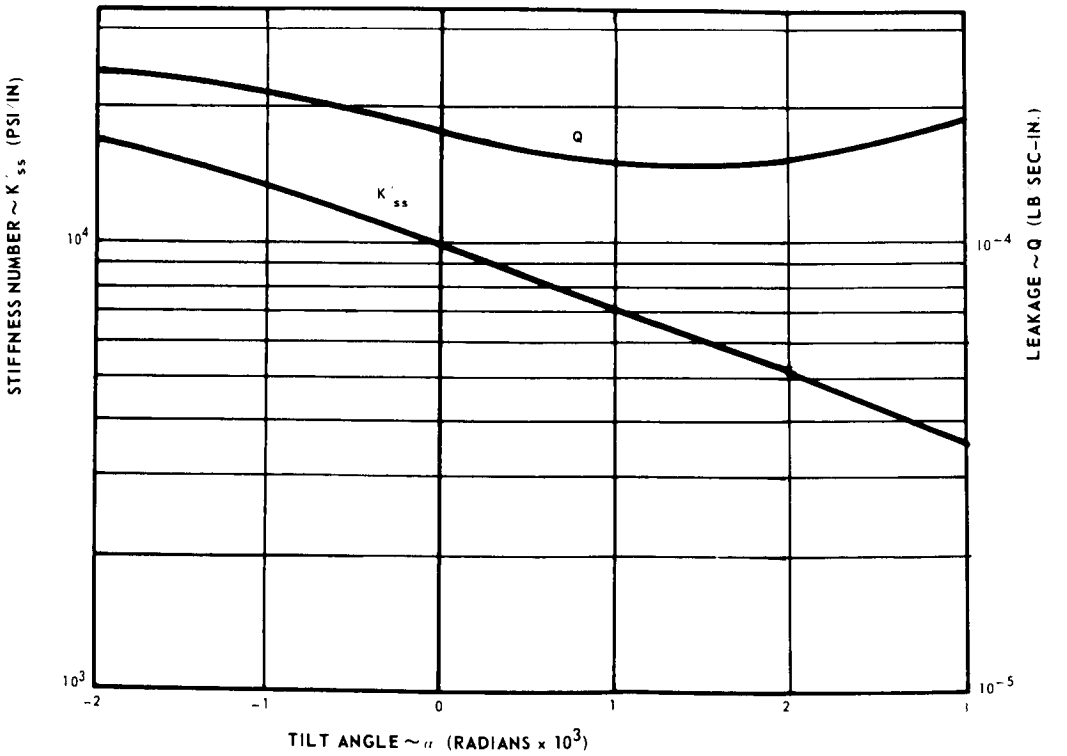

Figure 32 Leakage and Stiffness of the Semirigid Interstage Seal at Cruise

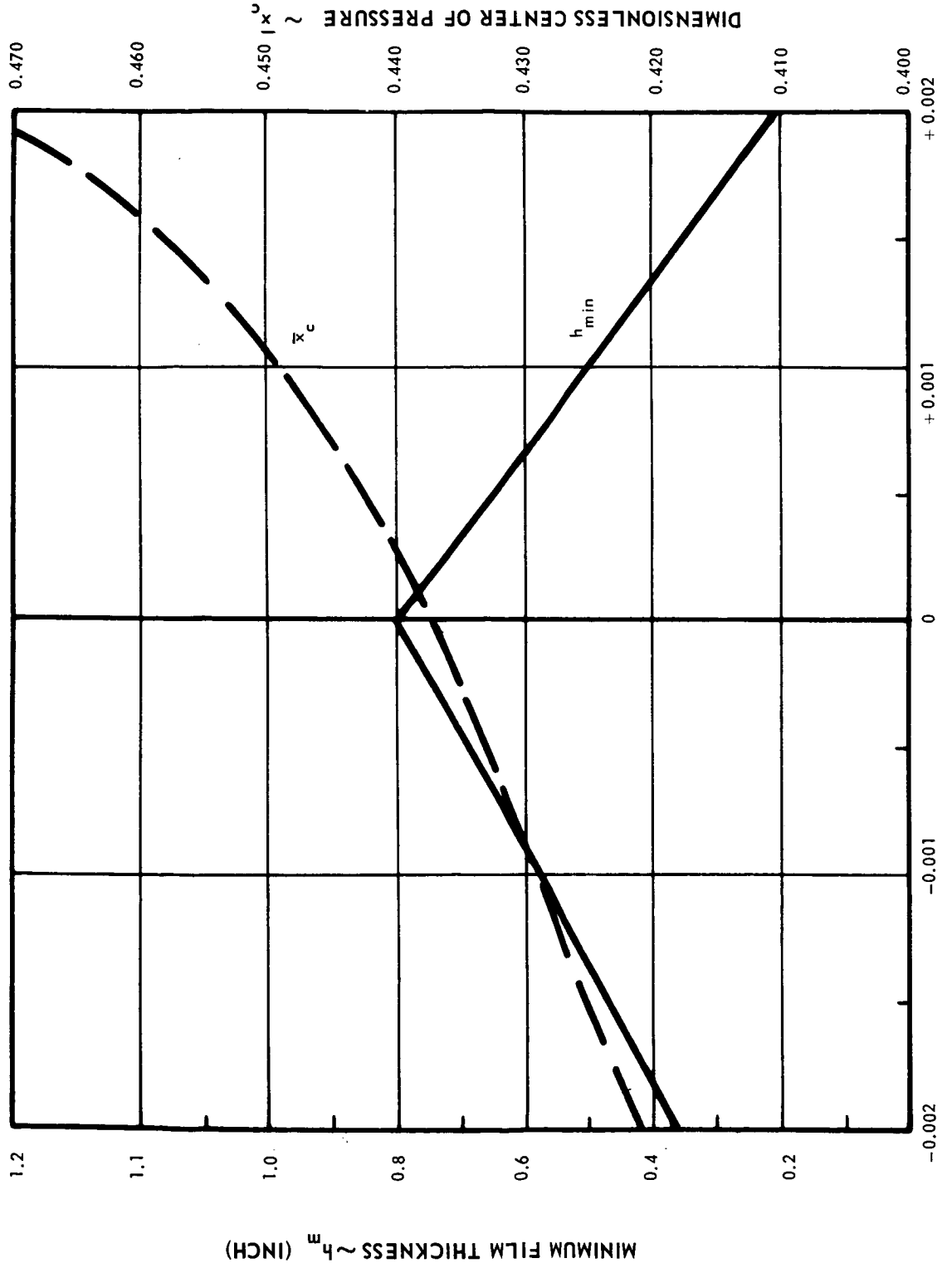

Figure 33 Minimum Film Thickness and Center of Pressure for the Semirigid Interstage Seal at Idle

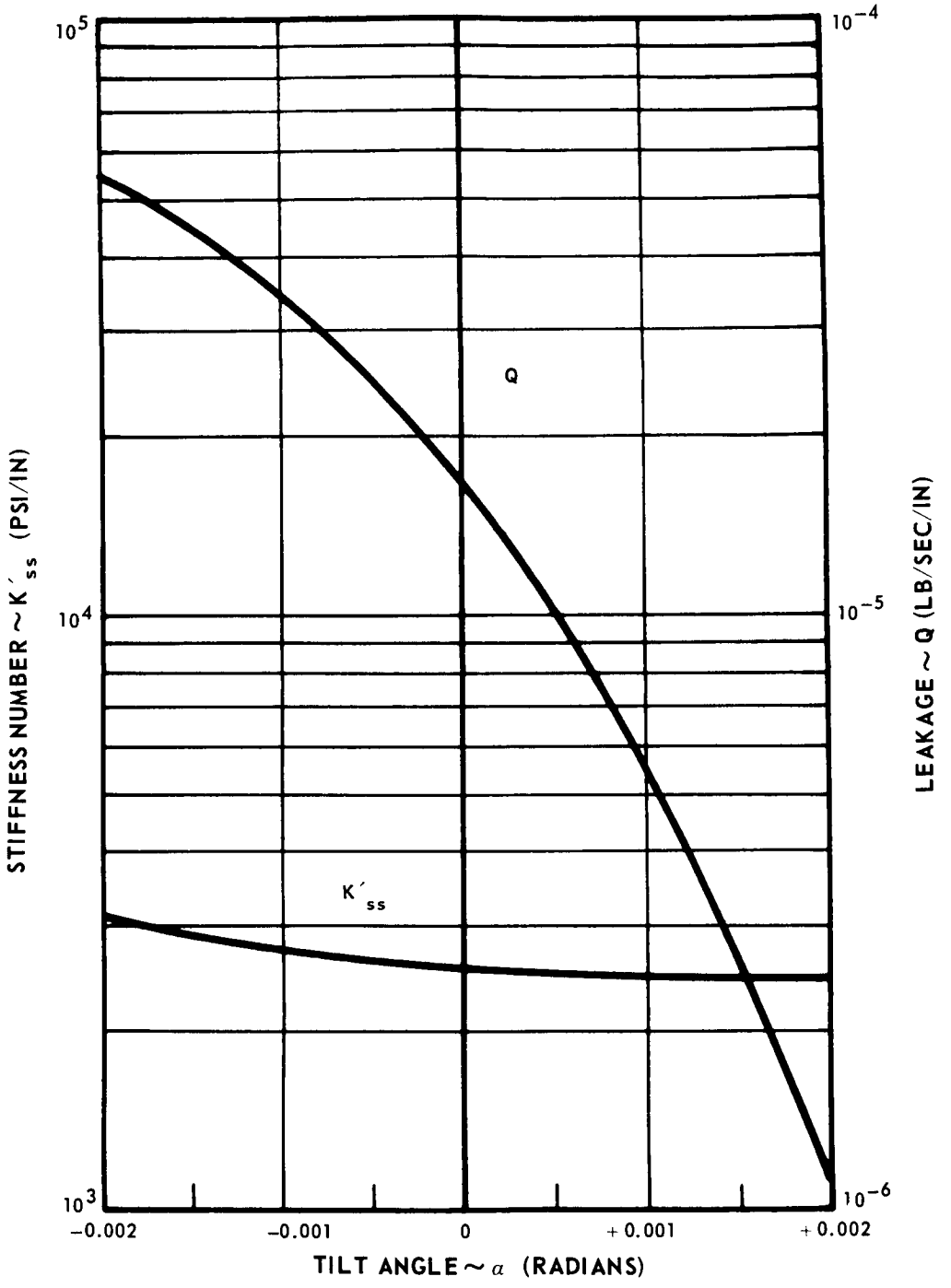

Figure 34 Leakage and Stiffness of the Semirigid Interstage Seal at Idle

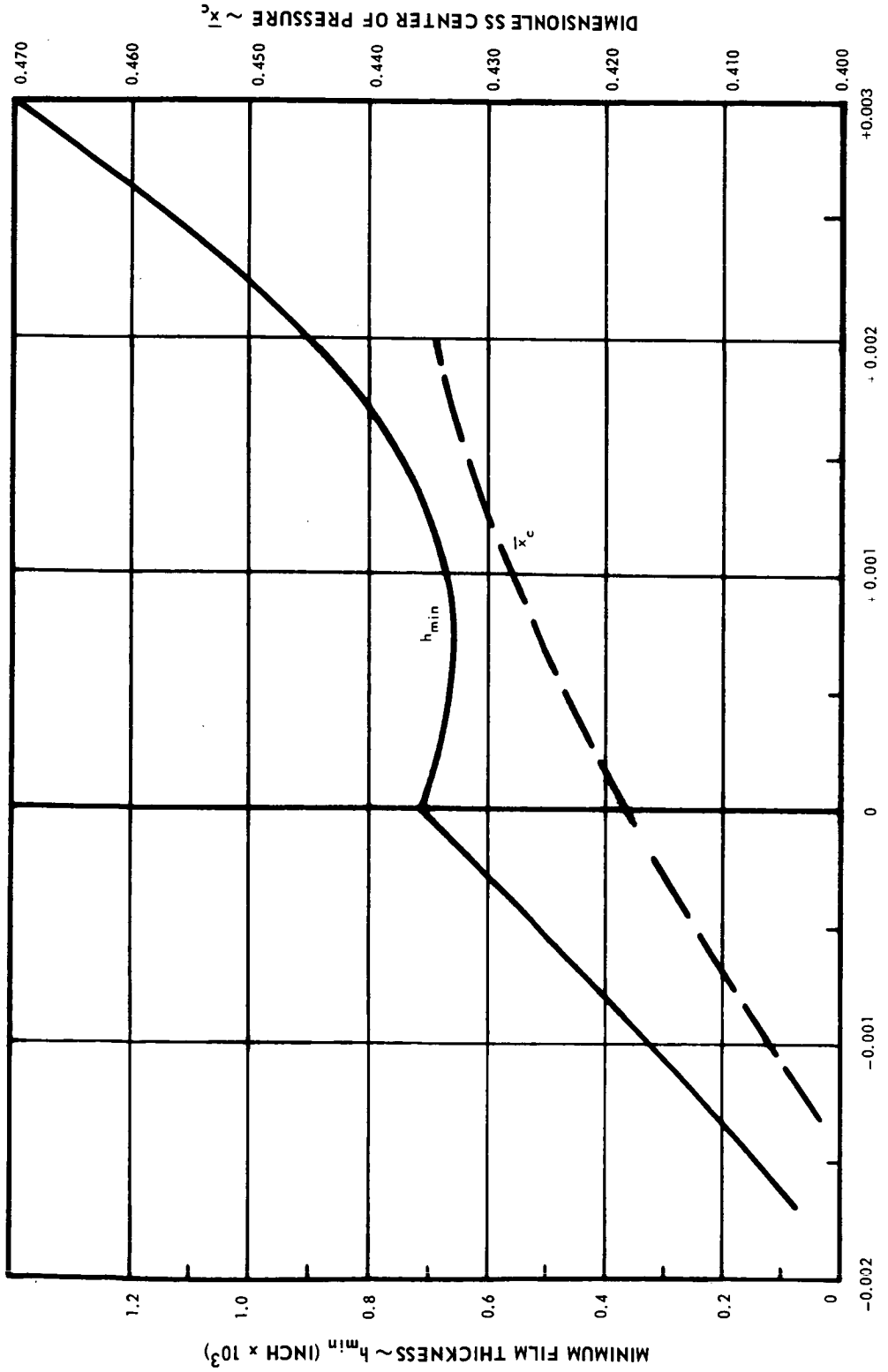

Figure 35 Minimum Film Thickness and Center of Pressure for the Semirigid Interstage Seal at Take-Off

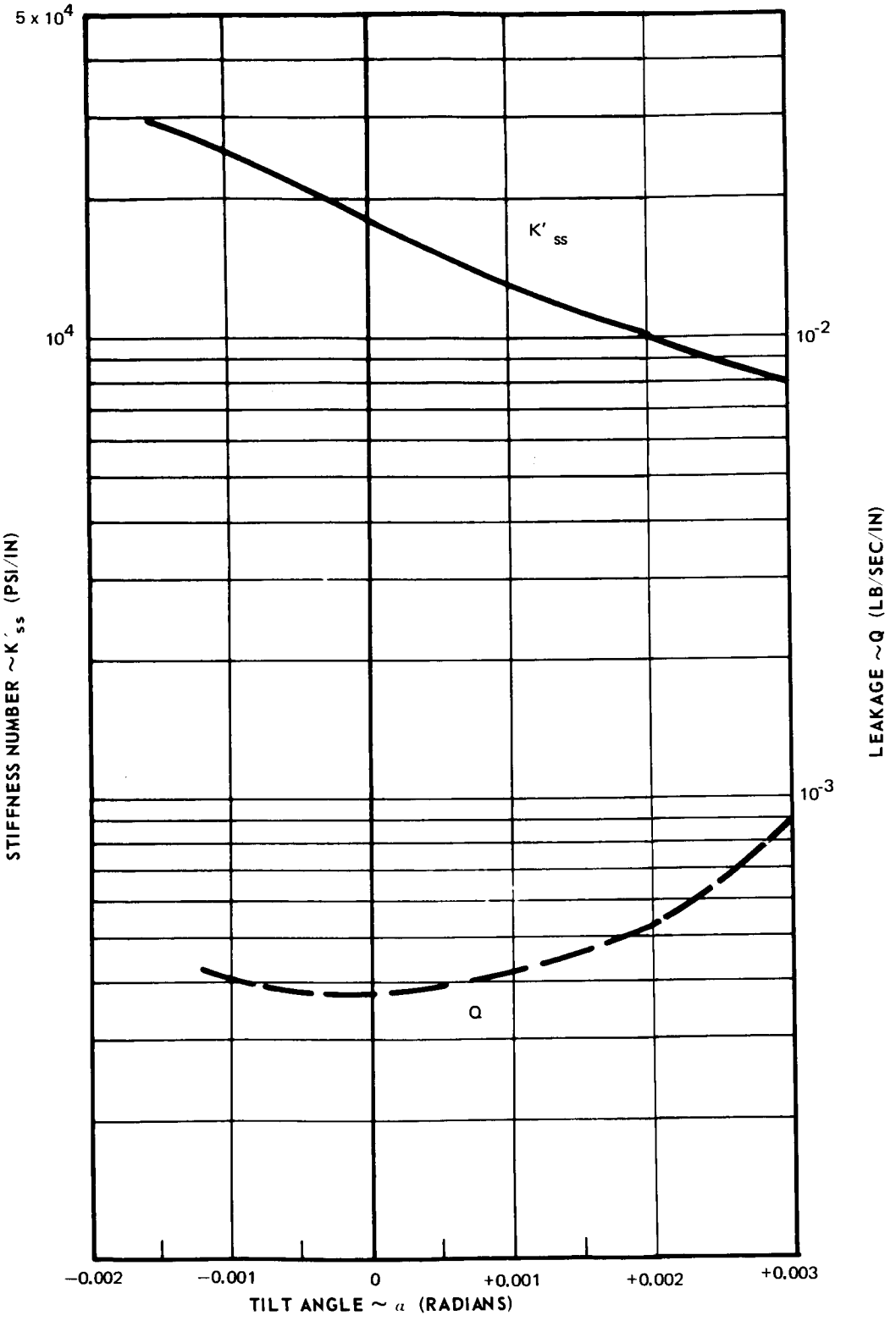

Figure 36 Leakage and Stiffness of the Semirigid Interstage Seal at Take-Off

(3) Leakage Flow

As shown in Figure 32, the leakage flow at cruise actually decreases at positive tilt angles. At take-off (Figure 36), the flow slightly increases as a function of tilt angle, but the over-all leakage magnitude is still of the order of 0.07 lb/sec. at 0.003 radians. At idle (Figure 34), the decrease in leakage at positive tilt is very pronounced, although at these conditions the over-all leakage magnitude is extremely low and has no bearing upon the seal-design requirements.

(4) Static Performance

Summarizing, the static seal performance of the semirigid configuration is quite satisfactory over a range of positive tilt angles of 0 to 0.003 radians at cruise and take-off conditions. At idle (in particular for the interstage seal) the tilt angle tolerance is severely affected, but tilt due to thermal gradients at these conditions is expected to be low during actual operation due to low speed and low ambient temperature levels.

6. TEMPERATURE DISTRIBUTION AND DISTORTIONS IN THE SEMIRIGID INTERSTAGE SEAL

a. THERMAL GRADIENTS

The interstage seal is more prone to the development of axial thermal gradients than the end stage seal because of lower film thickness and larger seal diameters, which contribute to higher heat generation; and lower pressure differentials, resulting in low leakage flow, and hence less heat carried away by the air. Because of these reasons, the thermal analysis performed on the interstage seal was formulated with more attention to detail than that for the end seal. Thus, the number of nodes was increased, and the effect of orifice air supply passages, and turbulence in the outer diameter 0.060 inch recess region at the entrance to the seal face, normally neglected in the end stage analysis, were included in the analysis of the interstage seal.

The nodal point distribution with adjacent subvolumes is shown in Figure 40 together with the surface coefficient values at the seal boundaries. The final temperature distribution obtained is shown in Figure 38. All thermal calculations are summarized in Appendix D.

Although, as expected, the over-all temperature levels are higher than those obtained on the end seal, the actual thermal gradients contributing to seal ring tilt are not appreciably different.

b. THERMAL DISTORTIONS

As previously indicated, the semirigid seal is sensitive to distortion-producing thermal gradients. This sensitivity is vividly demonstrated by the differences in the thermal distortions obtained on the end and interstage seals.

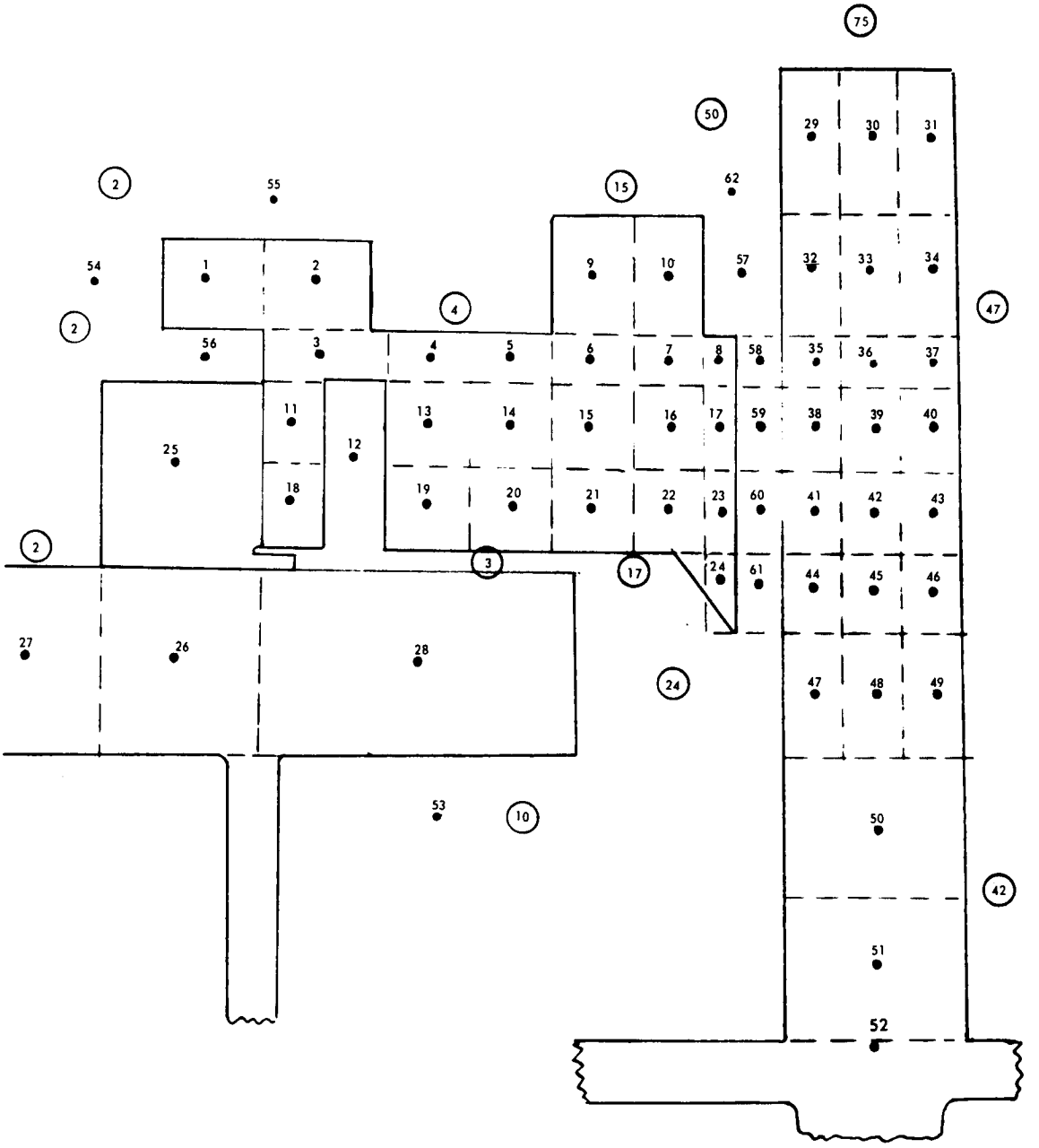

Figure 37 Diagram of Nodal Points and Subvolumes for Thermal Analysis of the Semirigid Interstage Seal

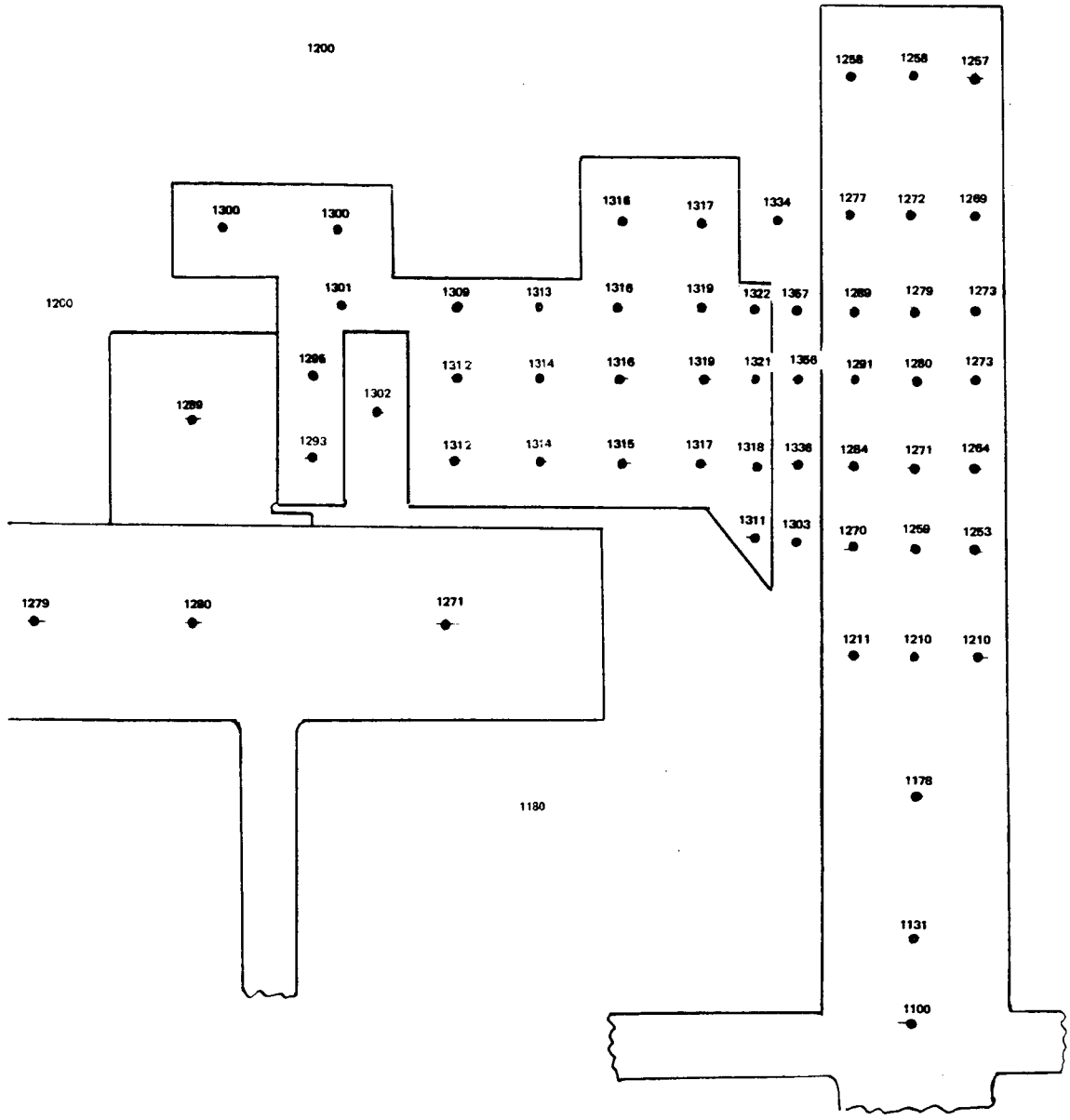

Figure 38 Temperature Distribution (in °F) in the Semirigid Interstage Seal

The end seal thermal analysis was based upon laminar conditions existing in the originally assumed 0.020-inch clearance between the upper portion of the seal ring and the runner. In the interstage thermal analysis, the calculated turbulent heat generation in the increased (0.060-inch) gap was included. The effect of this turbulence is important, inasmuch as it raises the temperature difference between the average upper seal ring addition and the lower main ring. This fact negates some of the restraining action of the upper seal ring on over-all ring tilt resulting from the axial thermal gradients.

The calculations of thermal deformation of the semirigid interstage seal are given in Appendix F. The results indicate a seal face tilt of 0.00343 radian for the interstage seal. The increase in deformation in the interstage seal can be attributed to the additional heat input in the 0.060-inch gap, as well as to the difference in operating conditions. Further substantial increases in the 0.060-inch gap to reduce the heat generation are subject to physical limitations, and increases of a smaller order of magnitude, such as doubling the original clearance value of 0.060-inch does not offer any appreciable decrease in heat generation.

7. TRACKING ANALYSIS

The general approach to the semirigid seal tracking analysis is the same as that for the OC diaphragm seal. Thus, for symbol definition and analytical details the reader referred back to Section IB of this report. The analysis of the semirigid seal was performed using the inputs shown in Table XII.

TABLE XII

INPUT DISTORTIONS USED IN THE TRACKING ANALYSIS OF THE SEMIRIGID END AND INTERSTAGE SEALS

	Mode Number n	δ (inches)	ϵ_n (radians)	ζ (radians)
Cruise	0	0	0	0.003
	1	0.0015	-0.00011	-
	2	0.0005	-0.000037	-
Idle	0	0	0	0.0004
	1	0.0015	-0.00011	-
	2	0.0005	-0.000037	-
Take-Off	0	0	0	0.003
	1	0.0015	-0.00011	-
	2	0.0005	-0.000037	-

Note that, in line with the conclusions arrived at in the thermal distortion analysis, a tilt angle (α) of 0.003 radian was assumed at both cruise and take-off conditions in the calculations of air-film thicknesses. At idle, where the likelihood of severe thermal gradients is greatly reduced, the air film characteristics were taken at a tilt angle of 0.0004 radian.

The influence coefficients are listed in Table XIII, and final tracking results are given in Table XIV. As in the OC diaphragm seal tracking analysis, separate values of minimum film thickness are given for the n = 0, n = 1, and n = 2 conditions. The minimum film thickness values for n = 0 were obtained from Figures 31, 33, and 35. It is then assumed that all minimum film thickness losses are in phase and thus directly additive, yielding the combined worst-case minimum film thickness shown.

Due to the positive tilt, at high pressure differentials such as the ones encountered at take-off conditions, the minimum film thickness actually increases over the original parallel film thickness. For lower pressure differentials, appreciable film losses can be noted. The idle condition in particular, where the pressure differential across the seal is only 2 psi indicates a 58 percent loss in film thickness in the minimum film thickness area. In general, however, considering the conservative assumptions used, the tracking characteristics of the semirigid seal are quite satisfactory.

TABLE XIII

INFLUENCE COEFFICIENTS FOR THE TRACKING ANALYSIS OF THE SEMIRIGID INTERSTAGE SEAL

Condition	n	C_{A1}	C_{A2}	C_{B1}	C_{B2}	C_{u1}	C_{u2}	C_{v1}	C_{v2}
	0	0.0052	0.0	0.9948	0.0	0.4434	1.0000	-0.4434	0.0
Cruise	1	-9,0164	-0.0458	1.0126	0.0372	0.4987	1.1267	-0.4499	-0.0166
	2	-0.0603	-0.1417	1.0325	0.0785	0.7012	1.5881	-0.4333	0.0186
	0	0.0019	0.0	0.9980	0.0	-0.0784	1.0000	0.0784	0.0
Idle	1	0.0045	-0.0385	0.9956	0.0366	-0.0815	1.0307	0.0789	0.0029
	2	0.0078	-0.0872	0.9932	0.0752	-0.0850	1.0630	0.0745	0.0683
	0	0.4756	0.0	0.5244	0.0	0.2996	1.0000	-0.2996	0.0
Take Off	1	0.3958	-0.0253	0.6034	0.0222	0.2954	1.0457	-0.2854	-0.0105
	2	0.2576	-0.0738	0.7384	0.0579	0.2911	1.1153	-0.2522	0.0016

TABLE XIV

SEMIRIGID INTERSTAGE SEAL TRACKING RESULTS

	Mode Number n	α, radians	Mean Film Thickness h_m	Minimum Film Thickness h_{min}	Total Minimum Film Thickness h_{Tmin}
Cruise	0	0.003	0.00102	0.000850	0.00041
	1			0.000851	
	2			0.000713	
Idle	0	0.0004	0.00080	0.000700	0.00049
	1			0.00075	
	2			0.00064	
Take Off	0	0.003	0.00079	0.001400	0.00126
	1			0.000736	
	2			0.000708	

PRECEDING PAGE BLANK NOT FILMED.

II. TASK II

COMPRESSOR END SEAL AND STATOR INTERSTAGE SEAL EXPERIMENTAL EVALUATION

A. INTRODUCTION

This phase of the program provides for final design and procurement of compressor end seals and stator interstage seals, design and fabrication of a test rig, and experimental evaluation of the compressor seals.

The final design of the four compressor seal concepts selected for experimental evaluation includes all calculations, material determinations, analyses, and drawings necessary for seal optimization, procurement and experimental evaluation. A test rig will be designed and fabricated to evaluate the selected compressor end seals and stator interstage seals under simulated compressor operating conditions. The test apparatus will simulate the last stages of a full-scale compressor including supporting members and bearing system in order to faithfully duplicate structural flexibility and thermal gradients.

The compressor end seals and stator interstage seals will be calibrated in incremental steps at room-temperature static conditions, room-temperature dynamic conditions, and subsequently over the full speed, pressure, and temperature operating ranges. The seals will then be subjected to endurance testing and finally will undergo a take-off and cruise cyclic test.

Final design layouts and detailed drawings have been completed for the one-side floated-shoe end and interstage seals and for the full-scale test rig in which the seals will undergo experimental evaluation. Hardware procurement is progressing for each of the above items.

B. ONE-SIDE FLOATED-SHOE SEAL

The fourth semi-annual progress report (Reference 7) contained a general review of the progress made in the design and manufacture of the floated-shoe seal configuration. The results of the primary gas film calculations using the triple-pad version of the shrouded Rayleigh Step Bearing computer program were presented in Tables XX and XXI of Reference 7. During the past month these calculations have been expanded, and the results are plotted in Figures 39 and 40 for end and interstage seals. The figures illustrate the effect of spring load on the design point dimensionless load capacity and film thickness. A final tabulation of end and interstage seal design point gas film characteristics is presented in Table XV. The values represent the ideal parallel film situation and the effects of thermal distortion or seal plate runout on the gas film characteristics have not been considered.

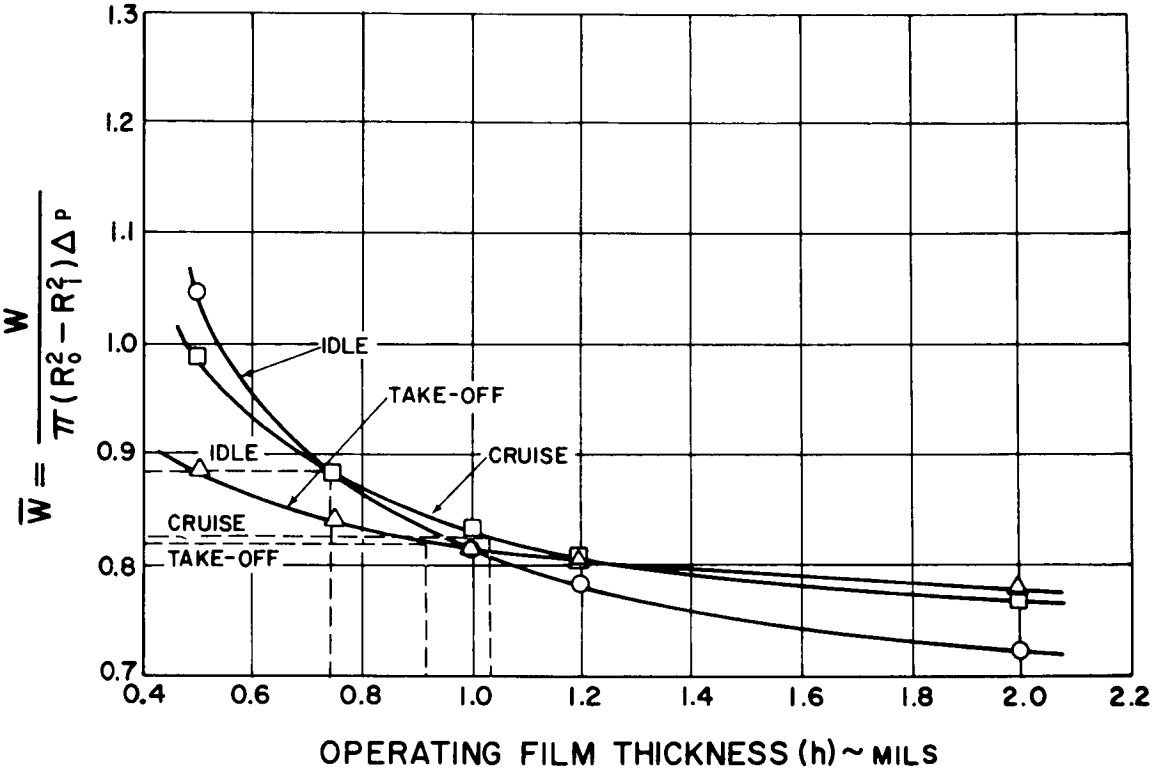

Figure 39 One-Side Floated-Shoe End Seal Gas Film Calculation

1. ONE-SIDE FLOATED-SHOE END SEAL

Most of the recent work on the end seal has consisted of procurement and fabrication of parts and instrumentation. At the end of December, 1967, all small parts, such as pins, springs, cups, etc. were completed and ready for assembly. The seal ring, seal-ring support, and piston rings were ready for finish machining, and the sealing shoes were ready for final machining.

TABLE XV

DESIGN POINT GAS FILM CHARACTERISTICS

End Seal, One Side Floated Shoe

	Idle	Cruise	Take Off
Applied Pressure (psia)	33	100	170
Back Pressure (psia)	20	20	20
Air Temperature (psia)	200	1200	680
Mean Radius* (Inches)	13.620	13.725	13.669
Primary Film Thickness (Mils)	0.75	1.03	0.92
Secondary Film Thickness (Mils)	0.36	0.5	0.55
Seal Leakage (lb/sec)			
Primary	0.003	0.020	0.083
Secondary (4 Seals)	0.011	0.047	0.335
Shoe Gap	0.010	0.039	0.080
Total	0.024	0.106	0.498
Primary Film Stiffness (lb/in)	209663	457054	566839

*The Room Temperature Mean Radius is 13.6 Inches

Interstage Seal, One Side Floated Shoe

	Idle	Cruise	Take Off
Applied Pressure (psia)	33	100	170
Back Pressure (psia)	31	75	120
Air Temperature (°F)	200	1200	680
Mean Radius* (Inches)	14.309	14.419	14.360
Primary Film Thickness (Mils)	0.99	1.03	0.725
Secondary Film Thickness (Mils)	0.36	0.40	0.42
Seal Leakage (lb/sec)			
Primary	0.006	0.009	0.020
Secondary (4 Seals)	0.007	0.015	0.099
Shoe Gap	0.002	0.016	0.031
Total	0.015	0.040	0.149
Primary Film Stiffness (lb/in)	107887	358764	645119

*The Room Temperature Mean Radius is 14.288 Inches

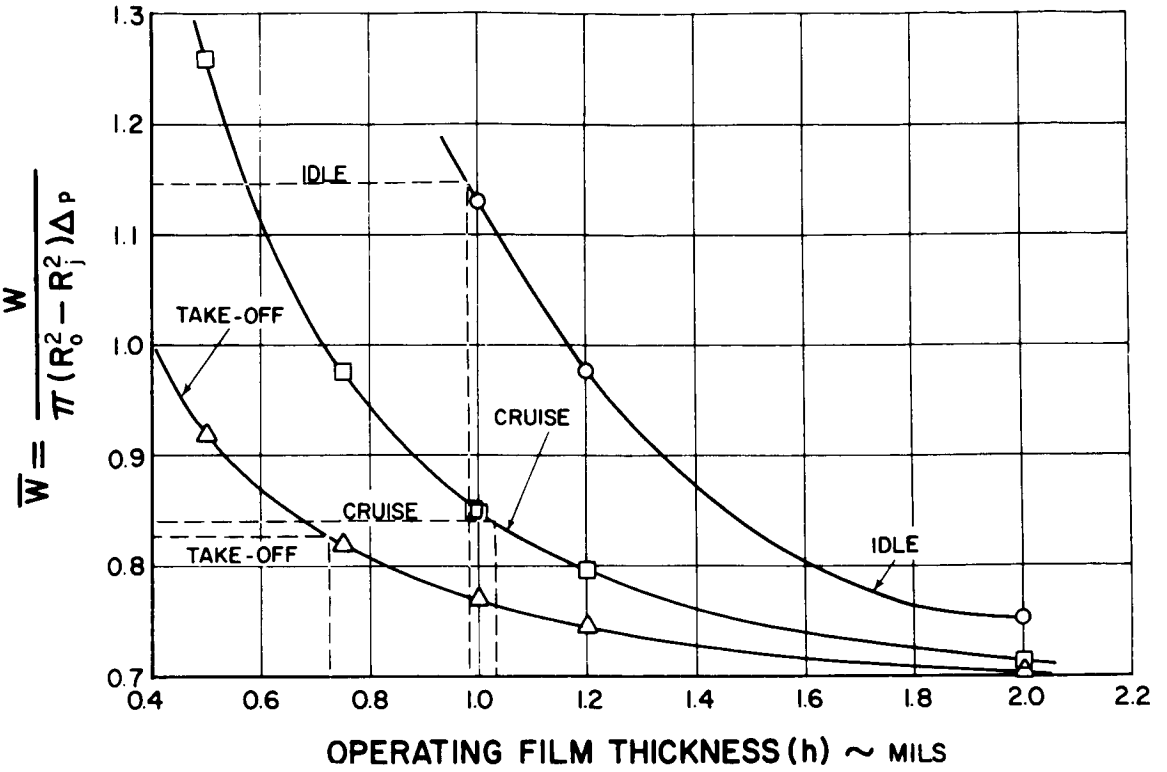

Figure 40 One-Side Floated-Shoe Interstage Seal Gas Film Calculation

The contractor has decided to use capacitance proximity probes for measuring film thickness. These probes will be embedded in two shoes 90 degrees apart. Six probes are now on order. A shoulder on the probe will be electron-beam welded to the rear of the floated seal shoe. The rear side of the shoe will have a counterbore to accept the shoulder on the probe. A high-temperature ceramic cement will fill the 0.030-inch radial clearance between the body of the probe and the cavity in the shoe. The utility of the probe will, however, be limited by the temperature limits on the electrical insulation of the probe's coaxial cable.

Pressure probes will consist of coiled stainless steel tubing fastened to the sealing shoe by a suitable connecting element, which will be electron-beam welded to the shoe. Sample parts are now being made up to test the feasibility of this connection and to test the effects of thermal growth and thermal cycling on the very small welds. This type of probe will provide almost pin-point pressure data, an advantage not provided by the relatively large area of the dynamic pressure transducers.

2. ONE-SIDE FLOATED-SHOE/INTERSTAGE SEAL

Pratt & Whitney Aircraft has completed a detailed thermal analysis of the one-side floated-shoe interstage seal. This analysis includes the heat-transfer effects of the primary and secondary leakage air and a more accurate determination of the convection and conduction paths within the seal parts, than had been available for the preliminary analysis. The results of this analysis are presented in the thermal map shown in Figure 41. It appears from the map that the temperature gradient across the seal carrier will be on the order of 100

degrees Fahrenheit, which is considered excessive. To reduce this gradient, the contractor is considering the use of a heat shield. The shield would provide a more nearly uniform seal temperature by keeping the 800-degree Fahrenheit cooling air for the disk from coming in contact with the interstage seal parts.

The more sophisticated methods to be used in the final thermal analysis are being incorporated in the TOSS computer program. These changes include a more accurate method of determining the thermal effects of leakage air and an improved method of determining conduction paths.

Fabrication of parts and instrumentation has started. At the end of December, 1967, the vendor was preparing to rough machine the large rings for the seal ring, seal-ring support, and piston rings. Instrumentation will be the same as that for the one-side floated-shoe end seal, although modifications may be made when the contractor has gained more experience with the end seal.

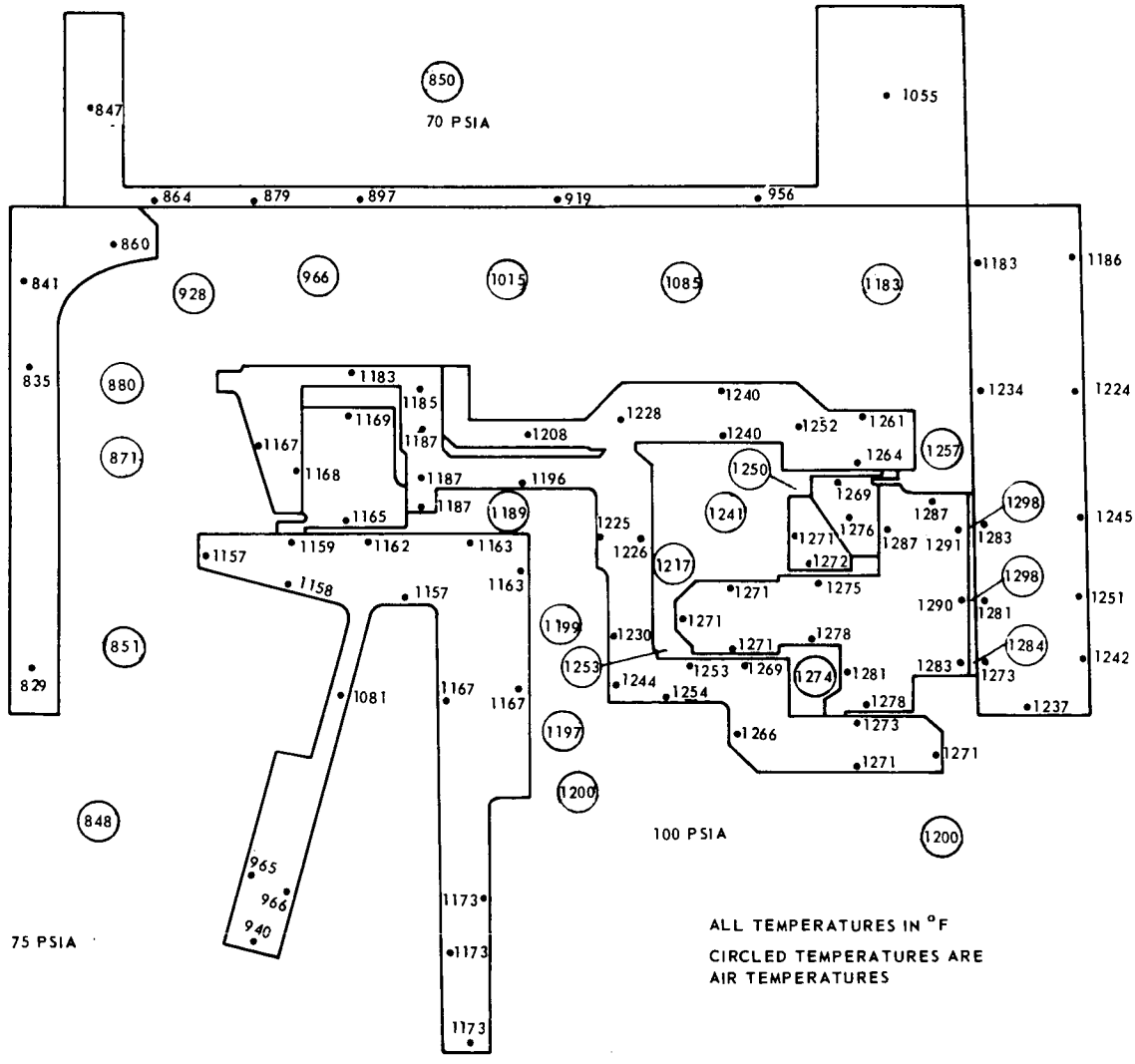

Figure 41 Thermal Map of the One-Side Floated-Shoe Interstage Seal at Cruise Conditions

C. OC DIAPHRAGM END SEAL AND SEMIRIGID INTERSTAGE SEAL

NASA approved both the OC diaphragm end seal and the semi-rigid interstage seal for investigation under Task II in November, 1967. Detailing of the OC diaphragm end seal has been completed, and the drawings are being checked before release. Detailing of the semi-rigid interstage seal is still in process. However, the results of the tracking analyses of these seals are still preliminary in nature.

1. MODIFICATION OF THE CROSS SECTION

The semi-rigid seal cross-section is shown in Figure 42 in its final configuration. The changes included further widening of the thermal barrier to reduce the axial temperature gradient of the seal and the redistributing of the mass to keep the centroid at the original position. The position of the centroid is important because it could affect the mechanically induced distortions.

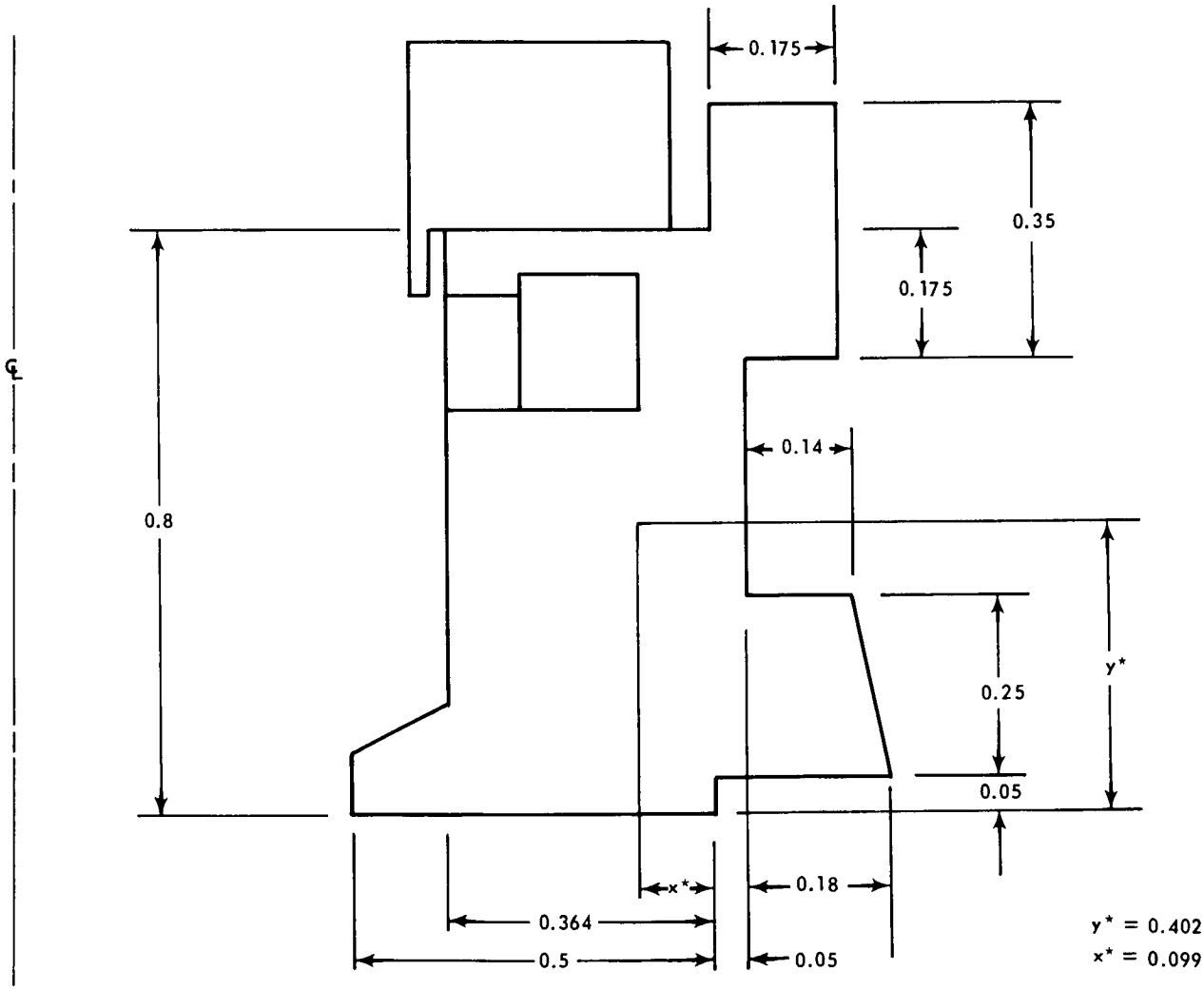

Figure 42 Semirigid Interstage Seal

2. THERMOELASTIC ANALYSIS OF SEMI-RIGID INTERSTAGE SEAL

Thermally induced distortions on the semi-rigid interstage seal were formulated with a thermoelastic finite element computer program (Reference 10). The temperature distribution is basically the same as the one shown in Figure 38 but it was redistributed to account for the new geometry. Figure 43 shows the results of the analysis and gives axial and radial displacement for certain selected points. The rotation of the seal face is 0.00337 radians in the direction that creates a converging flow passage with the runner, which agrees with the results (0.00343 radians) discussed in Appendix F. The numbers inside the cross-section indicate the subdivision as it was used in the finite element computer deck. The table lists the temperature for each element.

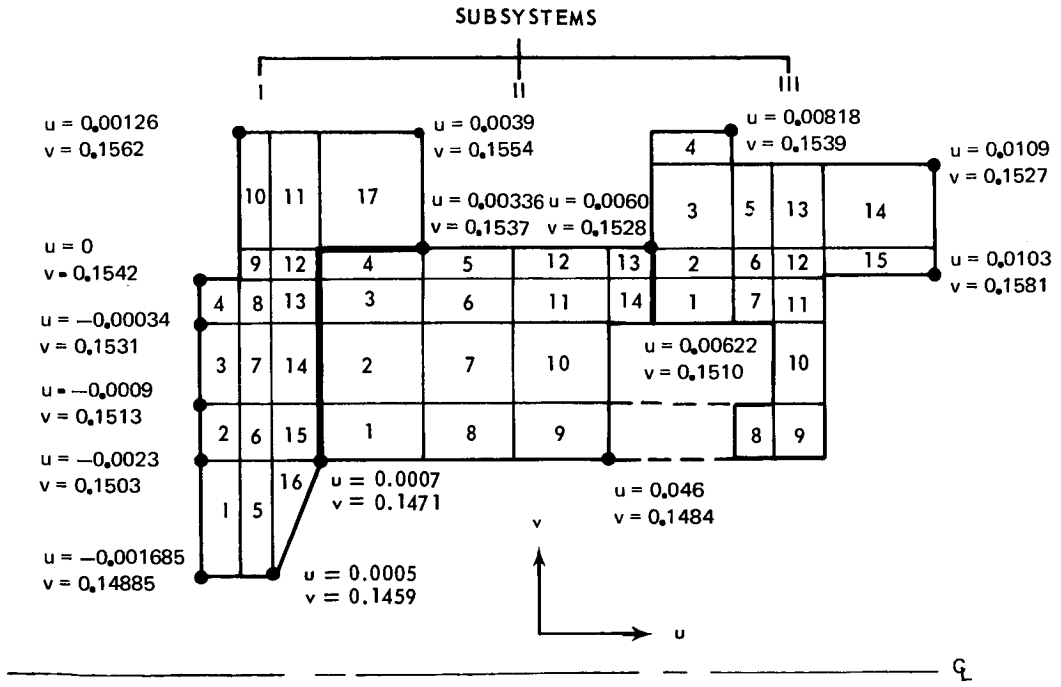

Figure 43 Semirigid Interstage Seal Thermal Deflection

TEMPERATURE DISTRIBUTION (SEMI-RIGID INTERSTAGE)

SUBSYSTEMS

I		II		III	
ELEM	TEMP °F	ELEM	TEMP °F	ELEM	TEMP °F
1	1311	1	1316	1	1300
2	1318	2	1316	2	1301
3	1320	3	1315	3	1300
4	1322	4	1315	4	1300
5	1311	5	1313	5	1300
6	1318	6	1314	6	1301
7	1320	7	1314	7	1300
8	1321	8	1314	8	1290
9	1319	9	1312	9	1291
10	1317	10	1312	10	1293
11	1317	11	1311	11	1295
12	1318	12	1309	12	1300
13	1319	13	1305	13	1300
14	1319	14	1301	14	1300
15	1317			15	1300
16	1312				
17	1316				

3. SEMI-RIGID SEAL SUPPORT

Seal support is the name given the structure that serves as the span between the seal ring and the rig case. It functions as a surface on which the secondary seal piston ring rides, and also an attachment for the torque pins and coil springs.

It is imperative that this sealing surface remain parallel (less than 1 milliradian slope) with the centerline. This is complicated by the fact that the pressure forces that act on the structure are large and cause slopes as high as 20 milliradians in some sections of the structure. To keep this large angular distortion from being transmitted to the sealing surface, a thin cylinder was placed in the structure to damp out the angular distortions and allow the sealing surface to remain a true cylinder.

In Figure 44, a sketch of the structure is presented along with curves that describe how the structure behaves when subjected to the pressure loads. It also shows the radial deflections and slopes when the piston ring carrier assembly and runner are in the extended position (no dashed arrows), and shows the deflections and slopes with these parts in the retracted position (with dashed arrows).

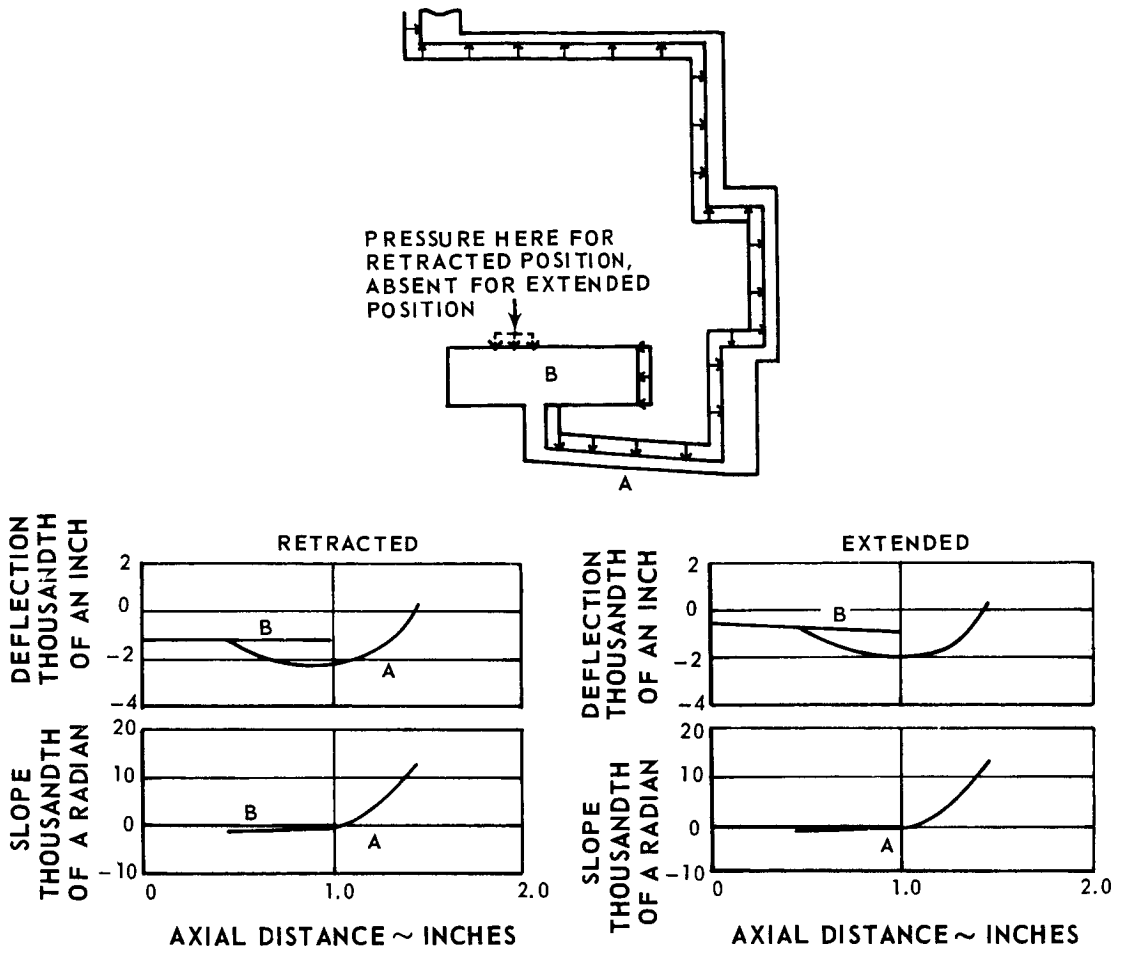

Figure 44 Pressure-Induced Deflections in the Semirigid Interstage Seal. Runner in Retracted and Extended Position.

D. TEST RIG AND TEST STAND

During the past six months, the contractor has been procuring and fabricating the required parts for the test rig and the test stand. All of the parts required to assemble the rotor of the test rig have been received and are being inspected. Three parts will receive some reworking in order to achieve a satisfactory surface finish. Detailed plans for the rotor instrumentation have been completed.

All required instruments and hardware for the test stand are either on order or in-house. The required time for building up the stand has been reduced, since a better stand has become available. The new stand already has many of the service lines for air, water, and electricity in place. A high-capacity fan is installed at one end of the stand, and a vent is installed at the other. An instrument panel is in place, and partially instrumented. The new stand already has double doors, so that phase of the build-up is now unnecessary. The rails for the drive and rig support have been installed in the stand. A remotely controlled hatch has been installed so that outside air can be drawn into the stand for rig cooling. The drive support system, consisting of the stand, engine, transmission, and gearbox has been assembled and is ready for installation in the stand. The ceiling monorails and chainfalls have been installed.

III. TASK III

COMPRESSOR STATOR PIVOT BUSHING AND SEAL CONCEPT FEASIBILITY ANALYSIS

Work performed under Task III was completed in the first year of the project. It is discussed in the first two semiannual reports (PWA-2752 and PWA-2875).

IV. TASK IV

PIVOT BUSHING AND SEAL EXPERIMENTAL EVALUATION

A. INTRODUCTION

This phase of the program provides for final design and procurement of bushings and seals, design and fabrication of a test rig, and experimental evaluation of bushing and seal assemblies.

The final design of the two selected concepts for experimental evaluation includes all calculations, material determinations, analyses, and drawings necessary for pivot bushing and seal optimization, procurement, and experimental evaluation.

A single-vane test rig has been designed and fabricated to evaluate two selected pivot bushing and seal designs under simulated operating conditions for the last compressor stage. The vane and actuating mechanism are applicable to current advanced engine practice.

The pivot bushing and seal assemblies will be calibrated in incremental steps over the full pressure and temperature range, with a maximum pressure of 135 psi and a maximum temperature of 1200 degrees Fahrenheit.

The seals will be subjected to a cyclic endurance run of at least 40 hours duration following a test program which provides for simulation of take-off (20 hours) and cruise (20 hours) conditions typical of advanced engine designs through duplication of:

Compressor stage air temperatures
Supporting structure geometry
Supporting structure temperatures
Pivot movements as required for the vanes
Pivot loading (mechanical loading to simulate air loading is acceptable)
Compressor stage pressure drop

The pivot movement will be a minimum of 13 degrees at 10 cycles per minute. The pivot loading will include a vibratory load at a convenient frequency super-imposed on the steady load and equal to approximately ±15 percent of the steady load.

Final design layouts and detailed drawings have been completed for the single bellows and spherical seat vane pivot seals and for the test rig in which the seals will undergo experimental evaluation. Hardware procurement is complete.

B. DESCRIPTION OF SEALS AND TEST RIG

During the six-month period covered by this report, the Task IV work has largely consisted of hardware procurement and instrumentation. Most of this work has now been completed, and the first test run has been initiated.

Testing to date has been conducted with a single-bellows vane pivot seal in the test rig. A schematic of the seal assembly is shown in Figure 45, and the seal is shown assembled on a simulated vane (rod) in Figure 46. As shown in the photograph, thermocouples were installed to measure the temperature of the seal seat, the base of the simulated vane, and the seal bushing. The seal seat and seal bellows are shown before assembly in Figure 47, and the seal installed in its housing is shown in Figure 48.

The push rod used to transmit the static vane-bending moment and the superimposed vibratory load is shown in Figure 49 with a close-up view of the strain gauge. The strain gauges are installed in a four-arm bridge mounted on a tube 0.042 OD x 0.038 ID to measure the bending load applied to the simulated vane. The gauges are made from Constantan foil with grid size of 0.015 x 0.020 inch. They are accurate within a temperature range of −100 to +400 degrees Fahrenheit. In installation, the push-rod support arm was misaligned so that the rod did not follow the cam properly. This problem was remedied by increasing the inside diameter of the carbon bearing. The vane cycling motor and linkage operated smoothly.

Figures 50 and 51 show the vane actuation link and its strain gauge. Like the gauge on the push rod, this strain gauge is made by the Budd Company, and is accurate within a temperature range of −100 to +400 degrees Fahrenheit. Unlike the other, this gauge is made of nichrome base alloy, and has a grid size of 0.062 x 0.067 inch.

Some difficulties have been encountered in procuring the seal parts. In the case of the spherical-seat seals, some of the test pieces did not conform to specified dimensions for spherical radii. The divergence was significant, and rework was required. In the case of the bellows seals, inspection revealed that the free lengths of some bellows were below the minimum required operating length. In some instances, the squareness of the sealing face also required rework in order to provide a more nearly uniform face loading against the seat. In order to solve these problems and to prevent the recurrence of similar problems, Pratt & Whitney Aircraft has set up a continuing program with both seal vendors to assist them in reoperating the parts to the required tolerances.

As previously mentioned, the first assembly of the test rig included a single-bellows vane pivot seal test configuration. Photographs of the assembly installed in the test stand are shown in Figures 52, 53, and 54. Instruments used include a Brown indicator for temperature readout, two pressure gages to monitor "air-in" pressures to the rig, a capillary flowmeter, and a water monometer to measure the pressure differential across the flowmeter. All of the instruments are standard except the flowmeter, which is a steel "hypodermic" tube, 0.008 inches ID by 20 inches long, brazed into end fittings and supported by an external shell. The laminar air flow through the tube is linear to the pressure drop across the length. The flowmeter was designed and calibrated for the operating pressure range and the anticipated air loss through the test seals.

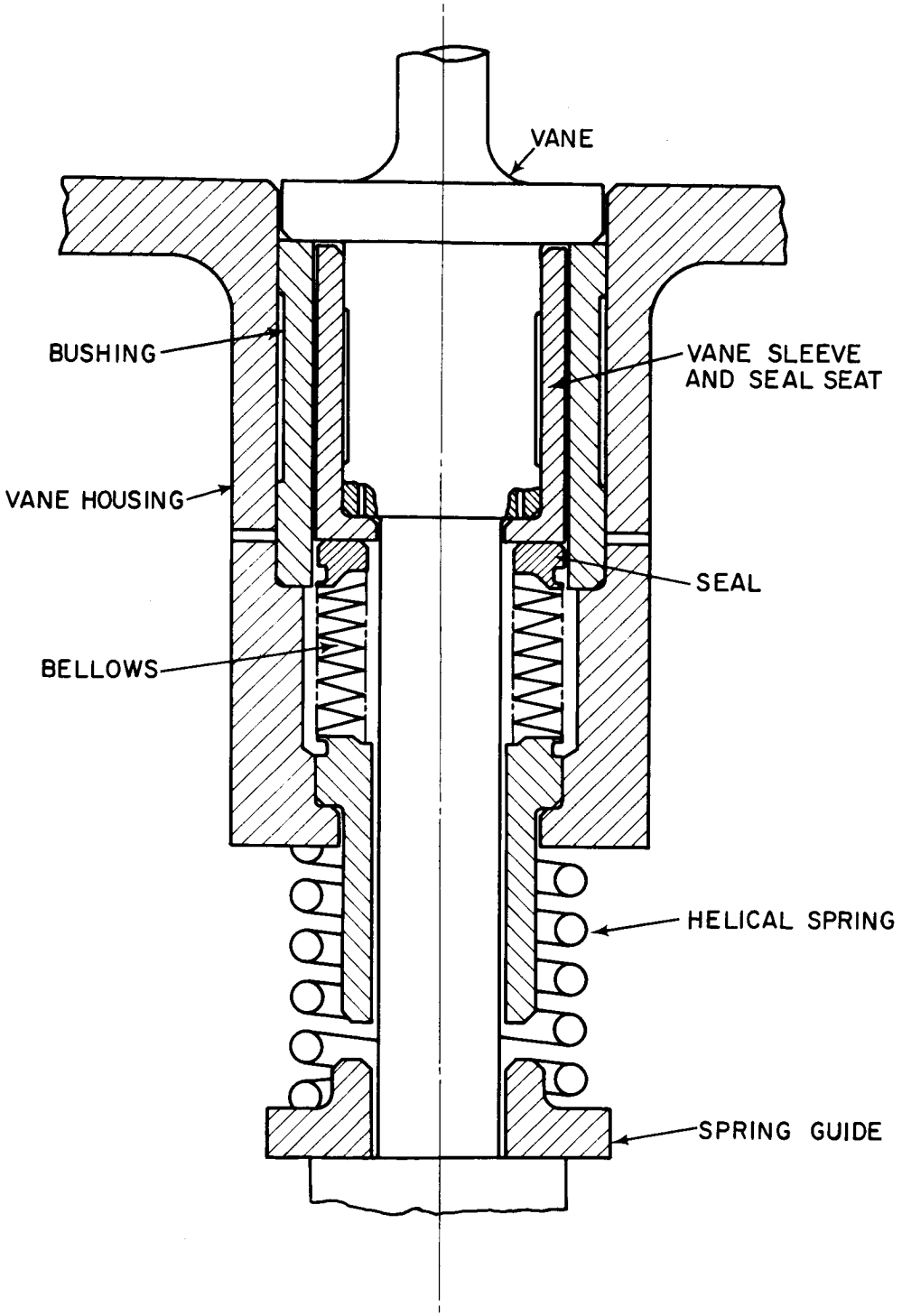

Figure 45 Single-Bellows Vane Pivot Seal

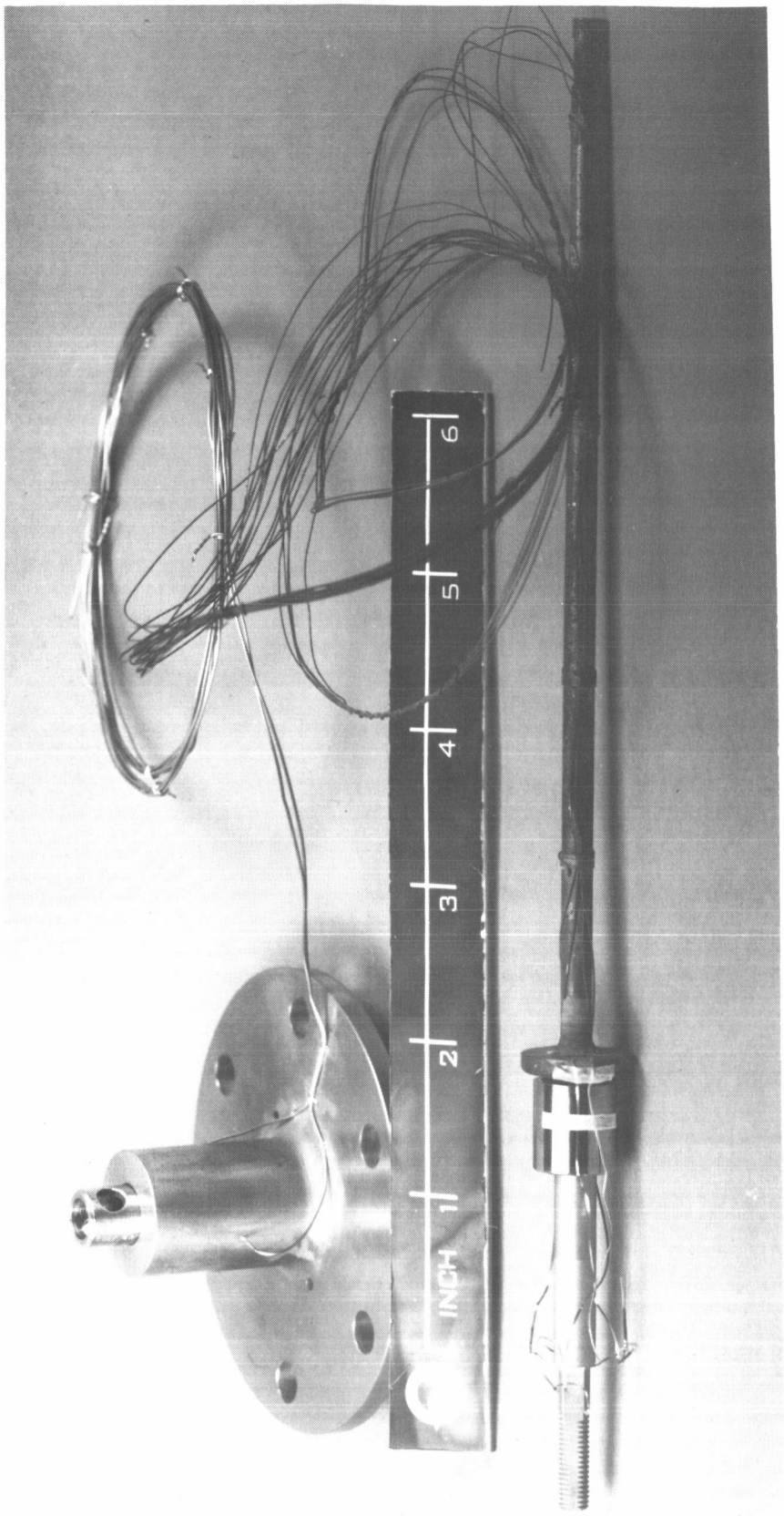

Figure 46 Instrumentation on Single-Bellows Vane Pivot Seal (XP-80138)

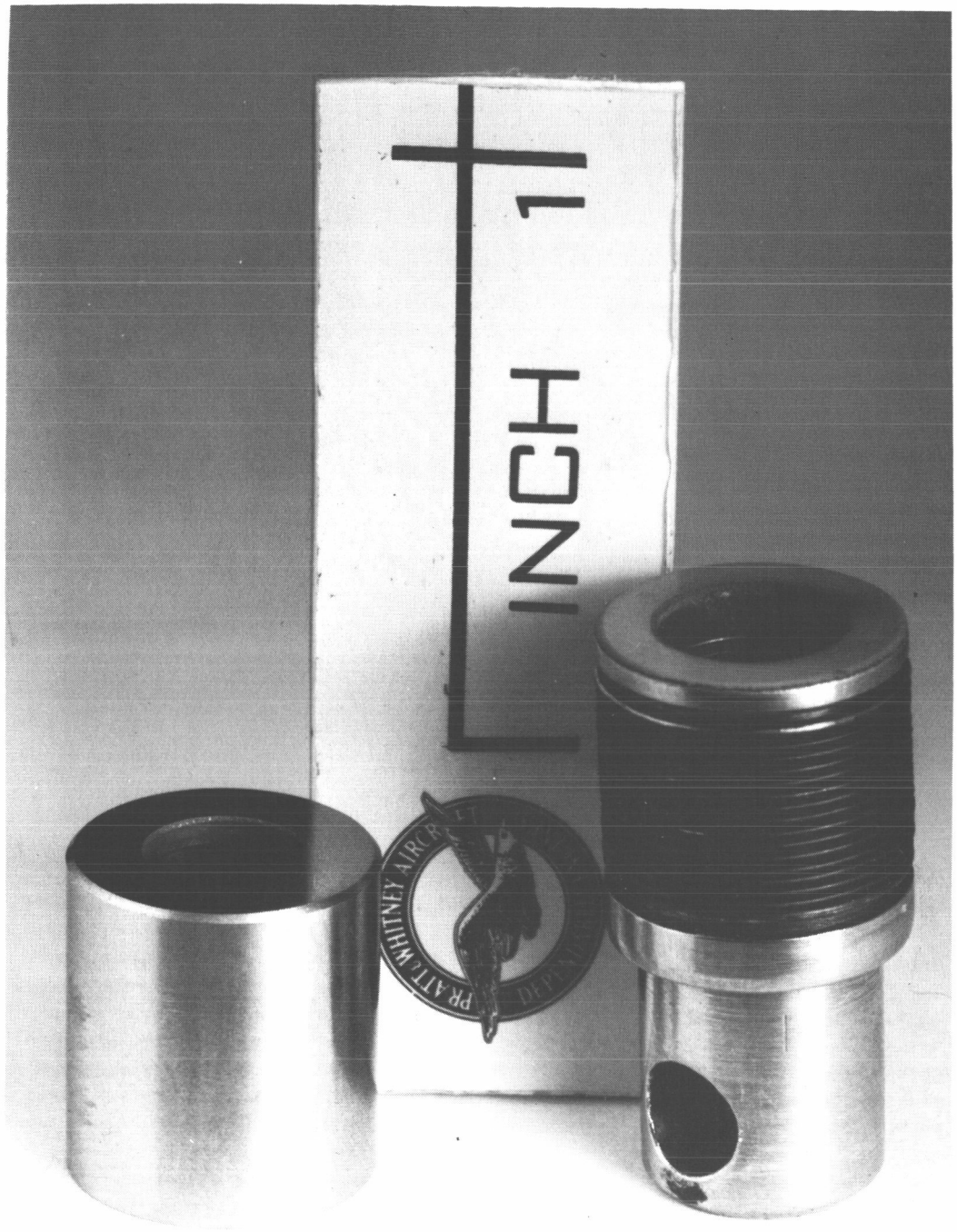

Figure 47 Seal (Left) for Single-Bellows Vane Pivot Seal, and Bellows (Right) (XP-79777)

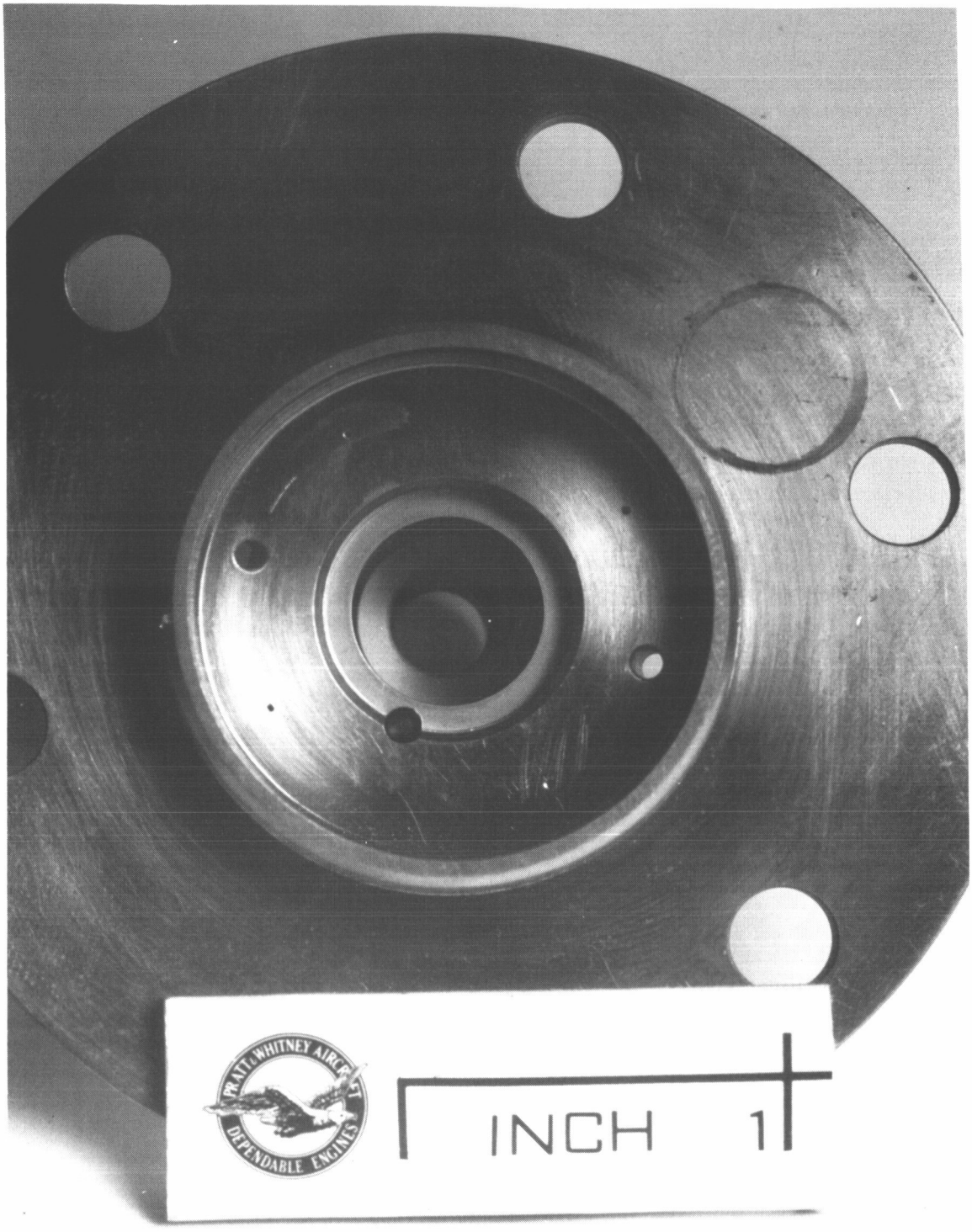

Figure 48 Seal Housing with Bellows Seal Installed (XP-80136)

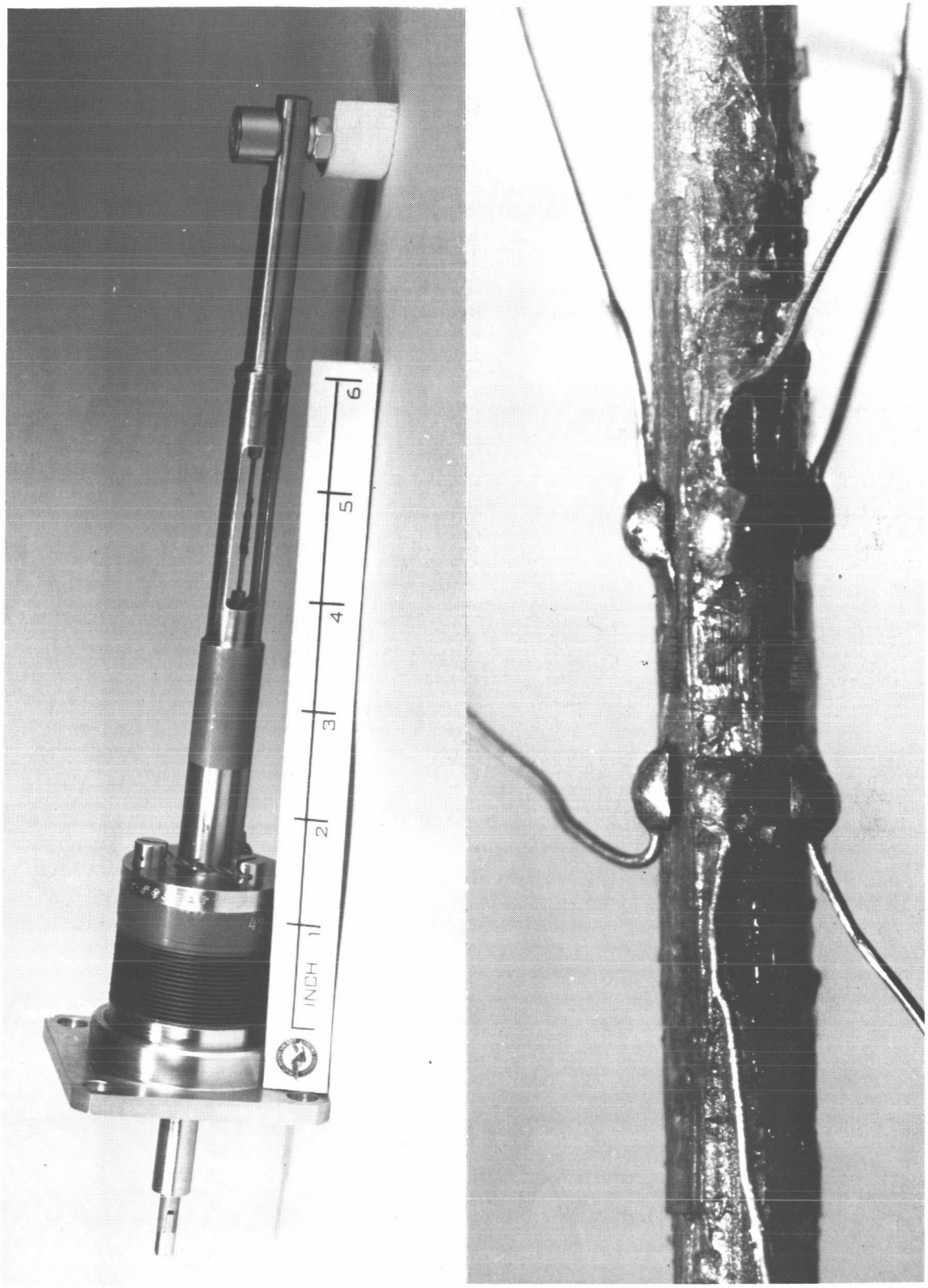

Figure 49 Push Rod and 25X View of Strain Gauge (XP-78644, XP-80223)

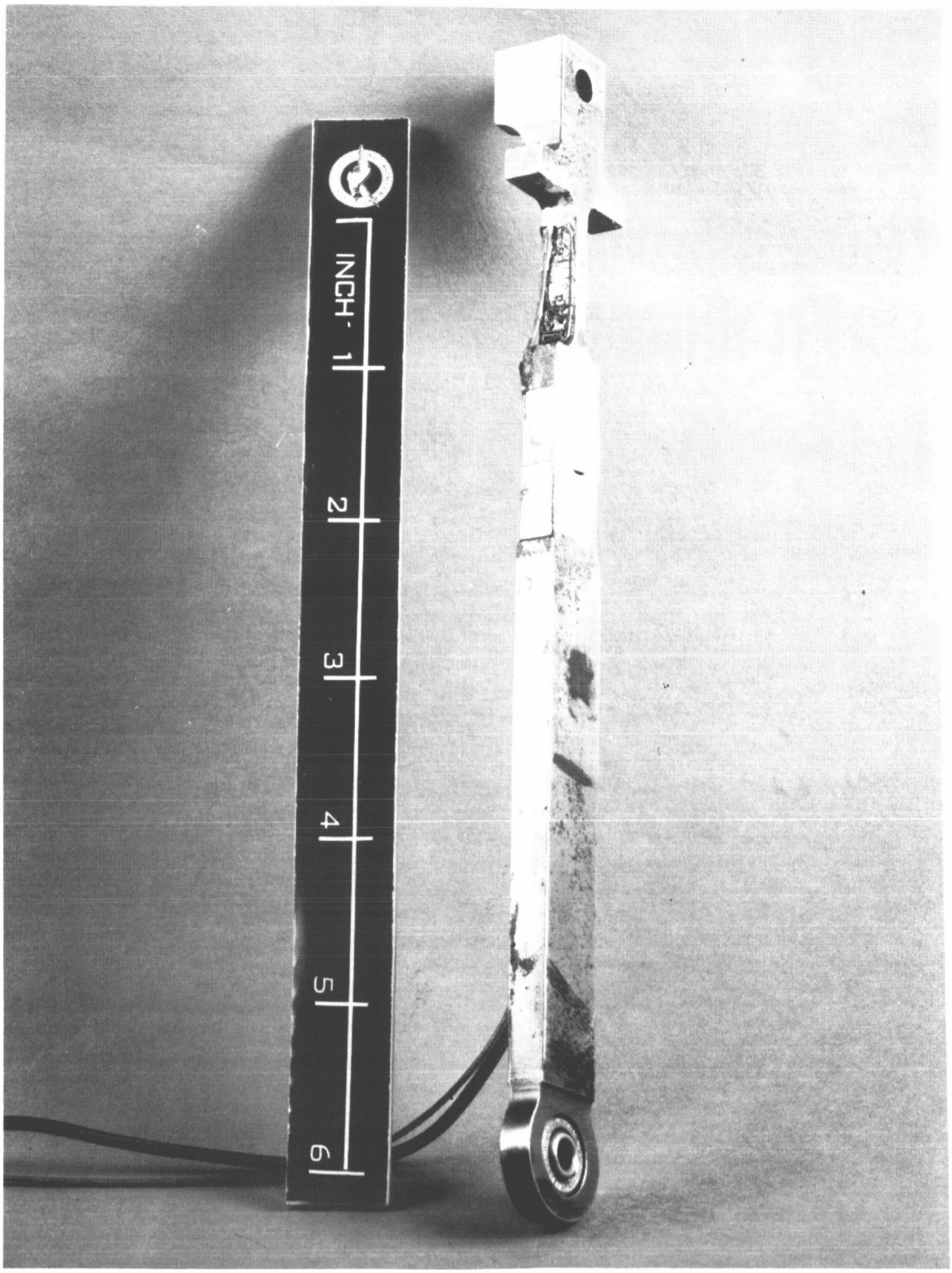

Figure 50 Vane Actuation Link (XP-80487)

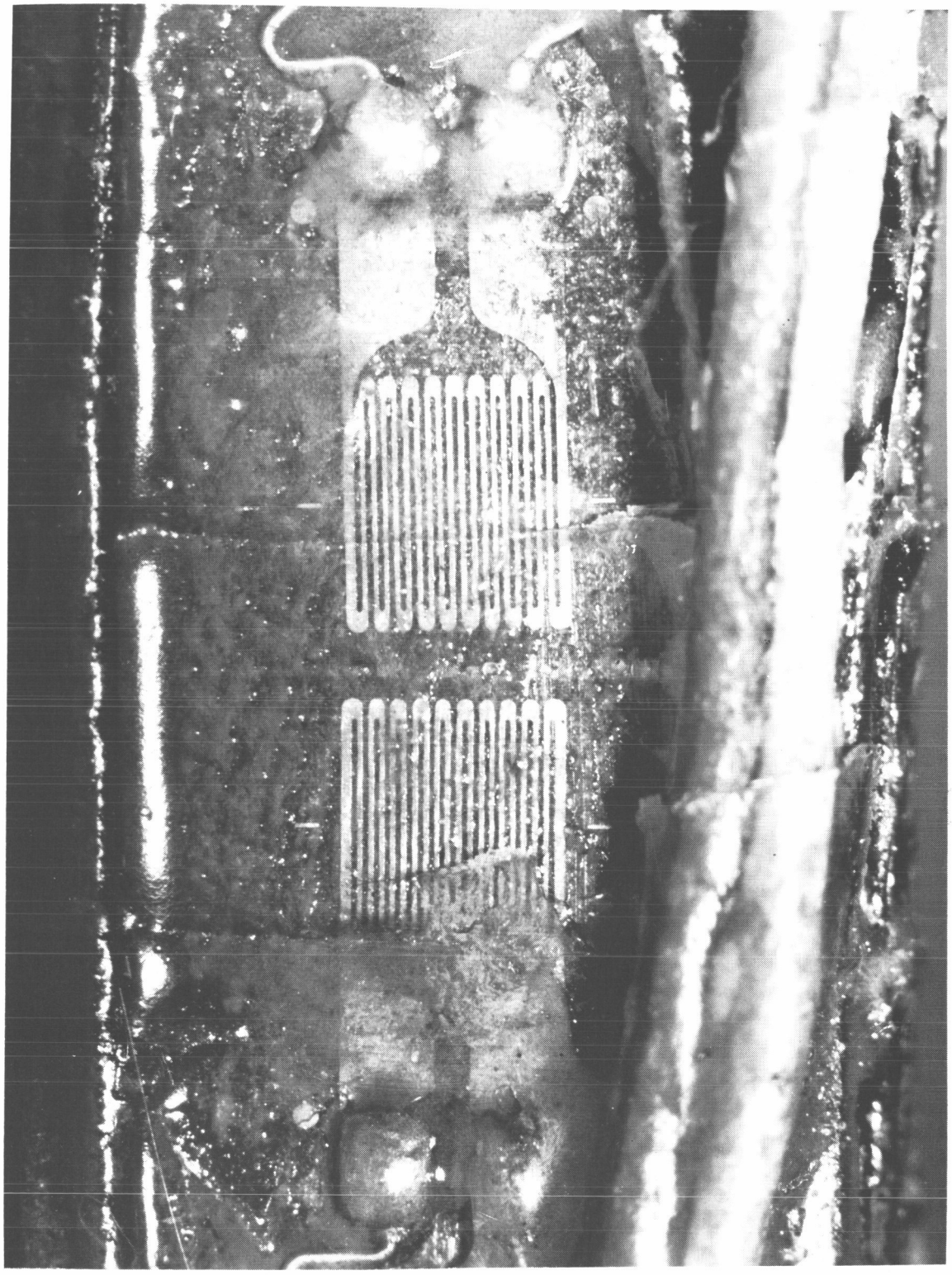

Figure 51 Strain Gauge for Vane Actuation Link (XP-80488)

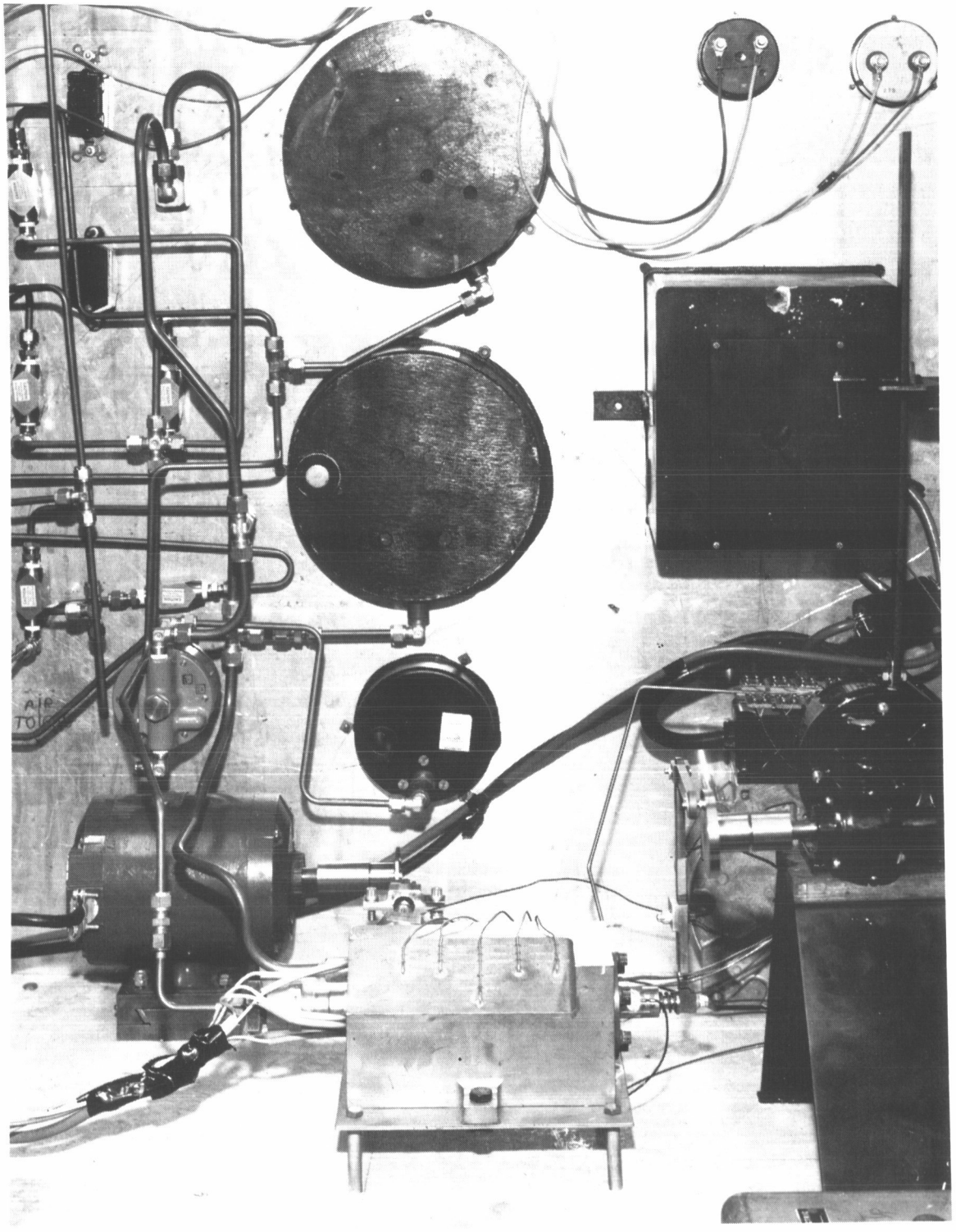

Figure 52 Test Rig and Instrumentation (XP-80959)

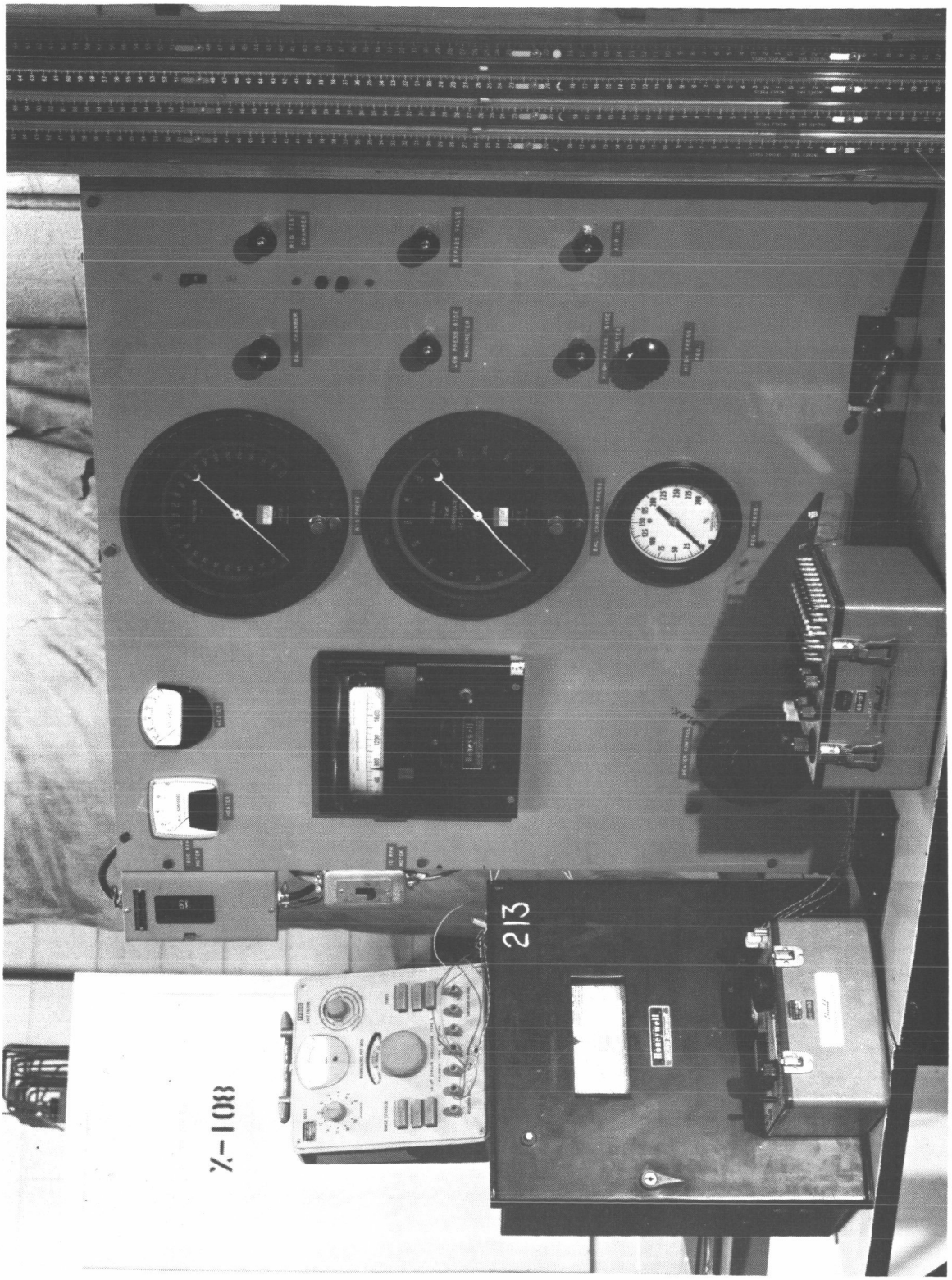

Figure 53 Instrumentation and Control Panel (XP-80960)

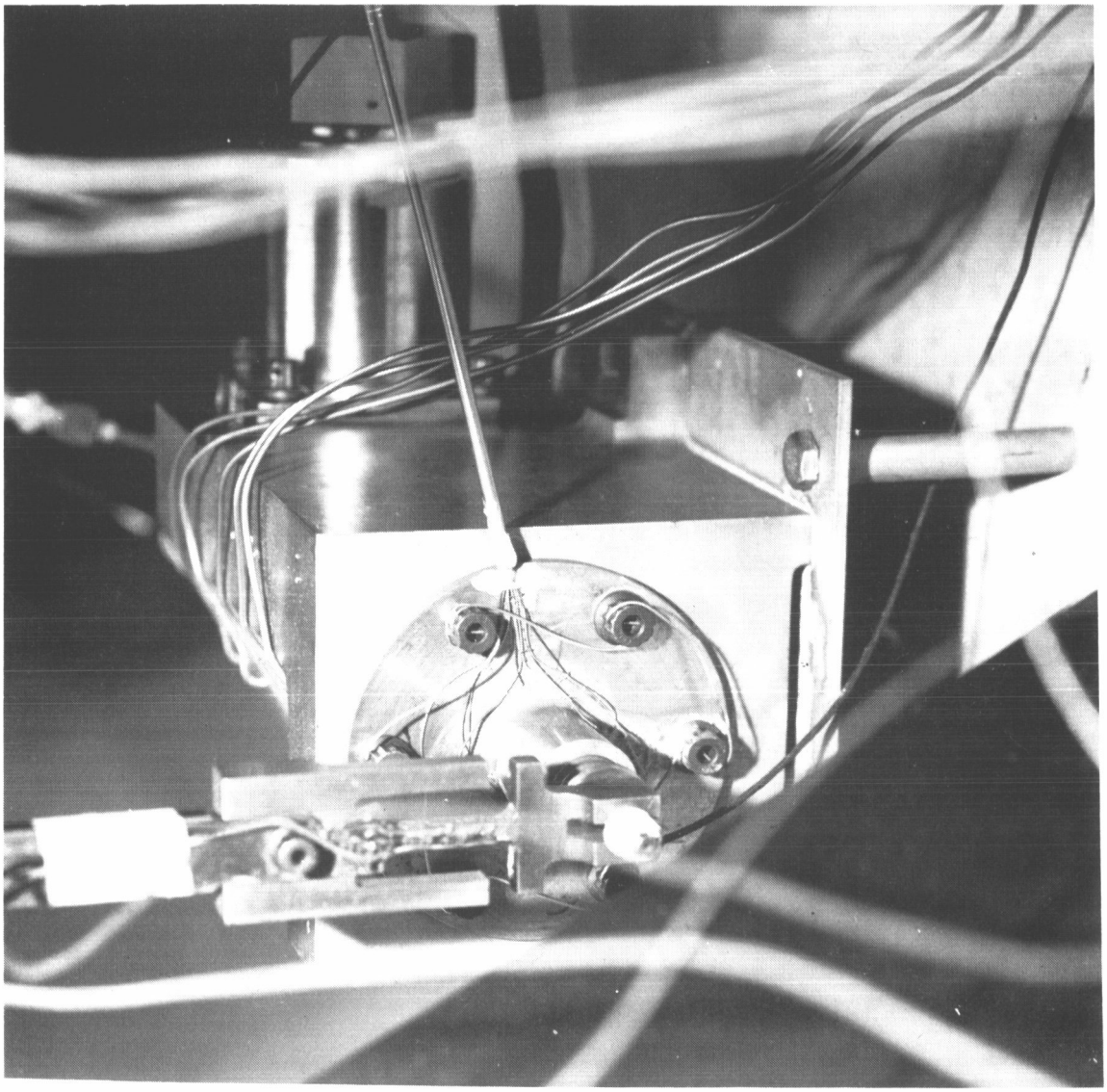

Figure 54 Close-Up of Thermocouple Leads (XP-80903)

On the first test run, readings from the strain gauges and thermocouples indicated that the rig was working properly. However, pressurization revealed some air losses past the holes for the thermocouple leads (shown in the foreground of Figure 54). The loss of air through these holes invalidated the seal loss indications because they are determined by measuring flow upstream of the rig. To eliminate the leakage, the contractor has decided to braze small-bore stainless steel tubing into the existing thermocouple holes. Instrumentation leads will be passed through the tubing and sealed with epoxy cement or low-temperature solder at the end of the tubing, some distance away from the hot rig. The testing which has been accomplished so far has successfully demonstrated the mechanical design concepts employed in the rig, and has demonstrated the ability of the instrumentation to provide the required data.

FOLDOUT FRAME 1

PRATT & WHITNEY AIRCRAFT

FOLDOUT FRAME 2

PWA-3302

PRECEDING PAGE BLANK NOT FILMED.

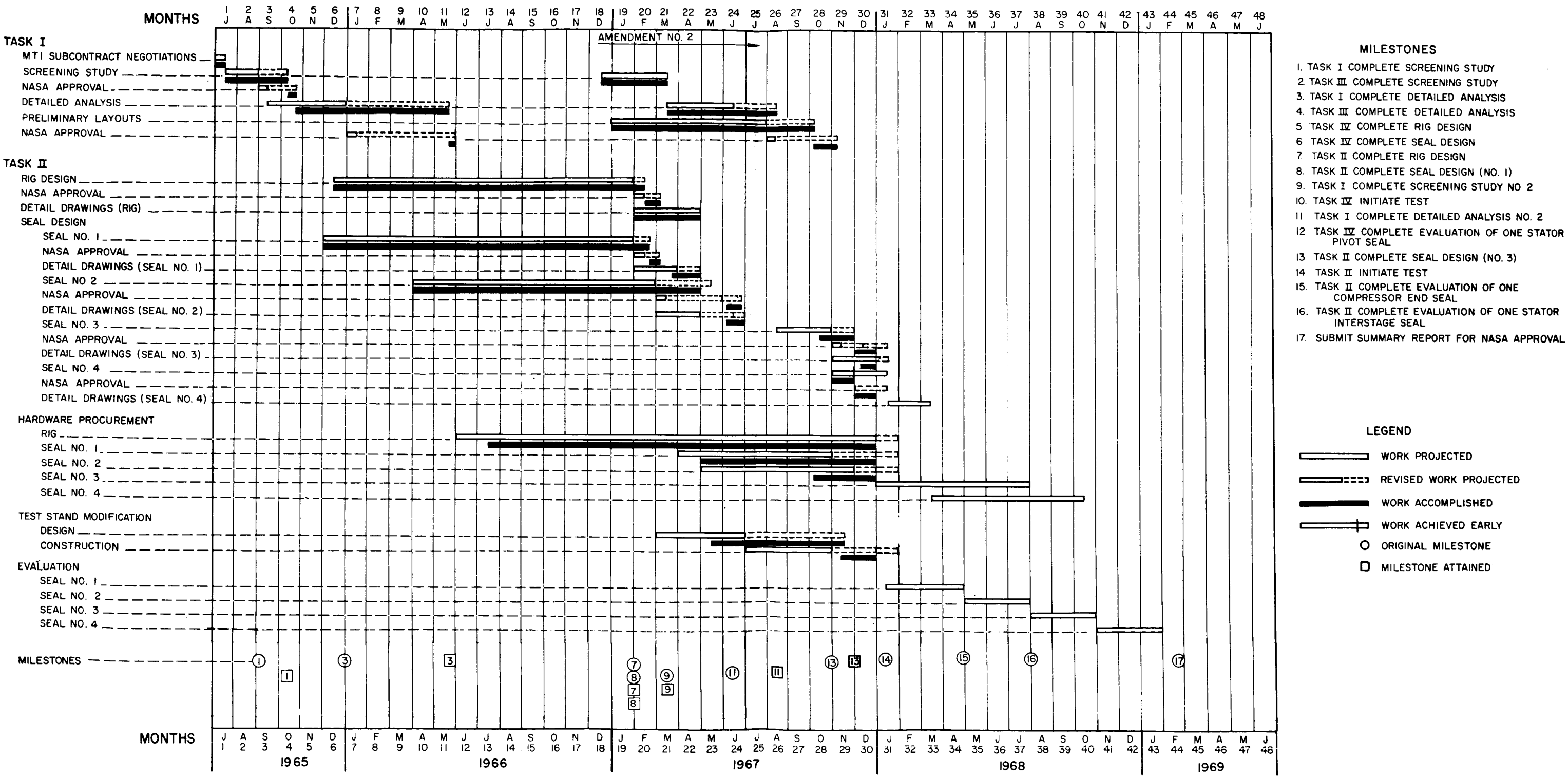

MILESTONES

1. TASK I COMPLETE SCREENING STUDY
2. TASK III COMPLETE SCREENING STUDY
3. TASK I COMPLETE DETAILED ANALYSIS
4. TASK III COMPLETE DETAILED ANALYSIS
5. TASK IV COMPLETE RIG DESIGN
6. TASK IV COMPLETE SEAL DESIGN
7. TASK II COMPLETE RIG DESIGN
8. TASK II COMPLETE SEAL DESIGN (NO. 1)
9. TASK I COMPLETE SCREENING STUDY NO 2
10. TASK IV INITIATE TEST
11. TASK I COMPLETE DETAILED ANALYSIS NO. 2
12. TASK IV COMPLETE EVALUATION OF ONE STATOR PIVOT SEAL
13. TASK II COMPLETE SEAL DESIGN (NO. 3)
14. TASK II INITIATE TEST
15. TASK II COMPLETE EVALUATION OF ONE COMPRESSOR END SEAL
16. TASK II COMPLETE EVALUATION OF ONE STATOR INTERSTAGE SEAL
17. SUBMIT SUMMARY REPORT FOR NASA APPROVAL

LEGEND

- WORK PROJECTED
- REVISED WORK PROJECTED
- WORK ACCOMPLISHED
- WORK ACHIEVED EARLY
- ORIGINAL MILESTONE
- MILESTONE ATTAINED

PRECEDING PAGE BLANK NOT FILMED.

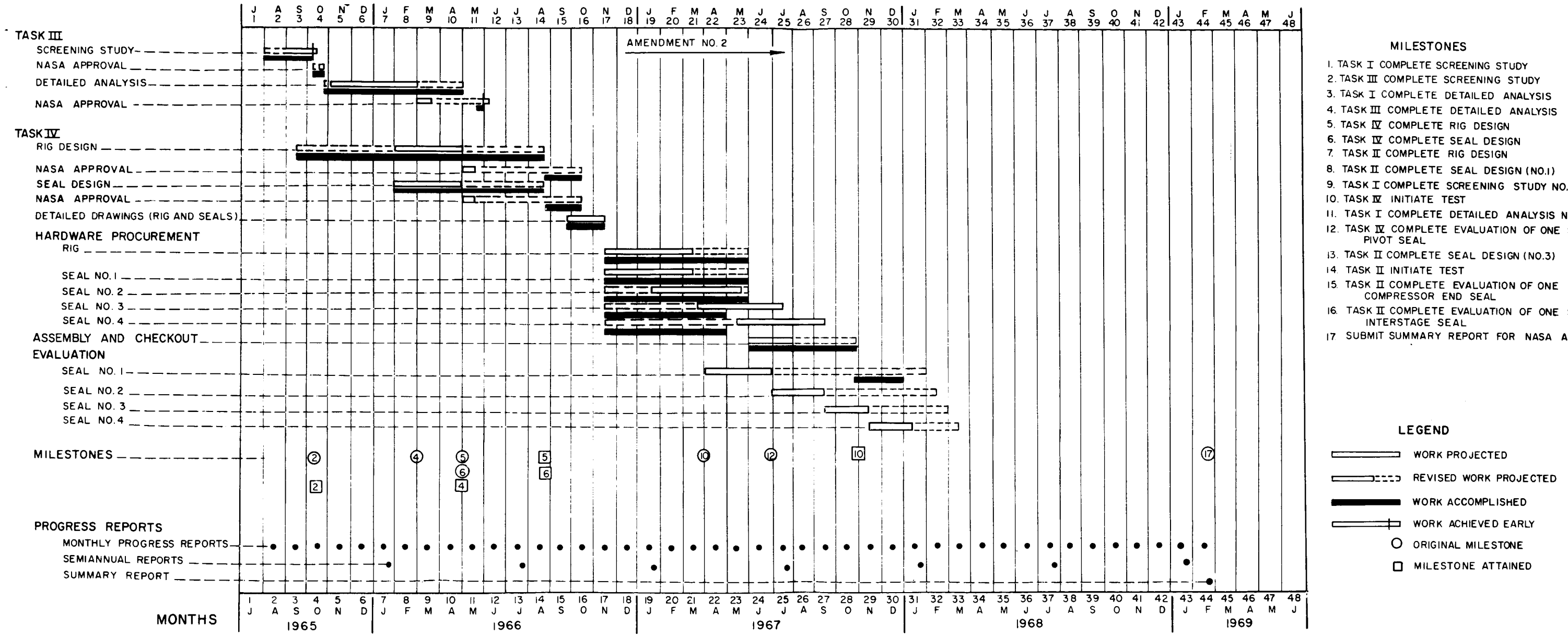

APPENDIX A

FLEXIBLE SEAL TRACKING ANALYSIS CONPUTER PROGRAM

The computer program is comprised of an executive program and a subroutine KCAL. The executive program performs all the calculations necessary for the solution of natural frequency and dynamic response. The subroutine KCAL is used when the gas film stiffnesses are not known.

1. EXECUTIVE PROGRAM

Seven major input cards are required for each set of input for the main program.

Card 1. Title Card (80H)

Card 2. Format (8 (E10.3))

Item Number (8 items)

1.	A	Dummy thickness of seal ring (inches)
2.	G	Modulus of rigidity (lb/in^2)
3.	E	Modulus of elasticity (lb/in^2)
4.	OMEGA	Rotational frequency (rad/sec)
5.	R	Mean radius of the seal ring (inches)
6.	AM1	Mass of the carrier ($lb\text{-}sec^2/in$)
7.	CK1	Spring rate of the carrier spring (lb/in)
8.	RHO	Mass density of the seal ring material ($lb\ sec^2/in^4$)

Card 3. Format (10I5)

Item Number (6 items)

1.	IND	1 for more cases, O for last case.
2.	NGASTF	Number of sets gas film stiffness values
3.	NKSSS	Number of sets of flexible support stiffness
4.	NAIP	Number of sets of polar moment of inertia
5.	NEN	Number of modes of distortion present in the runner
6.	NSW	1 for use of KCAL subroutine and 0 for direct input of gas-film characteristics
7.	NOPAD	Number of pads (0 for double pad, 1 for single pad)

Card 4. Format (5 (E12.5))

Item Number (5 items)

Note: One Card 4 needed for each NGASTF value used.

1. HMN Nominal film thickness (inches)
2. CKSS Axial stiffness of the gas film (lb/in/in)
3. CKSA Axial change of load on the gas film due to angular displacement of the rotor (lb/rad/in)
4. CKAS Change of moment load on the gas film due to axial displacement of the rotor (in-lb/in/in)
5. CKAA Angular stiffness of the gas film (in-lb/rad/in)

Card 5. Format (5 (E12.5))

Item Number (5 items)

Note: One Card 5 needed for each NKASS value used.

1. KSSS Axial stiffness of the flexible support (lb/in/in)
2. KSAS Change of axial load on the flexible support due to angular displacement (lb/rad/in)
3. KASS Change of moment load on the flexible support due to axial displacement (in-lb/in/in)
4. KAAS Angular stiffness of the flexible support (in-lb/rad/in)
5. AM2 Mass of the seal ring (lb-sec^2/in)

Card 6. Format (5 (E12.5))

Item Number (5 items)

Note: One Card 6 needed for each NAIP value used.

1. B Radial dimension of active seal width (inches)
2. AI Section moment of inertia (in^4)
3. AIP Section polar moment of inertia (in^4)
4. AITT Section mass moment of inertia (lb-in-sec^2)
5. AREA Cross sectional area of the seal ring (in^2)

Card 7. Format (5 (E12.5))

Item Number (5 items)

Note: One Card 8 needed for each NEN value used.

1. EN Mode of seal ring and rotor distortion present (0 = conical, 1 = out of plane, 2 saddle shape)
2. SDELM Transverse displacement of the rotor δ (inches)
3. ETAM Transverse displacement of the seal ring η (inches)
4. EPSN Angular displacement of the rotor ϵ_n (radians)
5. ZETAN Angular distortion of seal ring ζ_n (radians)

2. SUBROUTINE KCAL

This subroutine is required only if NSW = 1 (see instructions for Card 4). The angular and cross-coupling stiffnesses of a seal, as shown in Figure 23, are computed from the basic performance data of the gas film. The subroutine KCAL will compute these stiffnesses at a given nominal film thickness.

a. DOUBLE-PAD INPUT INSTRUCTIONS

For a double-pad seal (Figure 23), the gas film's performance characteristics needed for KCAL are the load capacity and the center of pressure for each pad at different film thicknesses and tilted positions. It should be noted that the load capacities and centers of pressure are dimensionless quantities, while film thickness is in inches. Five cards are required for each double-pad KCAL computation.

For a parallel film, three sets of data are required. Each set consists of the film thickness and the load capacities and centers of pressure of both pads at that thickness. H0P = h_o + Δh. At H0P, the load capacities of the lower and upper pads are represented by W20P and W10P respectively, and their centers of pressure are represented by X20P and X10P respectively. H0 = h_o. At H0, the load capacities of the lower and upper pads are represented by W20 and W10 respectively and their centers of pressure are represented by X20 and X10 respectively. H0M = h_o - Δh. At H0M, the load capacities of the lower and upper pads are represented by W20M and W10M respectively, and their centers of pressure are represented by X20M and X10M respectively.

For a tilted film, two sets of data are required. Each set consists of the tilt angle and film thicknesses for both pads, load capacities of both pads, and centers of pressure for both pads. ANGM = - $\Delta\alpha$, where $\Delta\alpha$ is a positive small angle in radians. At a tilt angle ANGM, the film thicknesses at the middles of the lower and upper pads are given by H2M = $h_o + (\Delta\alpha/2)(b_3 + b_2)$ and H1M = $h_o - (\Delta\alpha/2)(b_3 + b_1)$ respectively, the load capacities are given by W2M at (-$\Delta\alpha$,H2M) and W1M at (-$\Delta\alpha$, H1M) respectively, and the centers of pressure are given by X2CM at (-$\Delta\alpha$, H2M) and X1CM at (-$\Delta\alpha$, H1M) respectively. ANGP = $\Delta\alpha$. At a tilt angle ANGP the film thicknesses are given by H2P = $h_o - (\Delta\alpha/2)(b_3 + b_2)$ and

$H1P = h_o + (\Delta a/2)(b_3 + b_1)$, the load capacities by W2P at (Δa, H2P) and W1P at (Δa, H1P), and the centers of pressure by X2CP at (Δa, H2P) and X1CP at (Δa, H1P).

Five data items are required to describe the pads' geometry and pressure difference. The centroid of the section from the high-pressure side is denoted by XSTAR (in inches). The widths of the lower and upper pads are given by B2 and B1 respectively (in inches). The pressure difference between the pads is represented by DELTP (in psi). $DELTP = P_2 - P_1$. The width of the pad recess is given by SDST (in inches). $SDST = b-(b_1 + b_2)$.

The above data should be arranged in FORMAT (8(F10.5)) in the following order:

Card 1.

Item Number (8 items)

1.	H0P	Film thickness h_o^+ (inches)
2.	X20P	Center of pressure of the lower pad at ($a = 0$, h_o^+)
3.	W20P	Load capacity of the lower pad at ($a = 0$, h_o^+)
4.	X10P	Center of pressure of the upper pad at ($a = 0$, h_o^+)
5.	W10P	Load capacity of the upper pad at ($a = 0$, h_o^+)
6.	H0	Film thickness h_o (inches)
7.	X20	Center of pressure of the lower pad at ($a = 0$, h_o)
8.	W20	Load capacity of the lower pad at ($a = 0$, h_o)

Card 2.

Item Number (8 items)

1.	X10	Center of pressure of the upper pad at ($a = 0$, h_o)
2.	W10	Load capacity of the upper pad at ($a = 0$, h_o)
3.	H0M	Film thickness h_o^- (inches)
4.	X20M	Center of pressure of the lower pad at ($a = 0$, h_o^-)
5.	W20M	Load capacity of the lower pad at ($a = 0$, h_o^-)
6.	X10M	Center of pressure of the upper pad at ($a = 0$, h_o^-)
7.	W10M	Load capacity of the upper pad at ($a = 0$, h_o^-)
8.	ANGM	$-\Delta a$ small angle of seal tilt (radians)

Card 3.

Item Number (8 items)

1.	H2M	Film thickness at the middle of the lower pad at $a = -\Delta a$
2.	X2CM	Center of pressure of the lower pad at ($a = -\Delta a$, H2M)
3.	W2M	Load capacity of the lower pad at ($a = -\Delta a$, H2M)
4.	H1M	Film thickness at the middle of the upper pad at ($a = -\Delta a$)
5.	X1CM	Center of pressure of the upper pad at ($a = -\Delta a$, H1M)
6.	W1M	Load capacity of the upper pad at ($a = -\Delta a$, H1M)

7. ANGP Δa small angle of tilt (radians)
8. H2P Film thickness at the middle of the lower pad at ($a = \Delta a$)

Card 4.

Item Number (8 items)

1. X2CP Center of pressure of the lower pad at ($a = \Delta a$, H2P)
2. W2P Load capacity of the lower pad at ($a = \Delta a$, H2P)
3. H1P Film thickness at the middle of the upper pad at ($a = \Delta a$)
4. X1CP Center of pressure of the upper pad at ($a = \Delta a$, H1P)
5. W1P Load capacity of the upper pad at ($a = \Delta a$, H1P)
6. XSTAR Section centroid (inches)
7. B2 Width of the lower pad (inches)
8. B1 Width of the upper pad (inches)

Card 5.

Item Number (2 items)

1. DELTP Pressure differential (psi)
2. SDST Pad recess (inches)

An example will indicate the method used to determine the input numbers. The seal under consideration is the end seal, which consists of the spiral-grooved, orifice-compensated upper pad and Rayleigh-step lower pad at cruise conditions.

Card 1.

H0P = .00105 inches
X20P = .5
W20P = .62
X10P = .4296
W10P = .833
H0 = .001
X20 = .5
W20 = .635

Card 2.

X10 = .4315
W10 = .842
H0M = .00095
X20M = .5
W20M = .648
X10M = .4332
W10M = .852
ANGM = .001

Card 3.

H2M = .0014
X2CM = .512
W2M = .55
H1M = .0006
X1CM = .4326
W1M = .915
ANGP = .001
H2P = .0006

Card 4.

X2CP = .488
W2P = .808
H1P = .0014
X1CP = .4315
W1P = .825
XSTAR= .65
B2 = .5
B1 = .5

Card 5.

DELTP = 80.
SDST = .3

b. SINGLE PAD INPUT INSTRUCTIONS

The angular and cross-coupling stiffnesses of a single-pad seal, as shown in Figure 20, are computed in the same manner as for the double-pad seal. The subroutine KCAL will compute these stiffnesses at specific film conditions. The gas-film performance characteristics needed for the input of KCAL are the load capacity and center of pressure at the perturbed film thicknesses and tilted positions of the nominal film thickness. To compute the single-pad stiffnesses the gas film-data described below is needed.

For a parallel film, at $h = h_o$ = H0, the load capacity and center of pressure are represented by W0 and XC0 respectively. At $h = h_o + \Delta h = h_o^+$ = H0P, the load capacity and center of pressure are represented by W0P and SC0P respectively. At $h = h_o - \Delta h = h_o^-$ = H0M, the load capacity and center of pressure are represented by W0M and XC0M respectively.

For a tilted film at $\alpha = -\Delta\alpha$ = ANGM (where $\Delta\alpha$ is a small positive angle in radians), the load capacity and center of pressure are given by WM and XCM respectively at h = H0
At $\alpha = \Delta\alpha$ = ANGP, the load capacity and center of pressure are given by WP and XCP respectively at h = H0.

Three items of data concerning geometry and pressure-differences are required. The centroid of the section from the high-pressure side is given by XSTAR (in inches). The width of the seal pad is denoted by B (in inches). The pressure difference $\Delta P = P_2 - P_1$ is represented by DELTP (in psi).

A total of three cards is required for each single pad KCAL computation. The above data should be arranged in FORMAT (8(F10.5)) in the following order:

Card 1.

Item Number (8 items)

1.	H0	Film thickness ho (inches)
2.	XC0	Center of pressure at ($\alpha = 0$, ho)
3.	W0	Load capacity at ($\alpha = 0$, ho)
4.	H0P	Film thickness h_o^+ (inches)
5.	XC0P	Center of pressure at ($\alpha = 0$, h_o^+)
6.	W0P	Load capacity at ($\alpha = 0$, h_o^+)
7.	H0M	Film thickness h_o^- (inches)
8.	XC0M	Center of pressure at ($\alpha = 0$, h_o^+)

Card 2.

Item Number (8 items)

1.	WOM	Load capacity at ($\alpha = 0, h_o^-$)
2.	ANGP	$\Delta\alpha$ small angle of tilt (radians)
3.	ANGM	$-\Delta\alpha$ small angle of seal tilt (radians)
4.	XCP	Center of pressure at ($\alpha = \Delta\alpha, h_o$)
5.	WP	Load capacity at ($\alpha = \Delta\alpha, h_o$)
6.	XCM	Center of pressure at ($\alpha = -\Delta\alpha, h_o$)
7.	WM	Load capacity at ($\alpha = -\Delta\alpha, h_o$)
8.	XSTAR	Section centroid (inches)

Card 3.

Item Number (2 items)

1.	B	Width of the pad (inches)
2.	DELTP	Pressure differential (psi)

The gas film values are determined from the upper pad data in Appendix B. The output from the subroutine is K_{ss}, $K_{s\alpha}$, $K_{\alpha s}$, and $K_{\alpha\alpha}$.

The output from the main program using the values determined in the subroutine KCAL is essentially the same as the output of the double pad program.

3. EXPLANATION OF OUTPUT

a. TRACKING PARAMETERS

GAM	1	Defined by Equation 27
GAM	2	Defined by Equation 27
GAM	3	Defined by Equation 27
GAM	4	Defined by Equation 27
GAM	5	Defined by Equation 27
GAM	6	Defined by Equation 27
GAM	7	Defined by Equation 27
GAM	8	Defined by Equation 27
GAM	9	Defined by Equation 27
GAM	10	Defined by Equation 27
GAM	11	Defined by Equation 27
F1		Defined by Equation 28
F2		Defined by Equation 28
A1		Defined by Equation 53
A2		Defined by Equation 53

$$C_1/C_2 = (C_1/C_3)\ (1/C_2/C_3) = \frac{K_2}{K_1 + K_2 - M_1\omega^2}$$

b. NATURAL FREQUENCY ELASTIC VIBRATIONS

NUN	1	Defined by Equation 41
NUN	2	Defined by Equation 42

c. DYNAMIC RESPONSE ELASTIC VIBRATIONS

CDELN	Defined by Equation 47
ALFAN	Defined by Equation 50
BETAN	Defined by Equation 50
UN	Defined by Equation 50
VN	Defined by Equation 50
CA1	Defined by Equation 51
CA2	Defined by Equation 51
CB1	Defined by Equation 51
CB2	Defined by Equation 51
CU1	Defined by Equation 51
CU2	Defined by Equation 51
CV1	Defined by Equation 51
CV2	Defined by Equation 51

d. NATURAL FREQUENCIES RIGID BODY VIBRATION

NU	1	Defined by Equation 54
NU	2	Defined by Equation 54

e. DYNAMIC RESPONSE RIGID BODY VIBRATION

C_1/C_3	Defined by Equation 67
C_2/C_3	Defined by Equation 68

f. DIMENSIONAL RESULTS

PHI	$\phi = \epsilon_n \cdot (\alpha_n + \beta_n)$
DELTA H	$\delta_h = b\{[(u_n + v_n) - \delta_n] + 0.5\|\phi\|\}$
DELTA	$\delta = b\delta_n$
ETA	$\eta = b\eta_n$
HMIN	$h_{min} = h_m - \delta_h$

```
C     P356 GENERAL COMPUTER PROGRAM FOR FLEXIBLE SEAL TRACKING ANALYSIS
C     PROGRAM REVISED BY DR.CHAS.C.W.NG ,PRATT AND WHITNEY AIRCRAFT,FEB,68
C     FOR SINGLE PAD,N=0 MODE,THE AXIAL GAP REDUCTION IN MINIMUM FILM THICKNESS
C     CALCULATION IS RELIEVED FROM ITS ABSOLUTE SIGN,IT IMPLIES THAT THE WORST
C     CONDITION OF THE MINIMUM FILM THICKNESS IS NOT OBTAINED FOR THIS CASE
      DIMENSION  ZP1(10),ZP2(10),ZP3(10),ZP4(10),ZP5(10)
      DIMENSION  ZO1(10),ZO2(10),ZO3(10),ZO4(10),ZO5(10)
      DIMENSION  ZT1(10),ZT2(10),ZT3(10),ZT4(10),ZT5(10)
      DIMENSION  ZL1(10),ZL2(10),ZL3(10),ZL4(10),ZL5(10)
   20 FORMAT (5(2XF12.5))
   21 FORMAT (5F10.3)
   22 FORMAT (10I5)
   25 FORMAT (8E10.3)
   31 FORMAT (30HP356 GENERAL COMPUTER PROGRAM FOR FLEXIBLE SEAL       )
   32 FORMAT (1H1,25X,7H OUTPUT)
   33 FORMAT (17X,39H NATURAL FREQUENCIES ELASTIC VIBRATIONS)
   34 FORMAT (18X,36H DYNAMIC RESPONSE ELASTIC VIBRATIONS)
   36 FORMAT (17X,41H NATURAL FREQUENCIES RIGID BODY VIBRATION)
   37 FORMAT (17X,38H DYNAMIC RESPONSE RIGID BODY VIBRATION)
   38 FORMAT (27H DATA RUN ELASTIC SEAL RING)
   39 FORMAT (25X,21H DIMENSIONAL RESULTS )
   40 FORMAT (7X,1HA,13X,1HB,14X,1HR,13X,1HG,13X,1HE)
   41 FORMAT (5X,3HKSS,11X,3HKSA,11X,3HKAS,11X,3HKAA,11X,3HRHO)
   42 FORMAT (5X,4HKSS*,10X,4HKSA*,10X,4HKAS*, 10X,4HKAA*,10X,5HOMEGA)
   43 FORMAT (7X,1HI,13X,2HIP,13X,1HN,11X,4HEPSN,10X,5HSDELN)
   44 FORMAT (5X,5HZETAN,9X,4HETAN,10X,4HAREA,10X,4HAITT,8X6HH MEAN)
   45 FORMAT (5X,3HAM1,11X,3HAM2,11X,3HCK1,11X,3HCK2,11X,3HCK3)
   46 FORMAT (5X,2HA1,12X,2HA2,8X,5HC1/C2)
   47 FORMAT (5X,3HNU1,11X,3HNU2)
   48 FORMAT (3X,5HC1/C3,9X,5HC2/C3)
   49 FORMAT (7X,3HPHI,11X,7HDELTA H,8X,5HDELTA,6X,3HETA,11X,5HH MIN)
   50 FORMAT (4X,4HGAM1,10X,4HGAM2,10X,4HGAM3,10X,4HGAM4,10X,4HGAM5)
   51 FORMAT (4X,4HGAM6,10X,4HGAM7,10X,4HGAM8,10X,4HGAM9,10X,5HGAM10)
   52 FORMAT (4X,5HGAM11,11X,2HF1,12X,2HF2)
   53 FORMAT (5X,4HNUN1,10X,4HNUN2)
   54 FORMAT (5X,5HCDELN,9X,5HALFAN,9X,5HBETAN,11X,2HUN,12X,2HVN)
```

```
55 FORMAT (5X,3HCA1,11X,3HCA2,11X,3HCB1,11X,3HCB2)
56 FORMAT (5X,3HCU1,11X,3HCU2,11X,3HCV1,11X,3HCV2)
57 FORMAT(80H
  1                                )
58 FORMAT (5X,3HNU1)
99 FORMAT (1H1)
23 READ(5,57)
   READ(5,25) A,G,E,OMEGA,R,AM1,CK1,RHO
   WRITE(6,31)
   WRITE(6,57)
   CONST=6.28318*R
70 RSQ=R*R
   RCUB=R*RSQ
   READ(5,22) IND,NGASTF,NKSSS,NAIP,NEN,NSW,NOPAD
   DO 81 I=1,NGASTF
   READ(5,21) ZP1(I),ZP2(I),ZP3(I),ZP4(I),ZP5(I)
81 CONTINUE
   DO 85 I=1,NKSSS
   READ(5,21) ZO1(I),ZO2(I),ZO3(I),ZO4(I),ZO5(I)
85 CONTINUE
   DO 88 I=1,NAIP
   READ(5,21) ZT1(I),ZT2(I),ZT3(I),ZT4(I),ZT5(I)
88 CONTINUE
   DO 91 I=1,NEN
   READ(5,21) ZL1(I),ZL2(I),ZL3(I),ZL4(I),ZL5(I)
91 CONTINUE
   DO 100 I=1,NGASTF
   HMN  =ZP1(I)
   CKSS=ZP2(I)
   CKSA=ZP3(I)
   CKAS=ZP4(I)
   CKAA=ZP5(I)
   IF(NSW) 92,92,93
93 CALL KCAL(CKSS,CKAS,CKSA,CKAA,NOPAD)
92 CK3=CKSS*CONST
   DO 100 J=1,NKSSS
```

```
      CKSSS=Z01(J)
      CK2=CKSSS*CONST
      CKSAS=Z02(J)
      CKASS=Z03(J)
      CKAAS=Z04(J)
      AM2=Z05(J)
      DO 100 K=1,NAIP
      P=ZT1(K)
      AI=ZT2(K)
      AIP=ZT3(K)
      AITT=ZT4(K)
      AREA=ZT5(K)
      DO 100 L=1,NFN
      EN=ZL1(L)
      SDELM=ZL2(L)
      SDELN=SDELM/B
      ETAM=ZL3(L)
      ETAN=ETAM/B
      EPSN=ZL4(L)
      ZETAN=ZL5(L)
C     START OF CALCULATIONS
      E1=E*AI
      GIP=G*AIP
      XI=EI/GIP
      TEMP1=GIP*(1.+XI)
      GAM1=RCUB*(CKSA+CKSAS)/TEMP1
      GAM2=B*RCUB*(CKSS+CKSSS)/TEMP1
      GAM3=RCUB*CKSA/TEMP1
      GAM4=RCUB*CKSS*B/TEMP1
      GAM5=XI+RSQ*(CKAA+CKAAS)/GIP
      GAM6=(CKAS+CKASS)*B*RSQ/GIP
      GAM7=CKAA*RSQ/GIP
      GAM8=CKAS*B*RSQ/GIP
      GAM9=B*XI/(R*(1.+XI))
      GAM10=B/(R*(1.+XI))
      GAM11=B*(1.+XI)/R
```

```
      FS1=TEMP1/(RHO*AREA*B*RCUB)
      F1=SQRT(FS1)
      FS2=GIP/AITT
      F2=SQRT(FS2)
      EN2=EN*EN
      EN4=EN2*EN2
      EN6=EN2*EN4
      OMEGA2=OMEGA*OMEGA
      OMEGA4=OMEGA2*OMEGA2
      P1=FS2*(EN2+GAM5)+FS1*(GAM2+GAM10*EN2+GAM9*EN4)
      P2=GAM9*EN6+(GAM10+GAM5*GAM9-GAM11)*EN4+(GAM2-GAM6+GAM5*GAM10-
     1GAM1*GAM11)*EN2+GAM2*GAM5-GAM1*GAM6
      TEMP2=P1*P1-4.*FS1*FS2*P2
      TEMP3=SQRT(TEMP2)
      TEMP4=.5*(P1+TEMP3)
      TEMP5=.5*(P1-TEMP3)
      ZNUN1=SQRT(TEMP4)
      ZNUN2=SQRT(TEMP5)
      CDELN=(-EN4*OMEGA4+EN2*OMEGA2*P1)/(FS1*FS2)-P2
      Q1=GAM11*EN2+GAM6
      Q20=-GAM9*EN4-GAM10*EN2-GAM2
      Q2=Q20+EN2*OMEGA2/FS1
      CA1=(GAM3*Q1+GAM7*Q2)/CDELN
      CA2=(GAM4*Q1+GAM8*Q2)/CDELN
      CB1=(EN2*Q1+(EN2+XI)*Q20)/(-P2)
      CB2=((GAM9*EN4+GAM10*EN2)*Q1+EN2*GAM11*Q20)/(-P2)
      Q3=EN2+GAM1
      Q40=-EN2-GAM5
      Q4=Q40+EN2*OMEGA2/FS2
      CU1=(GAM7*Q3+GAM3*Q4)/CDELN
      CU2=(GAM8*Q3+GAM4*Q4)/CDELN
      CV1=((EN2+XI)*Q3+EN2*Q40)/(-P2)
      CV2=(GAM11*EN2*Q3+(GAM9*EN4+GAM10*EN2)*Q40)/(-P2)
      ALFAN=CA1*EPSN+CA2*SDELN
      BETAN=CB1*ZETAN+CB2*ETAN
      UN=CU1*EPSN+CU2*SDELN
```

```
      VN=CV1*ZETAN+CV2*ETAN
      A2=0.0
      IF(NOPAD)180,180,181
  180 A1=(CK1+CK2)/AM1+(CK2+CK3)/AM2
      A2=(CK1*CK2+CK2*CK3+CK3*CK1)/(AM1*AM2)
      GO TO 182
  181 A1=(CK2+CK3)/AM2
  182 TEMP6=A1*A1-4.*A2
      TEMP7=SQRT(TEMP6)
      TEMP8=(A1+TEMP7)*.5
      TEMP9=(A1-TEMP7)*.5
      ZNU1=SQRT(TEMP8)
      ZNU2=SQRT(TEMP9)
      TEMP10=1.0
      IF(NOPAD)183,183,184
  183 TEMP10=CK2/(-AM1*OMEGA2+CK1+CK2)
  184 C2=CK3/(-AM2*OMEGA2+CK2+CK3-CK2*TEMP10)
      C1=C2*TEMP10
  191 PHEE=EPSN-(ALFAN+BETAN)
      PH4=ABS(PHEE)
      PPPV=UN+VN-SDELN
      IF(NOPAD)196,196,197
  197 IF(EN)199,199,196
  196 DUV=ABS(PPPV)
      GO TO 198
  199 DUV=PPPV
  198 DELTA=(.5*PH4+DUV)*B
      HMIN=HMN-DELTA
C     END OF CALCULATIONS
      WRITE(6,38)
      WRITE(6,40)
      WRITE(6,20)   A,B,R,G,E
      WRITE(6,41)
      WRITE(6,20)   CKSS,CKSA,CKAS,CKAA,RHO
      WRITE(6,42)
      WRITE(6,20)   CKSSS,CKSAS,CKASS,CKAAS,OMEGA
```

```
      WRITE(6,43)
      WRITE(6,20)  A1,AIP,EN,EPSN,SDELN
      WRITE(6,44)
      WRITE(6,20)  ZETAN,ETAN,AREA,AITT,HMN
      WRITE(6,45)
      WRITE(6,20)  AM1,AM2,CK1,CK2,CK3
   90 WRITE(6,32)
      WRITE(6,50)
      WRITE(6,20)  GAM1,GAM2,GAM3,GAM4,GAM5
      WRITE(6,51)
      WRITE(6,20)  GAM6,GAM7,GAM8,GAM9,GAM10
      WRITE(6,52)
      WRITE(6,20)  GAM11,F1,F2
      WRITE(6,46)
      WRITE(6,20)  A1,A2,TEMP10
      WRITE(6,33)
      WRITE(6,53)
      WRITE(6,20)  ZNUN1,ZNUN2
      WRITE(6,34)
      WRITE(6,54)
      WRITE(6,20)  CDELN,ALFAN,BETAN,UN,VN
      WRITE(6,55)
      WRITE(6,20)  CA1,CA2,CB1,CB2
      WRITE(6,56)
      WRITE(6,20)  CU1,CU2,CV1,CV2
      WRITE(6,36)
      IF(NOPAD)192,192,193
  192 CONTINUE
      WRITE(6,47)
      WRITE(6,20)  ZNU1,ZNU2
      WRITE(6,37)
      WRITE(6,48)
      WRITE(6,20)  C1,C2
      GO TO 195
  193 WRITE(6,58)
      WRITE(6,20)  ZNU1
```

```
  195 WRITE(6,39)
      WRITE(6,49)
      WRITE(6,20) PHEE,DELTA,SDELM,ETAM,HMIN
      WRITE(6,99)
  100 CONTINUE
      IF(IND) 24,24,23
   24 STOP
      END


C     SUBROUTINE USED TO CALCULATE GAS FILM STIFFNESS FOR SINGLE AND DOUBLE PADS
      SUBROUTINE KCAL (CKSS,CKAS,CKSA,CKAA,NOPAD)
   20 FORMAT(//)
   21 FORMAT(8(E15.5))
   22 FORMAT(6X,3HH0P,11X,4HX20P,11X,4HW20P,11X,4HX10P,11X,4HW10P,12X,
     12HH0,13X,3HX20,12X,3HW20)
   23 FORMAT(//6X,3HX10,12X,3HW10,12X,3HH0M,11X,4HX20M,11X,4HW20M,11X,
     14HX10M,11X,4HW10M,11X,4HANGM)
   24 FORMAT(//6X,3HH2M,11X,4HX2CM,12X,3HW2M,12X,3HH1M,11X,4HX1CM,12X,
     13HW1M,11X,4HANGP,12X,3HH2P)
   25 FORMAT(//5X,4HX2CP,12X,3HW2P,12X,3HH1P,11X,4HX1CP,12X,3HW1P,11X,
     15HXSTAR,11X,2HB2,13X,2HB1)
   26 FORMAT(//5X,5HDELTP,10X,4HSDST)
   27 FORMAT(8(E10.5))
   28 FORMAT(//5X,4HXCTO,11X,4HXCTM,11X,4HXCTP,12X,3HXCP,12X,3HXCM)
   29 FORMAT(//5X,4HCKSS,11X,4HCKAS,11X,4HCKSA,11X,4HCKAA)
   40 FORMAT(6X,2HH0,12X,3HXC0,13X,2HW0,12X,3HH0P,11X,4HXC0P,12X,3HW0P,
     112X,3HH0M,11X,4HXC0M)
   41 FORMAT(//6X,3HW0M,11X,4HANGP,11X,4HANGM,12X,3HXCP,13X,2HWP,12X,
     13HXCM,13X,2HWM,13X,5HXSTAR)
   42 FORMAT(//7X,1HB,14X,5HDELTP)
      IF(NOPAD)60,60,251
   60 READ(5,27)  H0P,X20P,W20P,X10P,W10P,H0,X20,W20,X10,W10,H0M,X20M,
     1W20M,X10M,W10M,ANGM,H2M,X2CM,W2M,H1M,X1CM,W1M,ANGP,
     2H2P,X2CP,W2P,H1P,X1CP,W1P,XSTAR,B2,B1,DELTP,SDST
      WRITE(6,20)
```

```
      WRITE(6,22)
      WRITE(6,21)   H0P,X20P,W20P,X10P,W10P,H0,X20,W20
      WRITE(6,23)
      WRITE(6,21)   X10,W10,H0M,X20M,W20M,X10M,W10M,ANGM
      WRITE(6,24)
      WRITE(6,21)   H2M,X2CM,W2M,H1M,X1CM,W1M,ANGP,H2P
      WRITE(6,25)
      WRITE(6,21)   X2CP,W2P,H1P,X1CP,W1P,XSTAR,B2,B1
      WRITE(6,26)
      WRITE(6,21)   DELTP,SDST
      AK2=B2*DELTP
      AK1=B1*DELTP
      W10P=W10P*AK1
      W10M=W10M*AK1
      W10=W10*AK1
      W20P=W20P*AK2
      W20M=W20M*AK2
      W20=W20*AK2
      W1M=W1M*AK1
      W1P=W1P*AK1
      W2M=W2M*AK2
      W2P=W2P*AK2
      X10P=X10P*B1
      X10=X10*B1
      X10M=X10M*B1
      X1CM=X1CM*B1
      X1CP=X1CP*B1
      X20P=X20P*B2
      X20=X20*B2
      X20M=X20M*B2
      X2CM=X2CM*B2
      X2CP=X2CP*B2
      DWDH=(W10M-W10P)+(W20M-W20P)
      HDIFR=H0P-H0M
      DWDH=DWDH/HDIFR
      B12=B1+B2+SDST
```

```
      CKSS=DWDH
      W12=W10+W20
      XCTO=(W20*(B12-X20)+W10*X10)/W12
      XCTM=(W20M*(B12-X20M)+W10M*X10M)/(W10M+W20M)
      XCTP=(W20P*(B12-X20P)+W10P*X10P)/(W10P+W20P)
      DXCDH= (XCTP-XCTM)/HDIFR
      XCTOR=XCTO-XSTAR
      CKAS=DWDH*XCTOR-W12*DXCDH
      DALFA=ANGP-ANGM
      DWDA=(W1P-W1M+W2P-W2M)/DALFA
      CKSA=DWDA
      XCP=(W2P*(B12-X2CP)+W1P*X1CP)/(W1P+W2P)
      XCM=(W2M*(B12-X2CM)+W1M*X1CM)/(W1M+W2M)
      DXCDA=(XCP-XCM)/DALFA
      CKAA=DWDA*XCTOR+W12*DXCDA
      WRITE(6,28)
      WRITE(6,21) XCTO,XCTM,XCTP,XCP,XCM
      WRITE(6,29)
      WRITE(6,21) CKSS,CKAS,CKSA,CKAA
      GO TO 200
  251 READ(5,27) HO,XCO,WO,HOP,XCOP,WOP,HOM,XCOM,WOM,ANGP,ANGM,XCP,WP,
     1XCM,WM,XSTAR,B,DELTP
      WRITE(6,40)
      WRITE(6,21)   HO,XCO,WO,HOP,XCOP,WOP,HOM,XCOM
      WRITE(6,41)
      WRITE(6,21)   WOM,ANGP,ANGM,XCP,WP,XCM,WM,XSTAR
      WRITE(6,42)
      WRITE(6,21)   B,DELTP
      AK=B*DELTP
      WO=WO*AK
      WOP=WOP*AK
      WOM=WOM*AK
      WP=WP*AK
      WM=WM*AK
      XCO=XCO*B
      XCOP=XCOP*B
```

```
      XCOM=XCOM*B
      XCP=XCP*B
      XCM=XCM*B
      DWDH=(WOM-WOP)/(HOP-HOM)
      CKSS=DWDH
      DWDA=(WP-WM)/(ANGP-ANGM)
      CKSA=DWDA
      XCTO=XCO-XSTAR
      DXCDH=(XCOP-XCOM)/(HJP-HUM)
      CKAS=DWDH*XCTU-DXCDH*WU
      DXCDA=(XCP-XCM)/(ANGP-ANGM)
      CKAA=DWDA*XCTO+DXCDA*WU
      WRITE(6,29)
      WRITE(6,21) CKSS,CKAS,CKSA,CKAA
  200 CONTINUE
          RETURN
          END
```

APPENDIX B

THERMAL ANALYSIS

The methods of thermal analysis presented in this Appendix were used to determine the temperature distributions in the OC diaphragm seal and the semirigid seal. For the sake of clarity the analysis is discussed under the three headings:

1. The Temperature Distribution by Numerical Methods
2. Heat Generation
3. Surface Coefficients for Convective Heat Transfer

For all calculations, steady-state cruise conditions were assumed.

1. THE TEMPERATURE DISTRIBUTION BY NUMERICAL METHODS

The circumferential symmetry of the seal assemblies made a corresponding symmetry assumption for the temperature distribution possible. Consequently, the thermal analysis was simplified to that for a two-dimensional system.

The seal assemblies were broken down into a number of contiguous orthogonal subvolumes each of a shape suited to the requirements of local temperature information and the over-all geometry. The accuracy of the thermal maps computed depends on the small size of these subvolumes. As, however, the time taken to compute one thermal map for a particular configuration depends also on the number of subvolumes, a compromise had to be reached during the design stage to limit their number. Each subvolume contains one nodal point at which the temperature is determined. Details of nodal point numbers and locations are given in the appropriate sections for the seals.

The determination of the temperatures at the nodal points in the seal assemblies was carried out by conventional methods of thermal network theory. The physical basis of these methods is the analogy to Kirchhoff's first law for electrical circuits. This states that under steady-state conditions, the algebraic sum of heat flows into a junction point (nodal point) of the network is zero. As steady state conditions were postulated, the heat flow for each internal or surface nodal point by conduction and by convection is given by

$$\sum_i q_i = 0^*$$

Because no very large temperature differences existed across gaps between working elements of the seal assembly, heat exchange by radiation was considered to be negligible. The heat flows between adjacent nodal points is given by

$$q_\ell = \frac{\Delta_T}{\sum_m R_m}$$

*The symbols are identified in the Nomenclature

where the local conductive resistances have the form

$$R = \frac{L}{kA}$$

and the convective resistances

$$R = \frac{1}{\bar{h}A}$$

The scheme used for setting up the equations describing heat flow to the nodal points by convection and conduction only is illustrated by specific examples.

If the nodal point (i, j) is an interior point and heat transfer is by conduction only through the material which has a uniform thermal conductivity k, the thermal network is represented by the diagram shown in Figure 55.

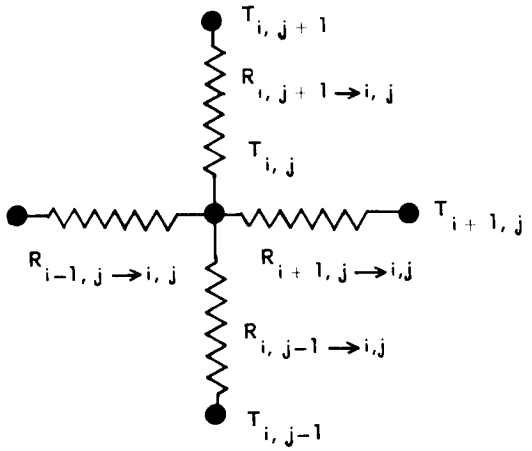

Figure 55 Thermal Network for Internal and Surface Nodal Points

The basic equation for heat flow in Figure 55 is

$$\frac{T_{i,j+1} - T_{i,j}}{R_{i,j+1 \rightarrow i,j}} + \frac{T_{i+1,j} - T_{i,j}}{R_{i+1,j \rightarrow i,j}} + \frac{T_{i,j-1} - T_{i,j}}{R_{i,j-1 \rightarrow i,j}} + \frac{T_{i-1,j} - T_{i,j}}{R_{i-1,j \rightarrow i,j}} = 0$$

and each R is equal to the appropriate $\frac{L}{kA}$.

If two nodal points, say (i-1, j) and (i, j), are located in two adjacent materials with thermal conductivities k_1 and k_2 then

$$R_{i-1,j \rightarrow i,j} = \frac{L_1}{k_1 A} + \frac{L_2}{k_2 A}$$

where $L_1 + L_2$ is equal to the total length of the pad between (i-1, j) and (i, j).

If the nodal point (i, j) is a surface point, then heat exchange with the adjacent air is by convection. Thus, if (i, j) lies on the surface and (i, j+1) lies in the air, then

$$R_{i,\,j+1 \rightarrow i,\,j} = \frac{1}{\bar{h}A}$$

If nodal point (i, j) is an interior point but the subvolume bounds on a surface with air adjacent to it, then for example

$$R_{i,\,j+1 \rightarrow i,\,j} = \frac{1}{\bar{h}A} + \frac{L}{kA}$$

Nodal points in subvolumes in the air film are treated similarly, except that there is heat transfer by mass flow and by heat generation due to shearing. Heat transferred by mass flow is calculated from

$$q_n = m_n c_p \Delta T$$

The heat generated in each subvolume is denoted by $\ddot{q}_{(i,\,j)}$. Details of its determination are discussed below. Nodal points in the air film are located midway between the adjacent working surfaces.

Determination of the gap Reynolds number indicated that flow was laminar. Consequently the heat transfer across the gap was calculated as by pure conduction. The thermal network for each nodal point in the film is shown in Figure 56.

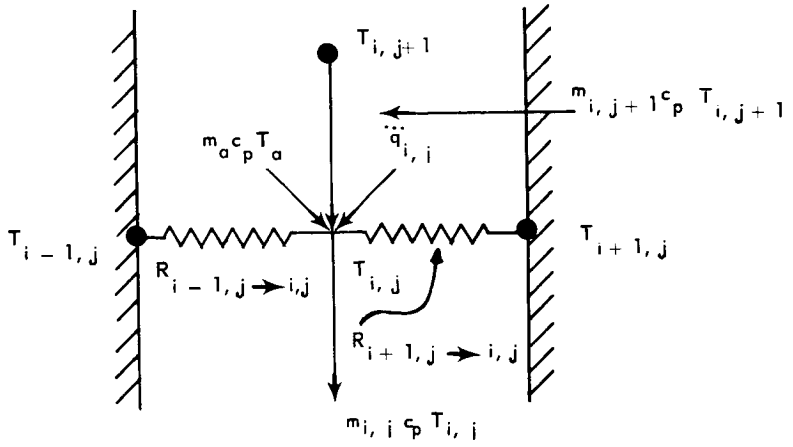

Figure 56 Thermal Network for Nodal Points in the Gap between Seal and Seal Plate

The mass flow rates of air through the gap are calculated in Section IB of this report. The basic equation for heat flow is

$$\frac{T_{i+1,j} - T_{i,j}}{R_{i+1,j \rightarrow i,j}} + \frac{T_{i-1,j} - T_{i,j}}{R_{i-1,j \rightarrow i,j}} + \dddot{q}_{i,j} + m_{i,j+1}\, c_p\, T_{i,j+1} + m_a\, c_p\, T_a - m_{i,j}\, c_p\, T_{i,j} = 0$$

where

$$m_{i,j} = m_{i,j+1} + m_a$$

The term $m_a c_p T_a$ represents heat transferred to (i, j) by air flow from an external supply such as through an air port.

The physical properties of air at 1200°F used in the thermal analysis are

Thermal conductivity	$k = 0.037$ BTU/hr-ft^2-°F/ft
Absolute viscosity	$\mu = 0.0955$ lb/hr/ft
Specific heat at constant pressure	$c_p = 0.269$ BTU/lb-°F
Prandtl number	$P_r = 0.6975$

2. HEAT GENERATION

If the velocity profile in the gap between seal and seal plate in the axial direction is linear

$$\partial U/\partial h = U/h$$

The shear force is consequently $F = \mu A\, U/h$, and the heat generated is $q = FU/J$. Thus, for an air-film subvolume with an area of 7.75 in^2 on the seal and seal plate surfaces, the heat generation is

$$\dddot{q}_{i,j} = \frac{0.0955 \times 7.75 \times 850 \times 850}{12 \times 32.2 \times 0.001 \times 778}$$

$$\approx 1780 \text{ BTU/hr.}$$

if the gap is 0.001 inch, the surface velocity is 850 ft/sec and the air viscosity is 0.0955 lb/hr-ft.

In the spiral-groove orifice configuration, the groove depths are deemed to be so small that for purposes of these calculations they can be neglected. The heat generation in the sub-volumes adjacent to the grooved surfaces of the seal are therefore also calculated as outlined above. The heat generation for the shrouded Rayleigh pad design is calculated taking into account the area covered by recesses and the recess depth.

3. SURFACE COEFFICIENTS FOR CONVECTIVE HEAT TRANSFER

For a number of the surfaces, the geometrics were similar enough to older seals that the coefficients for convective heat transfer could be based on experience. Thus, for example, on the back of the runner the values of $\bar{h}$ = 52 BTU/hr-ft^2-°F at the larger diameters and $\bar{h}$ = 42 BTU/hr-ft^2-°F were used. Over other surfaces, this experience factor was not available, and coefficients for those surfaces were therefore calculated from dimensionless expressions available in the heat-transfer literature. It is realized that these expressions apply more directly to the simpler geometries for which they were obtained, but in the absence of more precise information they were accepted as at least reasonably realistic for the seal geometries analyzed. The details of the expressions used are given below.

a. HORIZONTAL ROTATING CYLINDER WITH NO CLOSE OBSTRUCTIONS

For turbulent flow (i.e. for Re > 15000) the dimensionless equation is

$$Nu = 0.073\ Re^{0.7}$$

The Nusselt number is

$$Nu = \bar{h}D/k$$

and the rotational Reynolds number is

$$Re = \omega D^2 \rho / 2\mu$$

Thus, for the end seal at cruise conditions, the Reynolds Number is 1.172 x 10^7 and the surface coefficient is $\bar{h}$ = 100 BTU/hr-ft^2 - °F if the runner is unobstructed over its perimeter.

b. CYLINDER ROTATING WITH A CONCENTRIC TUBE WITH SMALL AXIAL FLOW

For conditions above critical flow (i.e. for Ta > 90) the dimensionless equation is

$$Nu = 0.350\ Nu_c\ Ta^{0.5}$$

The Nusselt number is

$$Nu = \bar{h}d/k$$

The Nusselt number for pure conduction is

$$Nu_c = \frac{\frac{d}{r_i}}{\ln\left(1+\frac{d}{r_i}\right)}$$

The Reynolds number is

$$Re = r_i \omega d \rho / \mu$$

and the Taylor number is

$$Ta = Re\left(\frac{d}{r_i}\right)^{0.5}$$

For small radial clearances between the cylinder and the tube, the Nusselt number for pure conduction approaches unity. Thus, if it is assumed that the runner-to-compressor casing clearance is 0.25 inch, the Reynolds number is

$$Re = 1.15 \times 10^5,$$

the corresponding Taylor Number is

$$Ta = 1.52 \times 10^4,$$

the Nusselt number for pure condition is

$$Nu_c \approx 1,$$

and the surface coefficient of convective heat transfer is

$$\overline{h} = 75 \text{ BTU/hr-ft}^2\text{-}^\circ\text{F}$$

c. ROTATING DISC WITH A CENTRAL HOLE WHICH ROTATES NEAR A STATIONARY WALL

For turbulent flow (i.e. $Re > 3.1 \times 10^5$) the dimensionless equation is

$$Nu = 0.0149\, Pr^{1/3}\, Re^{0.8} \left[1 + \left(\frac{r_i}{r_o}\right)^{0.5}\right] \left(\frac{s}{r_o}\right)^{0.1}$$

The Nusselt number is

$$Nu = \bar{h}r_o/k$$

The Prandtl number is

$$Pr = c_p\mu/k$$

and the Reynolds number is

$$Re = \omega\rho r_o^2/\mu$$

As an example, the low-pressure face of the runner adjacent to the seal is considered. Here $Re = 6.87 \times 10^4$, so the flow is turbulent, and $Nu = 1238$. The surface coefficient $\bar{h} = 41$ BTU/hr-ft²-°F. Flow is greatly restricted, however, by the drum-like flange of the runner and the surface coefficient of convective heat transfer was therefore estimated as $\bar{h} = 24$ BTU/hr-ft²-°F.

d. CHANNEL FLOW

For laminar flow the dimensionless expression is

$$Nu = \bar{h}t/k = 3.75$$

The Reynolds number of flow over the convex surface of the C-spring, for example, is 1200 and the surface coefficient is

$$\bar{h} = 3 \text{ BTU/hr-ft}^2\text{-°F}$$

e. SURFACES ON THE SEALS EXPOSED TO LITTLE OR NO FLOW

Surface coefficients for convective heat transfer over seal surfaces which are sheltered from windage effects of the runner could not be calculated, and estimates based on the expected circulation were made. Thus, for the back surfaces of the seals, essentially stagnant conditions were assumed, the surface coefficient $\bar{h} = 2$ BTU/hr-ft²-°F. For surfaces closer to the runner, larger coefficients were assumed, for example $\bar{h} = 4$ BTU/hr-ft²-°F over the recessed portion of the outer diameter of the semirigid seal.

The estimates of circulation and surface coefficients were more difficult, for example, in the space bounded by the semirigid seal, the piston ring and the compressor casing. The values of the surface coefficient were assumed here to vary from $\bar{h} = 10$ BTU/hr-ft²-°F to $\bar{h} = 2$ BTU/hr-ft²-°F depending on how much the circulation had been attenuated over the surface considered.

4. NOMENCLATURE

A	area (in^2)
D	diameter (in.)
F	force (to shear air film) (lb)
J	mechanical equivalent of heat (ft-lb/BTU)
L	length dimension, total distance between nodal points, (in.)
R	thermal resistance (hr^oF/BTU)
T	temperature (^oF)
U	runner surface velocity (ft/sec)
a,i,j, ℓ,m,n	indices
b	thickness (inches)
c_p	specific heat (BTU/lb ^oF)
d	radial clearance (inches)
h_m	gap between seal and runner (inches)
$\overline{h}$	mean surface coefficient of convective heat transfer (BTU/hr ft^2 ^oF)
k	thermal conductivity (BTU/hr ft ^oF)
$\dot{m}$	mass flow rate (lb/hr)
q	heat flux (BTU/hr)
$\dddot{q}$	volumetric heat generation (BTU/hr/subvolume)
r	radius (in)
r_i	inner radius (in)
r_o	outer radius (in)
s	mean axial gap between rotor and stationary part (in)
t	channel depth (distance between bounding walls) (in)

APPENDIX C

OC DIAPHRAGM END SEAL

TASK I THERMAL CALCULATIONS

1. INTRODUCTION

The design which is analyzed in this Appendix is shown in Figure 1. Other conditions which define the design are listed below.

Core ambient temperature	1136°F
Outer ambient temperature	1200°F
Supply flow	10×10^{-4} lb/sec-in
Vent flow	8.4×10^{-4} lb/sec-in
Conductivity of rotating element (inco 901)	11.2 BTU/hr-ft-°F
Conductivity of stationary element (Inco 750)	11.9 BTU/hr-ft-°F
Rotational speed	4.4×10^{5} rev/hr
Average seal radius	13.5 inches

For the temperature calculations, all surface heat-transfer coefficients were derived from the calculations discussed in Appendix B. The seal clearances which are used for the heat generation and admittance calculations take into account the relative areas of the land and recess regions. Also, the effect of flow through the piston ring seal is included.

The results of the calculations are shown in Figure 57 in the form of a steady-state temperature map of the OC diaphragm end seal.

2. ANALYSIS

a. HEAT GENERATION

Heat generation in the seal clearance is calculated using the equation for a rotating disk and stationary wall, and a linear velocity profile due to rotation.

$$q = 0.318 \left(\frac{R^3 \ell}{b}\right) N^2 \mu$$

where
- q = heat generation (BTU/hr)
- R = mean radius of the element (ft)
- ℓ = radial length of the element (ft)
- b = axial clearance (ft)
- N = rotational speed (rev/hr)
- μ = dynamic viscosity (lb_f-hr/ft^2)

For gas nodes 73 and 77 in the seal clearance, the value of the axial clearance "b" is obtained by taking the area-weighted average of the clearances of the land and recess. The

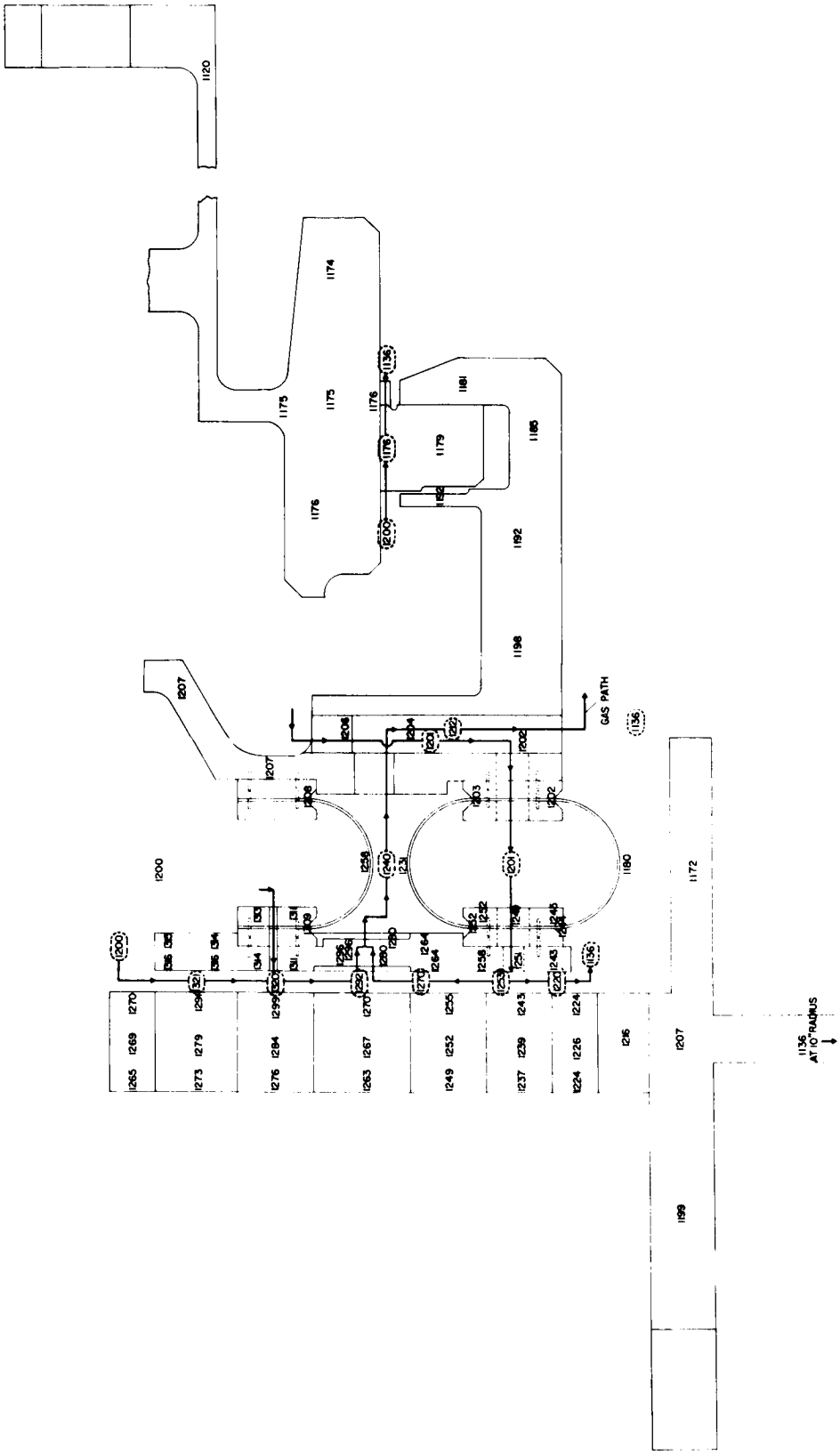

Figure 57 Temperature Distribution (in Degrees Fahrenheit) in the OC Diaphragm End Seal at Cruise Conditions

nodal network used is shown in Figure 58. The area loss due to the presence of supply and vent holes is neglected.

In all cases

$$N = 4.4 \times 10^5 \text{ (rev/hr)}$$

and

$$\mu = 2.29 \times 10^{-10} \text{ (lb}_f\text{-hr/ft}^2\text{)}$$

so that

$$N^2\mu = 44.4$$

and

$$q = 14.1\left(\frac{R^3 \ell}{b}\right) \tag{70}$$

For nodes 73 and 77, Equation 70 is rewritten

$$Q = 14.1\, R^3 \ell \left(\frac{A_\ell}{A_t}\,\frac{1}{b_\ell} + \frac{A_r}{A_t}\,\frac{1}{b_r}\right)$$

where the subscripts ℓ, r, and t refer to the land, recess and added properties. The heat generation for nodes 73 through 78 is tabulated in Table XVI.

TABLE XVI

HEAT GENERATION

Node	Radius Mean R (ft)	Radial Length ℓ (ft)	Axial Clearance b_ℓ (ft)	Axial Clearance b_r (ft)	Area Ratio $\frac{A_\ell}{A_t}$	Area Ratio $\frac{A_r}{A_t}$	Heat Generation q (Btu/hr)
73	1.17	0.0208	8.35×10^{-5}	2.71×10^{-4}	0.62	0.38	4170
74	1.15	0.0208	8.35×10^{-5}	0.0	1.0	0.0	5350
75	1.13	0.0250	1.46×10^{-3}	0.0	1.0	0.0	340
76	1.11	0.0067	8.35×10^{-5}	0.0	1.0	0.0	1510
77	1.09	0.0278	8.34×10^{-5}	1.875×10^{-4}	0.47	0.53	1390
78	1.07	0.0067	8.35×10^{-5}	0.0	1.0	0.0	4300
						TOTAL	17060

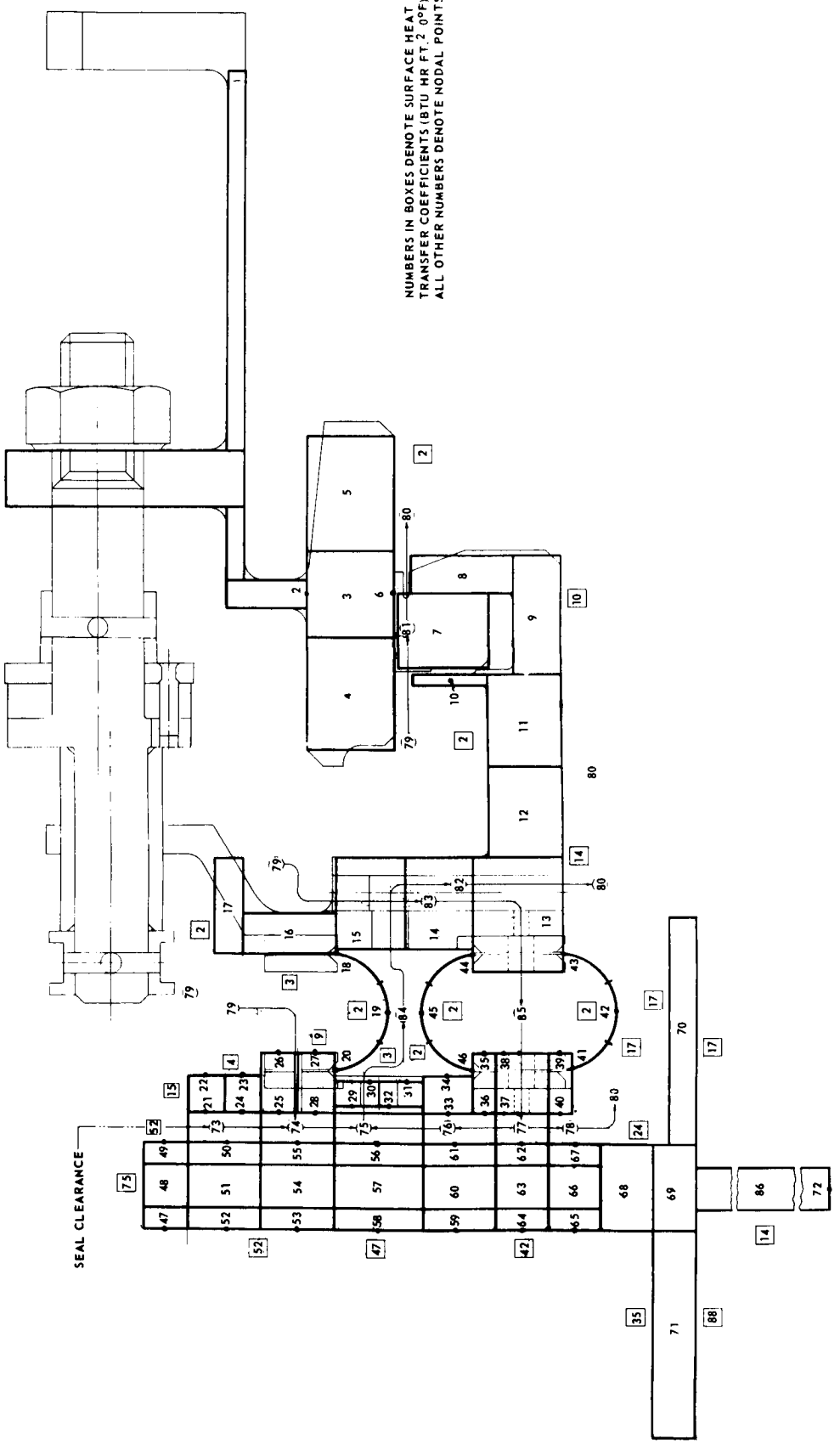

Figure 58 Nodal Network for the OC Diaphragm End Seal

b. HEAT TRANSFER COEFFICIENTS

(1) Seal Clearances

Pure conduction (k = 0.037 Btu/hr-ft-°F) is assumed across the seal clearances at nodes 73 to 78 inclusive. The width of the clearance used in these calculations is the area-weighted average of the clearances at the land and recess. The quantity "b" is tabulated in Table XVII.

$$b = \frac{A_\ell b_\ell + A_r b_r}{A_t}$$

TABLE XVII

WEIGHTED AXIAL CLEARANCE

Node	Area Ratio $\frac{A_\ell}{A_t}$	Area Ratio $\frac{A_r}{A_t}$	Land Axial Clearance b_ℓ (in)	Recess Axial Clearance b_r (in)	Weighted Axial Clearance b (in)
73	0.62	0.38	0.0010	0.00325	0.0018
74	1.0	0.0	0.0010	0.0	0.0010
75	1.0	0.0	0.0175	0.0	0.0175
76	1.0	0.0	0.0010	0.0	0.0010
77	0.47	0.53	0.0010	0.00225	0.0017
78	1.0	0.0	0.0010	0.0	0.0010

(2) Piston Ring Clearance

The average clearance at the piston ring (between metal nodes 7 and 6) is calculated using the same method which is used at the seal clearances. In this case

$$b = 0.125(0.0005) + 0.875(0.001) = 0.00098 \text{ inch}$$

(3) Vent and Supply Holes

The total vent flow is

$$w = 8.4 \times 10^{-4} \text{ lb/sec-in}$$

so that using an average radius of 13.5 inches, and assuming 154 vent holes, the amount of flow per hole is

$$w_v = \frac{8.4 \times 10^{-4} (13.5)}{154} = 4.63 \times 10^{-4} \text{ lb/sec}$$

The Reynold's number for pipe flow in any one hole is

$$Re = \frac{\rho VD}{\mu} = \frac{\rho w_v}{\rho A} D = \frac{4 w_v D}{\pi D^2 \mu} = \frac{4 w_v}{\pi \mu D}$$

where

$D = 0.125/12 = 1.04 \times 10^{-2}$ ft
$\rho = 2.4 \times 10^{-2}$ lb/ft^3
$\mu = 2.65 \times 10^{-5}$ lb/sec.ft

so that

$$Re = 2140 \text{ (low transition range)}$$

For laminar conditions, the Graetz chart (which includes entrance effects for a sharp-edged sudden contraction) yields a mean film coefficient of h = 60 BTU/hr-ft-°F).

For the supply flow of

$$w = 10 \times 10^{-4} \text{ lb/sec-in}$$

at 13.5 (in) and 77 holes, the flow per hole yields a Reynolds number of 5100 (mid-transition). Using a Latzko connection factor for entrance effects and the Colburn-Reynolds type equation for turbulent pipe flow, the mean film coefficient is h = 110 BTU/hr-ft^2-°F).

c. ADMITTANCE MATRIX

The heat transfer areas between the vent and supply holes and the metal (nodes 13, 14, 15) are summarized in the following tabulation.

		Area/Node (ft^2)	
Node	A_o (Area/hole node) (ft^2)	$A_v = 154 A_o$	$A_s = 77 A_1$
13	4.85×10^{-4}	7.47×10^{-2}	3.74×10^{-2}
14	6.23×10^{-4}	9.60×10^{-2}	4.80×10^{-2}
15	6.92×10^{-4}	10.65×10^{-2}	5.33×10^{-2}
TOTAL	17.97×10^{-4}		

Using the film coefficients of 60 and 110 for the vent and supply holes respectively, the admittances for nodes 13, 14, 15 are summarized in the following tabulation.

Node	$A_v(ft^2)$	h_a(Btu/hr-ft²-°F)	Y_v(Btu/hr-°F)	A_s	h_s	Y_s
13	7.47×10^{-2}	60	4.48	3.74×10^{-2}	110	4.12
14	9.6×10^{-2}	60	5.76	4.8×10^{-2}	110	5.28
15	10.65×10^{-2}	60	6.38	5.33×10^{-2}	110	5.87

Thus,

	Nodes	Admittance Y (Btu/hr°F)
	13/82	4.5
Vent	14/82	5.8
	15/82	6.4
	13/83	4.1
Supply	14/83	5.3
	15/83	5.9

All other admittances are computed using MTI Program PN0317. The pertinent input and output data are included as Tables XVIII and XIX.

d. HEAT BALANCE EQUATIONS

(1) Heat Exchanger

The region which is represented by metal nodes 13, 14, 15 is a complex heat transfer network. In this region, the 77 supply holes exchange heat with the 154 vent holes by forced convection, and by conduction through the metal. This is shown in the model given in Figure 59. The way in which the nodes of the model are connected to construct the heat balance equations is shown in the flow chart at the bottom of the same figure. Figure 60 shows the connection between this flow chart and the over-all fluid network for the end seal heat-balance calculation.

TABLE XVIII

INPUT DATA FROM ADMITTANCE CALCULATION

			PW OC FINAL NODES 1* TO 7*						6 9 67			
			RL THORKILDSEN						RD501 10			
1	1	2		13.96	14.02				.65			11.9
2	2	79				13.99	14.02	14.02	1.3		2.0	11.9
3	2	80	2 79									
4	2	3		13.96	14.02				.7			
5	3	4				13.99	14.377		.2			11.9
6	4	79		14.02	14.794				.1		2.0	11.9
7	4	79		14.02	14.794				.1		2.0	11.9
8	4	79				14.377	14.794	14.794	.2		2.0	11.9
9	3	5		13.96	14.02				.275			11.9
10	5	3	3 5									
11	5	79				13.99	14.02	14.02	.35		2.0	11.9
12	5	80				13.96	13.99	13.96	.25		2.0	11.9
13	5	6				13.852	13.99		.11			11.9
14	6	5	5 6									
15	6	79		13.744	13.96				.05		2.0	11.9
16	6	80	6 79									
17	6	7				13.744	13.852		.1			11.9
			PW OC FINAL COMPLETE						6 12 67			
			RL THORKILDSEN						RD501 10			
1	2	3				13.594	13.744		.3			11.9
2	3	6	2 3									
3	3	4		13.444	13.744				.35			11.9
4	3	5	3 4									
5	4	79				13.594	13.744	13.744	.5		2.0	11.9
6	4	79		13.444	13.744				.2		2.0	11.9
7	4	79				13.444	13.594	13.444	.3		2.0	11.9
8	4	3	3 4									
9	5	3	3 5									

10	5	80					13.594	13.744	13.744	.5	2.0	11.9
11	5	80			13.444	13.744				.2	2.0	11.9
12	5	80					13.444	13.594	13.444	.45	2.0	11.9
13	6	3	3	6								
~~14~~	6	7					13.276	13.444		.306		11.9
~~15~~	7	6	6	7								
16	7	10			13.126	13.384				.13		11.9
17	7	10			13.126	13.384				.014		.037
18	7	8			13.126	13.384				.2		11.9
19	7	9					13.051	13.276		.27		11.9
20	7	9					13.025	13.126		.263		.037
21	8	7	7	8								
22	8	80			13.025	13.38				.065	2.0	11.9
23	8	9					13.00	13.275		.13		11.9
24	9	8	8	9								
25	9	80					12.925	13.00	12.925	.42	2.0	11.9
26	9	7					13.051	13.276		.27		11.9
27	9	7					13.025	13.126		.263		.037
28	9	11			12.925	13.075				.4		11.9
29	10	7			13.126	13.38				.13		11.9
30	10	7			13.126	13.38				.014		.037
31	10	79			13.126	13.38				.025	2.0	11.9
32	10	11					13.1	13.276		.05		11.9
33	11	9	9	11								
34	11	10	10	11								
35	11	79					13.025	13.126	13.126	.275	2.0	11.9
36	11	80					12.925	13.025	12.925	.32	2.0	11.9
37	11	12			12.925	13.126				.325		11.9
38	12	11	11	12								
39	12	79					13.025	13.126	13.126	.32	2.0	11.9
40	12	80	11	80								
41	12	13			12.925	13.20				.35		11.9
42	13	12	12	13								
43	13	14					13.025	13.314		.32		11.9
44	13	80					12.925	13.025	12.925	.36	2.0	11.9
45	13	43					12.925	13.025		.15		11.9

46	13	44	13	43								
47	13	82										
48	13	83										
49	14	13	13	14								
50	14	15					13.314	13.538		.32		11.9
51	14	79										
52	14	82										
53	14	83										
54	15	14	14	15								
55	15	79										
56	15	82										
57	15	83										
58	15	16					13.65	13.775		.16		11.9
59	16	15	15	16								
60	16	17					13.775	14.01		.16		11.9
61	16	79			13.65	13.96				.13	2.0	11.9
62	16	79			13.65	13.9				.13	2.0	11.9
63	17	16	16	17								
64	17	79			13.96	14.07				.2	2.0	11.9
65	17	79					14.01	14.07	14.07	.4	2.0	11.9
66	17	79			13.96	14.07				.2	2.0	11.9
67	17	79					13.96	14.01	13.96	.33	2.0	11.9
68	18	16					13.65	13.775		.14		11.9
69	18	19			13.575	13.581				.314		11.9
70	18	79			13.538	13.65				.003	2.0	11.9
71	18	84			13.538	13.65				.003	3.0	11.9
72	19	18	18	19								
73	19	79					13.5	13.503	13.503	.3	2.0	11.9
74	19	84					13.497	13.5	13.497	.3	3.0	11.9
75	19	20	18	19								
76	20	19	19	20								
77	20	79	18	79								
78	20	84	18	84								
79	20	27					13.65	13.775		.1		11.9
80	21	73			14.01	14.15				.000924		.037
81	21	79					14.08	14.15	14.15	.0625	15.0	11.9

82	21	22			14.01	14.15			•125		11.9
83	21	24					13.925	14.08	•0625		11.9
84	22	21	21	22							
85	22	79	21	79							
86	22	79			14.01	14.15			0•	4.0	11.9
87	22	23	21	24							
88	23	22	22	23							
89	23	79			13.9	14.01			0•	4.0	11.9
90	23	26					13.8	13.935	•1		11.9
91	23	24			13.9	14.01			•125		11.9
92	24	23	23	24							
93	24	21	21	24							
94	24	73			13.9	14.01			•000924		•037
95	24	25					13.8	13.935	•0625		11.9
96	25	24	24	25							
97	25	26			13.775	13.9			•21		11.9
98	25	28					13.71	13.8	•1		11.9
99	25	74			13.775	13.9			•0005		•037
100	26	23	23	26							
101	26	25	25	26							
102	26	79			13.775	13.9			0•	2.0	11.9
103	26	27	25	28							
104	27	26	26	27							
105	27	79			13.65	13.775			0•	2.0	11.9
106	27	20					13.65	13.71	•1		11.9
107	27	28			13.65	13.775			•21		11.9
108	28	25	25	28							
109	28	27	27	28							
110	28	29					13.575	13.71	•045		11.9
111	28	30	28	29							
112	28	74			13.65	13.775			•0005		•037
113	29	28	28	29							
114	29	30			13.5	13.65			•087		11.9
115	29	32					13.43	13.575	•043		11.9
116	29	75			13.5	13.65			•00875		•037
117	30	29	29	30							
118	30	28	28	30							

119	30	84			13.5	13.65				0.	3.0	11.9
120	30	31					13.43	13.575		.043		11.9
121	31	30	30	31								
122	31	84			13.35	13.5				0.	3.0	11.9
123	31	34					13.273	13.43		.05		11.9
124	31	32			13.35	13.5				.0625		11.9
125	32	29	29	32								
126	32	31	31	32								
127	32	33	31	34								
128	32	75			13.35	13.5				.00875		.037
129	33	32	32	33								
130	33	34			13.189	13.35				.125		11.9
131	33	36					13.148	13.273		.125		11.9
132	33	76			13.273	13.35				.0005		.037
133	33	77			13.189	13.273				.00083		.037
134	34	31	31	34								
135	34	84			13.189	13.35				0.	2.0	11.9
136	34	36	33	36								
137	34	33			13.189	13.35				.125		11.9
138	35	46					13.148	13.189		.1		11.9
139	35	85			13.11	13.189				0.	2.0	11.9
140	35	38					13.03	13.148		.1		11.9
141	35	36			13.11	13.189				.2		11.9
142	36	33	33	36								
143	36	34	34	36								
144	36	35	35	36								
145	36	37	35	38								
146	36	77			13.11	13.189				.00083		.037
147	37	36	36	37								
148	37	38			12.94	13.11				.2		11.9
149	37	40					12.9	13.03		.1		11.9
150	37	77			12.94	13.11				.00083		.037
151	38	35	35	38								
152	38	85			12.94	13.11				0.	2.0	11.9
153	38	39	37	40								
154	38	37	37	38								

155	39	38	38	39							
156	39	85			12.86	12.94				0.	2.0	11.9
157	39	41					12.86	12.9		.1		11.9
158	39	40			12.86	12.94				.2		11.9
159	40	37	37	40								
160	40	39	39	40								
161	40	80					12.86	12.9	12.86	.1	17.0	11.9
162	40	78			12.86	12.9				.0005		.037
163	41	39	39	41								
164	41	85			12.76	12.86				.003	2.0	11.9
165	41	42			12.76	12.766				.314		11.9
166	41	80			12.76	12.86				.003	17.0	11.9
167	42	41	41	42								
168	42	85					13.76	13.763	13.763	.3	2.0	11.9
169	42	43	41	42								
170	42	80					13.757	13.76	13.757	.3	17.0	11.9
171	43	42	42	43								
172	43	85	41	85								
173	43	44					12.9	13.189		.125		11.9
174	43	80	41	80								
175	43	13	13	43								
176	43	85			12.9	13.03				.125	2.0	11.9
177	44	43	43	44								
178	44	13	13	44								
179	44	14	44	13								
180	44	85	18	79								
181	44	84	44	85								
182	44	45	18	19								
183	45	46	44	45								
184	45	84	19	79								
185	45	44	45	46								
186	45	85	45	84								
187	46	45	45	46								
188	46	85	44	85								
189	46	35	35	46								
190	46	84	44	84								

191	47	79			14.15	14.3					0.	52.0	11.2
192	47	79					14.23	14.3	14.3	.075	75.0	11.2
193	47	48			14.15	14.3				.157		11.2
194	47	52					14.03	14.23		.075		11.2
195	48	47	47	48								
196	48	79					14.23	14.3	14.3	.313	75.0	11.2
197	48	49	48	47								
198	48	51					14.03	14.23		.313		11.2
199	49	48	48	49								
200	49	79			14.15	14.3				0.	52.0	11.2
201	49	79					14.23	14.3	14.3	.075	75.0	11.2
202	49	50	47	52								
203	50	51			13.9	14.15				.157		11.2
204	50	49	49	50								
205	50	73			13.9	14.15				.000924		.037
206	50	55					13.775	14.03		.075		11.2
207	51	52	50	51								
208	51	48	48	51								
209	51	50	50	51								
210	51	54					13.775	14.03		.157		11.2
211	52	47	47	52								
212	52	51	51	52								
213	52	53	50	55								
214	52	79			13.9	14.15				0.	52.0	11.2
215	53	52	52	53								
216	53	54			13.65	13.9				.157		11.2
217	53	58					13.5	13.775		.075		11.2
218	53	79			13.65	13.9				0.	52.0	11.2
219	54	53	53	54								
220	54	51	51	54								
221	54	55	53	54								
222	54	57					13.5	13.775		.157		11.2
223	55	54	54	55								
224	55	50	50	55								
225	55	74			13.65	13.9				.0005		.037
226	56	57			13.35	13.65				.157		11.2

227	56	55	53	58							
228	56	75			13.35	13.65			•00875		•037
229	56	61					13.23	13.5	•075		11.2
230	57	58	56	57							
231	57	54	54	57							
232	57	56	56	57							
233	57	60					13.23	13.5	•157		11.2
234	58	53	53	58							
235	58	57	57	58							
236	58	59	56	61							
237	58	79			13.35	13.65			0.	47.0	11.2
238	59	58	58	59							
239	59	60			13.11	13.35			•157		11.2
240	59	64					13.03	13.23	•075		11.2
241	59	79			13.11	13.35			0.	42.0	11.2
242	60	59	59	60							
243	60	57	57	60							
244	60	61	59	60							
245	60	63					13.03	13.23	•157		11.2
246	61	60	60	61							
247	61	56	59	58							
248	61	76			13.273	13.35			•0005		•037
249	61	77			13.11	13.273			•00083		•037
250	61	62	59	64							
251	62	63			12.94	13.11.			•157		11.2
252	62	61	61	62							
253	62	77			12.94	13.11			•00083		•037
254	62	67					12.85	13.03	•075		11.2
255	63	64	62	63							
256	63	60	60	63							
257	63	62	62	63							
258	63	66					12.85	13.03	•157		11.2
259	64	59	59	64							
260	64	63	63	64							
261	64	65					12.85	13.03	•075		11.2
262	64	79			12.94	13.11			0.	42.0	11.2

263	65	64	64	65								
264	65	66			12.76	12.94				.157		11.2
265	65	68					12.68	12.85		.116		11.2
266	65	79			12.76	12.94				0.	42.0	11.2
267	66	65	65	66								
268	66	63	63	66								
269	66	67	65	66								
270	66	68					12.68	12.85		.157		11.2
271	67	66	66	67								
272	67	62	65	64								
273	67	78			12.86	12.94				.0005		.037
274	67	68	65	68								
275	67	80			12.76	12.85				0.	24.0	11.2
276	68	65	65	68								
277	68	66	66	68								
278	68	67	67	68								
279	68	80			12.59	12.76				.157	24.0	11.2
280	68	79			12.59	12.76				.157	42.0	11.2
281	68	69					12.52	12.68		.313		11.2
282	69	68	68	69								
283	69	70			12.44	12.54				.475		11.2
~~284~~	69	72					10.0	12.52		.156		11.2
285	69	71			12.44	12.59				.45		11.2
286	70	69	69	70								
287	70	80					12.52	12.54	12.54	.79	17.0	11.2
288	70	80			12.44	12.54				.4	17.0	11.2
289	70	80					12.44	12.52	12.44	.79	17.0	11.2
290	71	69	69	71								
291	71	80					12.44	12.52	12.44	.73	8.8	11.2
292	71	79					12.52	12.59	12.59	.73	35.0	11.2

PW OC FINAL ADDITIONAL CALCS 6 13 67
RLT RD 501 10

1	14	84			13.189	13.413				.16	2.0	11.9
2	15	84			13.413	13.65				.16	2.0	11.9
3	6	81					13.444	13.4448		.35		.037
4	7	81	6	81								

```
 5  7 81                          13.276 13.4443     .30            11.9
 6 69 86                          11.22  12.52       .156           11.2
 7 72 86                          10.00  11.22       .156           11.2
 8 86 80      10.00   12.44                          .078    14.0   11.2
 9 86 80      10.00   12.44                          .078    14.0   11.2
10 16 18                          13.663 13.775      .175           11.9
```

TABLE XIX

OUTPUT DATA FROM ADMITTANCE CALCULATION

TITLE PW OC FINAL NODES 1* TO 7* * DATE 6 9 67

ENGINEER RL THORKILDSEN CHARGE NO. RD501 10

			********** RESISTANCE *******				ADMITTANCES	
			CONDUCTION		CONVECTION		BTU/HR DEGREE F	
N	I	J	AXIAL	RADIAL	AXIAL	RADIAL	AXIAL	RADIAL
1	1	2	0.1242E 00				0.8046E 01	
2	2	79		0.2644E-03		0.6287E 00		0.1589E 01
3	2	80		0.2644E-03		0.6287E 00		0.1589E 01
4	2	3		0.0000E 00				0.0000E 00
5	3	4		0.2189E-01				0.4566E 02
6	4	79	0.1439E-02		0.1027E 01		0.9717E 00	
7	4	79	0.1439E-02		0.1027E 01		0.9717E 00	
8	4	79		0.2294E-01		0.3872E 01		0.2566E 00
9	3	5	0.5258E-01				0.1901E 02	
10	5	3	0.5258E-01				0.1901E 02	
11	5	79		0.9821E-03		0.2335E 01		0.4280E 00
12	5	80		0.1378E-02		0.3283E 01		0.3044E 00
13	5	6		0.1446E-01				0.6914E 02
14	6	5		0.1446E-01				0.6914E 02
15	6	79	0.2682E-02		0.3829E 01		0.2609E 00	
16	6	80	0.2682E-02		0.3829E 01		0.2609E 00	
17	6	7		0.1256E-01				0.7960E 02

*This calculation is used to determine the effect of conduction and connection which takes place between nodes 1 and 2 which are indicated on Figure 58.

TITLE PW OC FINAL COMPLETE DATE 6 12 67

ENGINEER RL THORKILDSEN CHARGE NO. RD501 10

			********** RESISTANCE *******				ADMITTANCES	
			CONDUCTION		CONVECTION		BTU/HR DEGREE F	
N	I	J	AXIAL	RADIAL	AXIAL	RADIAL	AXIAL	RADIAL
1	2	3		0.5870E-02				0.1703E 03
2	3	6		0.5870E-02				0.1703E 03
3	3	4	0.1377E-01				0.7260E 02	
4	3	5	0.1377E-01				0.7260E 02	
5	4	79		0.3522E-02		0.1667E 01		0.5984E 00
6	4	79	0.7870E-02		0.2809E 01		0.3548E 00	
7	4	79		0.5935E-02		0.2841E 01		0.3512E 00
8	4	3	0.1377E-01				0.7260E 02	
9	5	3	0.1377E-01				0.7260E 02	
10	5	80		0.3522E-02		0.1667E 01		0.5984E 00
11	5	80	0.7870E-02		0.2809E 01		0.3548E 00	
12	5	80		0.3957E-02		0.1894E 01		0.5268E 00
13	6	3		0.5870E-02		0.0000E 00		0.1703E 03
~~14~~	~~6~~	~~7~~		0.6595E-02				0.1516E 03
~~15~~	~~7~~	~~6~~		0.6595E-02				0.1516E 03
16	7	10	0.6101E-02				0.1639E 03	
17	7	10	0.2113E 00				0.4732E 01	4.6
18	7	8	0.9386E-02				0.1065E 03	
19	7	9		0.1016E-01			0.65	0.9842E 02
20	7	9		0.1515E 01				0.6596E 00
21	8	7	0.9386E-02				0.1065E 03	
22	8	80	0.2225E-02		0.2444E 01		0.4086E 00	
23	8	9		0.2584E-01				0.3869E 02
24	9	8		0.2584E-01				0.3869E 02
25	9	80		0.2210E-02		0.2110E 01		0.4732E 00
26	9	7		0.1016E-01				0.9842E 02
27	9	7		0.1515E 01				0.6596E 00

28	9	11	0.3292E-01				0.3037E 02	
29	10	7	0.6198E-02				0.1613E 03	
30	10	7	0.2146E 00				0.4658E 01	
31	10	79	0.1191E-02		0.3404E 01		0.2936E 00	
32	10	11		0.4283E-01				0.2334E 02
33	11	9	0.3292E-01				0.3037E 02	
34	11	10		0.4283E-01				0.2334E 02
35	11	79		0.4507E-02		0.3174E 01		0.3145E 00
36	11	80		0.3865E-02		0.2770E 01		0.3604E 00
37	11	12	0.1992E-01				0.5019E 02	
38	12	11	0.1992E-01				0.5019E 02	
39	12	79		0.3873E-02		0.2728E 01		0.3660E 00
40	12	80		0.3865E-02		0.2770E 01		0.3604E 00
41	12	13	0.1563E-01				0.6394E 02	
42	13	12	0.1563E-01				0.6394E 02	
43	13	14		0.1100E-01				0.9085E 02
44	13	80		0.3435E-02		0.2462E 01		0.4054E 00
45	13	43		0.8246E-02				0.1212E 03
46	13	44		0.8246E-02				0.1212E 03
47	13	82		0.0000E 00				0.0000E 00
48	13	83		0.0000E 00				0.0000E 00
49	14	13		0.1100E-01				0.9085E 02
50	14	15		0.8367E-02				0.1195E 03
51	14	79		0.0000E 00				0.0000E 00
52	14	82		0.0000E 00				0.0000E 00
53	14	83		0.0000E 00				0.0000E 00
54	15	14		0.8367E-02				0.1195E 03
55	15	79		0.0000E 00				0.0000E 00
56	15	82		0.0000E 00				0.0000E 00
57	15	83		0.0000E 00				0.0000E 00
58	15	16		0.9143E-02				0.1093E 03
59	16	15		0.9143E-02				0.1093E 03
60	16	17		0.1696E-01				0.5893E 02
61	16	79	0.4875E-02		0.2677E 01		0.3727E 00	
62	16	79	0.6058E-02		0.3327E 01		0.2999E 00	
63	17	16		0.1696E-01				0.5893E 02

64	17	79	0.2082E-01			0.7433E 01			0.1341E 00		
65	17	79		0.1714E-02			0.2036E 01			0.4907E 00	
66	17	79	0.2082E-01			0.7433E 01			0.1341E 00		
67	17	79		0.1738E-02			0.2487E 01			0.4017E 00	
68	18	16		0.1045E-01						0.9569E 02	
69	18	19	0.6185E 00						0.1616E 01		
70	18	79	0.3162E-03			0.7526E 01			0.1328E 00		
71	18	84	0.3162E-03			0.5017E 01			0.1992E 00		
72	19	18	0.6185E 00						0.1616E 01		
73	19	79		0.1187E-03			0.2828E 01			0.3534E 00	
74	19	84		0.1188E-03			0.1886E 01			0.5299E 00	
75	19	20	0.6185E 00						0.1616E 01		
76	20	19	0.6185E 00						0.1616E 01		
77	20	79	0.3162E-03			0.7526E 01			0.1328E 00		
78	20	84	0.3162E-03			0.5017E 01			0.1992E 00		
79	20	27		0.1463E-01						0.6835E 02	
80	21	73	0.2419E-01						0.4132E 02		
81	21	79		0.1273E-01			0.1727E 01			0.5745E 00	
82	21	22	0.1017E-01						0.9825E 02		
83	21	24		0.2842E-01						0.3517E 02	
84	22	21	0.1017E-01						0.9825E 02		
85	22	79		0.1273E-01			0.1727E 01			0.5745E 00	
86	22	79				0.2906E 01			0.3440E 00		
87	22	23		0.2842E-01						0.3517E 02	
88	23	22		0.2842E-01						0.3517E 02	
89	23	79				0.3732E 01			0.2679E 00		
90	23	26		0.1562E-01						0.6400E 02	
91	23	24	0.1306E-01						0.7651E 02		
92	24	23	0.1306E-01						0.7651E 02		
93	24	21		0.2842E-01						0.3517E 02	
94	24	73	0.3107E-01						0.3218E 02		
95	24	25		0.2499E-01						0.4000E 02	
96	25	24		0.2499E-01						0.4000E 02	
97	25	26	0.1948E-01						0.5132E 02		
98	25	28		0.1050E-01						0.9522E 02	
99	25	74	0.1492E-01						0.6701E 02		

100	26	23		0.1562E-01				0.6400E 02
101	26	25	0.1948E-01				0.5132E 02	
102	26	79			0.6625E 01		0.1509E 00	
103	26	27		0.1050E-01				0.9522E 02
104	27	26		0.1050E-01				0.9522E 02
105	27	79			0.6685E 01		0.1495E 00	
106	27	20		0.7038E-02				0.1420E 03
107	27	28	0.1966E-01				0.5085E 02	
108	28	25		0.1050E-01				0.9522E 02
109	28	27	0.1966E-01				0.5085E 02	
110	28	29		0.3529E-01				0.2833E 02
111	28	30		0.3529E-01				0.2833E 02
112	28	74	0.1505E-01				0.6641E 02	
113	29	28		0.3529E-01				0.2833E 02
114	29	30	0.6857E-02				0.1458E 03	
115	29	32		0.4008E-01				0.2494E 02
116	29	75	0.2218E 00				0.4508E 01	
117	30	29	0.6857E-02				0.1458E 03	
118	30	28		0.3529E-01				0.2833E 02
119	30	84			0.3751E 01		0.2665E 00	
120	30	31		0.4008E-01				0.2494E 02
121	31	30		0.4008E-01				0.2494E 02
122	31	84			0.3793E 01		0.2636E 00	
123	31	34		0.3774E-01				0.2649E 02
124	31	32	0.4981E-02				0.2007E 03	
125	32	29		0.4008E-01				0.2494E 02
126	32	31	0.4981E-02				0.2007E 03	
127	32	33		0.3774E-01				0.2649E 02
128	32	75	0.2242E 00				0.4458E 01	
129	33	32		0.3774E-01				0.2649E 02
130	33	34	0.9390E-02				0.1064E 03	
131	33	36		0.1214E-01				0.8231E 02
132	33	76	0.2518E-01				0.3971E 02	
133	33	77	0.3854E-01				0.2594E 02	
134	34	31		0.3774E-01				0.2649E 02
135	34	84			0.5363E 01		0.1864E 00	

136	34	36		0.1214E-01						0.8231E 02	
137	34	33	0.9390E-02					0.1064E 03			
138	35	46		0.4996E-02						0.2001E 03	
139	35	85			0.1103E 02			0.9065E-01			
140	35	38		0.1446E-01						0.6911E 02	
141	35	36	0.3089E-01					0.3236E 02			
142	36	33		0.1214E-01						0.8231E 02	
143	36	34		0.1214E-01						0.8231E 02	
144	36	35	0.3089E-01					0.3236E 02			
145	36	37		0.1446E-01						0.6911E 02	
146	36	77	0.4124E-01					0.2424E 02			
147	37	36		0.1446E-01						0.6911E 02	
148	37	38	0.1449E-01					0.6898E 02			
149	37	40		0.1609E-01						0.6214E 02	
150	37	77	0.1934E-01					0.5168E 02			
151	38	35		0.1446E-01						0.6911E 02	
152	38	85			0.5175E 01			0.1932E 00			
153	38	39		0.1609E-01						0.6214E 02	
154	38	37	0.1449E-01					0.6898E 02			
155	39	38		0.1609E-01						0.6214E 02	
156	39	85			0.1110E 02			0.9005E-01			
157	39	41		0.4984E-02						0.2006E 03	
158	39	40	0.3110E-01					0.3215E 02			
159	40	37		0.1609E-01						0.6214E 02	
160	40	39	0.3110E-01					0.3215E 02			
161	40	80		0.4984E-02		0.1048E 01				0.9493E 00	
162	40	78	0.5009E-01					0.1996E 02			
163	41	39		0.4984E-02						0.2006E 03	
164	41	85	0.3758E-03		0.8945E 01			0.1117E 00			
165	41	42	0.6581E 00					0.1519E 01			
166	41	80	0.3758E-03		0.1052E 01			0.9498E 00			
167	42	41	0.6581E 00					0.1519E 01			
168	42	85		0.1165E-03		0.2775E 01				0.3602E 00	
169	42	43	0.6581E 00					0.1519E 01			
170	42	80		0.1165E-03		0.3266E 00				0.3060E 01	
171	43	42	0.6581E 00					0.1519E 01			

172	43	85	0.3758E-03			0.8945E 01			0.1117E 00		
173	43	44		0.2844E-01						0.3515E 02	
174	43	80	0.3758E-03			0.1052E 01			0.9498E 00		
175	43	13		0.8246E-02						0.1212E 03	
176	43	85	0.1190E-01			0.6798E 01			0.1468E 00		
177	44	43		0.2844E-01						0.3515E 02	
178	44	13		0.8246E-02						0.1212E 03	
179	44	14		0.8246E-02						0.1212E 03	
180	44	85	0.3162E-03			0.7526E 01			0.1328E 00		
181	44	84	0.3162E-03						0.1328E 00		
182	44	45	0.6185E 00						0.1616E 01		
183	45	46	0.6185E 00						0.1616E 01		
184	45	84		0.1187E-03			0.2828E 01			0.3534E 00	
185	45	44	0.6185E 00						0.1616E 01		
186	45	85		0.1187E-03						0.3534E 00	
187	46	45	0.6185E 00						0.1616E 01		
188	46	85	0.3162E-03						0.1328E 00		
189	46	35		0.4996E-02						0.2001E 03	
190	46	84	0.3162E-03						0.1328E 00		
191	47	79				0.2065E 00			0.4841E 01		
192	47	79		0.1115E-01			0.2849E 00			0.3377E 01	
193	47	48	0.1254E-01						0.7969E 02		
194	47	52		0.3218E-01						0.3107E 02	
195	48	47	0.1254E-01						0.7969E 02		
196	48	79		0.2673E-02			0.6827E-01			0.1409E 02	
197	48	49	0.1254E-01						0.7969E 02		
198	48	51		0.7711E-02						0.1296E 03	
199	49	48	0.1254E-01						0.7969E 02		
200	49	79				0.2065E 00			0.4841E 01		
201	49	79		0.1115E-01			0.2849E 00			0.3377E 01	
202	49	50		0.3218E-01						0.3107E 02	
203	50	51	0.7635E-02						0.1309E 03		
204	50	49		0.3218E-01						0.3107E 02	
205	50	73	0.1360E-01						0.7351E 02		
206	50	55		0.4170E-01						0.2397E 02	
207	51	52	0.7635E-02						0.1309E 03		

208	51	48		0.7711E-02				0.1296E 03	
209	51	50	0.7635E-02				0.1309E 03		
210	51	54		0.1992E-01				0.5019E 02	
211	52	47		0.3218E-01				0.3107E 02	
212	52	51	0.7635E-02				0.1309E 03		
213	52	53		0.4170E-01				0.2397E 02	
214	52	79			0.1257E 00		0.7955E 01		
215	53	52		0.4170E-01				0.2397E 02	
216	53	54	0.7774E-02				0.1286E 03		
217	53	58		0.4584E-01				0.2181E 02	
218	53	79			0.1279E 00		0.7813E 01		
219	54	53	0.7774E-02				0.1286E 03		
220	54	51		0.1992E-01				0.5019E 02	
221	54	55	0.7774E-02				0.1286E 03		
222	54	57		0.2190E-01				0.4565E 02	
223	55	54	0.7774E-02				0.1286E 03		
224	55	50		0.4170E-01				0.2397E 02	
225	55	74	0.7494E-02				0.1334E 03		
226	56	57	0.6610E-02				0.1512E 03		
227	56	55		0.4584E-01				0.2181E 02	
228	56	75	0.1115E 00				0.8967E 01		
229	56	61		0.4593E-01				0.2177E 02	
230	57	58	0.6610E-02				0.1512E 03		
231	57	54		0.2190E-01				0.4565E 02	
232	57	56	0.6610E-02				0.1512E 03		
233	57	60		0.2194E-01				0.4557E 02	
234	58	53		0.4584E-01				0.2181E 02	
235	58	57	0.6610E-02				0.1512E 03		
236	58	59		0.4593E-01				0.2177E 02	
237	58	79			0.1204E 00		0.8305E 01		
238	59	58		0.4593E-01				0.2177E 02	
239	59	60	0.8431E-02				0.1186E 03		
240	59	64		0.3463E-01				0.2887E 02	
241	59	79			0.1718E 00		0.5818E 01		
242	60	59	0.8431E-02				0.1186E 03		
243	60	57		0.2194E-01				0.4557E 02	

244	60	61	0.8431E-02			0.1186E 03	
245	60	63		0.1654E-01			0.6044E 02
246	61	60	0.8431E-02			0.1186E 03	
247	61	56		0.4593E-01			0.2177E 02
248	61	76	0.2518E-01			0.3971E 02	
249	61	77	0.1992E-01			0.5018E 02	
250	61	62		0.3463E-01			0.2887E 02
251	62	63	0.1209E-01			0.8270E 02	
252	62	61		0.3463E-01			0.2887E 02
253	62	77	0.1934E-01			0.5168E 02	
254	62	67		0.3162E-01			0.3161E 02
255	63	64	0.1209E-01			0.8270E 02	
256	63	60		0.1654E-01			0.6044E 02
257	63	62	0.1209E-01			0.8270E 02	
258	63	66		0.1510E-01			0.6618E 02
259	64	59		0.3463E-01			0.2887E 02
260	64	63	0.1209E-01			0.8270E 02	
261	64	65		0.3162E-01			0.3161E 02
262	64	79			0.2464E 00	0.4057E 01	
263	65	64		0.3162E-01			0.3161E 02
264	65	66	0.1157E-01			0.8639E 02	
265	65	68		0.1957E-01			0.5107E 02
266	65	79			0.2359E 00	0.4238E 01	
267	66	65	0.1157E-01			0.8639E 02	
268	66	63		0.1510E-01			0.6618E 02
269	66	67	0.1157E-01			0.8639E 02	
270	66	68		0.1446E-01			0.6913E 02
271	67	66	0.1157E-01			0.8639E 02	
272	67	62		0.3162E-01			0.3161E 02
273	67	78	0.2500E-01			0.3998E 02	
274	67	68		0.1957E-01			0.5107E 02
275	67	80			0.8286E 00	0.1206E 01	
276	68	65		0.1957E-01			0.5107E 02
277	68	66		0.1446E-01			0.6913E 02
278	68	67		0.1957E-01			0.5107E 02
279	68	80	0.1242E-01		0.4431E 00	0.2194E 01	

280	68	79	0.1242E-01			0.2532E 00		0.3764E 01		
281	68	69		0.6918E-02					0.1445E 03	
282	69	68		0.6918E-02					0.1445E 03	
283	69	70	0.6485E-01					0.1541E 02		
~~284~~	~~69~~	~~72~~		0.2456E 00					~~0.4070E-01~~	
285	69	71	0.4087E-01					0.2446E 02		
286	70	69	0.6485E-01					0.1541E 02		
287	70	80		0.3445E-03			0.1360E 00		0.7329E 01	
288	70	80	0.5461E-01			0.1079E 01		0.8818E 00		
289	70	80		0.1383E-02			0.1371E 00		0.7216E 01	
290	71	69	0.4087E-01					0.2446E 02		
291	71	80		0.1497E-02			0.2867E 00		0.3468E 01	

ENGINEER RLT CHARGE NO. RD 501 10

			********** RESISTANCE *******				ADMITTANCES	
			CONDUCTION		CONVECTION		BTU/HR DEGREE F	
N	I	J	AXIAL	RADIAL	AXIAL	RADIAL	AXIAL	RADIAL
1	14	84	0.8618E-02		0.3846E 01		0.2594E 00	
2	15	84	0.8007E-02		0.3573E 01		0.2792E 00	
3	6	81		0.5449E-02				0.1834E 03
4	7	81		0.5449E-02			53.3	0.1834E 03
5	7	81		0.6739E-02				0.1483E 03
6	69	86		0.1198E 00				0.8344E 01
7	72	86		0.1258E 00				0.7947E 01
8	86	80	0.4858E-03		0.5979E-01		0.1658E 02	
9	86	80	0.4858E-03		0.5979E-01		0.1658E 02	
10	16	18		0.7487E-02				0.1335E 03

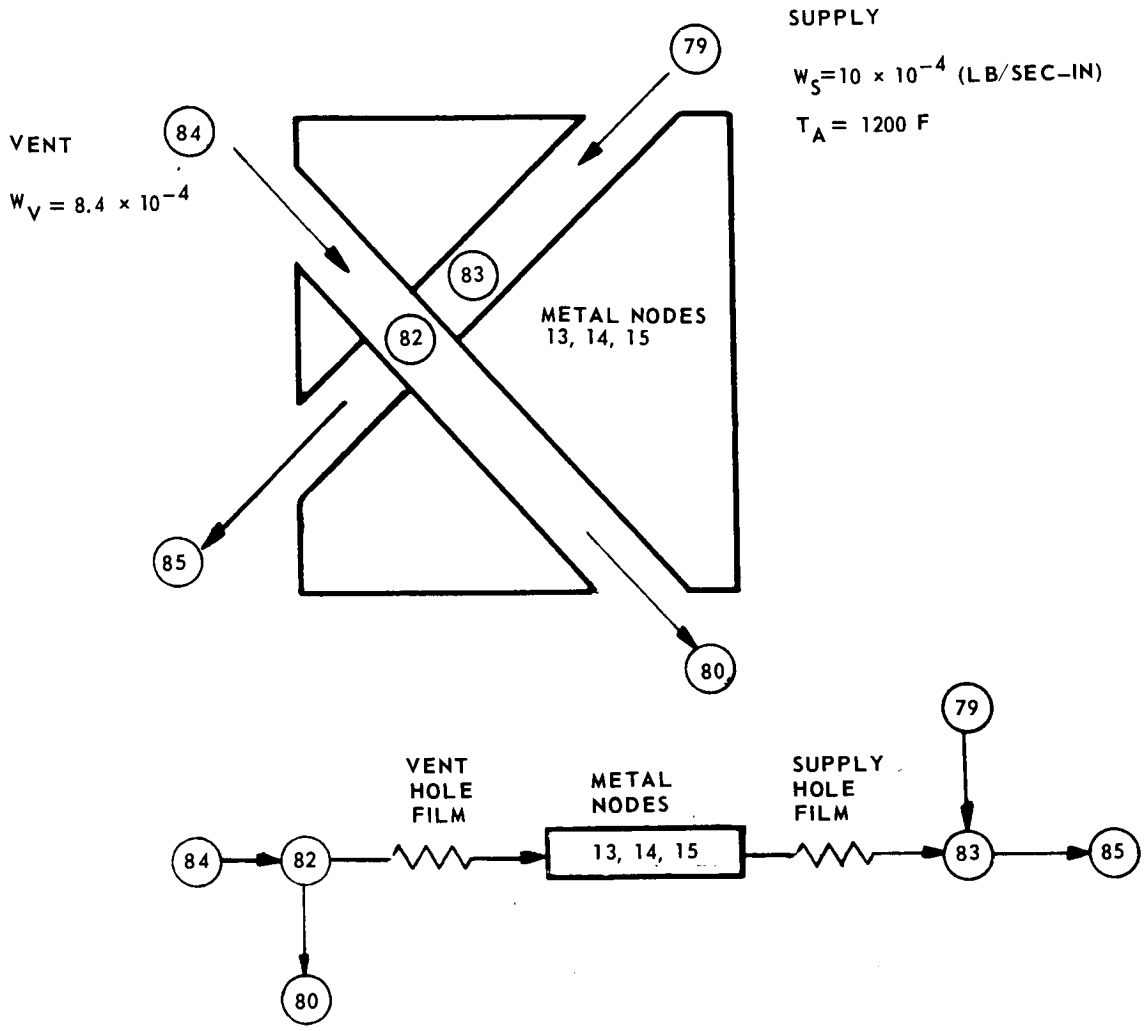

Figure 59 Model and Heat Flow Path for Heat Transfer in the Region of Metal Nodes 13, 14, and 15

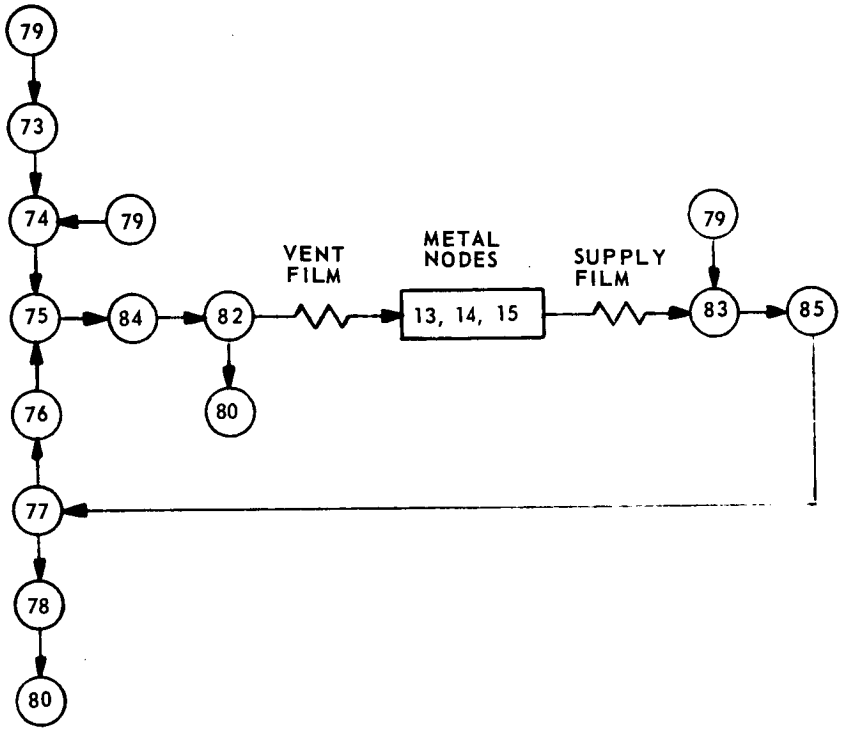

Figure 60 Flow Chart of the Entire Fluid Heat Transfer Path for the OC Diaphragm End Seal

(2) Flow Terms

A summary of the flow terms which are required in the heat balance equations are tabulated below.

Nodes	Flow (lb/sec-in x 10^4)	Flow w (lb/hr)*	wc_p $\left(\frac{\text{BTU/hr}}{°\text{F}}\right)$**
79/73	1.7	51	13.8
73/74	1.7	51	13.8
79/74	1.7	51	13.8
74/75	3.4	102	27.6
79/83	10.0	300	81.0
83/85	10.0	300	81.0
85/77	10.0	300	81.0

* w(lb/hr) = 3.10^5 w (lb/sec-in) at a radius of 13.5 inches

** c_p = 0.27 (BTU/lb-°F) at 1200°F

77/78	5.0	150	40.5
78/80	5.0	150	40.5
77/76	5.0	150	40.5
76/75	5.0	150	40.5
75/84	8.4	252	68.0
84/82	8.4	252	68.0
82/80	8.4	252	68.0
79/81		28.6	7.7
81/80		28.6	7.7

(3) Heat Balance Matrix

The over-all heat balance is obtained using MTI program PN0060 (READ 1). The defined temperatures in the 86 x 86 matrix inversion are:

$T_1 = 1120°F$

$T_{72} = 1136°F$

$T_{79} = 1200°F$

$T_{80} = 1136°F$

APPENDIX D

TEMPERATURE ANALYSIS OF THE SEMIRIGID INTERSTAGE SEAL

1. INTRODUCTION

The semirigid interstage seal design which is used in the temperature calculations is shown in Figure 2. Pertinent design parameters for this configuration are listed below.

Orifice supply flow	8.68×10^{-5} lb/sec-in
Main supply flow	9.02×10^{-5} lb/sec-in
Seal conductivity (Duranickle)	25.0 BTU/hr-ft°F
Runner conductivity (Inco 901)	11.2 BTU/hr-°F
Carrier conductivity (Inco 750)	11.8 BTU/hr-ft°F
Rotational speed	4.4×10^5 rev/hr
Mean radius of the seal	14.3 inches

The results of the calculations are shown in Figure 41 in the form of a steady-state temperature map of the semirigid interstage seal.

2. ANALYSIS

a. HEAT GENERATION

Heat is generated in the seal clearance by both Couette and turbulent action according to Reference 9. In the calculations which follow, it is initially assumed that the seal has undergone a 3-milliradian counterclockwise tilt with respect to the runner. This is the free-body tilt which would result if the seal were subjected to a linear axial temperature gradient of about 23 degrees Fahrenheit along its axial dimension. The mean operating film thickness which corresponds to this amount of tilt is 1.6 mils. The reason for making the assumption of an initial tilt is to compute realistic values of heat generation, thermal resistance across the seal clearance, and seal flow. The table below gives the dimensions used for Nodes 58-61.

Node	b_m (mils)	R (in)	ℓ (mils)	b (mils)	b_r (mils)	$\frac{A_\ell}{A_t}$	$\frac{A_r}{A_t}$	Q $\left(\frac{\text{Btu}}{\text{hr}}\right)$
58	1.60	14.49	100	2.16	4.41	.62	.38	2220
59	1.60	14.37	140	1.79	4.04	.62	.38	3131
60	1.60	14.23	130	1.37	0.0	1.00	0.0	2974
61	1.60	14.10	130	1.00	0.0	1.00	0.0	3094
							TOTAL	11419

Here nodes 58 and 59 are for the land and groove and nodes 60 and 61 are for the orifice regions. Also, it is assumed that the average recess depth is 2.25 mils.

Heat generation for the turbulent region (Node 57) is computed using Reference 9 for merged turbulent boundary layers. A value of 2144 BTU/hr was obtained, raising the total amount of heat generation to 13,503 BTU/hr.

b. HEAT-TRANSFER COEFFICIENTS

(1) Seal Clearances

Equivalent heat-transfer coefficients, which correspond to pure conduction across Nodes 58-61 are calculated using a gas conductivity of 0.037 BTU/hr-ft-^{o}F. The total seal clearance at each node is computed assuming the 2 milliradian tilt discussed above, and is modified according to the relative amounts of land and recess areas present. The results are tabulated below based on the equation of the weighted clearance.

$$b = (A_{\ell}\, b_{\ell} + A_r\, b_r)/A_t$$

Node	b_{ℓ} (mils)	b_r (mils)	$\frac{A_{\ell}}{A_t}$	$\frac{A_r}{A_t}$	b (mils)	h_{equiv} (BTU/hr-ft^2-^{o}F)
58	1.73	3.98	.62	.38	2.58	340
59	1.49	3.74	.62	.38	2.34	380
60	1.21	0.0	1.00	0.0	1.21	730
61	0.95	0.0	1.00	0.0	0.95	930

For Node 57, a forced convection value of h = 130 BTU/hr-ft^2 - ^{o}F was obtained from Reference 9, assuming a clearance of 60 mils.

(2) Supply Holes

There are 360 supply holes which pass through the seal. These carry the total supply flow of 9.02×10^{-5} lb/sec-in to the orifice region. Using a mean radius of 14.3 inches, this gives a flow of 4.64 lb/hr and a value, for each hole, of

$$w = 1.29 \times 10^{-2} \text{ lb/hr}$$

Using a gas viscosity of $\mu = 9.7 \times 10^{-2}$ lb/hr-ft, the approximate Reynold's numbers for this flow, as it passes through the seal are

Nodes	$Re = \frac{4w}{\pi\mu D} = \frac{0.169}{D}$
9, 6, 16	25
22	51
24	82

The corresponding surface heat-transfer coefficients for these low laminar conditions are calculated from Nu = 4, or

$$\bar{h} = 4\frac{k}{D}$$

Nodes	$\bar{h}$ (BTU/hr ft² °F)
9, 6, 16	22
22	45
24	71

Because these $\bar{h}$ values are quite low (equivalent to about 4 to 12 inches of metal), the film resistance is large, compared to the resistance due to conduction between holes. The metal conduction resistance between holes is therefore neglected in all further calculations.

c. ADMITTANCE MATRIX

The admittance between the flow in the supply holes and the seal is calculated below. In the tabulation below, the values of hole diameter D, length ℓ, area A, and coefficient $\bar{h}$ are the values for a single hole. The value of admittance Y is for the combination of 360 holes.

Node	D (ft)	ℓ (ft)	A (ft²)	$\bar{h}$ BTU/hr-ft²-°F	$Y = 360\,\bar{h}A$ BTU/hr-°F
9, 16, 16	6.83×10^{-3}	0.12	2.14×10^{-4}	22	1.8
22	3.33×10^{-3}	0.18	1.57×10^{-4}	45	2.5
24	2.08×10^{-3}	0.06	3.27×10^{-5}	71	0.7

For the heat-balance calculations, Nodes 9, 16, 16 are connected to gas node 63. Nodes 22, 24 are connected to gas node 64. All other admittances are calculated using MTI computer program PN0317. Input and output data are shown in Tables XX and XXI, respectively.

d. HEAT BALANCE EQUATIONS

(1) Defined Temperatures

Temperatures are defined at Nodes 52, 53, 54, 55, 56, and 62 as follows:

$$T_{52} = 1100°F$$

$$T_{53} = 1180°F$$

$$T_{54} = T_{55} = T_{56} = T_{62} = 1200°F$$

The value for Node 52 is believed to be a reasonable estimate based on previous calculations.

(2) Flow Terms

A summary of flow terms which are used in the heat balance equations are tabulated below.

Nodes	10^5 x Flow (lb/sec-in)	Flow* w (lb/hr)	c_p** (BTU/hr-°F)
62/57	8.68	28.1	7.58
57/58	8.68	28.1	7.58
58/59	8.68	28.1	7.58
59/60	8.68	28.1	7.58
60/61	8.68	28.1	7.58
62/63	9.02	29.2	7.88
63/64	9.02	29.2	7.88
64/61	9.02	29.2	7.88
61/53	17.7	57.3	15.46

* Mean radius assumed to be 14.3 inches

** c_p = 0.27 BTU/lb-°F at 1200°F

TABLE XX

INPUT DATA FOR ADMITTANCE CALCULATION ON THE SEMIRIGID INTERSTAGE SEAL

PW SR INTER FINAL 8 3 67
RL THORKILDSEN RD 501

1	1	55					14.61	14.69	14.69	.175	2.0	25.0
2	1	56					14.54	14.61	14.54	.175	2.0	25.0
3	1	2			14.54	14.69				.18		25.0
4	1	54			14.54	14.69				.088	2.0	25.0
5	2	55	1	55								
6	2	3					14.49	14.61		.175		25.0
7	2	62	1	54								
8	2	1	1	2								
9	3	2	2	3								
10	3	12					14.31	14.44		.1		.037
11	3	11					14.36	14.49		.1		25.0
12	3	4			14.44	14.54				.175		25.0
13	3	56			14.44	14.54				.1	2.0	25.0
14	4	62					14.49	14.54	14.54	.15	4.0	25.0
15	4	13					14.36	14.49		.15		25.0
16	4	5			14.44	14.54				.15		25.0
17	4	3	3	4								
18	5	62	4	62								
19	5	14	4	13								
20	5	6	4	5								
21	5	4	4	5								
22	6	9					14.49	14.64		.13		25.0
23	6	15					14.36	14.49		.13		25.0
24	6	7			14.44	14.54				.123		25.0
25	6	5	5	6								
26	7	10	6	9								
27	7	16	6	15								
28	7	8			14.44	14.54				.088		25.0
29	7	6	6	7								

30	8	57					14.49	14.54	14.54	.06	130.0	25.0
31	8	17					14.36	14.49		.06		25.0
32	8	58		14.44	14.54					.03	340.0	25.0
33	8	7		14.44	14.54					0.9		25.0
34	9	62					14.64	14.74	14.74	.13	15.0	25.0
35	9	6					14.49	14.64		.13		25.0
36	9	10		14.54	14.74					.12		25.0
37	9	55		14.54	14.74					.065	4.0	25.0
38	10	62	9 62									
39	10	7	9 6									
40	10	57		14.54	14.74					.06	130.0	25.0
41	10	9	9 10									
42	11	3	3 11									
43	11	18					14.23	14.36		.1		25.0
44	11	12		14.29	14.44					.05		.037
45	11	25		14.29	14.44					.05		25.0
46	11	25		14.23	14.36					.13		11.8
47	12	3	3 12									
48	12	13	11 12									
49	12	19		14.17	14.29					.05		.037
50	12	11	11 12									
51	12	18	12 19									
52	13	4	4 13									
53	13	19					14.23	14.36		.15		25.0
54	13	14		14.29	14.44					.145		25.0
55	13	12	12 13									
56	14	5	5 14									
57	14	20	13 19									
58	14	15	13 14									
59	14	13	13 14									
60	15	6	6 15									
61	15	21					14.23	14.36		.13		25.0
62	15	16		14.29	14.44					.123		25.0
63	15	14	14 15									
64	16	7					14.36	14.49		.115		25.0
65	16	22					14.23	14.36		.115		25.0
66	16	17		14.29	14.44					.088		25.0

67	16	15	15	16								
68	17	8	8	17								
69	17	23					14.23	14.36		.06		25.0
70	17	59			14.3	14.44				.03	380.0	25.0
71	17	16	16	17								
72	18	11	11	18								
73	18	53					14.17	14.23	14.17	.1	3.0	25.0
74	18	12	12	18								
75	18	25			14.17	14.29				.05		25.0
76	18	25			14.17	14.29				.13		11.8
77	19	13	13	19								
78	19	53					14.17	14.23	14.17	.15	3.0	25.0
79	19	20			14.17	14.29				.145		25.0
80	19	12	12	19								
81	20	14	14	20								
82	20	53	19	53								
83	20	21	19	20								
84	20	19	19	20								
85	21	15					14.23	14.36		.13		25.0
86	21	53					14.17	14.23	14.17	.13	17.0	25.0
87	21	22			14.17	14.29				.123		25.0
88	21	20	20	21								
89	22	16	16	22								
90	22	53					14.17	14.23	14.17	.115	17.0	25.0
91	22	23			14.17	14.29				.088		25.0
92	22	21	21	22								
93	23	17	17	23								
94	23	24					14.14	14.23		.06		25.0
95	23	60			14.17	14.29				.03	730.0	25.0
96	23	22	22	23								
97	24	23	23	24								
98	24	53					14.04	14.14	14.04	.06	24.0	25.0
99	24	61			14.04	14.17				.03	930.0	25.0
00	24	53			14.04	14.17				.03	17.0	25.0
101	25	56					14.28	14.44	14.44	.26	2.0	11.8
102	25	26					14.01	14.28		.26		11.8
03	25	11			14.29	14.44				.05		25.0

104	25	11			14.23	14.36				.13		11.8
105	25	18			14.17	14.29				.05		25.0
06	25	18			14.17	14.29				.13		11.8
107	25	54			14.15	14.44				.13	2.0	11.8
108	26	25	25	26								
09	26	54					13.85	14.01	13.85	.26	2.0	11.8
110	26	28			13.85	14.15				.35		11.8
111	26	27			13.85	14.15				.275		11.8
12	27	55					14.01	14.15	14.15	.29	2.0	11.8
113	27	54					13.85	14.01	13.85	.29	2.0	11.8
114	27	26	26	27								
15	27	54			13.85	14.15				.145	2.0	11.8
116	28	54					14.01	14.15	14.15	.45	3.0	11.8
117	28	53					13.85	14.01	13.85	.45	10.0	11.8
18	28	53			13.85	14.15				.225	20.0	11.8
119	28	26	26	28								
120	29	62					14.87	14.99	14.99	.1	75.0	11.2
121	29	32					14.64	14.87		.1		11.2
122	29	30			14.74	14.99				.1		11.2
123	29	55			14.74	14.99				.05	50.0	11.2
124	30	62	29	62								
125	30	33	29	32								
126	30	31	29	30								
127	30	29	29	30								
128	31	62	29	62								
129	31	34	29	32								
130	31	55			14.74	14.99				.055	52.0	11.2
131	31	30	29	30								
132	32	29	29	32								
133	32	35					14.49	14.64		.1		11.2
134	32	33			14.54	14.74				.1		11.2
135	32	57			14.54	14.74				.05	130.0	11.2
136	33	30	29	32								
137	33	36	32	35								
138	33	34	32	33								
139	33	32	32	33								

140	34	31	29	32							
141	34	37	32	35							
142	34	55			14.54	14.74			.055	52.0	11.2
143	34	33	32	33							
144	35	32	32	35							
145	35	38					14.36	14.49	.1		11.2
146	35	36			14.44	14.54			.1		11.2
147	35	58			14.44	14.54			.05	340.0	11.2
148	36	33	32	35							
149	36	39	35	38							
150	36	37	35	36							
151	36	35	35	36							
152	37	34	32	35							
153	37	40	35	38							
154	37	55			14.44	14.54			.055	47.0	11.2
155	37	36	35	36							
156	38	35	35	38							
157	38	41					14.23	14.36	.1		11.2
158	38	39			14.29	14.44			.1		11.2
159	38	59			14.29	14.44			.05	380.0	11.2
160	39	36	35	38							
161	39	42	38	41							
162	39	40	38	39							
163	39	38	38	39							
164	40	37	35	38							
165	40	43	38	41		14.49					
166	40	55			14.31	~~14.47~~			.055	47.0	11.2
167	40	39	38	39							
168	41	38	38	41							
169	41	44					14.14	14.23	.1		11.2
170	41	42			14.17	14.29			.1		11.2
171	41	60			14.17	14.29			.05	730.0	11.2
172	42	39	38	41							
173	42	45	41	44							
174	42	43	41	42							
175	42	41	41	42							

176	43	40	36	41								
177	43	46	41	44								
178	43	55			14.17	14.29				.055	47.0	11.2
179	43	42	41	42								
180	44	41	41	44								
181	44	47					13.9	14.14		.1		11.2
182	44	45			14.04	14.17				.1		11.2
183	44	61			14.04	14.17				.05	930.0	11.2
184	45	42	41	44								
185	45	48	44	47								
186	45	46	44	45								
187	45	44	44	45								
188	46	43	41	44								
189	46	49	44	47								
190	46	55			14.04	14.17				.055	42.0	11.2
191	46	45	44	45								
192	47	44	44	47								
193	47	50					13.7	13.9		.13		11.2
194	47	48			13.8	14.04				.1		11.2
195	47	53			13.8	14.04				.05	24.0	11.2
196	48	45	44	47								
197	48	50	47	50								
198	48	49	47	48								
199	48	47	47	48								
200	49	46	44	47								
201	49	50	47	50								
202	49	55			13.8	14.04				.055	42.0	11.2
203	49	48	47	48								
204	50	47	47	50								
205	50	48	47	50								
206	50	49	47	50								
207	50	51					13.47	13.7		.313		11.2
208	50	55			13.6	13.8				.156	42.0	11.2
209	50	53			13.6	13.8				.156	24.0	11.2
210	51	50	50	51								
211	51	52					13.34	13.47		.313		11.2

212	51	55			13.34	13.6	.156	42.0	11.2
213	51	53			13.34	13.6	.156	17.0	11.2
214	57	32	32	57					
215	57	10	10	57					
216	58	35	35	58					
217	58	8	8	58					
218	59	38	38	59					
219	59	17	17	59					
220	60	41	41	60					
221	60	23	23	60					
222	61	44	44	61					
223	61	24	24	61					

TABLE XXI

OUTPUT DATA FROM ADMITTANCE CALCULATION ON THE SEMIRIGID INTERSTAGE SEAL

TITLE PW SR INTER FINAL DATE 8 3 67

ENGINEER RL THORKILDSEN CHARGE NO. RD 501

			********** RESISTANCE *******				ADMITTANCES	
			CONDUCTION		CONVECTION		BTU/HR DEGREE F	
N	I	J	AXIAL	RADIAL	AXIAL	RADIAL	AXIAL	RADIAL
1	1	55		0.2383E-02		0.4457E 01		0.2242E 00
2	1	56		0.2096E-02		0.4503E 01		0.2219E 00
3	1	2	0.6272E-02				0.1594E 03	
4	1	54	0.3066E-02		0.5227E 01		0.1911E 00	
5	2	55		0.2383E-02		0.4457E 01		0.2242E 00
6	2	3		0.3600E-02				0.2777E 03
7	2	62	0.3066E-02		0.5227E 01		0.1911E 00	
8	2	1	0.6272E-02				0.1594E 03	
9	3	2		0.3600E-02				0.2777E 03
10	3	12		0.4668E 01				0.2142E 00
11	3	11		0.6884E-02				0.1452E 03
12	3	4	0.9226E-02				0.1083E 03	
13	3	56	0.5272E-02		0.7908E 01		0.1263E 00	
14	4	62		0.1754E-02		0.2627E 01		0.3804E 00
15	4	13		0.4589E-02				0.2178E 03
16	4	5	0.7908E-02				0.1264E 03	
17	4	3	0.9226E-02				0.1083E 03	
18	5	62		0.1754E-02		0.2627E 01		0.3804E 00
19	5	14		0.4589E-02				0.2178E 03
20	5	6	0.7908E-02				0.1264E 03	
21	5	4	0.7908E-02				0.1264E 03	
22	6	9		0.6052E-02				0.1652E 03

23	6	15		0.5296E-02					0.1888E 03
24	6	7	0.6484E-02					0.1542E 03	
25	6	5	0.7908E-02					0.1264E 03	
26	7	10		0.6052E-02					0.1652E 03
27	7	16		0.5296E-02					0.1888E 03
28	7	8	0.4639E-02					0.2155E 03	
29	7	6	0.6484E-02					0.1542E 03	
30	8	57		0.4385E-02		0.2020E 00			0.4843E 01
31	8	17		0.1147E-01					0.8714E 02
32	8	58	0.1581E-02		0.4651E-01			0.2078E 02	
33	8	7	0.4744E-01					0.2107E 02	
34	9	62		0.4000E-02		0.7973E 00			0.1247E 01
35	9	6		0.6052E-02					0.1652E 03
36	9	10	0.3130E-02					0.3193E 03	
37	9	55	0.1695E-02		0.1956E 01			0.5105E 00	
38	10	62		0.4000E-02		0.7973E 00			0.1247E 01
39	10	7		0.6052E-02					0.1652E 03
40	10	57	~~0.2522E-03~~		~~0.9703E-02~~		14.7	~~0.1004E-03~~	
41	10	9	0.3130E-02					0.3193E 03	
42	11	3		0.6884E-02					0.1452E 03
43	11	18		0.6947E-02					0.1439E 03
44	11	12	0.1197E 01					0.8348E 00	
45	11	25	0.1772E-02	.00177 .01132			76.3	~~0.5641E-03~~	
46	11	25	0.1132E-01	.01309				~~0.8831E-02~~	
47	12	3		0.4668E 01					0.2142E 00
48	12	13	0.1197E 01					0.8348E 00	
49	12	19	0.1511E 01					0.6616E 00	
50	12	11	0.1197E 01					0.8348E 00	
51	12	18	0.1511E 01					0.6616E 00	
52	13	4		0.4589E-02					0.2178E 03
53	13	19		0.4631E-02					0.2159E 03
54	13	14	0.5140E-02					0.1945E 03	
55	13	12	0.1197E 01					0.8348E 00	
56	14	5		0.4589E-02					0.2178E 03
57	14	20		0.4631E-02					0.2159E 03
58	14	15	0.5140E-02					0.1945E 03	

59	14	13	0.5140E-02				0.1945E 03	
60	15	6		0.5296E-02				0.1888E 03
61	15	21		0.5344E-02				0.1871E 03
62	15	16	0.4360E-02				0.2293E 03	
63	15	14	0.5140E-02				0.1945E 03	
64	16	7		0.5986E-02				0.1670E 03
65	16	22		0.6041E-02				0.1655E 03
66	16	17	0.3119E-02				0.3205E 03	
67	16	15	0.4360E-02				0.2293E 03	
68	17	8		0.1147E-01				0.8714E 02
69	17	23		0.1157E-01				0.8636E 02
70	17	59	0.1139E-02		0.2997E-01		0.3213E 02	
71	17	16	0.3119E-02				0.3205E 03	
72	18	11		0.6947E-02				0.1439E 03
73	18	53		0.3227E-02		0.5391E 01		0.1853E 00
74	18	12	0.1511E 01				0.6616E 00	
75	18	25	0.2236E-02	.00224			~~0.4470E-03~~	
76	18	25	0.1232E-01	.01232 / .01456		68.7	~~0.8115E-02~~	
77	19	13		0.4631E-02				0.2159E 03
78	19	53		0.2151E-02		0.3594E 01		0.2780E 00
79	19	20	0.6486E-02				0.1541E 03	
80	19	12	0.1511E 01				0.6616E 00	
81	20	14		0.4631E-02				0.2159E 03
82	20	53		0.2151E-02		0.3594E 01		0.2780E 00
83	20	21	0.6486E-02				0.1541E 03	
84	20	19	0.6486E-02				0.1541E 03	
85	21	15		0.5344E-02				0.1871E 03
86	21	53		0.2483E-02		0.7318E 00		0.1361E 01
87	21	22	0.5502E-02				0.1817E 03	
88	21	20	0.6486E-02				0.1541E 03	
89	22	16		0.6041E-02				0.1655E 03
90	22	53		0.2806E-02		0.8273E 00		0.1204E 01
91	22	23	0.3936E-02				0.2540E 03	
92	22	21	0.5502E-02				0.1817E 03	
93	23	17		0.1157E-01				0.8636E 02
94	23	24		0.8078E-02				0.1237E 03
95	23	60	0.1342E-02		0.1838E-01		0.5069E 02	

96	23	22	0.3936E-02				0.2540E 03		
97	24	23		0.8078E-02				0.1237E 03	
98	24	53		0.9036E-02		0.1133E 01		0.8751E 00	
99	24	61	0.1249E-02		0.1343E-01		0.6807E 02		
100	24	53	0.1249E-02		0.7352E 00		0.1357E 01		
101	25	56		0.6935E-02		0.3052E 01		0.3268E 00	
102	25	26		0.1188E-01				0.8415E 02	
103	25	11	0.1772E-02				76.3 ~~0.5641E 03~~		
104	25	11	0.1132E-01				~~0.8831E 02~~		
105	25	18	0.2236E-02				68.7 ~~0.4470E 03~~		
106	25	18	0.1232E-01				~~0.8115E 02~~		
107	25	54	0.5075E-02		0.2764E 01		0.3611E 00		
108	26	25		0.1188E-01				0.8415E 02	
109	26	54		0.7150E-02		0.3182E 01		0.3135E 00	
110	26	28	0.1348E-01				0.7414E 02		
111	26	27	0.1059E-01				0.9436E 02		
112	27	55		0.5549E-02		0.2792E 01		0.3573E 00	
113	27	54		0.6410E-02		0.2853E 01		0.3497E 00	
114	27	26	0.1059E-01				0.9436E 02		
115	27	54	0.5587E-02		0.2728E 01		0.3657E 00		
116	28	54		0.3576E-02		0.1199E 01		0.8310E 00	
117	28	53		0.4131E-02		0.3677E 00		0.2689E 01	
118	28	53	0.8670E-02		0.2728E 00		0.3552E 01		
119	28	26	0.1348E-01				0.7414E 02		
120	29	62		0.1370E-01		0.2038E 00		0.4596E 01	
121	29	32		0.2658E-01				0.3762E 02	
122	29	30	0.4588E-02				0.2179E 03		
123	29	55	0.2294E-02		0.1233E 00		0.7959E 01		
124	30	62		0.1370E-01		0.2038E 00		0.4596E 01	
125	30	33		0.2658E-01				0.3762E 02	
126	30	31	0.4588E-02				0.2179E 03		
127	30	29	0.4588E-02				0.2179E 03		
128	31	62		0.1370E-01		0.2038E 00		0.4596E 01	
129	31	34		0.2658E-01				0.3762E 02	
130	31	55	0.2523E-02		0.1185E 00		0.8256E 01		
131	31	30	0.4588E-02				0.2179E 03		

132	32	29		0.2658E-01				0.3762E 02
133	32	35		0.1756E-01				0.5694E 02
134	32	33	0.5823E-02			0.1717E 03		
135	32	57	0.2911E-02		0.6020E-01	0.1584E 02		
136	33	30		0.2658E-01				0.3762E 02
137	33	36		0.1756E-01				0.5694E 02
138	33	34	0.5823E-02			0.1717E 03		
139	33	32	0.5823E-02			0.1717E 03		
140	34	31		0.2658E-01				0.3762E 02
141	34	37		0.1756E-01				0.5694E 02
142	34	55	0.3203E-02		0.1505E 00	0.6504E 01		
143	34	33	0.5823E-02			0.1717E 03		
144	35	32		0.1756E-01				0.5694E 02
145	35	38		0.1536E-01				0.6507E 02
146	35	36	0.1176E-01			0.8497E 02		
147	35	58	0.5884E-02		0.4651E-01	0.1908E 02		
148	36	33		0.1756E-01				0.5694E 02
149	36	39		0.1536E-01				0.6507E 02
150	36	37	0.1176E-01			0.8497E 02		
151	36	35	0.1176E-01			0.8497E 02		
152	37	34		0.1756E-01				0.5694E 02
153	37	40		0.1536E-01				0.6507E 02
154	37	55	0.6472E-02		0.3365E 00	0.2915E 01		
155	37	36	0.1176E-01			0.8497E 02		
156	38	35		0.1536E-01				0.6507E 02
157	38	41		0.1550E-01				0.6448E 02
158	38	39	0.7913E-02			0.1263E 03		
159	38	59	0.3956E-02		0.2799E-01	0.3130E 02		
160	39	36		0.1536E-01				0.6507E 02
161	39	42		0.1550E-01				0.6448E 02
162	39	40	0.7913E-02			0.1263E 03		
163	39	38	0.7913E-02			0.1263E 03		
164	40	37		0.1536E-01				0.6507E 02
165	40	43		0.1550E-01				0.6448E 02
166	40	55	~~-0.1016E-03~~		-0.5282E-02	4.5 ~~-0.1857E-03~~		
167	40	39	0.7913E-02			0.1263E 03		

168	41	38		0.1550E-01			0.6448E 02
169	41	44		0.1081E-01			0.9242E 02
170	41	42	0.9986E-02			0.1001E 03	
171	41	60	0.4993E-02		0.1838E-01	0.4277E 02	
172	42	39		0.1550E-01			0.6448E 02
173	42	45		0.1081E-01			0.9242E 02
174	42	43	0.9986E-02			0.1001E 03	
175	42	41	0.9986E-02			0.1001E 03	
176	43	40		0.1550E-01			0.6448E 02
177	43	46		0.1081E-01			0.9242E 02
178	43	55	0.5492E-02		0.2855E 00	0.3435E 01	
179	43	42	0.9986E-02			0.1001E 03	
180	44	41		0.1081E-01			0.9242E 02
181	44	47		0.2919E-01			0.3425E 02
182	44	45	0.9299E-02			0.1075E 03	
183	44	61	0.4649E-02		0.1343E-01	0.5528E 02	
184	45	42		0.1081E-01			0.9242E 02
185	45	48		0.2919E-01			0.3425E 02
186	45	46	0.9299E-02			0.1075E 03	
187	45	44	0.9299E-02			0.1075E 03	
188	46	43		0.1081E-01			0.9242E 02
189	46	49		0.2919E-01			0.3425E 02
190	46	55	0.5114E-02		0.2975E 00	0.3303E 01	
191	46	45	0.9299E-02			0.1075E 03	
192	47	44		0.2919E-01			0.3425E 02
193	47	50		0.1901E-01			0.5260E 02
194	47	48	0.5104E-02			0.1959E 03	
195	47	53	0.2552E-02		0.2858E 00	0.3467E 01	
196	48	45		0.2919E-01			0.3425E 02
197	48	50		0.1901E-01			0.5260E 02
198	48	49	0.5104E-02			0.1959E 03	
199	48	47	0.5104E-02			0.1959E 03	
200	49	46		0.2919E-01			0.3425E 02
201	49	50		0.1901E-01			0.5260E 02
202	49	55	0.2807E-02		0.1633E 00	0.6018E 01	
203	49	48	0.5104E-02			0.1959E 03	

204	50	47		0.1901E-01			0.5260E 02
205	50	48		0.1901E-01			0.5260E 02
206	50	49		0.1901E-01			0.5260E 02
207	50	51		0.9223E-02			0.1084E 03
208	50	55	0.9708E-02		0.1991E 00	0.4787E 01	
209	50	53	0.9708E-02		0.3485E 00	0.2791E 01	
210	51	50		0.9223E-02			0.1084E 03
211	51	52		0.5283E-02			0.1892E 03
212	51	55	0.7595E-02		0.1558E 00	0.6119E 01	
213	51	53	0.7595E-02		0.3849E 00	0.2547E 01	
214	57	32	0.2911E-02		0.6020E-01	0.1584E 02	
215	57	10	~~0.2522E-03~~		~~0.9703E-02~~	14.7 ~~0.1004E 03~~	
216	58	35	0.5884E-02		0.4651E-01	0.1908E 02	
217	58	8	0.1581E-02		0.4651E-01	0.2078E 02	
218	59	38	0.3956E-02		0.2799E-01	0.3130E 02	
219	59	17	0.1139E-02		0.2997E-01	0.3213E 02	
220	60	41	0.4993E-02		0.1838E-01	0.4277E 02	
221	60	23	0.1342E-02		0.1838E-01	0.5069E 02	
222	61	44	0.4649E-02		0.1343E-01	0.5528E 02	
223	61	24	0.1249E-02		0.1343E-01	0.6807E 02	

APPENDIX E

STIFFNESS AND DISPLACEMENT CALCULATIONS FOR COMPOSITE THIN RINGS

1. INTRODUCTION

The analyses which follow apply to small rotations of thin rings which do not change cross-sectional shape during rotation. These conditions are reasonably satisfied if the sine of the rotation angle is approximately equal to the rotation angle (in radians), the over-all radial length of the cross section is less than 10 percent of the radius of the centroid, and the cross section is compact. The analysis is in three parts: rotation stiffness of a ring for a prescribed center of rotation, rotation of a two-section ring for prescribed values of initial radial and angular mismatch, and thermal distortion of a two-section ring.

2. ANALYSIS

a. ROTATIONAL STIFFNESS FOR A PRESCRIBED CENTER OF ROTATION

(1) Hoop Stress and Force

Referring to Figure 61, the prescribed center of rotation is at C_r and the rotation is θ. As point A moves to point B, a hoop strain ϵ is developed.

$$\epsilon = \frac{x}{r} \approx \frac{x}{a}$$

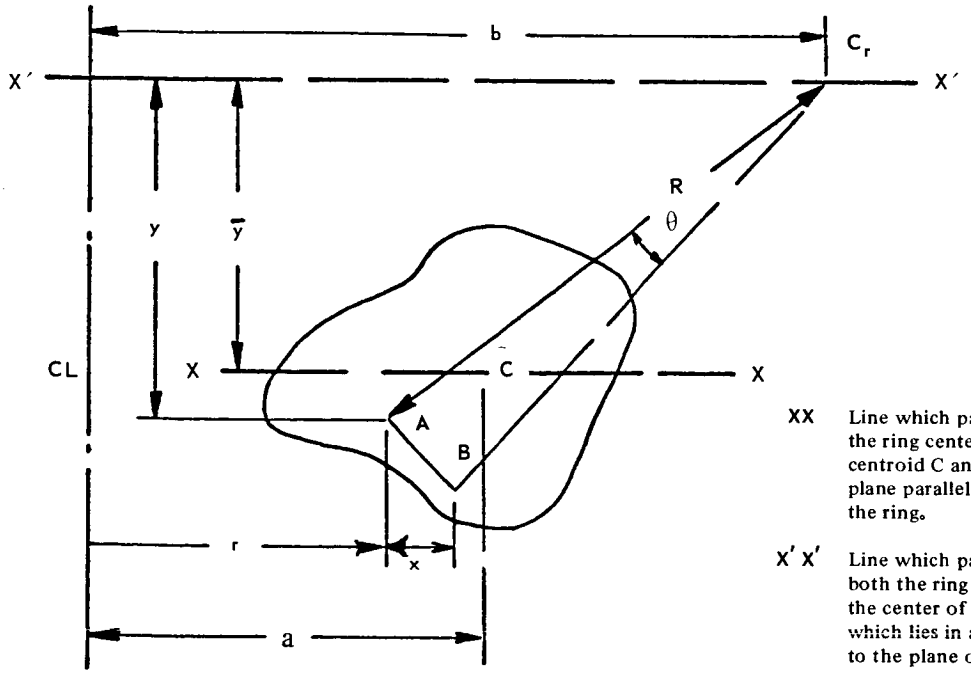

Figure 61 Rotation of the Cross Section of a Ring Around a Prescribed Center of Rotation

where, from geometry

$$\frac{x}{R\theta} = \frac{y}{R}$$

or $$x = y\theta$$

so that $$\epsilon = \frac{y\theta}{a}$$

The corresponding hoop stress at any point in the cross section is therefore

$$\sigma = E\epsilon = \frac{Ey}{a}\theta \tag{71}$$

The corresponding net hoop force over the cross section A is

$$F = \int_A \sigma dA = \frac{E\theta}{a}\int_A ydA = \frac{E\bar{y}A\theta}{a} \text{ (lb)}$$

where y is the distance measured from a line X'X'. Line X'X' is defined to be in a plane parallel to the plane of the ring and to pass through the center of rotation C_r.

Also, $\bar{y}A$ is the first moment of area of cross section A with respect to line X'X', and a line XX which passes through the centroid C of the cross section.

(2) Moment Due to Hoop Stress

The moment around line X'X'of the forces due to the hoop stress σ is (from Figure 61)

$$M = \int_A (\sigma dA)y \text{ (in-lb)} \tag{72}$$

combining Equations 71 and 72,

$$M = \int_A \frac{Ey\theta}{a}(dA)y = \frac{E\theta}{a}\int_A y^2 dA = \frac{EI\theta}{a} \tag{73}$$

where I is the second moment of area of A with respect to line X'X'.

(3) Equilibrium

Suppose that the prescribed rotation is caused by a uniformly distributed moment M_b (in-lb/in) only. Consider half of the ring (as shown in Figure 62) as a free body. Then for equilibrium

$$2M = 2\int_0^{\frac{\pi}{2}} M_b \ (b \sin \phi) \ d\phi \tag{74}$$

Substituting M from Equation 73 into 74,

$$2\frac{EI}{a}\theta = 2bM_b\int_0^{\frac{\pi}{2}} \sin\phi \, d\phi$$

or

$$M_b = \frac{EI}{ab}\theta \tag{75}$$

Next, suppose that from geometry, the motion of the cross section is written in terms of an outward radial motion x_c of the centroid plus a rotation θ_c around the centroid

$$\theta_c = \theta \tag{76}$$

$$x_c = \bar{y}\theta \tag{77}$$

Consider first the moment M_θ required only to produce θ_c around the centroid.

From Equation 75 and 76

$$M_\theta = \frac{EI}{ab}\theta_c = \frac{EI}{ab}\theta \tag{78}$$

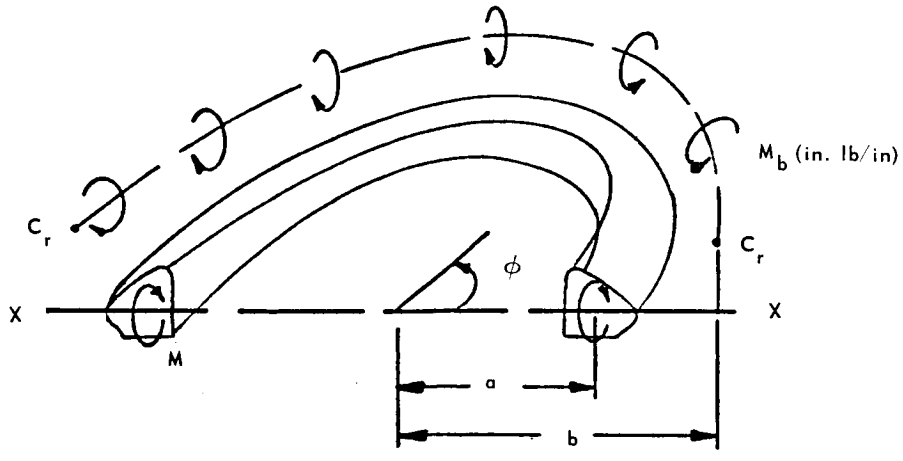

Figure 62 Free-Body Diagram of One Half of a Ring

but, because the rotation is defined to be around the centroid (which has the radius a),

$$b = a \tag{79}$$

Also, the line X′X′ coincides with line XX, so that $\bar{y} = 0$.

But
$$I = \bar{I} + A\bar{y}^2 \tag{80}$$

where $\bar{I}$ is the second moment of area of A with respect to line XX

so that combining Equations 78, 79, and 80 with $\bar{y} = 0$,

$$M_\theta = \frac{E\bar{I}}{a^2}\theta \tag{81}$$

Note that this moment could be applied anywhere in the plane of the cross section as long as its radius is equal to a.

Next, from geometry

$$x_c = \epsilon\, a$$

but
$$\epsilon = \frac{\sigma}{E} \simeq \frac{F}{AE}$$

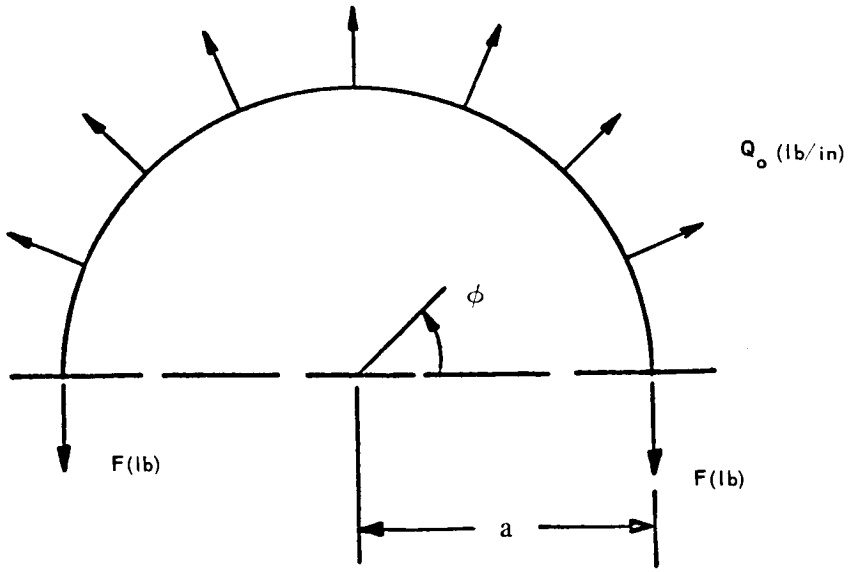

Figure 63 Free-Body Diagram of One Half of a Ring with a Uniform Radial Force (Q_o) Applied Outward through the Centroid

where F (net hoop force over the cross section) is the force required to produce the outward motion of the centroid, i.e.

$$F = \frac{AE}{a} x_c \tag{82}$$

For equilibrium (see Figure 63),

$$2F = 2 \int_0^{\frac{\pi}{2}} Q_o \, (a \sin \phi) \, d\phi \tag{83}$$

so that combining Equations 82 and 83

$$Q_o = \frac{F}{a} \tag{84}$$

Note that the combined moment (of M_θ and Q_o) around any other point of rotation, say $C_r = C$, would be

$$M_o = M_\theta + Q_o \, \bar{y} \tag{85}$$

where $\bar{y}$ is the perpendicular distance from the line of action of Q_o to a parallel line through C_r. Using Equations 77, 82 and 84, Equation 85 can be rewritten

$$M_o = \frac{E\bar{I}}{a^2} \theta + \bar{y} \left(\frac{AE}{a}\right) \bar{y} \, \theta = \frac{E\theta}{a^2} (\bar{I} + A\bar{y}^2)$$

or

$$M_o = \frac{E\theta}{a^2} I$$

which checks with Equation 75.

Finally, suppose that a pure moment is applied to the ring, i.e.

$$M_o = M_o$$

$$Q_o = 0$$

The last eqution indicates that the net hoop force over the cross section is zero, so that from Equation 81, the radial displacement of the centroid must be zero. This can be true if and only if the center of rotation coincides with the centroid.

b. TWO-SECTION THIN RING WITH PRESCRIBED INITIAL RADIAL AND ANGULAR MISMATCH

The composite ring shown in Figure 64 is assumed to consist of two sections (1 and 2) which are mismatched due to thermal distortion by the radial displacement x and rotation θ. (See Section c). It is desired to find the equilibrium angle θ_o of the composite ring.

For compatibility of displacement and rotation,

$$x = x_1 - x_2 \tag{86}$$

$$\theta = \theta_1 - \theta_2 \tag{87}$$

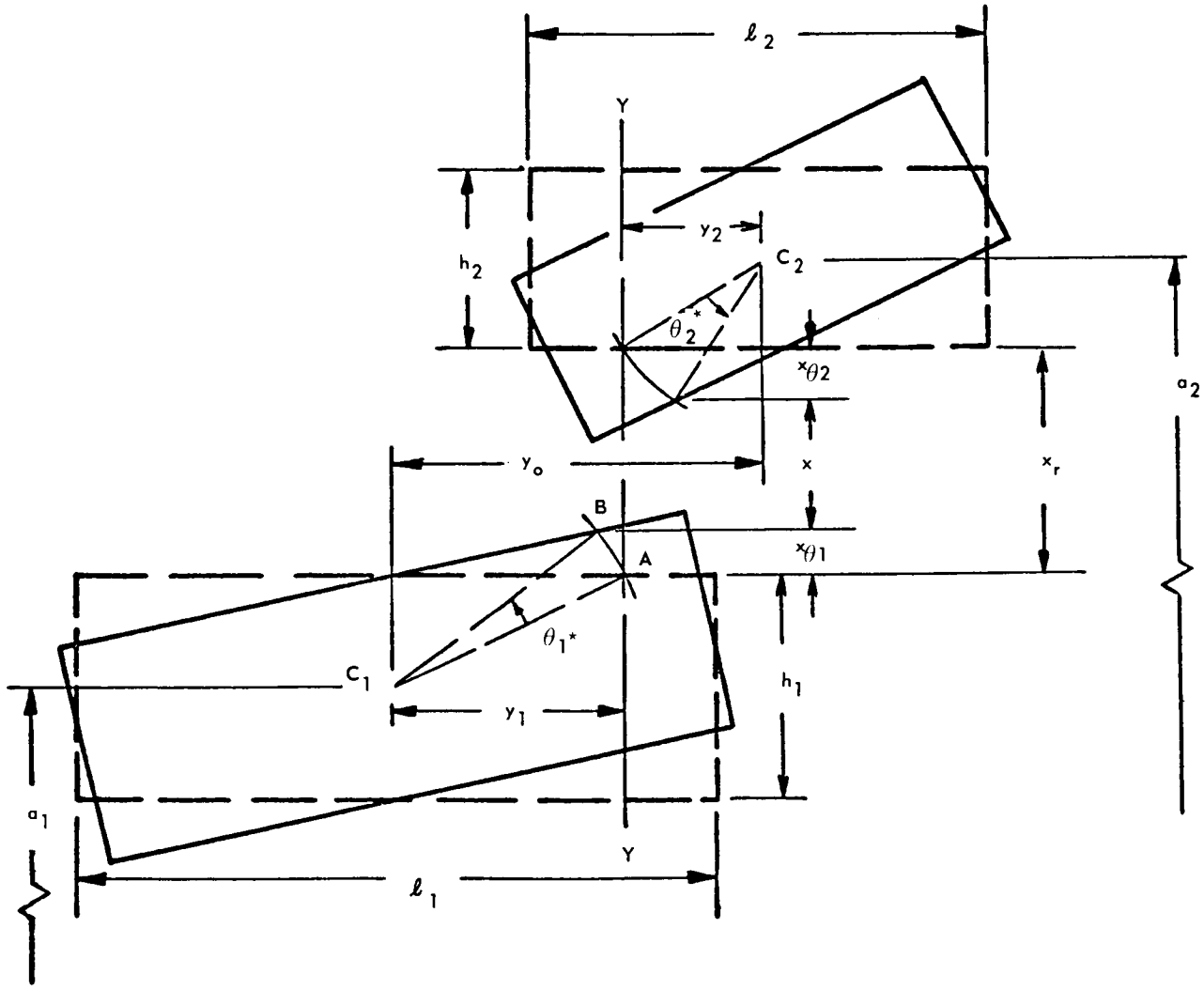

YY = LINE THROUGH THE AXIAL CENTER OF THE CYLINDRICAL SURFACE OF INTERACTION OF THE TWO SECTIONS.

Figure 64 Mismatch Conditions for a Two-Section Ring

From Equations 82 and 84, the radial forces required to displace the centroids of sections 1 and 2 by the amounts x_1 and x_2 are:

$$Q_1 = \frac{A_1 E}{a_1^2} x_1 \tag{88}$$

$$Q_2 = \frac{A_2 E}{a_2^2} x_2 \tag{89}$$

For equilibrium

$$\Sigma Q = 0 = Q_1 + Q_2$$

so that from Equations 88 and 89,

$$\frac{A_1}{a_1^2} x_1 + \frac{A_2}{a_2^2} x_2 = 0 \tag{90}$$

Solving Equations 86 and 90 simultaneously,

$$x_1 = \left[\frac{a_1{}^2 A_2}{a_2^2 A_1 + a_1^2 A_2}\right] x$$

$$x_2 = \left[\frac{-a_2{}^2 A_1}{a_2^2 A_1 + a_1^2 A_2}\right] x$$

so that, substituting x_1 and x_2 back into Equations 88 and 89

$$Q_1 = \left[\frac{E A_1 A_2}{a_2^2 A_1 + a_1^2 A_2}\right] x$$

$$Q_2 = -\left[\frac{E A_1 A_2}{a_2^2 A_1 + a_1^2 A_2}\right] x \tag{91}$$

These are the forces which are required, if applied at the centroids of sections 1 and 2, to close the initial mismatch x.

The elastic forces which oppose the forces Q_1 and Q_2 form a couple M_x which causes a rotation θ_x.

$$M_x = Q_1 y_o \tag{92}$$

where $y_o \equiv \pm (y_1 + y_2)$. The value of y_o is taken to be positive if the centroids of sections 1 and 2 are to the left and right, respectively, of the interaction line YY in Figure 64.

Thus, combining Equations 91 and 92,

$$M_x = \left(\frac{E y_o A_1 A_2}{a_2^2 A_1 + a_1^2 A_2} \right) x$$

so that from Equations 80 and 81,

$$\theta_x = \frac{a^2}{E\bar{I}} M_x = \frac{a^2 y_o A_1 A_2}{\bar{I}\left(a_2^2 A_1 + a_1^2 A_2\right)} x \tag{93}$$

The moments required to close the mismatch rotation θ between sections 1 and 2 are (from Equation 75)

$$M_1 = \frac{EI_1}{a_1^2} \theta_1 \tag{94}$$

$$M_2 = \frac{EI_2}{a_2^2} \theta_2 \tag{95}$$

For equilibrium

$$\Sigma M = 0 = M_1 + M_2$$

so that from Equations 94 and 95

$$\frac{I_1}{a_1^2} \theta_1 + \frac{I_2}{a_2^2} \theta_2 = 0 \tag{96}$$

Solving Equations 87 and 96 simultaneously,

$$\theta_1 = \left(\frac{a_1^2 I_2}{a_2^2 I_1 + a_1^2 I_2}\right)\theta \tag{97}$$

$$\theta_2 = -\left(\frac{a_2^2 I_1}{a_2^2 I_1 + a_1^2 I_2}\right)\theta \tag{98}$$

If $\theta_1{}^*$ is the initial angle of section 1, the final angle caused by the moments M_1 and M_2 is

$$\theta_M = (\theta_1{}^* + \theta_1) = (\theta_2{}^* + \theta_2) \tag{99}$$

so that, combining Equations 99 and 97 or 98,

$$\theta_M = \left[\theta_1{}^* + \left(\frac{a_1^2 I_2}{a_2^2 I_1 + a_1^2 I_2}\right)\theta\right] = \left[\theta_2{}^* - \left(\frac{a_2^2 I_1}{a_2^2 I_1 + a_1^2 I_2}\right)\theta\right] \tag{100}$$

With respect to a perpendicular to the plane of the ring, the final angle θ_o due to the initial mismatch (x, θ) is obtained by adding Equations 93 and 100.

$$\theta_o = \theta_x + \theta_M = \frac{a^2 y_o A_1 A_2}{\bar{I}(a_2^2 A_1 + a_1^2 A_2)} x + \frac{a_1{}^2 I_2}{a_2^2 I_1 + a_1^2 I_2}\theta + \theta_1{}^*$$

or if $$a_1^2 \simeq a_2^2 \simeq a^2$$

$$\theta_o = \frac{y_o A_1 A_2}{\bar{I}(A_1 + A_2)} x + \frac{I_2}{I_1 + I_2}\theta + \theta_1{}^* \tag{101}$$

or $$\theta_o = \frac{y_o A_1 A_2}{\bar{I}(A_1 + A_2)} x - \frac{I_1}{I_1 + I_2}\theta + \theta_2{}^* \tag{102}$$

But $$I_1 + I_2 = \bar{I}$$

$$A_1 + A_2 = A$$

so that Equations 101 and 102 can be rewritten

$$\theta_o = \theta_{1,2}{}^* + \left[\frac{\frac{A_1 A_2 y_o}{A} x \pm I_{2,1}\theta}{\bar{I}}\right]$$

NOMENCLATURE

A	Defined by $(A_1 + A_2)$
$A_{1,2}$	Cross-Section areas of sections 1 and 2 (in^2)
C	Combined centroid of the two-section ring
$C_{1,2}$	Centroids of $A_{1,2}$
E	Elastic Modulus (psi)
$\bar{I}$	Second moment of A with respect to a line which both passes through C and the ring center line, and is parallel to the plane of the ring (in^4). Defined by $(I_1 + I_2)$
$I_{1,2}$	Second moments of $A_{1,2}$ with respect to a line which both passes through C and the ring center line, and is parrallel to the plane of the ring (in^4).
$M_{1,2}$	Uniformly distributed moments which are required on sections 1 and 2 to close the mismatch rotation (in lb/in)
M_x	Uniformly distributed moment which is produced by radial forces $Q_{1,2}$ and the lever arm y_0 (in lb/in)
$Q_{1,2}$	Uniformly distributed radially outward forces required to produce centroid displacements $x_{1,2}$ (lb/in)
YY	Interaction line (Figure 4). A line, perpendicular to the ring center line, which defines the axial center of the cylindrical surface of interaction between sections 1 and 2.
$a_{1,2}$	Radii of the centroids C_1, C_2, of sections 1 and 2 (in)
$h_{1,2}$	Radial heights of sections 1 and 2 (in)
$\ell_{1,2}$	Axial lengths of sections 1 and 2 (in)
x	Total radial mismatch of free body sections 1 and 2 defined by $(x_r - x_\theta)$
$x_{1,2}$	Radial displacements of $C_{1,2}$ from their initial (free body) positions to their positions at final equilibrium. Positive radially outward (in)
y_o	Defined by $\pm (y_1 + y_2)$. Use (+) if C_1, C_2 are to the left and right, respectively, of the interaction line YY (in). Use (−) for the reversed positions. See Figure 4.

NOMENCLATURE (Cont'd)

$y_{1,2}$	Distance measured axially from $C_{1,2}$ to the interaction line YY (in).
θ	Initial angular mismatch between free body sections 1 and 2. Defined by ($\theta_2^* - \theta_1^*$)
$\theta_{1,2}$	Rotations from their initial (free body) positions (θ_1^*, θ_2^*) to their positions at final equilibrium. Positive counterclockwise (radians)
θ_x	The portion of θ_o which is caused by the moment M_x (radians)
θ_M	The portion of θ_o which is caused by moments $M_{1,2}$ (radians)
θ_o	Final equilibrium angle which the complete ring makes with the ring center line (radians). Defined by ($\theta_x + \theta_M$), positive counterclockwise.

c. THERMAL DISTORTION OF A TWO-SECTION RING

Suppose that a two-section ring as shown in Figure 65 has linear axial temperature gradients G_1, G_2 in the two sections. For a uniform coefficient of thermal expansion in the ring, the free-body angular positions of the two sections are

$$\theta_1^* = a\,\alpha\,G_1 \tag{103}$$

$$\theta_2^* = a\,\alpha\,G_2 \tag{104}$$

so that the initial angular mismatch is

$$\theta \equiv \theta_2^* - \theta_1^* = a\,\alpha\,(G_2 - G_1)$$

where a = radius of the combined centroid C (in)

Next, the values of initial radial position of section 1 and 2 are expressed by x_1^* and x_2^* below

$$x_1^* = a\,\alpha\,(\overline{T}_1 - \overline{T}_o)$$

$$x_2^* = a\,\alpha\,(\overline{T}_2 - T_o)$$

where T_o = initial uniform temperature of the ring, ^oF

$\overline{T}_{1,2}$ = average temperatures of the two sections, ^oF

so that $$x_r \equiv x_2^* - x_1^* = a\,\alpha\,\Delta\,\overline{T}$$

where $$\Delta\,\overline{T} \equiv (\overline{T}_2 - \overline{T}_1)$$

and the value of x_r is taken to be positive if $\Delta\overline{T}$ tends to cause a clearance. The value of x_θ is

$$x_\theta = x_{\theta 1} + x_{\theta 2} \equiv \left[\theta_1^* \left(y_1 - \frac{h_1}{4}\,\theta_1^*\right) + \theta_2^* \left(y_2 - \frac{h_2}{4}\,\theta_2^*\right)\right]$$

where values of θ_1^*, θ_2^* are given by Equations 103 and 104. The value of x is positive if the centroids C_1 and C_2 are to the left and right, respectively, of the interaction line YY.

The initial radial mismatch x is

$$x = x_r - x_\theta$$

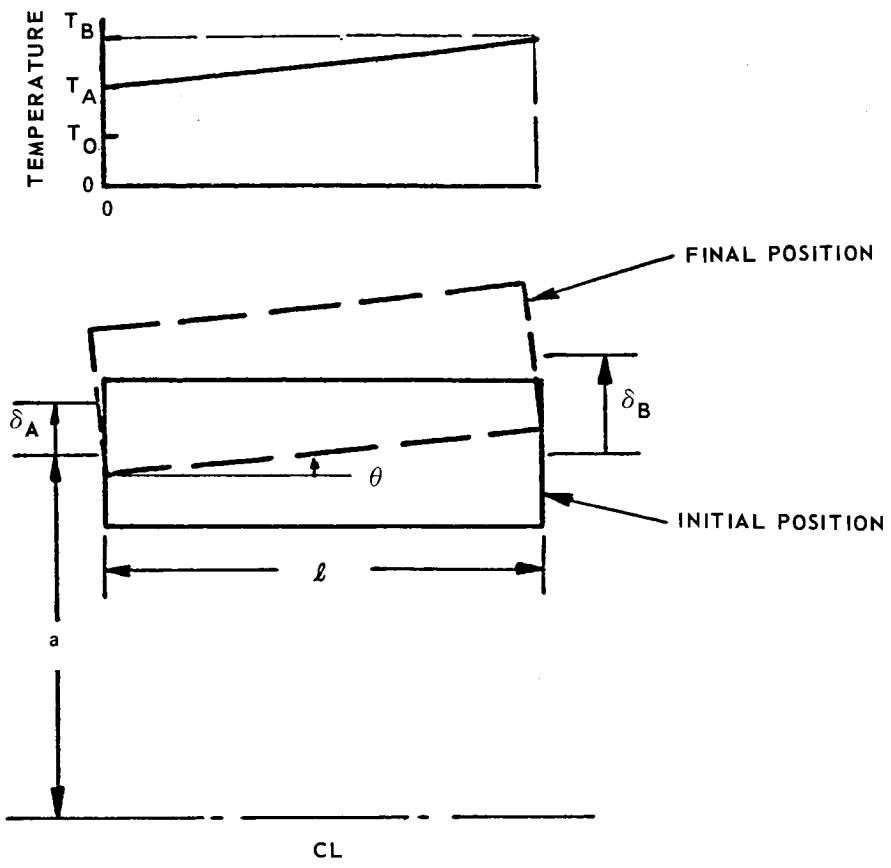

Radial Growths $\quad \delta_B \cong a\,\alpha\,(T_B - T_o)$

$$\delta_A \cong a\,\alpha\,(T_A - T_o)$$

Angle of Rotation $\quad \theta = \tan^{-1}\left(\frac{\delta_B - \delta_A}{\ell}\right) \cong \frac{\delta_B - \delta_A}{\ell}$

so that $\quad \theta = \frac{a\alpha}{\ell}(T_B - T_A)$

or $\quad \theta = a\alpha G$

Figure 65 Rotation of a Thin Ring with a Linear Axial Temperature Gradient

APPENDIX F

THERMAL ROTATION CALCULATIONS FOR SEMIRIGID INTERSTAGE SEAL

1. INTRODUCTION

The final Task I semirigid interstage seal design is shown in Figure 2. The steady-state temperature distribution used in these calculations is given in Figure 41. For the rotation calculation, the cross section is divided into four sections with the temperatures that are indicated in Figure 66. Finally, the calculation of thermal rotation is done using equations from Appendix E. Because of the temperature gradients predicted in Reference 9, the thermal rotation of the interstage seal should not exceed 2.8 millradians.

2. ANALYSIS

The semirigid seal is divided into four sections as indicated in Figure 66. In the analysis which follows, sections 1 and 2 are matched and the resulting rotation and radial motion calculated. This is also done for sections 3 and 4. Finally, sections 1 and 2 are matched to sections 3 and 4 and the final rotation of the entire seal is computed.

a. SECTIONS 1 AND 2

The following dimensions are used in conjunction with the ring analysis given in Appendix E.

$a = 14.0$ inches

$A_1 = 0.0464\ (in^2)$ $\qquad \bar{T}_2 = 1300\ (°F)$

$A_2 = 0.0525\ (in^2)$ $\qquad \bar{T}_1 = 1294\ (°F)$

$A = 0.0989\ (in^2)$ $\qquad \Delta\bar{T} = \bar{T}_2 - \bar{T}_1 = 6\ (°F)$

$\bar{I} = 7.79 \times 10^{-4}\ (in^4)$ $\qquad \theta_1^* = \theta_2^* = 0$ (radian)

$\alpha = 8.5 \times 10^{-6}$ (radian) $\qquad \theta = 0$ (radian)

$y_o = -0.072$ (in) $\qquad x = a\alpha\Delta\bar{T} = 14\ (8.5 \times 10^{-6})\ (6) = 6.7 \times 10^{-4}$

$$\theta_{12}^* = \frac{A_1 A_2 y_o x}{A\bar{I}} = -1.61\ (10^{-3}) \text{ radians (clockwise)}$$

The amount of outward relative radial motion of the section 2 with respect to section 1 is given by

$$x_{12}^* = \frac{A_2}{A} x = 3.74\ (10^{-4})$$

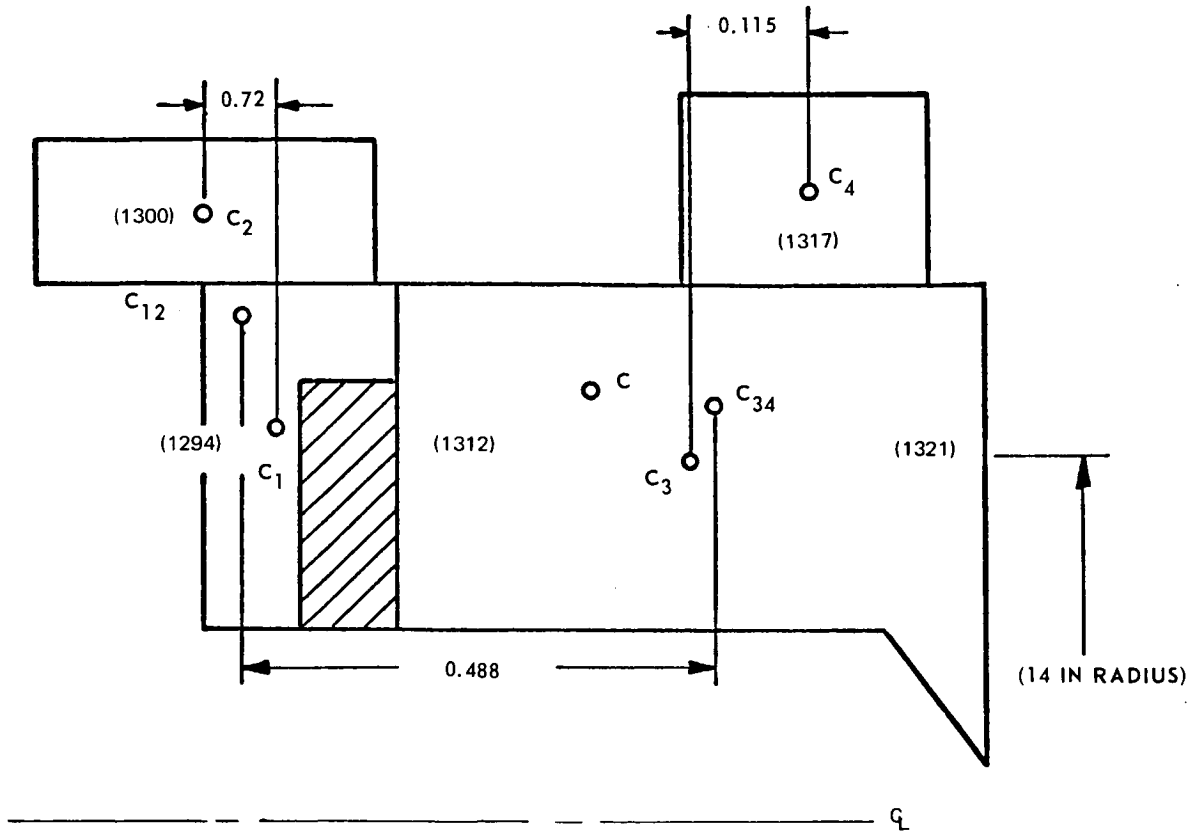

C = Centroid of entire solid section

C_{12} = Centroid of combined sections 1 and 2

C_{34} = Centroid of combined sections 3 and 4

( ) = Temperatures (°F)

Figure 66 Thermal Rotation Model of the Semirigid Interstage Seal

b. SECTIONS 3 AND 4

For this calculation,

$a = 14$ (inches)

$A_3 = 0.218$ (in^2)

$A_4 = 0.05$ (in^2)

$A = 0.268$ (in^2)

$\ell_3 = 0.6$ (inch)

$\ell_4 = 0.25$ (inch)

$\alpha = 8.5 \times 10^{-6}$ (radian)

$\overline{T}_3 = \frac{1312 + 1321}{2} = 1316.5$ (^{o}F)

$\overline{T}_4 = 1317$ (^{o}F)

$\theta_3^* = a\alpha G_3 = 1.79 \times 10^{-3}$ (radian)

$\theta_4^* = 0$

$\theta = \theta_4^* - \theta_3^* = -1.79 \times 10^{-3}$ (radian)

$y_o = 0.115$ (inch)

$y_3 = 0.115$ (inch)

$y_4 = 0$ (inch)

$I_3 = 6.65 \times 10^{-3}$ (in^4)

$I_4 = 6.95 \times 10^{-4}$ (in^4)

$\overline{I} = 7.35 \times 10^{-3}$ (in^4)

$G_3 = 9/0.6 = 15$ (^{o}F/in)

$G_4 = 0$ (^{o}F/in)

$\Delta\overline{T} = \overline{T}_4 - \overline{T}_3 = 0.5$ (^{o}F)

$x_\theta = \theta_3^* \left(y_3 - \frac{h_3}{4}\theta_3^*\right) = 2.05 \times 10^{-4}$ (inch)

$x_r = a\alpha\,\Delta\overline{T} = 0.059 \times 10^{-3}$ (inch)

$x = x_r - x_\theta = 1.46 \times 10^{-4}$ (inch)

$$\theta_{34}^* = \theta_4^* + \frac{\frac{A_3 A_4 y_o}{A} \times -I_3\ \theta}{\overline{I}} = 1.53 \times 10^{-3} \text{ (radian, counterclockwise)}$$

The corresponding outward relative radial motion of the section 4 with respect to section 3 is given by

$$x_{34}^* = \frac{A_4}{A} x = -2.75 \times 10^{-5} \text{ (inch)}$$

c. COMPLETE SEAL RING

The conditions used to compute rotation of the complete seal are:

$a = 14.0$ (inch)

$A_{12} = 0.0989$ (in^2)

$A_{34} = 0.269$ (in^2)

$A = 0.367$ (in^2)

$I_{12} = 0.01328\ (in^4)$ $\quad \overline{T}_{34} = 1316.5\ (^oF)$

$I_{34} = 0.012\ (in^4)$ $\quad \overline{T}_{12} = 1294\ (^oF)$

$\overline{I} = 0.0253\ (in^4)$ $\quad x_{12}^* = 3.74 \times 10^{-4}$ (inch)

$y_o = 0.488$ (in) $\quad x_{34}^* = 2.55 \times 10^{-5}$ (inch)

$y_{12} = 0.356$ (in) $\quad x_r = x_{34}^* - x_{12}^* + a\alpha\,(\overline{T}_{34} - \overline{T}_{12}) = 22.75 \times 10^{-4}$ (inch)

$y_{34} = 0.132$ (in) $\quad x_{\theta_{12}} = -0.58 \times 10^{-3}$ (inch)

$\theta_{12}^* = -1.61 \times 10^{-3}$ (radian) $\quad x_{\theta_{34}} = 1.58 \times 10^{-4}$ (inch)

$\theta_{34}^* = 1.18 \times 10^{-3}$ (radian) $\quad x_\theta = -4.2 \times 10^{-4}$ (inch)

$\theta = (1.18 + 1.61) \times 10^{-3} = 2.79 \times 10^{-3}$ (radian) $\quad x = 2.7 \times 10^{-3}$ (inch)

Thus,

$$\theta_o = \theta_{34}^* + \left(\frac{\frac{A_{12} A_{34} y_o}{A} x - I_{12}\,\theta}{\overline{I}} \right) = 3.43 \times 10^{-3}\ (\text{radian})$$

REFERENCES

1. R. J. Roark, Formular for Stress and Strain, Third Edition, McGraw-Hill Book Co., Inc., N.Y., N.Y., 1954

2. Sokolnickoff, I.S., Mathematical Theory of Elasticity, Second Edition, McGraw-Hill Book Co., Inc., N.Y., N.Y., 1956

3. Love, A.E.H., The Mathematical Theory of Elasticity, Fourth Edition, Dover Press, 1944

4. Den Hartog, J.P., Advanced Strength of Materials, McGraw-Hill Book Co., Inc., N.Y., N.Y., 1952

5. H. Cheng, C. Chow, and F.S. Murray, The Hydrodynamic Gas Journal Bearing and the Hydrodynamic Gas Thrust Bearing, Vol. I, MTI-65TR5-II, Mechanical Technology Inc., Latham, N.Y., 1965.

6. R.M. Hawkins, et. al., Development of Compressor End Seals, Stator Interstage Seals, and Stator Pivot Seals in Advanced Air Breathing Engines, PWA-2995, Pratt & Whitney Aircraft, E. Hartford, Conn., 1967

7. R.M. Hawkins, et. al., Development of Compressor End Seals, Stator Interstage Seals, and Stator Pivot Seals in Advanced Air Breathing Engines, PWA-3147, Pratt & Whitney Aircraft, E. Hartford, Conn., 1967

8. R.M. Hawkins, et. al., Development of Compressor End Seals, Stator Interstage Seals, and Stator Pivot Seals in Advanced Air Breathing Engines, PWA-2875, Pratt & Whitney Aircraft, E. Hartford, Conn., 1966

9. J.W. Daily and R.W. Nece, "Chamber Dimension Effects on Induced Flow and Frictional Resistance of Enclosed Rotating Disks," Journal of Basic Engineering, March, 1960

10. M. Van Duyn and W. B. Large, Rotor Stress Analysis, United Aircraft of Canada Limited, July 1966

Semiannual Reports Distribution List
NAS 3-7605

Addressee	No. of Copies
1. NASA-Lewis Research Center Air-Breathing Engine Procurement Section Attn: John H. DeFord	3
2. NASA-Lewis Research Center Air Breathing Engine Division Attn. J. Howard Childs MS 60-4	1
W. H. Roudebush MS 60-6	1
D. P. Townsend MS 60-6	4
L. E. Macioce MS 60-6	1
3. NASA-Lewis Research Center Technical Utilization Office Attn. John Weber	1
4. NASA-Lewis Research Center Reports Control Office	1
5. NASA-Lewis Research Center Attn. Library	2
Norman T. Musial	2
6. NASA-Scientific and Technical Information Facility Box 5700 Bethesda, Maryland Attn. NASA Representative	6
7. NASA-Lewis Research Center Fluid System Components Division Attn. I. I. Pinkel	1
E. E. Disson	1
R. L. Johnson	1
W. R. Loomis	1
L. P. Ludwig	1
R. A. Swikert	1
M. J. Hartmann	1
8. Air Force Materials Laboratory Wright-Patterson Air Force Base, Ohio Attn. NAML, R. Adamczak	1
NANE, R. Headrick & J. M. Keible	1
NAAE, P. Rouse	1
9. Air Force Systems Engineering Group Wright-Patterson Air Force Base, Ohio Attn. SESWS, J. L. Wilkins	1
SEJPF, S. Proto	1

Addressee	No. of Copies
10. Air Force Aero Propulsion Lab. Wright-Patterson Air Force Base, Ohio Attn. AFAPL (APFL), K. L. Berkey & L. DeBrohum	1
AFAPL (APTC), C. Simpson	1
APTP, J. J. Gershon	1
11. FAA Headquarters 800 Independence Avenue, S.W. Washington, D.C. Attn. J. Chavkin SS/120	1
M. Lott FS/141	1
12. NASA Headquarters Washington, D.C. 20546 Attn. N. F. Rekos (RAP)	1
A. J. Evans (RAD)	1
J. Maltz (RRM)	1
13. NASA-Langley Research Center Langley Station Hampton, Virginia 23365 Attn. Mark R. Nichols	1
14. Mechanical Technology, Inc. 968 Albany-Shaker Road Latham, New York Attn. D. Wilcock	1
15. Clevite Corporation Cleveland Graphite Bronze Div. 17000 St. Clair Ave. Cleveland, Ohio 44110 Attn. T. H. Koenig	1
16. Koppers Company, Inc. Metal Products Div. Piston Ring and Seal Department Baltimore 3, Maryland Attn. T. C. Kuchler	1
17. Stein Seal Company 20th Street and Indiana Ave. Philadelphia 32, Pennsylvania Attn. Dr. P. C. Stein	1
18. Wright Aeronautical Div. Curtiss-Wright Corporation 333 West 1st Street Dayton 2, Ohio Attn. S. Lombardo	1

Addressee	No. of Copies
19. General Electric Company Advanced Engine and Technology Department Cincinnati, Ohio 45215	
Attn. L. B. Venable	1
G. J. Wilo	1
C. C. Moore H-25	1
20. Huyck Metals Company P.O. Box 30 45 Woodmont Road Milford, Connecticut	
Attn. J. I. Fisher	1
21. Aerojet-General Corporation 20545 Center Ridge Road Cleveland, Ohio 44116	
Attn. W. L. Snapp	1
22. Lycoming Division Avco Corporation Stratford, Connecticut	
Attn. R. Cuny	1
23. Battelle Memorial Institute 505 King Avenue Columbus 1, Ohio	
Attn. C. M. Allen	1
24. Bendix Corporation Fisher Building Detroit 2, Michigan	
Attn. R. W. Isaacs	1
25. Boeing Aircraft Company 224 W. Wilkinson Dayton, Ohio 45402	
Attn. H. W. Walker	1
26. Douglas Aircraft Company Holiday Office Center 16501 Brookpark Road Cleveland, Ohio 44135	
Attn. J. J. Pakiz	1
27. General Dynamics Corporation 16501 Brookpark Road Cleveland, Ohio 44135	
Attn. George Vila	1
28. General Motors Corporation Allison Division Plant #8 Indianapolis, Indiana	
Attn. E. M. Deckman	1
29. Lockheed Aircraft Company 16501 Brookpark Road Cleveland, Ohio 44135	
Attn. Mr. L. Kelly	1

Addressee	No. of Copies
30. Martin Company 16501 Brookpark Road Cleveland, Ohio 44135	
Attn. Z. G. Horvath	1
31. North American Rockwell 16901 Brookpark Road Cleveland, Ohio 44135	
Attn. George Bremer	1
32. Fairchild-Hiller Corporation Republic Aviation Division Farmingdale, Long Island New York 11735	
Attn. D. Schroeder	1
33. Westinghouse Electric Corporation 55 Public Square Cleveland, Ohio 44113	
Attn. Lynn Powers	1
34. I.I.T. Research Foundation 10 West 35 Street Chicago, Illinois 60616	
Attn. Dr. Strohmeler	1
35. Pesco Products Division Borg-Warner Corporation 24700 N. Miles Bedford, Ohio	1
36. Stanford Research Institute Menlo Park, California	
Attn. R. C. Fey	1
37. Franklin Institute Lab. 20th and Parkway Philadelphia 3, Pennsylvania	
Attn. J. V. Carlson	1
38. Industrail Tectonics Box 401 Hicksville, New York 11801	
Attn. J. Cherubin	1
39. Sealol Incorporated P.O. Box 2158 Providence 5, Rhode Island	
Attn. Justus Stevens	1
40. Continental Aviation & Engineering 12700 Kercheval Detroit 15, Michigan	
Attn. A. J. Fallman	1
41. Northrop Corporation 1730 K. Street, N.W. Suite 903-5 Washington, D.C.	
Attn. S. W. Fowler, Jr.	1

Addressee	No. of Copies
42. Chicago Rawhide Manufacturing Co. 1311 Elston Ave. Chicago, Illinois Attn. R. Blair	1
43. Midwest Research Institute 425 Volker Blvd. Kansas City 10, Missouri Attn. V. Hopkins	1
44. Southwest Research Institute San Antonio, Texas Attn. P. H. Ku	1
45. E. I. DuPont de Nemours & Co. 1007 Market Street Wilmington 98, Delaware Attn. A. J. Cheney R. J. Laux	1 1
46. Fairchild Engine & Airplane Corp. Stratos Division Bay Shore, New York	1
47. Borg-Warner Corporation Roy C. Ingersoll Research Center Wolf and Algonguin Roads Des Plaines, Illinois	1
48. U.S. Naval Air Material Center Aeronautical Engine Laboratory Philadephia 12, Pennsylvania Attn. A. L. Lockwood	1
49. Department of the Navy Bureau of Naval Weapons Washington, D.C. Attn. A. B. Nehman, RAAE-3 C. C. Singleterry, RAPP-4	1 1
50. Department of the Navy Bureau of Ships Washington 25, D.C. Attn. Harry King, Code 634-A	1
51. SKF Industries, Inc. 1100 First Avenue King of Prussia, Pennsylvania Attn. L. B. Sibley	1
52. Crane Packing Company 6400 W. Oakton Street Morten Grove, Illinois Attn. Harry Tankus	1
53. B. F. Goodrich Company Aerospace and Defense Products Div. Troy, Ohio Attn. L. S. Blalkowski	1
54. The University of Tennessee Department of Mechanical & Aerospace Engineering Knoxville, Tennessee Attn. Professor W. K. Stair	1
55. Hughes Aircraft Company International Airport Station P.O. Box 98515 Los Angeles 9, California	1
56. U.S. Navy Marine Engineering Lab. Friction and Wear Division Annapolis, Maryland Attn. R. B. Snapp	1
57. Metal Bellows Corporation 20977 Knapp Street Chatsworth, California Attn. Sal Artino	1
58. Rocketdyne 6633 Canoga Ave. Canoga Park, California Attn. M. Butner	1
59. Carbon Products Div. of Union Carbide Corporation 270 Park Avenue New York 17, New York Attn. J. Curran	1
60. Garlock, Incorporated Palmyra, New York 14522 Attn. E. W. Fisher	1
61. Chemicals Div. of Union Carbide Corporation Technical Service Lab. P.O. Box 65 Tarrytown, New York Attn. J. E. Haaga	1
62. Durametallic Corporation Kalamazoo, Michigan Attn. H. Hummer	1
63. Morganite, Incorporated 33-02 48th Avenue L.I.C. 1, New York Attn. S. A. Rokaw	1
64. United States Graphite Company 1621 Holland Saginaw, Michigan Attn. F. F. Ruhl	1
65. Cartiseal Corporation 3515 West Touhy Lincolnwood, Illinois Attn. R. Voltik	1

Addressee	No. of Copies
66. Department of the Army U.S. Army Aviation Material Labs. Fort Eustis, Virginia 23604 Attn. John W. White, Chief	1
Propulsion Division	1
67. Prof. George A. Brown Dept. of Mechanical Engineering University of Rhode Island Kingston, R.I. 02881	1
68. AVCOM AMSAVEGTT Mart Building 405 South 12th Street St. Louis, Mo. 63100 Attn. E. England	1
69. Commanding Officer U.S. Naval Underwater Weapons Research and Engineering Section Newport, R.I. 02840 Attn. Technical Library, CS12 (B-566)	1
70. Stevens Institute of Technology Mechanical Engineering Department Hoboken, N. J. 07030 Attn. Prof. E. Bales	
71. Small Steam & Gas Turbine Engineering B-4 Lester Branch P.O. Box 9175 Philadelphia, Penn. 19113 Attn. S. M. DeCorso	1
72. George B. Manning U.S.A.E.R.G. Research & Technology Dept. Ft. Belvoir, Virginia 22060	1